

UNIVERSITY OF SOUTHAMPTON  
FACULTY OF ENGINEERING, SCIENCE & MATHEMATICS  
School of Ocean & Earth Sciences

# The Application of High Temperature Superconducting Materials to Power Switches

by

Stephen A. March

Thesis for the degree of Doctor of Philosophy

October 2009



UNIVERSITY OF SOUTHAMPTON

ABSTRACT

FACULTY OF ENGINEERING, SCIENCE & MATHEMATICS  
SCHOOL OF OCEAN & EARTH SCIENCES

Doctor of Philosophy

**THE APPLICATION OF HIGH TEMPERATURE SUPERCONDUCTING  
MATERIALS TO POWER SWITCHES**

by Stephen A. March

Superconducting switches may find application in superconducting magnet systems that require energy extraction. Such superconducting switches could be bypass-switches that are operated in conjunction with a parallel resistor or dump-switches where all of the energy is dissipated in the switch itself. Bypass-switches are more suited to higher energy circuits as a portion of the energy can be dissipated in the external dump resistor. Dump-switches require less material and triggering energy as a lower switch resistance is needed to achieve the required total dump resistance.

Both superconducting bypass-switches and superconducting dump-switches can be thermally activated. Switching times that are comparable to those obtained with mechanical bypass-switch systems can be achieved using a co-wound heater that is powered by a capacitor discharge. Switches that have fast thermal diffusion times through the insulation can be modelled as a lumped system whereas those with slow thermal diffusion times were modelled with the full heat diffusion equation.

Superconducting switches can be formed of either high temperature superconductors (HTS) or low temperature superconductors (LTS). Switches based on HTS materials allow operation at higher temperatures where the cost of cooling is less. Extracting the magnet energy and depositing the heater energy at higher temperatures will also reduce the load on the overall cryogenic system during switching and energy extraction. For magnet circuits that are based on high temperature superconductors the switch must also be formed of HTS material. Due to the approximately  $T^3$  dependence of specific heat capacity, switches that operate at higher temperatures have slower heat diffusion times and require higher triggering energies than those operating at low temperature. HTS based dump-switches and HTS based bypass-switches were tested in liquid nitrogen to show that the required switching time could be achieved at these high temperatures.

The design and optimisation of superconducting switches that were formed of various superconducting materials were performed for example magnet circuits to provide reference designs of switches. These example circuits were based on selected Large Hadron Collider 600 A circuits that had a stored energy of 5.5 kJ. Superconducting switches may also find application in magnet circuits with higher transport currents and higher energies. The scaling and suitability of the reference designs to higher energy circuits was also described.



# Contents

<b>Declaration of Authorship</b>	<b>xviii</b>
<b>Acknowledgements</b>	<b>xix</b>
<b>1 Introduction</b>	<b>1</b>
1.1 Energy Extraction in the LHC	4
1.2 Switches for Superconducting Electrical Systems	6
1.3 Energy Extraction Switches in the LHC	6
1.4 Magnetically and Thermally Triggered Superconducting Switches for LTS Coils	8
1.5 Thermally Triggered LTS Switches for the Very Large Hadron Collider	9
1.6 Fault Current Limiters that Utilise Superconductors	10
1.7 Switches for Maglev and SMES	12
1.8 Summary of Switch Usage and Triggering Mechanisms	12
<b>2 Materials for use in Switches that Utilize Superconductors</b>	<b>14</b>
2.1 Introduction to Superconductivity	15
2.2 HTS Materials that have the Potential to be Used in Switches	17
2.2.1 YBCO Produced by American Superconductor	18
2.2.2 YBCO Produced by SuperPower	20
2.2.3 MgB <sub>2</sub> Produced by Columbus	22
<b>3 Description of Models for Superconducting Switches</b>	<b>25</b>
3.1 Switch Concepts: Bypass-Switch and Dump-Switch	26
3.2 Physical Layout of a Superconducting Switch	29
3.3 Heat Diffusion in the Switch	31
3.3.1 Heat Diffusion Equation	31
3.3.2 Initial and Boundary Conditions of the Heat Diffusion Equation	32
3.4 Electrical Circuits	32
3.4.1 Heater Circuit	33
3.4.2 Magnet Circuit	34
3.5 Heat Generation in the Current Sharing Regime	35
3.5.1 Configuration of Superconducting Composite Conductors	35
3.5.2 Heat Generation in LTS Composite Conductors	36
3.5.3 Heat Generation in HTS Composite Conductors	38
3.6 System of Equations for a Superconducting Switch	44
3.6.1 Switch Equations	44
3.6.2 Initial and Boundary Conditions for the Switch Equations	45

3.6.3	Possible Solution Methods . . . . .	46
3.7	Approximate Solution of the Switch Equations using a Lumped Model . . .	46
3.7.1	Diffusion Times in the Switch . . . . .	46
3.7.2	Description of the Lumped Approximation . . . . .	47
3.7.2.1	Heat Conduction through the Insulation . . . . .	49
3.7.2.2	Cooling to the Surrounds . . . . .	50
3.7.2.3	Enthalpy Changes in the Switch . . . . .	50
3.7.2.4	Electrical Circuits and Heat Generation . . . . .	51
3.7.3	Switch Equations for the Lumped Approximation . . . . .	52
3.7.4	Initial Conditions for the Lumped Approximation . . . . .	53
3.8	Solution of the Switch Equations Using Finite Element and Finite Difference Methods . . . . .	54
3.8.1	Solution with a Finite Element Method . . . . .	55
3.8.2	Solution with a Finite Difference Method . . . . .	55
3.9	Conclusions . . . . .	56
<b>4</b>	<b>Experimental HTS Switches</b>	<b>58</b>
4.1	Aim of the Experiments . . . . .	59
4.2	Design and Manufacture of HTS Switches . . . . .	61
4.2.1	Dump-Switches Based on YBCO Tape . . . . .	61
4.2.2	Bypass-Switches Based on Stainless Steel Clad YBCO . . . . .	62
4.3	Experimental Results of Dump-Switches . . . . .	65
4.3.1	Heater Dynamics . . . . .	65
4.3.2	Superconductor Dynamics . . . . .	69
4.3.3	Conclusions from Experiments on Dump-Switches . . . . .	77
4.4	Experimental Results of Bypass-Switches . . . . .	78
4.4.1	Heater Dynamics . . . . .	78
4.4.2	Switching Dynamics with a Single Coil Bypass-Switch . . . . .	80
4.4.3	Switching Dynamics with a Multi-Module Bypass-Switch . . . . .	85
4.4.4	Conclusions from Experiments on Bypass-Switches . . . . .	88
4.5	Modelling of HTS Switches Operating at 77 K . . . . .	88
4.5.1	Heater Dynamics . . . . .	88
4.5.2	Sensitivity of Switching Characteristics to Critical Surface . . . . .	89
4.5.3	Comparison of Experimental YBCO Based Dump-Switches to the Model . . . . .	91
4.5.4	Comparison of Experimental YBCO Based Bypass-Switches to the Model . . . . .	92
4.5.5	Modelled Switching Characteristics with Cooling . . . . .	95
4.5.6	Switching Characteristics Calculated with the PDE Model . . . . .	96
4.6	Summary of Experimental HTS Switches . . . . .	98
<b>5</b>	<b>Design and Optimisation of HTS Switches for Magnet Circuits</b>	<b>99</b>
5.1	Superconducting Switches for Discharging Energy from Magnet Circuits . .	100
5.1.1	Description of Existing Magnet Circuits in which Superconducting Switches could be Used . . . . .	101
5.1.2	Application of Superconducting Switches to Typical Magnet Circuits	102
5.1.2.1	Energy Extraction Using a Superconducting Bypass-Switch	102

5.1.2.2	Energy Extraction Using a Superconducting Dump-Switch	103
5.1.2.3	Cooling of a Superconducting Switch	104
5.2	Design and Characteristics of HTS Switches	105
5.2.1	Configuration of YBCO Based Switches	105
5.2.2	Discharge Characteristics of the MCD Magnets when Using a YBCO Based Bypass-Switch	108
5.2.3	Discharge Characteristics of the MCD Magnets when Using an YBCO Based Dump-Switch	110
5.2.4	Application of HTS Switches to Magnet Circuits such as MCD, Bypass- or Dump- Type?	112
5.3	Optimisation of HTS Dump-Switches for 600 A Magnet Circuits Similar to MCD	113
5.3.1	Required Magnet Discharge Characteristics	113
5.3.2	Minimisation of Switch Length that Meets the Discharge Requirements	114
5.3.3	Performance Metrics for Superconducting Switches	116
5.3.4	Heater Energy	120
5.3.5	Operating Temperature	126
5.3.6	Choice of Superconductor	132
5.3.7	Number of Tapes and Tape Width	138
5.3.8	Superconducting Tape Critical Current Density	142
5.3.9	Normal State Resistance of the Superconducting Tape	146
5.3.10	Insulation Thickness	156
5.3.11	Heater Dynamics with a Capacitor Discharge Powered Heater	159
5.3.11.1	Heater Dynamics when Operating at 50 K	160
5.3.11.2	Heater Dynamics when Operating at 20 K	163
5.3.11.3	Effect of Heater Thickness on Heater Dynamics	166
5.4	Application of Superconducting Switches to Higher Energy Circuits	171
5.4.1	Higher Energy Circuits with the Same Current and Dump Resistance	171
5.4.2	Higher Energy Circuits with a Higher Current and Lower Dump Resistance	174
5.5	Summary of Design Parameters and Reference Designs of HTS Switches	179
5.5.1	Summary of Design Parameters for Superconducting Switches	179
5.5.2	Reference Designs of HTS Dump-Switches	182
<b>6</b>	<b>Conclusions</b>	<b>186</b>
	<b>Bibliography</b>	<b>189</b>

# List of Figures

1.1	CERN, bringing together people, science, and technology. . . . .	2
1.2	A view down the LHC tunnel showing the feed box that contains the current leads on the right, and the cryostats for the superconducting magnets stretching off down the tunnel. . . . .	3
1.3	Energy extraction from long magnet chains using conventional mechanical switches and also with superconducting bypass-switches. . . . .	5
1.4	Energy extraction from short magnet chains using conventional mechanical switches and also with superconducting dump-switches. . . . .	5
1.5	The mechanical switch is formed of four smaller breakers that are linked together to meet the 13 kA current rating. The overall length of the switch is about 2.5 m. Due to the high noise levels and arcing during commutation the switches are housed in a dedicated room within the tunnel. . . . .	7
1.6	Schematic of a $\dot{B}$ triggered LTS switch with the winding configuration enlarged. The switch was produced by Hagedorn in 1974 for the protection of LTS coils. . . . .	8
1.7	Quench protection cell of the VLHC transmission line magnets. . . . .	9
1.8	A resistive FCL based on Bi-2212 cylinders that are surrounded by a cupronickel shunt that also provides mechanical support. The FCL is rated at 10 MVA and 10 kV, the $I_c$ is 850 A at 66 K. . . . .	11
1.9	An HTS FCL that utilises 750 m of stainless steel clad YBCO tape. The FCL is rated at 300 A and 7.5 kV, the $I_c$ is 440 A at 77 K. The FCL is operated in liquid nitrogen and there are cooling channels between layers of the coils to allow fast recovery. . . . .	11
2.1	The critical surface of bulk YBCO. . . . .	15
2.2	Effect of an applied magnetic field on a superconductor. The Meissner Effect occurs below the lower critical field ( $H_{c1}$ ) and is the expulsion of an applied magnetic field upon transition from the normal to superconducting state. Between the lower critical field and the upper critical field ( $H_{c2}$ ) the flux can enter the superconductor as regularly spaced quantised flux vortices. . . . .	16
2.3	Applications of superconductivity. Left to right, top to bottom, levitating train, transformer, power cable, MRI image, motor, particle accelerator, and a levitating magnet. . . . .	16
2.4	Typical resistivity profiles of a low temperature superconductor (LTS) and a high temperature superconductor (HTS). . . . .	17
2.5	Cross section of American Superconductor produced YBCO tape with copper cladding ( $4.3 \text{ mm} \times 0.2 \text{ mm}$ ). . . . .	18

2.6	Electrical properties of YBCO tape produced by American Superconductor. Shown are the engineering critical current density ( $J_{ce}$ ), the $n$ -value, and the normal state resistivity ( $\rho$ ). . . . .	19
2.7	Thermal properties of YBCO tape produced by American Superconductor. . . . .	20
2.8	Cross section of the corner of a SuperPower produced YBCO tape with copper stabilisation. . . . .	20
2.9	Electrical properties of YBCO tape with different thicknesses of copper stabilisation that is produced by SuperPower. Shown are the engineering critical current density ( $J_{ce}$ ), the $n$ -value, and the normal state resistivity ( $\rho$ ). . . . .	21
2.10	Thermal properties of YBCO tape with different thicknesses of copper stabilisation that is produced by SuperPower. . . . .	22
2.11	Cross sections of MgB <sub>2</sub> tapes with different matrices as produced by Columbus. . . . .	22
2.12	Electrical properties of MgB <sub>2</sub> tape produced by Columbus. Shown are the engineering critical current density ( $J_{ce}$ ), the $n$ -value, and the normal state resistivity ( $\rho$ ). . . . .	23
2.13	Thermal properties of MgB <sub>2</sub> tape produced by Columbus. . . . .	24
3.1	Conventional energy extraction scheme using a mechanical switch and a dump resistor. . . . .	26
3.2	Possible energy extraction schemes that use superconducting switches that operate at HTS temperature. (a) shows the concept for when the energy dissipation is in a warm dump resistor, (b) shows the concept for when there is energy dissipation in the switch. . . . .	27
3.3	Physical layout of a superconducting switch. The thermal profile relates to a switch where the heater and superconductor layers have high thermal diffusivity. . . . .	30
3.4	Circuit diagrams for powering a heater with capacitor discharge. (a) shows the simplified layout for analysis, (b) shows the functional diagram including power supplies to charge the capacitor bank. . . . .	33
3.5	Magnet circuit diagram during discharge when the power supply is shorted out. Line inductance and resistances are assumed to be zero. . . . .	34
3.6	Cross sections of composite LTS tapes. (a) is Nb-Ti in a Cu matrix (0.8 mm diameter) and (b) is Nb <sub>3</sub> Sn in a Cu matrix (0.8 mm diameter). . . . .	35
3.7	Cross sections of composite HTS tapes. (a) is multifilamentary Bi-2223 in an Ag matrix tape (4 mm × 0.22 mm) and (b) is YBCO on a nickel-tungsten substrate with copper cladding (4.3 mm × 0.2 mm). . . . .	36
3.8	Heat generation as a function of temperature for LTS materials where there is a narrow current sharing region. $J_c(T)$ decreases linearly with temperature. $\rho_m$ and $J_{op}$ are constant. . . . .	38
3.9	$E$ - $J$ characteristics of a multifilamentary BSCCO in silver matrix tape measured in liquid nitrogen. . . . .	39
3.10	Current sharing between tape components. . . . .	40
3.11	Heat generation per unit volume ( $G$ ) of a stainless steel clad YBCO tape that has $T_{cs}$ of 50 K. The heat generation is normalised to the normal state value at $T_c$ ( $G_{89}$ ). . . . .	42
3.12	Current sharing between tape components and a dump resistor. . . . .	43
3.13	Diffusion time as a function of thickness for materials used in typical switches. . . . .	47

3.14	Sketch of typical switch and thermal profiles within it. . . . .	48
3.15	Heat flow resulting in enthalpy increase of the insulation layer. . . . .	49
3.16	Flow charts for the solution of the partial differential form of the system of switch equations using either a coupled method (a) or a sequential method (b). . . . .	56
4.1	Sketch of 1.5 turns of a switch (not to scale) showing the non-inductive bifilar HTS winding co-wound with a heater and insulation. The HTS tape is shown in blue, the steel heater in red, and the insulation in grey. The indium solder between the two legs of the superconductor is shown in green. The inner diameter of the switch is about 100 mm. . . . .	61
4.2	Sketch of 1.5 turns of a switch (not to scale) showing the non-inductive winding of the HTS, heater, and insulation with the switch back located in the centre of the switch. The HTS is shown in blue, the heater in red, and the insulation in grey. The diameter of the switch is about 100 mm. . . . .	63
4.3	A machine for assisting with winding the multilayer bypass-switches. I indicates spools of insulation; H, spool of steel tape; Y, spool of YBCO tape; G, guides; C the coil. Friction brakes were mounted on each axle. . . . .	63
4.4	Photograph of the bypass-switch and test station. The switch is shown centre-bottom. Current leads, heater leads, and instrumentation wires lead up from the switch. The superconductor power supply is on the left, the heater controls are on the right. The cryostat is underneath the switch. . . . .	64
4.5	Heater voltage decays for YBCO dump-switches. Voltage decays are shown for the heater having a constant resistance equivalent to the 77 K resistance ( $0.49 \Omega$ ) and the 300 K resistance ( $1 \Omega$ ). Data for the YBCO SS switches was recorded for 5 ms. . . . .	65
4.6	Measured and fitted heater voltage decays. The fitting was performed with a smoothed spline. The measured voltage of the YBCO SS switch that had a $V_{HI}$ of 250 V was limited to a maximum of 82 V by the data acquisition system. . . . .	66
4.7	Measured heater voltage decay compared to an ideal $RLC$ circuit. Time of zero corresponds to the initiation of the heater voltage rise. . . . .	67
4.8	Heater energy deposition for capacitor charge voltages of 100 V, 200 V, 300 V, 500 V, 750, and 1 kV. The estimated heater energy is calculated from the heater voltage and its differential. . . . .	68
4.9	Voltages induced in the switch by the heater capacitor discharge. Due to the switch-back in the superconductor the short ( $\approx 75$ cm) leg has a voltage in the opposite sense to the heater and the long ( $\approx 100$ cm) leg of the switch. Time zero is the onset of capacitor voltage rise. Flat spots in the voltages are where the voltage is out of range of the acquisition system. . . . .	69
4.10	Induced voltage in the superconductor as a function of the peak heater voltage. The maximum $V^+$ occurs during the rise of the heater voltage, the maximum $V^-$ occurs during the discharge of the capacitor. . . . .	70
4.11	Voltage traces for the YBCO Cu switch when triggered with a 1 kV capacitor discharge. The applied current was 40 A. When no current was applied there are still voltages induced in the superconductor by the heater. Three experiments were performed and the fit represents the average voltage with the induced voltages subtracted. Time zero is when the heater voltage begins to rise. . . . .	70

4.12	Voltage traces for the YBCO Cu switch when triggered with a capacitor discharge. The applied current was 40 A. The fit represents the average voltage with the induced voltages subtracted. Time zero is when the heater voltage begins to rise. . . . .	71
4.13	Voltage traces for the YBCO SS switch when triggered with a 1 kV capacitor discharge. The applied current was 40 A. When no current was applied there are still voltages induced in the superconductor by the heater. The fit represents the voltage with the induced voltages subtracted. Time zero is when the heater voltage begins to rise. After about 3.75 ms the power supply tripped and the current reduced. . . . .	72
4.14	Voltage evolution for the YBCO based dump-switches with a constant operating current. . . . .	73
4.15	Energy dissipated in YBCO dump switches that were triggered by a capacitor that was charged to a voltage $V_{HI}$ . The switch length was about 1.75 m and the transport current ( $I_{op}$ ) was constant. . . . .	74
4.16	Voltage as a function of temperature of YBCO based tapes that have different critical currents and carry different transport currents. . . . .	74
4.17	Estimated temperatures of YBCO based switches that transport 40 A and are triggered by a 500 V capacitor discharge. Temperature estimations around or below $T_{cs}$ are not valid due to the zero resistance of the superconductor. . . . .	75
4.18	Switching time as a function of capacitor energy for YBCO Cu and YBCO SS based dump-switches that transport 40 A. . . . .	76
4.19	Switching time as a function of transport current for YBCO SS based dump-switches that are triggered with a 500 V (200 J) capacitor discharge. . . . .	77
4.20	Heater voltage decays for stainless steel clad YBCO based bypass-switches. The fit is a smoothed spline to the average of a number (2-5) of tests. Voltage decays are also shown for the heater having a constant resistance equivalent to the 77 K resistance (1.8 $\Omega$ ) and the 300 K resistance (3.7 $\Omega$ ). The recorded voltage for $V_{HI}$ of 500 V, 600 V, and 700 V saturated at 480 V. The data and fit are generally coincident. . . . .	78
4.21	Heater energy deposition. The estimated heater energy is calculated from the heater voltage decay, the energy stored in the capacitor is calculated from the charge voltage of the capacitor. . . . .	79
4.22	Voltages measured across the dump resistor for a one coil bypass-switch formed of stainless steel clad YBCO. The data is from a number of experiments and the fit is a smoothed spline of the average. . . . .	80
4.23	Current in a stainless steel clad YBCO bypass-switch. $I_{SW}$ is the current in the switch, $I_D$ is the current in the parallel dump resistor. The operating current ( $I_{op}$ ) does not decay with time. . . . .	81
4.24	Dump resistance of an YBCO bypass-switch with a room temperature resistance of 3.7 $\Omega$ connected in parallel with a 16.5 m $\Omega$ dump resistor. . . . .	81
4.25	Estimated temperature rise of a bypass-switch based on stainless steel clad YBCO. The temperature is estimated from the non-linear $V - I$ characteristics of the superconductor, the operating current, and the resistances of the matrix, dump resistor, and current leads. Temperature estimation not valid below $T_{cs}$ where there is a zero voltage. Above $T_c$ temperature estimation is less accurate as even large changes in temperature will only have a small effect on the voltage across the dump resistor. . . . .	82

4.26	Dump resistor voltages after switching. With an $I_{op}$ of 50 A and a $V_{HI}$ of 1 kV (800 J) the switch remains resistive after triggering. With an $I_{op}$ of 40 A and a $V_{HI}$ of 400 V (128 J) the switch does not fully trigger and starts to recover in less than 1 s. . . . .	83
4.27	Estimated temperature of the switch. . . . .	84
4.28	Switching time of a single coil YBCO based bypass-switch. The switching time is defined as the time taken to reach 95 % of the required dump resistance (16 m $\Omega$ ). When carrying 40 A the switch did not switch when triggered with heater energies of 128 J or 200 J. . . . .	85
4.29	Voltages measured across the dump resistor for a four module bypass-switch formed of stainless steel clad YBCO. The data is from a number of experiments and the fit is a smoothed spline of the average. . . . .	85
4.30	Current in a stainless steel clad YBCO bypass-switch. $I_{SW}$ is the current in the switch, $I_D$ is the current in the parallel dump resistor. The operating current ( $I_{op}$ ) does not decay with time. . . . .	86
4.31	Estimated temperature rise of a bypass-switch based on stainless steel clad YBCO. The temperature is estimated from the non-linear V-I characteristics of the superconductor, the operating current, and the resistances of the matrix, dump resistor, and current leads. Temperature estimation not valid below $T_{cs}$ where there is a zero voltage. Above $T_c$ temperature estimation is less accurate as even large changes in temperature will only have a small effect on the voltage across the dump resistor. . . . .	87
4.32	Dump resistance of an YBCO bypass-switch with a room temperature resistance of 410 m $\Omega$ connected in parallel with a 8.4 m $\Omega$ dump resistor. The initial resistance is due to the current leads that had a resistance of 2.6 m $\Omega$ . . . . .	87
4.33	Measured and modelled heater voltage decays for the single coil dump-switch when there is no transport current. The model with a $V_{HI}$ of 1 kV was calculated for the normal heater resistance and also for an increased resistance case ( $1.5R_H$ ). The model and experiment are coincident for $V_{HI}$ 100 V and 500 V. . . . .	89
4.34	Measured and modelled heater voltage decays for the single coil bypass-switch when there is no transport current. The recorded voltage for $V_{HI}$ of 500 V, 600 V, and 700 V saturated at 480 V. . . . .	90
4.35	Voltage-temperature characteristics of YBCO based dump-switches for different fitting parameters of the critical surface and $n$ -value. The transport current is 40 A, the length of the stainless steel clad YBCO switch is 1.7 m and of the copper clad YBCO switch 1.87 m. . . . .	90
4.36	Measured and predicted voltage rises of a copper clad YBCO dump switch that transports 40 A and operates in liquid nitrogen. Modelled results are shown for the experimental switch configuration, with twice the thickness of insulation, and with a more rapid decrease of $I_c$ with temperature ( $\alpha$ of 3). . . . .	91
4.37	Measured and predicted voltage rises of a stainless steel clad YBCO dump switch that transports 40 A and operates in liquid nitrogen. Modelled results are shown for the experimental switch configuration, with twice the thickness of insulation, and with a higher $I_c$ . . . . .	92
4.38	Measured and predicted voltage rise of a stainless steel clad YBCO bypass-switch that transports 40 A and operates in liquid nitrogen. Modelled results are shown for the experimental switch configuration, with twice the thickness of insulation, and with a higher $I_c$ . . . . .	93



4.39	Voltage-temperature of a stainless steel clad YBCO bypass-switch that transports 40 A. The parallel dump resistor is 16.5 m $\Omega$ and the current leads have a total resistance of 10.4 m $\Omega$ . The $I_c$ at 77 K is 57 A. . . . .	93
4.40	Measured and predicted voltage rise of a stainless steel clad YBCO bypass-switch that transports 40 A and operates in liquid nitrogen. Modelled results are shown for different $J_c(T)$ and $n(T)$ characteristics, the thermal conductivity of the insulation was reduced to allow for contact resistance between the layers. . . . .	94
4.41	Measured and predicted voltage rises of a stainless steel clad YBCO bypass-switch that operates in liquid nitrogen. The modelled results use $\alpha$ of 1.75, $n(0\text{ K})$ of 10, $n(T_c)$ of 5, and the thermal conductivity of the insulation is half of the theoretical value to account for thermal contact resistance between the layers. . . . .	94
4.42	Switching times for the experimental and modelled stainless steel clad YBCO bypass-switch. . . . .	95
4.43	Comparison between the experimental results and the modelled switch with different levels of cooling. Cooling is shown for an adiabatic switch, a switch with a thermal resistance ( $R_{cool}$ ) of 3.4 K/W, and with $R_{cool}$ of 3.4 mK/W. . . . .	95
4.44	Dump resistor voltages after switching with an $I_{op}$ of 50 A and a $V_{HI}$ of 1 kV (800 J). The modelled switch has cooling to the surrounds through a thermal resistance of 3.4 K/W. The voltage drop at 95 % of the required resistance is also shown. . . . .	96
4.45	Switch temperature calculates with the lumped approximation and the PDE form of the heat diffusion equation for the stainless steel clad YBCO bypass-switch with $I_{op}$ of 50 A and $V_{HI}$ of 600 V. . . . .	97
4.46	Voltage evolution calculated with the lumped approximation and the PDE form of the heat diffusion equation for the stainless steel clad YBCO bypass-switch with $I_{op}$ of 50 A and $V_{HI}$ of 600 V. . . . .	98
5.1	Circuit diagram for energy extraction in the LHC MCD magnet circuits. . .	102
5.2	Energy discharge profile for the LHC MCD magnet circuits operating at the maximum current of 600 A (nominal current is 550 A). . . . .	102
5.3	Magnet circuit layout with a superconducting bypass-switch, safety lead, and warm dump resistor. (a) is for when the bypass-switch operates at 50 K and there is a Nb-Ti bus-bar, (b) for when the switch operates at 20 K and there is a MgB <sub>2</sub> bus-bar. . . . .	103
5.4	Magnet circuit layout when the energy is dissipated in a superconducting dump-switch. (a) is for when the dump-switch operates at 50 K and there is a Nb-Ti bus-bar, (b) for when the switch operates at 20 K and there is a MgB <sub>2</sub> bus-bar. . . . .	104
5.5	Physical layout of a superconducting switch based on stainless steel clad YBCO. . . . .	106
5.6	Superconducting properties for stainless steel clad YBCO produced by American Superconductor. Shown are the engineering critical current density (measured at CERN), the heat generation when the tape is carrying 200 A, and the normal state resistivity (measured at the University of Southampton). . . . .	106

5.7	Thermal conductivity and specific heat capacity of materials used in the stainless steel clad YBCO (YBCO SS) based switch. (a) shows the temperature values and (b) the integrated values from 4.2 K. The YBCO tape was produced by American Superconductor. . . . .	107
5.8	Switching characteristics of a HTS bypass-switch. The top pane shows the thermal histories of the heater ( $T_H$ ) and superconductor ( $T_S$ ). The middle pane shows the magnet current ( $I_L$ ) decay and energy dissipated ( $E_D$ ) for the HTS bypass-switch and for a mechanical switch, both with a $0.7 \Omega$ dump resistor. The bottom pane shows the circuit voltage ( $V$ ) and the dump resistance ( $R_D$ ) for the two systems. Time zero is when the heater temperature instantly rises to $T_{HI}$ . . . . .	109
5.9	Currents in the magnet, switch, and dump resistor during energy extraction with a superconducting bypass-switch and with the existing mechanical bypass-switch. Inset is the circuit diagram of the energy extraction scheme; the power convertor is bypassed during energy extraction. . . . .	110
5.10	Switching characteristics of a HTS dump-switch. The top pane shows the thermal histories of the heater ( $T_H$ ) and superconductor ( $T_S$ ). The middle pane shows the magnet current ( $I_L$ ) decay and energy dissipated ( $E_D$ ) for the HTS dump-switch and for a mechanical switch with a $0.7 \Omega$ dump resistor. The bottom pane shows the circuit voltage ( $V$ ) and the dump resistance ( $R_D$ ) for the two systems. . . . .	111
5.11	Effect of changing the length on the thermal profiles of a superconducting dump-switch. . . . .	114
5.12	Effect of changing the length on the current decay (a) and on the energy dissipation (b). . . . .	115
5.13	Effect of changing the switch length on the circuit voltage (a) and on the dump resistance (b). . . . .	115
5.14	Star plot showing the performance metrics of superconducting bypass and dump switches that use stainless steel clad YBCO, operate at 50 K and have a heater that instantly warms to 300 K. A smaller enclosed area represents a better performing switch. . . . .	118
5.15	Relative and area scores for superconducting bypass and dump switches. Relative scores are read on the left axis; area scores are read from the right axis. Higher performing switches have higher scores and are a lighter colour at the top . . . . .	119
5.16	Effect of changing the initial heater temperature on the thermal profiles of a superconducting dump-switch. . . . .	121
5.17	Effect of changing the length on the current decay (a) and on the circuit voltage (b). . . . .	122
5.18	Effect of changing the initial heater temperature on the thermal profiles of a superconducting dump-switch. . . . .	123
5.19	Effect of changing the initial heater temperature on the current decay (a) and on the energy dissipation (b). . . . .	123
5.20	Effect of changing the initial heater temperature on the circuit voltage (a) and on the dump resistance (b). . . . .	124
5.21	Required total switch length, total heater energy, and $\overline{\Delta T}$ for switches where the heater is instantly warmed to an initial heater temperature. Circles represent results of analyses. . . . .	125

5.22	Star plot of the performance of superconducting dump-switches with different initial heater temperatures. . . . .	125
5.23	Effect of changing the initial heater temperature on the performance of a superconducting dump-switch. . . . .	126
5.24	Switching characteristics of a stainless steel clad YBCO dump-switch that operates at 20 K, has a $T_{HI}$ of 300 K, and develops a dump resistance of $0.7 \Omega$ at just above $T_c$ . . . . .	127
5.25	Required total switch length, total heater energy, and $\overline{\Delta T}$ for switches operating at 20 K and at 50 K where the heater is instantly warmed to an initial heater temperature. Circles represent results of analyses. . . . .	128
5.26	Thermal profiles of YBCO based dump-switches operating at 20 K and at 50 K. . . . .	129
5.27	Effect of reducing the operating temperature on the current decay (a) and on the energy dissipation (b). . . . .	130
5.28	Effect of reducing the operating temperature on the circuit voltage (a) and on the dump resistance (b). . . . .	130
5.29	Star plot of the performance metrics of superconducting dump-switches with different operating temperatures. . . . .	131
5.30	Effect of changing the operating temperature on the performance metrics of superconducting dump-switches. . . . .	132
5.31	Required total switch length, total heater energy, and $\overline{\Delta T}$ for $MgB_2$ and YBCO based switches that have resistive matrices and operate at 20 K. Circles represent results of analyses. . . . .	134
5.32	Required total switch length, total heater energy, and $\overline{\Delta T}$ for $MgB_2$ switches that operate at 20 K. Circles represent results of analyses. . . . .	135
5.33	Required total switch length, total heater energy, and $\overline{\Delta T}$ for YBCO switches that operate at 20 K. Circles represent results of analyses. . . . .	135
5.34	Thermal profiles dump-switches that utilize different superconducting tapes and have $T_{op}$ of 20 K. . . . .	136
5.35	Effect of utilizing different superconducting tapes on the current decay (a) and on the energy dissipation (b). The Cu stabilised tapes have almost identical current decays. . . . .	136
5.36	Effect of utilizing different superconducting tapes on the circuit voltage (a) and on the dump resistance (b). . . . .	137
5.37	Star plot of the performance of superconducting dump-switches that utilize different superconducting tapes. . . . .	138
5.38	Effect of utilizing different superconducting tapes on the performance of a superconducting dump-switch. . . . .	139
5.39	Required total switch length, total heater energy, and $\overline{\Delta T}$ for $MgB_2$ in Cu-Ni matrix switches and stainless steel clad YBCO switches that operate at 20 K. Markers represent results of analyses. . . . .	140
5.40	Thermal profiles of dump-switches that utilize different numbers of superconducting tapes. . . . .	140
5.41	Effect of utilizing different numbers of superconducting tapes on the current decay (a) and on the energy dissipation (b). The current decay with 2 tapes of YBCO is slightly faster than with the other switches. . . . .	141
5.42	Effect of utilizing different numbers of superconducting tapes on the circuit voltage (a) and on the dump resistance (b). . . . .	141

5.43	Star plot of the performance of superconducting dump-switches that utilize different numbers of tapes. . . . .	142
5.44	Effect of utilizing different numbers of tapes on the performance of a superconducting dump-switch. . . . .	143
5.45	Effect of changing the critical current density on the thermal profiles of a stainless steel clad dump-switch. Increasing the critical current density by 50 % allows one less tape to carry the magnet current at 50 K. . . . .	144
5.46	Star plot of the performance metrics of superconducting dump-switches with different critical current densities. . . . .	145
5.47	Effect of changing the critical current densities on the performance metrics of superconducting dump-switches. . . . .	145
5.48	MgB <sub>2</sub> based tapes can have different cupronickel matrices. (a) shows the resistivities of such tapes and (b) shows the thermal profiles of dump-switches based on these tapes. . . . .	146
5.49	Effect of using MgB <sub>2</sub> based dump-switches that have different matrix compositions on the current decay (a) and on the energy dissipation (b). . . . .	148
5.50	Effect of using MgB <sub>2</sub> based dump-switches that have different matrix compositions on the circuit voltage (a) and on the dump resistance (b). . . . .	148
5.51	Star plot of the performance metrics of MgB <sub>2</sub> based dump-switches that have different matrix compositions. . . . .	149
5.52	Effect of changing the matrix resistivity on the required length and heater energy of MgB <sub>2</sub> based dump-switches. . . . .	150
5.53	Performance scores of MgB <sub>2</sub> based dump-switches with different matrix compositions. . . . .	150
5.54	Normal state resistivity of YBCO tape with different thicknesses of copper stabilisation on a 50 $\mu\text{m}$ Hastelloy substrate and a 2 $\mu\text{m}$ silver layer. . . . .	151
5.55	Thermal profiles of YBCO based dump-switches that have different thicknesses of copper stabilisation. . . . .	152
5.56	Effect of using different thicknesses of copper stabilisation on YBCO based dump-switches on the current decay (a) and on the energy dissipation (b). The switch with 10 $\mu\text{m}$ of Cu stabilisation has a slightly fast current decay than the other switches. . . . .	153
5.57	Effect of using different thicknesses of copper stabilisation on YBCO based dump-switches on the circuit voltage (a) and on the dump resistance (b). . . . .	154
5.58	Effect of the thickness of the copper stabilization on the performance parameters of YBCO based dump-switches. . . . .	155
5.59	Star plot of the performance metrics of YBCO based dump-switches that have different matrix compositions. . . . .	155
5.60	Performance scores of YBCO based dump-switches with different matrix compositions. . . . .	156
5.61	Switching characteristics of a switch with 76.2 $\mu\text{m}$ of insulation when analysed with the lumped approximation (ODE) and also the PDE solution. . . . .	157
5.62	Effect of changing insulation thickness on the thermal profiles of a superconducting stainless steel clad YBCO dump-switch that operates at 50 K and has a $T_{HI}$ of 185 K. . . . .	158
5.63	Effect of changing insulation thickness on the current decay (a) and on the energy dissipation (b). . . . .	158
5.64	Effect of changing insulation thickness on the circuit voltage (a) and on the dump resistance (b). . . . .	159

5.65	Thermal profiles of YBCO based dump-switches that have different heater materials. The SS heater with a $V_{HI}$ of 1 kV is slower than the rest. . . . .	161
5.66	Effect of using different heater materials in YBCO based dump-switches on the current decay (a) and on the energy dissipation (b). The SS heater with a $V_{HI}$ of 1 kV is slower than the rest. . . . .	161
5.67	Effect of using different heater materials in YBCO based dump-switches on the circuit voltage (a) and on the dump resistance (b). The SS heater with a $V_{HI}$ of 1 kV is slower than the rest. . . . .	162
5.68	Required heater energy and heater capacitance, and the resulting average thermal gradient and heater discharge time constant for YBCO based dump-switches operating at 50 K. Results for a switch with a copper heater and also one with a stainless steel heater. . . . .	163
5.69	Thermal profiles for dump-switches that have capacitor discharge powered heaters with different charge voltages. A log time scale (a) is used to show the differences at early times and a linear time scale (b) to show differences at later times. The legend is the same for both figures. . . . .	164
5.70	Effect of utilizing different heater capacitor charge voltages on the current decay (a) and on the voltage decays (b). $V_L$ is the magnet circuit voltage and $V_H$ the heater circuit voltage. . . . .	165
5.71	Required heater energy and capacitance, and the resulting heater discharge time and average thermal gradients for $MgB_2$ based dump-switches that have 50 $\mu m$ thick heaters formed of either stainless steel or copper as a function of $V_{HI}$ . . . . .	166
5.72	Effect of the heater capacitor charge voltage on the required heater energy and capacitance, and the resulting heater discharge time and final temperature for dump-switches that operate at 20 K and have 50 $\mu m$ thick heaters formed of copper (RRR 100). . . . .	167
5.73	Thermal profiles of $MgB_2$ based dump-switches that have different stainless steel heater thicknesses ( $\delta_H$ ) that have a capacitor charge voltage of 1 kV. A log time scale (a) is used to show the differences at early times and a linear time scale (b) to show differences at later times. The legend is the same for both figures. . . . .	168
5.74	Effect of using different thicknesses stainless steel heaters in $MgB_2$ based dump-switches on the current decay (a) and on the circuit voltages (b). . . . .	168
5.75	Required heater energy and resulting capacitor discharge time ( $\tau_H^{calc}$ ), average thermal gradients and final temperatures for $MgB_2$ in 70Cu-30Ni based dump-switches that have different thickness heaters formed of either copper (RRR 100) or stainless steel. The capacitor charge voltage is 1 kV. . . . .	169
5.76	Required heater energy and resulting capacitor discharge time ( $\tau_H^{calc}$ ), average thermal gradients and final temperatures for $MgB_2$ based dump-switches that have different thickness copper heaters (RRR 100). . . . .	170
5.77	Thermal profiles of $MgB_2$ with copper stabilization based dump switches when they are used in magnet circuits that have different stored energies but the same current and dump resistance requirements. For a constant $R_D$ of 0.7 $\Omega$ , the magnet discharge times are 44 ms (5.5 kJ), 0.18 s (22.2 kJ), and 1.3 s (160 kJ) . . . . .	172

5.78	Current decay profiles (a) and energy dissipation profiles (b) of MgB <sub>2</sub> with copper stabilization based dump switches when they are used in magnet circuits that have different stored energies but the same current and dump resistance requirement. . . . .	173
5.79	Voltage traces (a) and dump resistance evolutions (b) of MgB <sub>2</sub> with copper stabilization based dump switches when they are used in magnet circuits that have different stored energies but the same current and dump resistance requirement. $V_M$ is the voltage obtained with the mechanical switch and dump resistor, $V_S$ is the voltage obtained with the HTS switch, and $V_H$ is the heater voltage. . . . .	174
5.80	Required length and heater energy and the resulting final temperature and magnet discharge voltage when using MgB <sub>2</sub> with copper stabilization based dump-switches in higher energy magnet circuits. . . . .	175
5.81	Final temperature of the bypass-switch as a function of length. The estimations have a constant dump resistance of 0.15 $\Omega$ . . . . .	179
5.82	Switching characteristics of a 19 km long MgB <sub>2</sub> in a 70Cu-30Ni matrix based bypass-switch for the 13 kA dipole circuits. The top pane shows the thermal histories of the heater ( $T_H$ ) and superconductor ( $T_S$ ). The middle pane shows the magnet current ( $I_L$ ) decay and energy dissipated ( $E_D$ ) for the HTS bypass-switch and for a mechanical switch with a 150 m $\Omega$ dump resistor. The bottom pane shows the circuit voltage ( $V$ ) and the dump resistance ( $R_D$ ) for the two systems. In the LHC there are two energy extraction facilities, one of which is grounded at its midpoint, thereby reducing the discharge voltage to < 500 V. . . . .	180
5.83	Temperature evolutions of the reference design dump-switches when used with the 5.5 kJ MCD magnet circuits. . . . .	183
5.84	Star plot of the performance metrics of the reference design dump-switches when used with the 5.5 kJ MCD magnet circuits. . . . .	185

# List of Tables

1.1	Stored energy in LHC circuits that have energy extraction with a mechanical switch and a dump resistor ( $R_D$ ). . . . .	4
2.1	Properties YBCO tape produced by American Superconductor. $W$ is the width, $\delta$ the thickness, $\gamma$ the density, $\lambda$ the superconductor filling factor, and $T_c$ the critical temperature. . . . .	19
2.2	Properties of copper stabilised YBCO tape produced by SuperPower. In addition to the copper stabilisation the tapes have a 50 $\mu\text{m}$ thick Hastelloy substrate, a 2 $\mu\text{m}$ thick silver layer, and about 1.2 $\mu\text{m}$ of other buffer layers. . . . .	21
2.3	Properties $\text{MgB}_2$ tape produced by Columbus. $W$ is the width, $\delta$ the thickness, $\gamma$ the density, $\lambda$ the superconductor filling factor, and $T_c$ the critical temperature. . . . .	23
4.1	Thermal diffusion times of different thickness polyimide insulation at 4.2 K and 77 K. . . . .	59
4.2	Metrics of YBCO based dump-switches with copper and stainless steel cladding. The total resistance includes the resistance of the HTS-HTS joint. . . . .	62
4.3	Metrics of YBCO based bypass-switches with stainless steel cladding. The length of each module is about 5 m. $R_S$ is the switch resistance, $R_L$ the total lead resistance, $R_H$ the heater resistance, and $R_{DR}$ the resistance of the parallel dump resistor. . . . .	63
4.4	Superconducting properties of the tested YBCO based dump-switches. . . . .	75
5.1	Parameters of selected LHC magnet circuits. $I_{\text{nom}}$ is the nominal current of the circuit, $I_{\text{max}}$ is the maximum current of the power convertor, and $\tau_{LR}$ is the time constant of the magnet decay through the dump resistance ( $R_D$ ). The stored energy is evaluated at the maximum current level. . . . .	100
5.2	Required conductor length for superconducting bypass-switches to dissipate over 95 % of the magnet energy in a 0.7 $\Omega$ dump resistor. The operating current is 600 A and the stored energy is 5.5 kJ. Lengths are given for switches formed of stainless steel clad YBCO, which was produced by American Superconductor, and also $\text{MgB}_2$ in 70%(70%Cu-30%Ni), 11%Nb matrix, which was produced by Columbus. . . . .	103
5.3	Required conductor length for superconducting dump-switches that have 0.7 $\Omega$ dump resistance just above $T_c$ . Lengths are given for switches formed of stainless steel clad YBCO produced by American Superconductor and also $\text{MgB}_2$ in a 70%(70%Cu-30%Ni), 11%Nb matrix produced by Columbus. . . . .	104
5.4	Properties of stainless steel clad YBCO tape produced by American Superconductor. . . . .	107

5.5	Properties of superconducting switches based on stainless steel clad YBCO over a range of operating temperatures with a magnet current of 600 A. . .	127
5.6	Heater energy ( $E_H$ ) and equivalent heater energy ( $\overline{E_H}$ ) delivered at the operating temperature for minimum energy switches formed of stainless steel clad YBCO. . . . .	131
5.7	Properties of dump-switches that operate at 20 K with a magnet current of 600 A. $L_{T_c}$ is the length required for a dump resistance of $0.7 \Omega$ at $T_c$ . . .	133
5.8	Parameters of minimum energy YBCO switches that have different critical current densities and which operate at 50 K. . . . .	143
5.9	Parameters of MgB <sub>2</sub> based dump-switches that have different matrix compositions. The lengths are set to meet the discharge requirements for the minimum heater energy. The Cu, Ni, & Fe matrix tape has a larger area than the cupronickel alloy tapes. . . . .	147
5.10	Parameters of HTS dump-switches that operate at 50 K and use YBCO tape with deposited copper (RRR 50) stabilisation. The tapes also contain a $50 \mu\text{m}$ Hastelloy substrate and a $2 \mu\text{m}$ Ag (RRR 100) layer. Three tapes are needed to carry the magnet current and the lengths are set to meet the discharge requirements for the minimum heater energy. . . . .	152
5.11	Parameters of YBCO based dump-switches operating at 50 K that have $50 \mu\text{m}$ thick heaters. Three tapes are required to carry the magnet current at 50 K. The magnet circuit discharge time constant ( $\tau_M^{\text{mech}}$ ) is 58.7 ms . . .	160
5.12	Parameters of dump-switches operating at 20 K that have $50 \mu\text{m}$ thick heaters powered by a 1 kV that provides the same energy as the $T_{HI}$ switch. The magnet circuit discharge time constant ( $\tau_M^{\text{mech}}$ ) is 58.7 ms. The YBCO has an $I_c$ of 90 A at 77 K and two tapes are required to carry the 600 A magnet current at 20 K. The MgB <sub>2</sub> switches only require one tape. . . . .	164
5.13	Parameters of MgB <sub>2</sub> in 70Cu-30Ni matrix based dump-switches that operate at 20 K and have different thickness heaters ( $\delta_H$ ) formed of stainless steel. One tape is needed to carry the magnet current and the lengths are set to meet the discharge requirements for the minimum heater energy. . . . .	167
5.14	Estimated energies that cause MgB <sub>2</sub> based switches that operate at 20 K to warm to 300 K. The switches have an $I_c$ of 700 A ( $J_{ce}$ (20 K) of $\approx 0.35 \text{ kA/mm}^2$ ) The magnet current is 600 A and the dump resistance is $0.7 \Omega$ . . . . .	176
5.15	Reference designs of switches that transport 600 A and develop a dump resistance of $0.7 \Omega$ . . . . .	182



# Declaration of Authorship

I, **Stephen A. March**, declare that the thesis entitled **The Application of High Temperature Superconducting Materials to Power Switches** and the work presented in the thesis are both my own, and have been generated by me as the result of my own original research. I confirm that:

- this work was done wholly or mainly while in candidature for a research degree at this University;
- where any part of this thesis has previously been submitted for a degree or any other qualification at this University or any other institution, this has been clearly stated;
- where I have consulted the published work of others, this is always clearly attributed;
- where I have quoted from the work of others, the source is always given. With the exception of such quotations, this thesis is entirely my own work;
- I have acknowledged all main sources of help;
- where the thesis is based on work done by myself jointly with others, I have made clear exactly what was done by others and what I have contributed myself;
- parts of this work have been published as:
  - S. A. March, A. Ballarino, and Y. Yang, “Power switches utilizing superconducting material for accelerator magnets”, *Applied Superconductivity, IEEE Transactions on*, vol. 19, pp. 1182 - 1185, 2009.
  - S. A. March, A. Ballarino, C. Beduz, K. H. Meß, and Y. Yang, “Towards the design of power switches utilizing HTS material”, *Journal of Physics: Conference Series*, vol. 97, p. 012002 (6pp), 2008.

Signed: .....



## Acknowledgements

I am indebted to my supervisors, Dr Amalia Ballarino at CERN and Prof Yifeng Yang at the University of Southampton, without whom this Ph.D. would not have been possible. My thanks to you both.

I am grateful to Dr Tom Taylor for his helpful and stimulating discussions. I would also like to thank Prof Carlo Beduz, Dr Karl-Hubert Meß, and Dr Maitham Al-Mosawi for their useful input at various stages throughout this work.

I would like to thank Mike Webb for his tips on how to make different devices and also all of the people in Southampton who made it a pleasant and welcoming place to be. Je voudrais remercier Pascal Chambouvet, Philippe Denis, Alain Gharib, Nassim Ben Redjeb et les gens du labo pour la réalisation des pièces mécaniques, l'assistance technique, et surtout leur amitié. I would like to thank Dr Thierry Boutboul for his help with testing the critical current of HTS materials at 4.2 K and also Dr Christian Scheuerlein for his help in taking micrographs of the YBCO and MgB<sub>2</sub> samples. My thanks to the administrative staff in both Southampton and at CERN for helping with the paperwork that was spread across both countries. I am also grateful for the financial support from CERN that allowed this research to be carried out and which is where I spent the majority of my time.

Finally, my love to my family and friends for their help and support throughout this time.

## Chapter 1

# Introduction

Switches formed of superconducting material may find application in superconducting magnet systems that require energy extraction. Conventional energy extraction schemes often use a mechanical switch and a dump resistor that are situated at room temperature. Superconducting switches may allow a direct replacement of the mechanical switch or they may allow novel energy extraction schemes to be utilised. Superconducting magnet systems are a key part of particle accelerators such as those found at CERN.

**CERN- The European Organization for Nuclear Research** was founded in 1954, and derives its name from the ‘Conseil Européen pour la Recherche Nucléaire’ which was setup in 1951 to allow physicists to explore the fundamental questions of nature. CERN is the world’s largest particle physics laboratory and whilst it is a European organization, the collaboration occurs on an international scale with twenty European member states, twenty eight non-member states, as well as eight observer states and organizations<sup>1</sup>. In addition to the fundamental physics research performed at CERN, there are a whole host of spin-off technologies including the World Wide Web [1]. This ground breaking research and development is only possible through the cooperation of thousands of people throughout the world, making CERN one of the best examples of effective international cooperation.

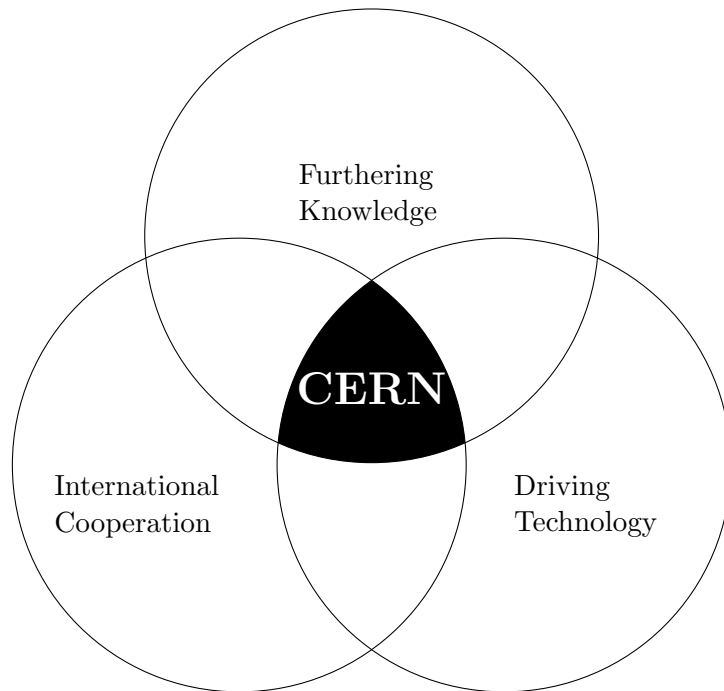


FIGURE 1.1: CERN, bringing together people, science, and technology.

**The Large Hadron Collider (LHC)** is a synchrotron particle accelerator with a circumference of 27 km. This makes it the world’s largest and most powerful particle accelerator and also one of the world’s largest machines. Figure 1.2 shows a view down the LHC

<sup>1</sup>At present, CERN’s Member States are Austria, Belgium, Bulgaria, the Czech Republic, Denmark, Finland, France, Germany, Greece, Hungary, Italy, Netherlands, Norway, Poland, Portugal, Slovakia, Spain, Sweden, Switzerland, and the United Kingdom. India, Israel, Japan, the Russian Federation, the United States of America, Turkey, the European Commission, and the United Nations Educational, Scientific, and Cultural Organization (UNESCO) have Observer status.

tunnel. The LHC consists of two counter rotating particle beams that are housed within the same cryostat. The beams, of either protons or lead ions, are accelerated to close to the speed of light and are bent around the ring by superconducting dipoles. There are four beam crossing points where the main experiments take place. These installations are ALICE, CMS, ATLAS, and LHCb. In normal operating conditions the collisions have an energy of 14 TeV for proton-proton collisions and 1150 TeV for lead ion collisions. One of the purposes of the LHC and its associated experiments is to search for the Higgs boson. The Higgs boson is a hypothetical particle that is believed to give fundamental particles their mass [2].



FIGURE 1.2: A view down the LHC tunnel showing the feed box that contains the current leads on the right, and the cryostats for the superconducting magnets stretching off down the tunnel.

The LHC consists of a variety of both superconducting and resistive magnets that are used to guide, correct, and focus/defocus the beams. The superconducting magnets and superconducting bus-bars, which utilise Nb-Ti as the superconductor, are cooled to as low as 1.9 K with superfluid helium and are housed with a variety of other accelerator components in a common cryostat. The LHC is divided into eight sectors thereby allowing a more manageable powering scheme when compared to a continuous ring, as well as modular construction and testing. Each sector contains superconducting magnets that have transports currents from 60 A to 13 kA. The individual magnet groups are connected in series and are connected to the same cooling circuits as the other magnet groups. In the event of a quench or other machine malfunction, the energy stored in the magnets must be rapidly extracted to prevent damage to the LHC.

## 1.1 Energy Extraction in the LHC

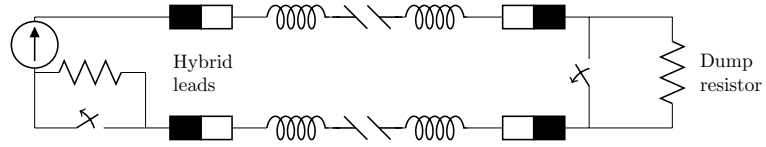
**The energy stored in the superconducting circuits** of the LHC amounts to about 11 GJ in total. This energy requires controlled extraction if there is a problem related to the superconducting magnets. The sectorization and separation of the various superconducting circuits mean that the energy extracted by a single circuit is a lower, but still significant amount. A maximum of 1.3 GJ of energy is stored within the main dipoles chains due to their high inductance (15.4 H) and maximum current of 13 kA (nominal current is 11.8 kA) [3]. The problem is further compounded by the fact that the magnets are connected in series, and so if a resistive transition (quench) occurs, the magnet chain will try to dump all of its energy into the quenching magnet leading to almost certain burnout. In order to avoid this happening, various ways of protecting the magnets are in place. These include, room temperature switches and energy extraction resistors, cold diodes, cold resistors, and also quench heaters [3]. Table 1.1 shows the stored energy in LHC circuits where the energy extraction system utilises mechanical switches and an external dump resistor [4]; superconducting switches may find application in these circuits.

Magnet Type	Inductance (mH)	Current (A)	No. of Circuits	Energy (kJ)	$R_D$ (m $\Omega$ )
Dipoles	15 400	11 810	8	$1.1 \times 10^6$	150
Quadrupoles	263	11 810	8	$18 \times 10^3$	6.6
	286	11 810	8	$20 \times 10^3$	7.7
Correctors	12 & 20	550	16 & 16	1.8 & 3.0	200
	31 to 600	550	8 to 32	4.7 to 91	700

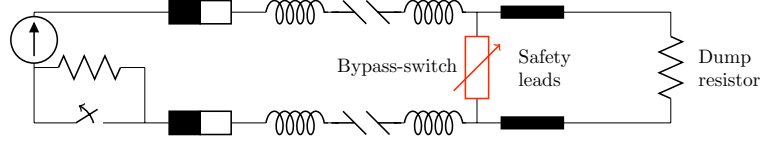
TABLE 1.1: Stored energy in LHC circuits that have energy extraction with a mechanical switch and a dump resistor ( $R_D$ ).

**Energy extraction schemes** are required so that the energy can be extracted from the magnet faster than in a normal ramp-down. If the energy is not extracted fast enough then the magnet will rapidly warm up potentially damaging the magnet and other accelerator components. In the LHC the maximum allowable temperature of the Nb-Ti is 300 K to 375 K [3]. In order to prevent this happening, the majority of the 13 kA and 600 A circuits require external dump resistors in which the energy is dissipated. These resistors, which for the dipoles weigh several tonnes, are connected in series with the magnet chain and are switched into the circuit using custom built circuit breakers. These switches are described in more detail in Section 1.3. The main magnets also have quench heaters that are used to warm up the entire magnet thereby minimising local hot spots.

Figure 1.3(a) shows a conventional energy extraction scheme for a long magnet chain that has mechanical switches and dump resistors at both ends of the chain. The LHC main dipole circuits have an energy extraction scheme similar to this; they also include cold diodes over each magnet and the grounding of the resistor midpoint to reduce the discharge voltage [4]. The disadvantage of such a scheme is that the full operating current



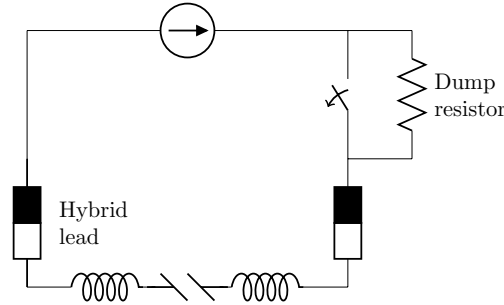
(a) Energy extraction from a long magnet chain using two mechanical switches, two dump resistors, and four full rated hybrid current leads.



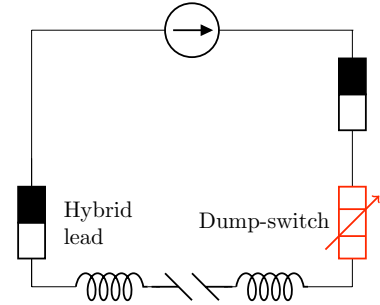
(b) Energy extraction from a long magnet chain where one mechanical switch has been replaced with a superconducting bypass-switch thereby allowing two full rated current leads to be replaced with lower heat leak safety leads.

FIGURE 1.3: Energy extraction from long magnet chains using conventional mechanical switches and also with superconducting bypass-switches.

of the magnets has to be extracted from the cryostat, pass through the switch at ambient temperature, and then return to the magnet chain. This leads to cryogenic losses along the current leads and ohmic losses in the resistive part of the current leads and in the switch. One possible application of a superconducting switch would be as a replacement for the room temperature DC breakers, as shown in Figure 1.3(b). The advantages of using a superconducting switch is a reduction in cryogenic losses due to the use of lower heat leak safety leads and a reduction in resistive losses as the leads do not normally carry the magnet current and the switch is superconducting.



(a) Energy extraction from a short magnet chain with a conventional mechanical switch and a dump resistor.



(b) Energy extraction from a short magnet chain with superconducting dump-switch.

FIGURE 1.4: Energy extraction from short magnet chains using conventional mechanical switches and also with superconducting dump-switches.

Figure 1.4(a) show a conventional energy extraction scheme for a magnet chain where there is single mechanical switch and dump resistor. Superconducting bypass-switches may provide advantages in such circuits as they do not suffer from arcing and erosion that is a problem for mechanical switches. However, the cryogenic losses would increase slightly as an extra safety lead would be required to bypass the switch when it is resistive. A novel application for superconductors would be as a dump-switch as shown in Figure 1.4(b).

Such a system eliminates the need for an extra safety lead and the dump resistor as all of the magnet energy is deposited in the switch itself. More details on superconducting bypass-switches and superconducting dump-switches are in Section 3.1.

## 1.2 Switches for Superconducting Electrical Systems

In section Section 1.1, the potential for using superconducting switches in energy extraction systems was discussed. Due to the large range of operating conditions of different superconducting magnet systems there is the potential for a range of different switches that are suitable for different circuits, similar to the different rated conventional mechanical switches. In the LHC, for example, the range of operating currents is 600 A to 13 kA, the energy that is to be dissipated is in the range of 5.5 kJ to 1.3 GJ, and the required dump resistances range from 6.6 m $\Omega$  to 700 m $\Omega$  (Table 1.1).

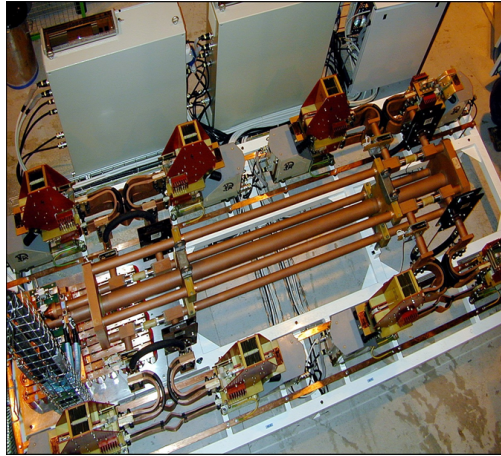
It is clear that a superconductor can be returned to its resistive state by exceeding any one of the critical values for temperature, magnetic field, or current density. In addition to this a superconducting switch could be operated mechanically, in a similar way to conventional switches. An examination of the literature shows that superconducting switches have been made utilising each of these triggering mechanisms, as described in Section 1.4 to Section 1.7. These power switches tend to be either slower acting persistent current switches or fault current limiters, both of which have limited applicability to energy extraction switches. The use of HTS power switches has been proposed since shortly after the discovery of this class of materials with their use for space launcher applications being investigated in the late 1980s [5]. Conventional mechanical switches that are currently used for energy extraction, can also provide an insight into the issues surrounding energy extraction switches.

## 1.3 Energy Extraction Switches in the LHC

This section details the mechanical switches [6] that are used commutate the current and allow energy extraction from the LHC circuits described in Section 1.1. Both the 13 kA and 600 A circuits require a switch to shunt the stored energy into a parallel dump resistor with the overriding design parameter for these switches being reliable operation as non-opening would lead to the energy being released into the magnets and bus-bars, which could result in damage to the collider. This in turn would lead to long and costly repairs. Other design parameters were longevity, radiation tolerance, and low ohmic losses. The choice for both of these switches were electromechanical breakers that had a similar principle of operation, but that was implemented differently due to the difference in current. Semiconductor devices would have been a possibility as the absence of moving parts provides advantages, but they were rejected as they rely on a single active system, have higher ohmic losses



during operation, and are less tolerant to radiation making them less suited for use near a particle accelerator.



(a) Mechanical switch for the LHC 13 kA circuits.



(b) Housing for the switch.

FIGURE 1.5: The mechanical switch is formed of four smaller breakers that are linked together to meet the 13 kA current rating. The overall length of the switch is about 2.5 m. Due to the high noise levels and arcing during commutation the switches are housed in a dedicated room within the tunnel.

The 13 kA switch comprised of four parallel connected DC breakers that were individually rated to 4.5 kA (Figure 1.5). At the time there was no existing breaker that could meet these demands and so a bespoke device to meet the LHC requirements was developed [7]. This device utilized components from existing breakers that had a reliable track record of being used in a variety of industries world wide. The breaker was fitted with arc chutes and mufflers in order to increase the lifetime of the switch. The breaker had two independent release mechanisms, one passive and one active. The active system was triggered by a pulsed release via a capacitor discharge, the passive system by de-energizing the holding coil. The active system resulted in opening times of  $5 \text{ ms} \pm 1 \text{ ms}$ , the passive  $20 \text{ ms} \pm 2 \text{ ms}$ , but both systems being triggered simultaneously [8]. One problem with mechanical breakers is that frequent maintenance is needed to replace the contacts. Conventional copper contacts would have worn out after 20-100 commutations, which would have led to unacceptable LHC downtime, and so specially developed tungsten-silver contacts having a lifetime of 300 commutations were used instead [6]. The voltage drop across a breaker was 60 mV at 4 kA. Further disadvantages of these large electromechanical breakers were the noise (100 dBA), shock waves (129 dBA at 3 m), high contact temperatures ( $160^\circ \text{C}$ ) during operation and hot ( $350^\circ \text{C}$ ) ionized air release during opening [9]. These problems necessitated the installation of the switches in a dedicated protection room (Figure 1.5(b)) within the tunnel. The 600 A breakers were based on standard 3-pole AC breakers that were then mechanically linked together. The breakers were fitted with arc chutes and capacitive snubber circuits and have similar release principles to the 13 kA breakers [8]. The active system resulted in opening times of 11 ms to 17 ms, the passive 20 ms to 22 ms.

## 1.4 Magnetically and Thermally Triggered Superconducting Switches for LTS Coils

The use of superconducting switches is not a new concept with their use following the development of other superconducting systems. In 1964 thermally and magnetically triggered switches were investigated for use in superconducting magnetic energy storage (SMES) systems at the Ion Physics Corporation by Ameen and Wiederhold [10]. The switches were formed of Nb-Zr wire that was wound in a non-inductive manner. The thermally activated switch had a critical current of 17 A and used 700 m to achieve a room temperature resistance of 21 k $\Omega$ . The magnetically triggered switch had a critical current of 26 A and used 1000 m of wire with a room temperature resistance of 31 k $\Omega$ . These switches met the zero resistance and zero inductance requirements of SMES, and also had fast rates of rise of resistance. The magnetically triggered switch was three times faster than the thermally triggered switch and had a rate of resistance increase of  $10^5$   $\Omega$ /s. When integrated into the SMES circuit this corresponded to a rise time of 26 ms for the magnetically triggered switch and 70 ms for the thermally triggered switch. These switches were dependent upon the operating current and had a size comparable to that of the coils which they were used in conjunction with.

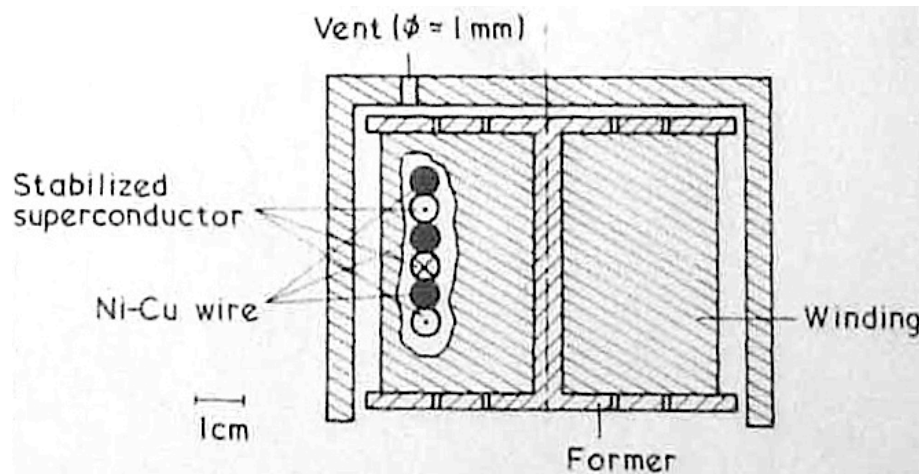


FIGURE 1.6: Schematic of a  $\dot{B}$  triggered LTS switch with the winding configuration enlarged. The switch was produced by Hagedorn in 1974 for the protection of LTS coils.

Thermally activated switches were investigated in 1971 at Oxford Instruments by Biltcliffe and Hanley [11] for safely discharging persistent LTS magnets when the helium level drops too low. In this case the magnet was shorted with a length of superconducting wire that was in thermal contact with a heater. A diode was connected in parallel to the switch so that the extracted energy did not destroy the switch but was instead dissipated in the diode. The forward voltage bias of the diode meant that there was some current through the switch that served to keep the switch latched open during de-excitation of the magnet. The transition time of this switch was around 2 s which meant that it was suitable for the

slow discharge of a magnet but not for the protection of a quenching magnet that requires energy extraction.

A superconducting switch for the protection of LTS magnets was developed in 1974 by Hagedorn and Dullenkopf [12]; shown in Figure 1.6. This switch was formed of 480 m of Nb-Ti in a cupronickel matrix which gave it maximum operating current of 90 A and also a high off state resistance. The resistance of the switch in the normal state was 195  $\Omega$ , which allowed energy extraction to occur in an 18  $\Omega$  room temperature resistor that was connected in parallel to the switch. The switch wire was co-wound with a control wire that was used to magnetically trigger the switch. The control wire was co-wound with the switch-wire in such a way that a magnetic field was applied to the superconductor but the overall switch had a low inductance (41  $\mu\text{H}$ ). The magnetic field was created by discharging a capacitor through the control wire leading to a high rate of change of magnetic flux density that exceeded the critical  $\dot{B}$  of the material. The switch was tested with transport currents from 20 A to 90 A with switching times from 3.5 ms to 1 ms.

## 1.5 Thermally Triggered LTS Switches for the Very Large Hadron Collider

The use of superconducting protection switches for energy extraction from large accelerator magnets was proposed for the Very Large Hadron Collider (VLHC) [13]. This was a design study into a particle accelerator that had a circumference of 233 km and was situated 120 m under Fermilab, Illinois. The large circumference of the VLHC allowed it to achieve beam energies of up to 40 TeV at Stage 1 and over 175 TeV after Stage 2. In this machine the protection of the 100 kA, 20 km long, 60 mH magnet strings was to be via parallel dump resistors, at either warm or cold, that were switched into the circuit with superconducting switches as shown in Figure 1.7.

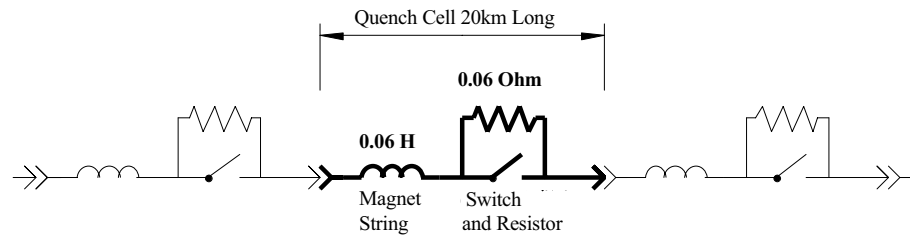


FIGURE 1.7: Quench protection cell of the VLHC transmission line magnets.

These switches were based upon a 65 m length of Nb-Ti in a Cu-Ni matrix giving a warm resistance of 1  $\Omega$  that allowed energy extraction via a 60 m $\Omega$  parallel dump resistor. The discharge time constant of this energy extraction circuit was about 1 s [14]. The switch was to be thermally activated using a capacitor discharge powered heater. Whilst the

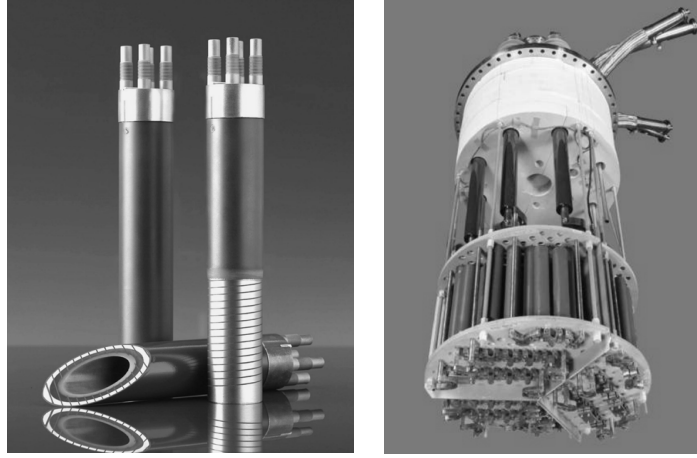
design called for commercially available LTS conductor, HTS material was also proposed as a possibility.

This switch did not evolve beyond a preliminary design stage due to termination of the VLHC project. However, the design of this superconducting dump switch was resurrected by a team at Fermilab in 2007 [15] for use in fast cycling accelerators. The new switch had the same design parameters as for the VLHC switch and was to be used as a back up to a power supply failure. The switch is not the primary protection system due to the long cool down time after energy extraction.

## 1.6 Fault Current Limiters that Utilise Superconductors

Whilst superconductors exhibit properties that make them inherently suitable for use in a fault current limiter (FCL) they were not developed for this application until the late 1980s and early 1990s [16] after the advent of LTS conductors with low AC losses and the discovery of HTS materials. The promise of FCL is such that their development has continued with a variety of designs now being researched [17]. HTS based FCLs emerged as a better choice than LTS due to the cryogenic savings and simplicity of working at liquid nitrogen temperatures despite their less sharp transition to the normal state and higher conductor cost. At present there is significant research into different designs of FCLs that utilize various HTS materials with whole sections of conferences being dedicated to them (*e.g.* ASC 2008 in Chicago and EUCAS 2007 in Brussels). FCLs can be inductive, resistive, or a combination of the two. For FCLs based on tape material, YBCO tape is favoured due to its higher normal state resistance when compared to silver matrix BSCCO tapes. If bulk material is to be used then BSCCO is generally favoured, although YBCO bulk based FCLs are also under development [18] [19]. FCLs based on thin films of YBCO are also possible [20]. The recent discovery of  $\text{MgB}_2$  and its subsequent rapid development has shown that it too can be used for FCL applications [21] with commercial versions of the high resistance matrix  $\text{MgB}_2$  wire suitable for FCLs under development [22]. Whilst FCLs are passive devices and protection switches are generally active devices their similar requirements in terms of high transport current, resistance, and reliability warrants their further description. Described below are two FCLs nearing grid usability, one formed of bulk BSCCO, the other YBCO tape.

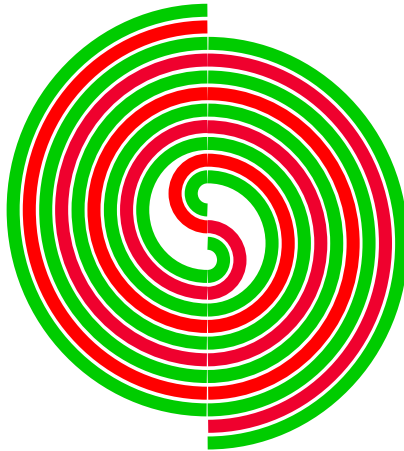
**FCLs formed of bulk HTS** materials are suited to switching applications due to their high current carrying ability and high normal state resistance. However, they are limited by poor mechanical properties and susceptibility to hot spots due to inhomogeneities, leading most practical devices to be made from tape materials. Despite this, successful FCLs have been formed of bulk BSCCO [23] and earlier demonstrators formed of bulk YBCO as well as BSCCO have also been investigated. A resistive FCL was formed of melt cast processed Bi-2212 with a rating of 10 MVA and 10 kV with an  $I_c$  of 850 A at



(a) Bulk BSCCO cylinders that have a cupronickel shunt, the height is  $\approx 0.3$  m. (b) FCL formed of bulk BSCCO.

FIGURE 1.8: A resistive FCL based on Bi-2212 cylinders that are surrounded by a cupronickel shunt that also provides mechanical support. The FCL is rated at 10 MVA and 10 kV, the  $I_c$  is 850 A at 66 K.

66 K. The base component is a BSCCO tube 30 cm long and 50 mm in diameter that was cut into a spiral bifilar resulting in a length of 540 cm. A continuous cupronickel shunt was connected to the superconductor to provide mechanical and electrical stability. Figure 1.8(a) shows the Bi-2212 cylinders with attached shunt, each phase required 30 of these components (Figure 1.8(b)). This device was field tested in a commercial grid and was suitable for medium voltage levels. Further development of a Bi-2212 FCL suitable for use at 130 kV is ongoing [24].



(a) Schematic of a non-inductively wound tape FCL. Red is the superconductor and green is the insulation.



(b) Assembled coils of a fault current limiter based on YBCO tape.

FIGURE 1.9: An HTS FCL that utilises 750 m of stainless steel clad YBCO tape. The FCL is rated at 300 A and 7.5 kV, the  $I_c$  is 440 A at 77 K. The FCL is operated in liquid nitrogen and there are cooling channels between layers of the coils to allow fast recovery.



**FCLs formed of tape HTS** can have many design similarities to power switches that are also formed of YBCO tapes. Due to the large international interest in FCLs there has been considerable research and development with devices nearing commercial level. One such device has been developed by Siemens and American Superconductor [25] and has been successfully tested [26]. The FCL is made from a total of 750 m of stainless steel clad YBCO that was manufactured using the RABiTS-MOD process (Section 2.2.1). This fault current limiter was measured to have an  $I_c$  of 440 A at 77 K with a nominal operating rating of 300 A<sub>rms</sub> and 7.5 kV. A length of 50 m of tape was wound into a low-inductance coil (Figure 1.9(a)) with five coils being connected in parallel to achieve the required  $I_c$  and three modules being connected in series to develop the required resistance (Figure 1.9(b)). In order to ensure rapid recovery to the superconducting state the windings of the bifilar coil were separated and exposed to liquid nitrogen.

## 1.7 Switches for Maglev and SMES

Maglev required a persistent current switch with a current carrying capacity of 600 A and an off state resistance of  $\approx 52 \Omega$  [27]. The switch had to be small and light with good stability against spurious quenches, which are particularly a problem on vibrating trains. A 1.7 kg Nb-Ti in cupronickel matrix switch was developed that had a switching time of  $< 10$  s. However, the  $I_c$  was only about a fifth of the  $I_c$  of a short sample and the switch was sensitive to disturbances. Changing the material to Nb<sub>3</sub>Sn in 70%Cu30%Ni matrix increased the critical temperature and critical-current density which led to a more stable switch. The Nb<sub>3</sub>Sn switch weighed  $\approx 30\%$  less than the Nb-Ti switch but it had a longer switching time, 37 s, for the same 13 W heater.

In order to allow operation at higher temperatures and an open circuit in the off state, mechanical HTS switches were investigated for Maglev and SMES applications [28]. To overcome the problems of the brittle bulk YBCO fracturing it was impregnated with epoxy. Cubes with a side area of 64 mm<sup>2</sup> were clamped together with a force of 500 N, allowing a current of 13.5 A to be passed. A mechanical switch using Nb-Ti was also developed for SMES applications [29]. Each switch could carry  $\approx 1$  kA, with several connected in parallel to achieve the required  $I_c$ . The transition time for the switch was 0.7 ms.

## 1.8 Summary of Switch Usage and Triggering Mechanisms

Whilst there are a range of superconducting switches in existence, none of them are suitable for use in magnetic energy extraction schemes that operate above 4.2 K. In order to allow energy extraction systems to operate at higher temperatures where the cryogenic cost is less a new switch is required. However, technologies used in existing superconducting

switches could be used in the design and manufacture of such a device. The advantages and limitations of the four different triggering mechanisms are discussed below.

**A thermally triggered switch** is one where the superconductor is taken out of the superconducting state by warming with a separate heating element. Fast acting heaters can be made by utilising a capacitor discharge powering system. This system has been used in practice to control both HTS and LTS switches and has similarities to quench heaters that are used to protect superconducting magnets. The disadvantage of a thermally triggered switch is the time taken for the heat to diffuse through the insulation that separates the heater and superconductor, this problem is compounded at high temperatures due to the  $T^3$  increase in specific heat capacity.

**Magnetically triggered switches** can provide benefits as the thermal diffusion time is not an issue and so fast switches can be formed even with thick insulation. In such a switch a magnet system is used to raise the applied field above the critical magnetic field. For HTS materials this can be a considerable field at low temperatures. A further complexity is the need of integrating a separate inductor into the switch and achieving a fast magnet ramping up time.

**Switches triggered by over-current** can provide fast switching times, as demonstrated by its successful use in FCLs. The disadvantage of such a system is the complexity in combining the discharging magnet circuit and the triggering circuit without one adversely affecting the other.

**Mechanical switches formed of superconductors** are suited to bypass-switches as they have an infinite resistance when they are opened. As for conventional mechanical switches they can have fast switching times ( $< 20$  ms), but also suffer from arcing and degradation of the contacts. This is a particular problem for brittle HTS materials.

**Thermal triggering is the most suitable** for switches based on HTS materials as the triggering circuit is simpler than that for an over-current switch or a magnetic field triggered switch and does not interfere with the magnet circuit. The slow diffusion time at HTS temperatures can be overcome by optimising the heater and insulation. HTS switches were tested in liquid nitrogen to investigate switching in the high temperature regime where the thermal diffusion time may be an issue (Chapter 4). Quench heaters that are used to warm up quenching superconducting magnets [30] are widely used and have similarities to the heaters used to thermally trigger a superconducting switch.

## Chapter 2

# Materials for use in Switches that Utilize Superconductors



In order to analyse and manufacture switches based upon superconducting materials both the thermophysical and electromechanical properties as well as the superconducting properties must be known. The thermophysical properties are the thermal conductivity, resistivity, specific heat capacity, and density. The electromechanical properties relate to the degradation of critical current with applied strain. For switches that operate with no applied field the relevant superconducting properties are the temperature dependent critical current density and the  $n$ -value of the transition. Where the required data was not available, experiments were conducted at the University of Southampton and also at CERN. Measurements of the thermophysical properties were performed on YBCO produced by American Superconductor and  $\text{MgB}_2$  with copper stabilisation that was produced by Columbus. YBCO tapes with both copper cladding and with stainless steel cladding were measured. The critical currents of the YBCO tapes were measured at 77 K. Critical current measurements at 4.2 K were performed on YBCO,  $\text{MgB}_2$  with copper stabilisation, and  $\text{MgB}_2$  in a cupronickel matrix that was also produced by Columbus. The electromechanical properties and soldered joint resistances of YBCO tapes were also measured.

## 2.1 Introduction to Superconductivity

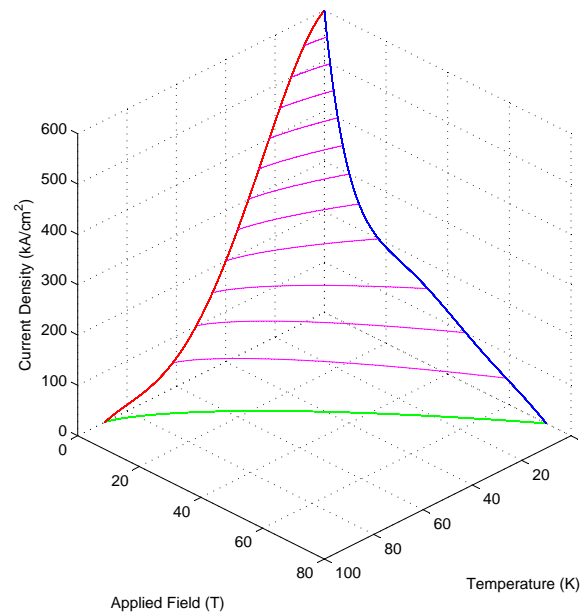


FIGURE 2.1: The critical surface of bulk YBCO.

A superconductor is a material that is both a perfect conductor and a perfect diamagnet. Superconductivity was discovered in Holland in 1911 by Heike Onnes whilst testing mercury at 4.2 K [31]. Superconductivity depends upon temperature, the applied magnetic field, and the current density; these variables are interdependent and place limits on the superconducting region of the material. Figure 2.1 shows the critical surface of

bulk YBCO estimated from measurements in [32]. Perfect conductivity is the flow of a non-time variant current without resistance. Under alternating current conditions superconductors have small, but not negligible, resistive losses due to movement of the flux vortices, hysteresis, and eddy currents [33].

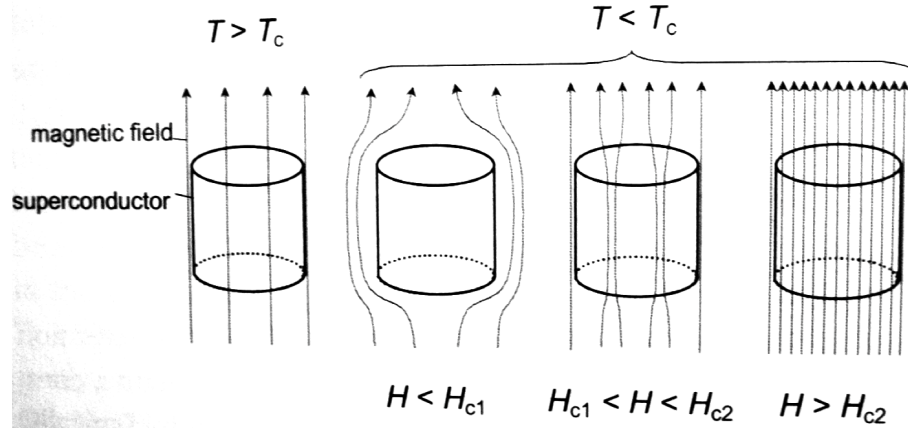


FIGURE 2.2: Effect of an applied magnetic field on a superconductor. The Meissner Effect occurs below the lower critical field ( $H_{c1}$ ) and is the expulsion of an applied magnetic field upon transition from the normal to superconducting state. Between the lower critical field and the upper critical field ( $H_{c2}$ ) the flux can enter the superconductor as regularly spaced quantised flux vortices.

Perfect diamagnetism is also known as the Meissner Effect following experiments by Meissner and Ochensfield in 1933 where they showed that magnetic fields were expelled from the interior of a material when it became superconducting [34]. Figure 2.2 [35] shows the Meissner Effect in a superconductor below the lower critical field, as well as flux pinning when the applied field is between the lower critical field and the upper critical field.



FIGURE 2.3: Applications of superconductivity. Left to right, top to bottom, levitating train, transformer, power cable, MRI image, motor, particle accelerator, and a levitating magnet.

Perfect conductivity and perfect diamagnetism are linked together, as without the ability to carry superconducting shielding currents a material can not be a perfect diamagnet. These properties have been exploited in various applications (Figure 2.3), including power transmission cables [36], magnets [37], medical imaging devices [38], generators [39], and levitating trains [40].

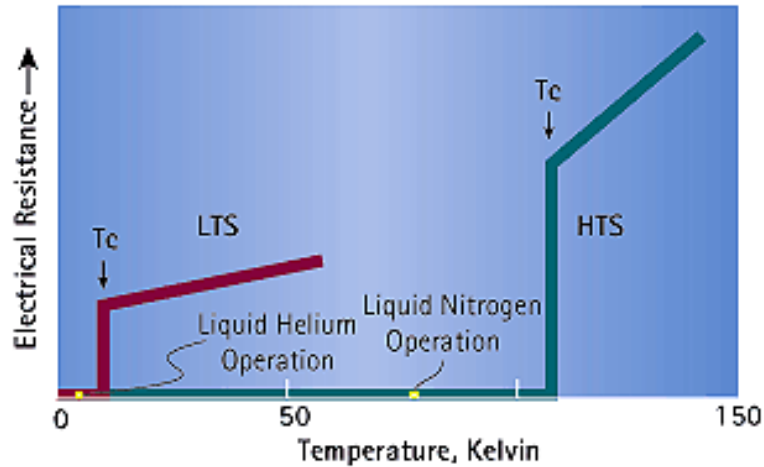


FIGURE 2.4: Typical resistivity profiles of a low temperature superconductor (LTS) and a high temperature superconductor (HTS).

Superconductivity was originally thought to be a low temperature phenomenon; BCS theory [41] predicted that it was impossible for a material to exhibit superconductivity above 30 K. However, in 1986 Bednorz and Müller discovered superconductivity in ceramic materials at 35 K [42]. This then led to the rapid development of superconductors with higher critical temperatures; cuprates with a critical temperature of 138 K was measured in 1995 [43]. Superconductors with a critical temperature of less than 30 K are known as low temperature superconductors (LTS), whilst those above are known as high temperature superconductors (HTS). Figure 2.4 [44] shows the typical resistivity profiles of both HTS and LTS materials. The higher operating temperatures that are possible with HTS materials allow cryogenic savings over systems that utilise LTS materials which usually operate in liquid helium at 4.2 K.

## 2.2 HTS Materials that have the Potential to be Used in Switches

HTS materials that are formed into composite tapes with metallic matrices have the potential to be used in switches due to their high critical temperature, high thermal conductivity, and good electromechanical properties. Suitable HTS materials include YBCO with either copper or stainless steel stabilisation, and  $\text{MgB}_2$  with copper or a copper alloy stabilisation. BSCCO in a silver alloy matrix is less suitable due to its low resistivity and heat capacity, and its potentially higher cost due to the large amount of silver that is used in

the matrix. Bulk materials less suitable for use in switches due to their poor mechanical properties and low thermal diffusion, which may lead to slow switching when thermally activated. LTS materials such as Nb-Ti may be suitable for operating temperatures at 4.2 K but are not suitable for operation at higher temperatures due to their low critical temperatures.

**Critical current density dependence on temperature** is given by

$$J_c(T) = a \left(1 - \frac{T}{T_c}\right)^\alpha. \quad (2.1)$$

Increasing temperature causes a decrease in the critical current until it is zero at  $T_c$ . An  $\alpha$  of one represents a linear relationship that would lead to a sharp voltage-temperature ( $V - T$ ) characteristic at  $T_c$ . Typical values of  $\alpha$  are in the range 1 to 3 and depend upon the superconductor with higher values leading to smoother  $V - T$  characteristics.

**$n$ -value dependence on temperature** is given by

$$n(T) = n(0) \left(1 - \frac{T}{T_c}\right)^{\frac{1}{2}} + n(T_c), \quad (2.2)$$

where  $n(0)$  is an assumed  $n$ -value at 0 K and  $n(T_c)$  is the  $n$ -value at the critical temperature. Like the critical current the  $n$ -value should fall to zero at  $T_c$ . However, for practical purposes a sufficiently low, typically less than five, value is used. The  $n$ -value is a measure of the sharpness of the superconducting to normal transition and is typically lower for HTS materials than for LTS materials.

### 2.2.1 YBCO Produced by American Superconductor



FIGURE 2.5: Cross section of American Superconductor produced YBCO tape with copper cladding (4.3 mm  $\times$  0.2 mm).

American Superconductor [44] produces coated conductor YBCO tapes that have either copper cladding (YBCO Cu) [45] or stainless steel cladding (YBCO SS) [46]. The cross section of the copper clad YBCO tape is shown in Figure 2.5. The dimensions of these tapes are given in Table 2.1

These tapes are manufactured by depositing a layer of YBCO on a Hastelloy<sup>1</sup> substrate by the metal organic deposition (MOD) process [47]. The Hastelloy substrate is 75  $\mu\text{m}$  thick and is deformation textured by the rolling assisted biaxially textured substrate (RABiTS) process. Texturing the substrate in this way assists in aligning the YBCO grains correctly.

<sup>1</sup>Hastelloy is a nickel alloy that contains 5% tungsten.

Cladding	$W$ (mm)	$\delta$ (mm)	$\gamma$ (kg/m <sup>3</sup> )	$\lambda$ (%)	$T_c$ (K)
Stainless steel	4.33	0.15	8518	$\approx 0.87$	89
Copper	4.35	0.2	8635	$\approx 0.67$	89

TABLE 2.1: Properties YBCO tape produced by American Superconductor.  $W$  is the width,  $\delta$  the thickness,  $\gamma$  the density,  $\lambda$  the superconductor filling factor, and  $T_c$  the critical temperature.

The YBCO film is about 1  $\mu\text{m}$  thick and there are a series of other buffer layers that have a total thickness of less than 1  $\mu\text{m}$ . The YBCO has a silver cap layer that is about 3  $\mu\text{m}$  thick. The tape is produced with a wide (up to 10 cm) width which is then slit into smaller tapes that have a width of about 4.3 mm. The cladding is attached with solder with a melting point of 179  $^{\circ}\text{C}$  during the manufacturing process and so the tape must subsequently not be exposed to temperatures exceeding 175  $^{\circ}\text{C}$  [48]. The copper cladding has a total thickness of 100  $\mu\text{m}$  and the stainless steel cladding has a total thickness of 70  $\mu\text{m}$  [25]. Soldered joints were made with 99.99 % pure indium at 160  $^{\circ}\text{C}$ . The resistances of the joints were measured at 77 K to be 213  $\text{n}\Omega/\text{cm}^2$  for the stainless steel clad tape and 54.2  $\text{n}\Omega/\text{cm}^2$  for the copper clad tape.

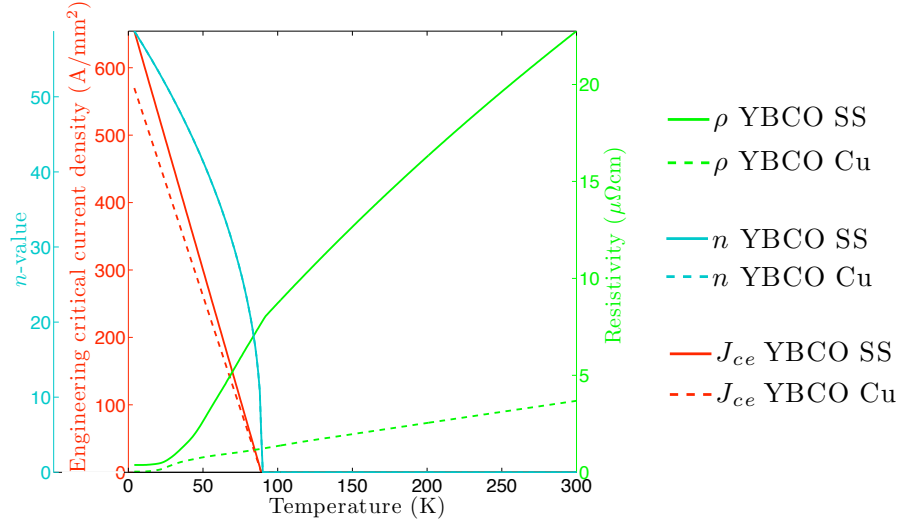


FIGURE 2.6: Electrical properties of YBCO tape produced by American Superconductor. Shown are the engineering critical current density ( $J_{ce}$ ), the  $n$ -value, and the normal state resistivity ( $\rho$ ).

The critical current of the YBCO tapes was measured at 4.2 K and at 77 K with the  $J_{ce}(T)$  curve shown in Figure 2.6;  $n(T)$  and  $\rho(T)$  are shown in the same figure. The  $n$ -value was assumed to be 25 at 77 K [49] [50] and was assumed to fall to 5 at  $T_c$ . The resistivity of both the copper stabilised tape and the stainless steel stabilised tape were measured between  $T_c$  and 300 K. The resistivity beneath  $T_c$  was based upon the resistivity of the substrate [51], the silver cap layer [52] and cladding. The resistivity of the stainless steel cladding and the copper cladding was based upon standard data [53] [54]. The copper

cladding had a low RRR that was probably due to large amounts of cold working that was used when rolling the cladding.

The thermal conductivity and specific heat capacity are shown in Figure 2.7. These properties were measured in the range 4.2 K to 300 K using a Quantum Design physical property measurement system [55]. The integrated values from 4.2 K are also shown for use in estimating the heat conduction along a thermal gradient and also the enthalpy change of the material.

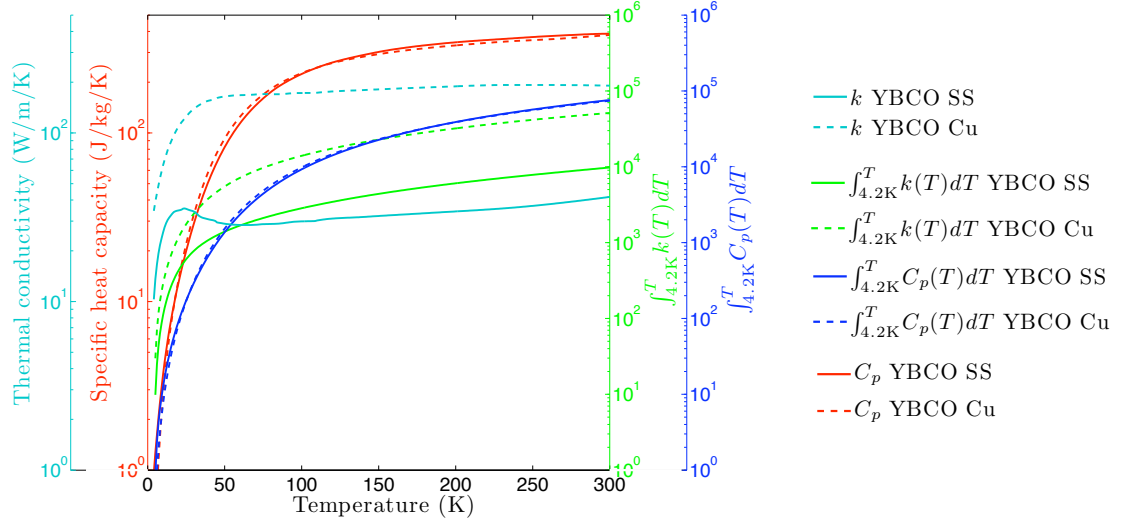


FIGURE 2.7: Thermal properties of YBCO tape produced by American Superconductor.

The degradation of critical current with applied strain was measured at 77 K. The strain that causes a 5 % degradation in the  $I_c$  was 0.4 % for YBCO Cu in compression and 0.7 % in bending, for the YBCO SS it was 0.4 % in compression and 0.5 % in bending. These YBCO based tapes are more strain tolerant than BSCCO based tapes that have a silver alloy matrix.

### 2.2.2 YBCO Produced by SuperPower



FIGURE 2.8: Cross section of the corner of a SuperPower produced YBCO tape with copper stabilisation.

SuperPower [56] produces coated conductor YBCO tapes that have an electro-deposited copper stabiliser layer [57]. The cross section of the copper clad YBCO tape is shown in Figure 2.8 and the dimensions of these tapes are given in Table 2.2. The total copper

thickness is in the range  $1\ \mu\text{m}$  to  $40\ \mu\text{m}$  [58] and has a residual resistivity ratio (RRR) to 4.2 K of 50 [59].

<b>Total thickness of Cu stabilisation</b>	<b><math>W</math> (mm)</b>	<b><math>\delta</math> (<math>\mu\text{m}</math>)</b>	<b><math>\gamma</math> (<math>\text{kg}/\text{m}^3</math>)</b>	<b><math>\lambda</math> (%)</b>	<b><math>T_c</math> (K)</b>
5 $\mu\text{m}$	4.00	58	8774	1.7	89
10 $\mu\text{m}$	4.01	63	8789	1.6	89
40 $\mu\text{m}$	4.04	93	8845	1.07	89

TABLE 2.2: Properties of copper stabilised YBCO tape produced by SuperPower. In addition to the copper stabilisation the tapes have a  $50\ \mu\text{m}$  thick Hastelloy substrate, a  $2\ \mu\text{m}$  thick silver layer, and about  $1.2\ \mu\text{m}$  of other buffer layers.

These tapes are manufactured by depositing a layer of YBCO on a Hastelloy substrate by the metal organic chemical vapor deposition (MOCVD) process [60]. The YBCO layer is about  $1\ \mu\text{m}$  thick and has a silver cap layer that is about  $2\ \mu\text{m}$  thick [61]. The substrate is textured by adding biaxially-textured buffer layers using ion beam assisted deposition (IBAD) of MgO; the buffer layers have a total thickness of less than  $0.2\ \mu\text{m}$ . The Hastelloy C276 substrate can be either  $50\ \mu\text{m}$  thick or  $100\ \mu\text{m}$  thick [62]. Soldering to the tape can be performed at temperatures up to  $250\ ^\circ\text{C}$  [63].

The  $J_{ce}(T)$ ,  $n(T)$ , and  $\rho(T)$  relationships are shown in Figure 2.9. The critical current of the YBCO tapes was 60 A at 77 K and 650 A at 4.2 K [64] [65]. Due to the rapid development of YBCO based tapes the critical current for a 4 mm width increased to over 100 A by 2009 [57] [66]. The  $n$ -value was assumed to be 25 at 77 K [67] and was assumed to fall to 5 at  $T_c$ . The resistivity of the tape between 4.2 K and 300 K was calculated from the resistivities of the substrate [51], the silver cap layer [52] and the copper stabilisation [54].

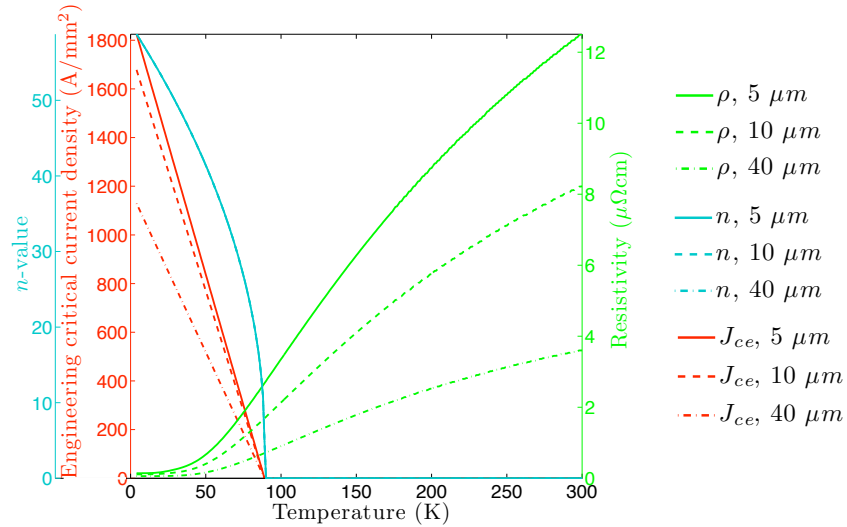


FIGURE 2.9: Electrical properties of YBCO tape with different thicknesses of copper stabilisation that is produced by SuperPower. Shown are the engineering critical current density ( $J_{ce}$ ), the  $n$ -value, and the normal state resistivity ( $\rho$ ).



The thermal conductivity and specific heat capacity are shown in Figure 2.10. These properties were estimated in the range 4.2 K to 300 K from the thermophysical properties of the tape components. The thermal conductivity of the silver cap layer is from [54] and the specific heat is from [68]. The thermal conductivity and specific heat capacity of the Hastelloy substrate is from [51]. The thermal conductivity and specific heat capacity of the copper stabilisation (RRR 50) is from [54]. The integrated values from 4.2 K are also shown for use in estimating the heat conduction along a thermal gradient and also the enthalpy change of the material.

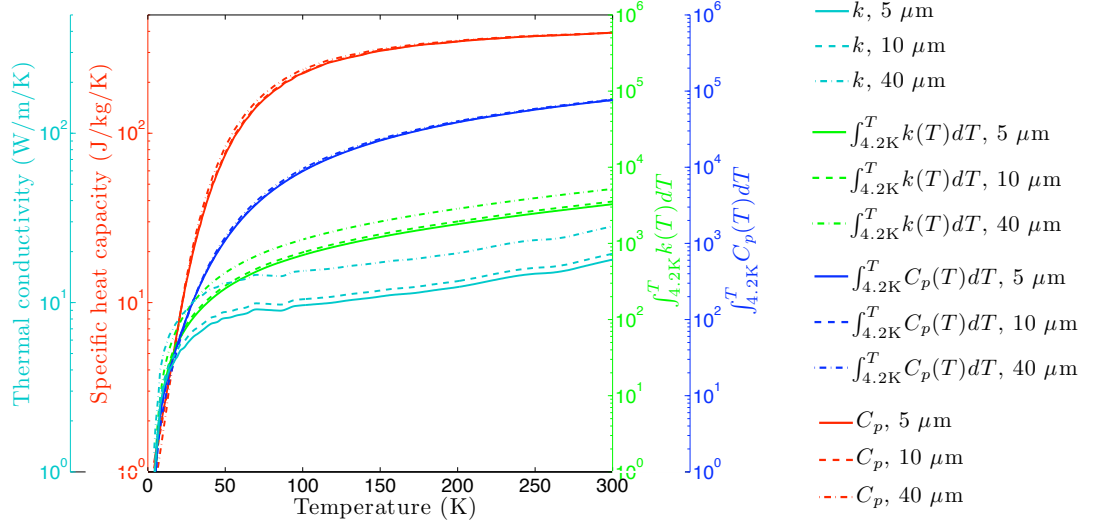


FIGURE 2.10: Thermal properties of YBCO tape with different thicknesses of copper stabilisation that is produced by SuperPower.

### 2.2.3 MgB<sub>2</sub> Produced by Columbus

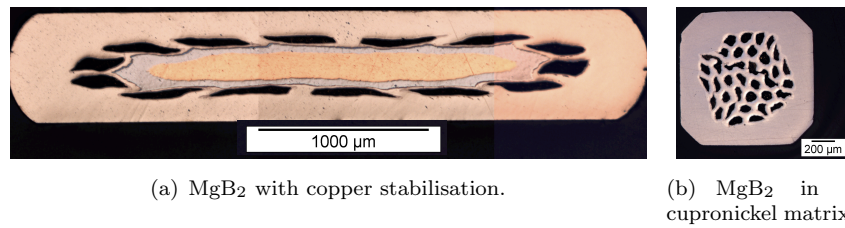


FIGURE 2.11: Cross sections of MgB<sub>2</sub> tapes with different matrices as produced by Columbus.

Magnesium diboride (MgB<sub>2</sub>) is produced by Columbus [69] via an *ex situ* powder in tube (PIT) process [21]. The MgB<sub>2</sub> can have either copper stabilisation Figure 2.11(a) or a cupronickel matrix Figure 2.11(b). The copper stabilised tape also contains nickel that makes up 66 % of the volume. An iron barrier, 8 % by volume, surrounds the copper. The MgB<sub>2</sub> in the cupronickel matrix tape is surrounded by a niobium barrier that makes up 11 % of the volume. Commonly 70Cu-30Ni is used but this could be changed for a less resistive alloy depending upon the requirements of the application. The dimensions of the



Columbus produced  $\text{MgB}_2$  tapes are given in Table 2.3.  $\text{MgB}_2$  is also produced by Hyper Tech Research [70] and can have copper or copper alloy stabilisation [71].

Matrix	$W$ (mm)	$\delta$ (mm)	$\gamma$ (kg/m <sup>3</sup> )	$\lambda$ (%)	$T_c$ (K)
15% Cu, 66% Ni, 8% Fe	3.6	0.65	8092	9	39
70% 90Cu-10Ni, 11% Nb	1.4	1.4	7685	19	39
70% 70Cu-30Ni, 11% Nb	1.4	1.4	7685	19	39

TABLE 2.3: Properties  $\text{MgB}_2$  tape produced by Columbus.  $W$  is the width,  $\delta$  the thickness,  $\gamma$  the density,  $\lambda$  the superconductor filling factor, and  $T_c$  the critical temperature.

The electrical properties of these tapes are shown in Figure 2.12 and the thermal properties are shown in Figure 2.13. The critical current of the tapes were measured by Columbus and also at CERN at 4.2 K. The  $n$ -value was  $\approx 100$  at 4.2 K [21],  $\approx 55$  at 30 K, falling to 5 at  $T_c$ ; the same  $n$ -value was used for both the Cu stabilised and Cu-Ni stabilised tape. The specific heat capacity, resistivity, and thermal conductivity of the copper stabilised tape was measured at the University of Southampton [72]. The thermal conductivity and resistivity of the  $\text{MgB}_2$  tapes with 70Cu-30Ni stabilisation was measured by Columbus [73]. The resistivity beneath  $T_c$  and the specific heat capacity was estimated from the tape components.

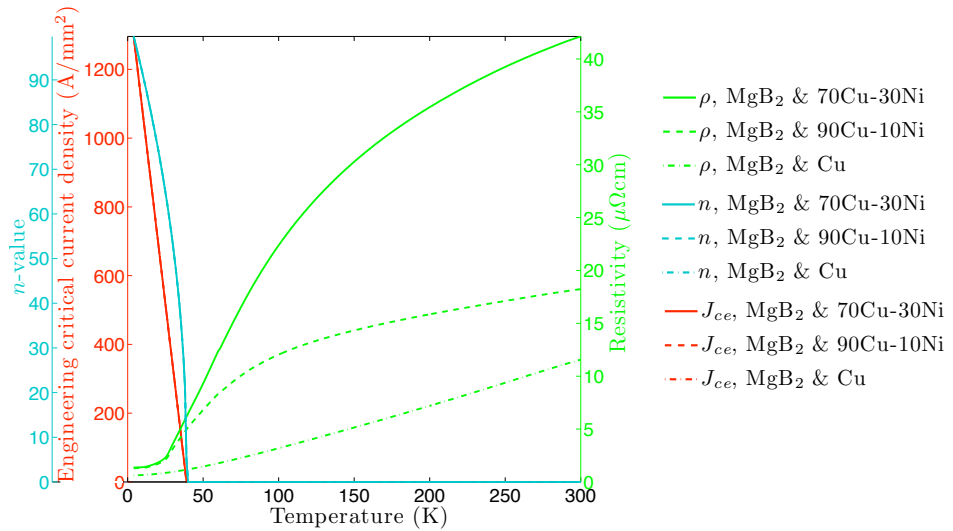


FIGURE 2.12: Electrical properties of  $\text{MgB}_2$  tape produced by Columbus. Shown are the engineering critical current density ( $J_{ce}$ ), the  $n$ -value, and the normal state resistivity ( $\rho$ ).

The properties of the 90Cu-10Ni matrix tape were based on the 70Cu-30Ni matrix tape and the properties of the different cupronickel alloys. The specific heat capacity, resistivity, and thermal conductivity of copper is given in [54]. The specific heat capacity of nickel is given in [74]. The thermal conductivity of nickel, copper, and cupronickel alloys is given in [75]. The resistivity of nickel, copper, and cupronickel alloys is given in [76]. The resistivity of niobium is given in [77] and the thermal conductivity in [78]. The specific heat capacity of iron is given in [79]. The thermal conductivity and electrical resistivity

of iron and nickel are given in [80]. Due to the large differences in resistivity that can occur within the same material, for example due to impurities or defects, the resistivity of a composite superconducting tape should be measured before it is used in a switch.

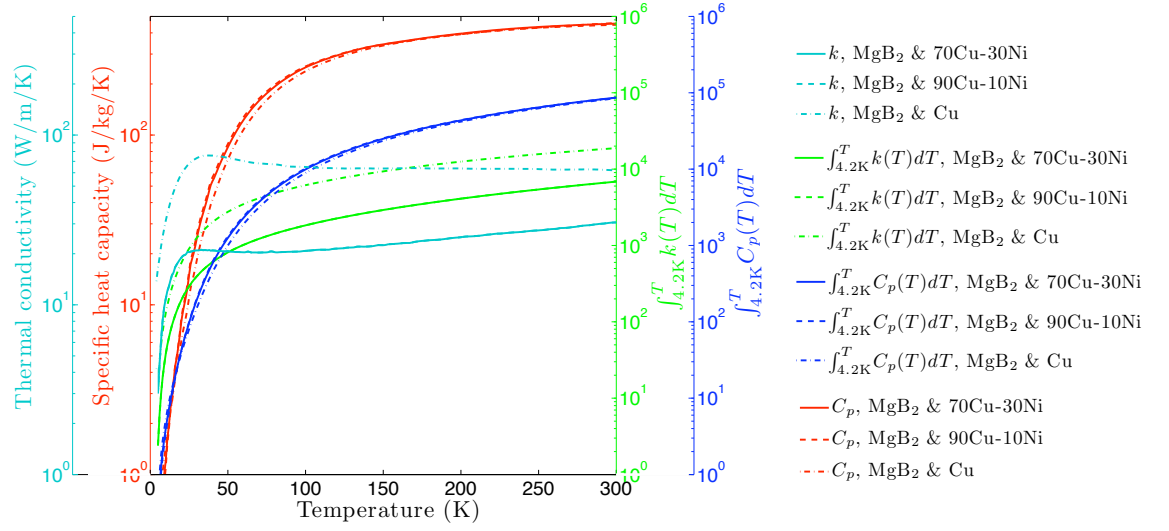


FIGURE 2.13: Thermal properties of  $\text{MgB}_2$  tape produced by Columbus.

## Chapter 3

# Description of Models for Superconducting Switches

### 3.1 Switch Concepts: Bypass-Switch and Dump-Switch

**Conventional energy extraction schemes** that utilise mechanical breakers have the circuit layout shown in Figure 3.1. In such circuits the mechanical switch is normally closed and the magnet is powered via a current source at room temperature. In the event of a problem in a magnet the mechanical switch is opened and the dump resistor is switched into the circuit. The magnet current then decays exponentially with a time constant of  $\frac{L}{R}$  and the magnet energy is dissipated at warm in the dump resistor. Such schemes are used to extract energy from certain LHC magnet circuits [4]. The LHC circuits also utilise hybrid current leads that have resistive and HTS sections to transfer the current from room temperature to the LTS bus-bar at 4.2 K [81].

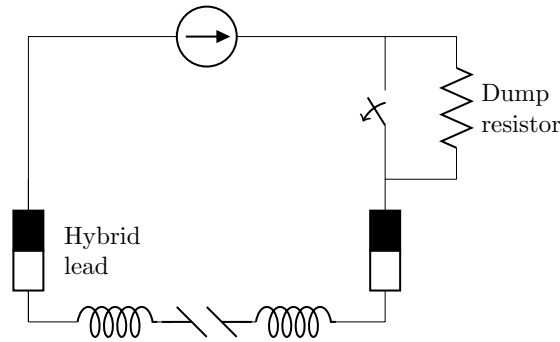


FIGURE 3.1: Conventional energy extraction scheme using a mechanical switch and a dump resistor.

**Superconducting switch based energy extraction schemes** could also be used to discharge quenching superconducting magnets and may provide benefits over conventional energy extraction schemes. Superconducting switches have a more gradual transition than mechanical switches and so they have the potential to reduce the peak voltage during discharge, whilst still meeting the energy extraction requirements, provided that the time to the start of magnet current decay is less than the opening time of the mechanical switch. Superconducting switches can be made with either HTS or LTS materials. HTS based switches can operate at either HTS temperatures or at LTS temperatures, but LTS based switches must necessarily operate at LTS temperatures. Switches formed of superconducting material can be of two types, either a bypass-switch or a dump-switch. In the case of a superconducting bypass-switch, the switch is connected in parallel with a dump resistor in which the magnet energy is dissipated. Dump-switches have no parallel resistor and so do not need to develop as high a resistance and so shorter switch lengths can be used. In dump-switches all of the magnet energy is dissipated in the switch itself. As the magnet energy is dissipated in the dump-switch, it forms a significant part of the heat energy input into the switch and so lower heater energies may be needed, this is in addition to the lower energy required by the shorter length. Figure 3.2 shows the circuit diagrams for the two different systems.

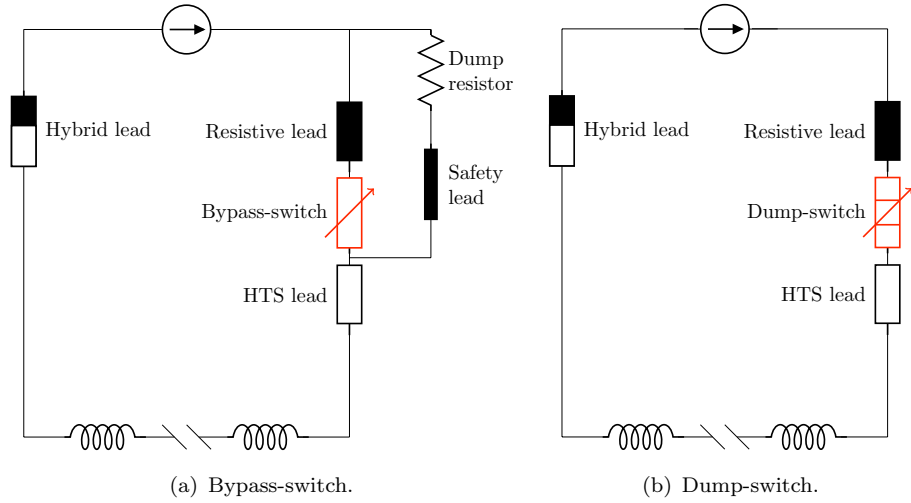


FIGURE 3.2: Possible energy extraction schemes that use superconducting switches that operate at HTS temperature. (a) shows the concept for when the energy dissipation is in a warm dump resistor, (b) shows the concept for when there is energy dissipation in the switch.

On long magnet chains where the energy extraction for the chain is divided into smaller units, some of the full rated current leads are required to bring the magnet current from cold to hot, through a mechanical switch and back to cold again. This has associated resistive and cryogenic losses that could be reduced with the use of superconducting switches. Distribution of energy extraction systems is used in the LHC in the 13 kA magnet circuits [3], as well as in other particle accelerators such as HERA [82] and the Tevatron [83]. If the mechanical bypass-switch is replaced with a superconducting switch then the extra full rated current leads can be replaced with leads that can be designed to have a lower heat leak as they do not normally carry the magnet current. These thinner leads are referred to as safety leads [84] and only carry current during energy extraction. Additionally, superconducting switches do not produce the arcing and high noise levels that require the mechanical switches to be specially isolated from the tunnel environment. Superconducting switches can be operated in series with the existing energy extraction schemes to increase the redundancy in the protection circuit.

**Superconducting bypass-switches** operate in a similar way to mechanical bypass-switches as they shunt the majority of the magnet current into a parallel dump resistor. Unlike a mechanical switch a superconducting bypass-switch has a finite “open” state resistance. This “open” switch resistance must be high with respect to the resistance of the parallel connected dump resistor in order to dissipate the magnet energy in the dump resistor. Long lengths of superconductor may be needed in order to achieve this high resistance. Switching whilst still in the current sharing regime may require less heater energy as the switch does not need to be warmed up as much; however, even longer lengths of switch are needed in order to develop the required voltage. In the case of a bypass-switch the required resistance of the switch ( $R_{ST}$ ) increases with the fraction of energy ( $f$ ) that

is to be dissipated with a total dump resistance ( $R_D$ ) with the relationship;

$$R_{ST} = \frac{R_D}{f}. \quad (3.1)$$

The long lengths required result in high heater energies also being needed. The problem is compounded by the fact that only a small fraction of the magnet energy can be used to assist the transition of the switch as the majority of the energy is dissipated in the external dump. This results in the thermal switching dynamics being dominated by the heater with the magnet energy only having a small affect. The experimental HTS switches described in the Chapter 4 were of this sort of bypass-switch and a similar concept is investigated for the MCD magnet circuits. Circuits that have a single energy extraction facility require the addition of an extra safety lead so that the current can bypass the switch when it is in the “open” (resistive) state. This third lead would increase the cryogenic losses during operation compared to the existing two lead set-up. For switch operation at HTS temperature the safety lead only operates between room temperature and HTS temperature and so there is lower heat leak than in the case of a switch operating at LTS temperatures.

**Superconducting dump-switches** require less resistance than equivalent superconducting bypass-switches, as the resistance must just be sufficient to achieve the correct magnet discharge characteristics and not to cause the current to be shunted into a parallel dump resistor. Due to this lower resistance requirement dump-switches require a correspondingly shorter length and therefore less heater energy than bypass-switches. However, as all of the magnet energy is dissipated in the switch itself, the thermal mass of the switch must be high enough to prevent an excessive temperature rise occurring during energy extraction from the magnet. As there is no external dump resistor the full magnet energy can be used to assist the transition. The magnet energy may therefore make up a significant proportion of the heat energy deposited in the switch and so the thermal dynamics of the switch rely on both the magnet and heater characteristics. Dump-switches that can dissipate the magnet energy whilst they are in the current sharing regime may be more desirable as there could be reduced thermal gradients within the switch as the fast temperature rise to the critical temperature ( $T_c$ ) required by bypass-switches is not needed. If the magnet energy is dumped in the switch itself then the existing powering scheme can be simplified as the safety leads and parallel resistor are not required.

**The switching characteristics** of switches formed of superconductors are based around the superconducting to normal transition and so it is essential to be able to fully model this change in state. Superconducting switches must be considered in conjunction with the electrical circuit into which they are integrated in as this can have a large effect on the transition. Irrespective of whether the superconducting switch acts as a bypass-switch or as a dump-switch the current passing through it must be known as it affects the superconducting to normal transition.

**The superconducting to normal transition** can be caused by over-current, an applied magnetic field, by raising the temperature, or by a combination of these factors. Transitions caused by over-current, which are inherently suited to fault current limiters, are less suitable for magnet energy extraction switches due to the complexity and practicality of combining the magnet circuit and the triggering circuit in such a way that neither adversely affects the other. Any switch formed of superconducting materials that is used in a real circuit must have sufficient current margin to provide a safety factor. Field induced transitions are also possible but they require fast acting magnet circuits that can be difficult to implement in a real system. Thermally activated switches can transition to the fully normal state in times of the order of milliseconds. This can be achieved using capacitor discharge powered heaters; similar capacitor discharges are used to power the quench heaters in the LHC superconducting dipoles [30]. The thermal characteristics of any superconductor based switch must be known and so the heat diffusion equation must be solved in conjunction with the electrical circuit characteristics.

In order to effectively model a superconducting switch the superconducting to normal transition must necessarily be modeled. This transition is highly non-linear and is critical in the operation of a switch, especially in the case of an HTS switch operating at LTS temperatures where there may be a large current sharing temperature range. It is possible to implement a superconducting switch where the magnet is discharged whilst the switch is in the current sharing regime if a sufficiently long length of superconductor is used. The heat generation in the current sharing regime is explained in Section 3.5.

## 3.2 Physical Layout of a Superconducting Switch

A thermally triggered superconducting switch consists of a superconducting tape, an insulation layer, and a heater layer. This layout, shown in Figure 3.3, is the same for both dump-switches and bypass-switches. For long switches the cooling from the  $yz$  faces is much larger than from the  $xz$  or  $xy$  faces and so the switch has uniform temperatures in the  $y$  and  $z$  directions ( $\frac{\partial T}{\partial y} = \frac{\partial T}{\partial z} = 0$ ). The heater is distributed along the length of the superconducting tape in order to raise the temperature of the whole superconductor at the same time. Switching via a propagating quench is possible but is slower than a distributed heater and is not suitable for HTS switches as they have low quench propagation velocities. High temperature superconductors have quench propagation velocities two to three orders of magnitude less than LTS materials; for copper clad YBCO it is in the range of 1 mm/s to 40 mm/s when tested at temperatures from 40 K to 77 K [85]. A distributed heater system can cause the whole switch to go normal at the same time, thereby preventing excessive local temperature rise of the superconductor during quench. A further advantage of a distributed heater is that it can act as a heat sink to limit the overall temperature rise of the switch when magnet energy is being deposited in the superconductor. Tape

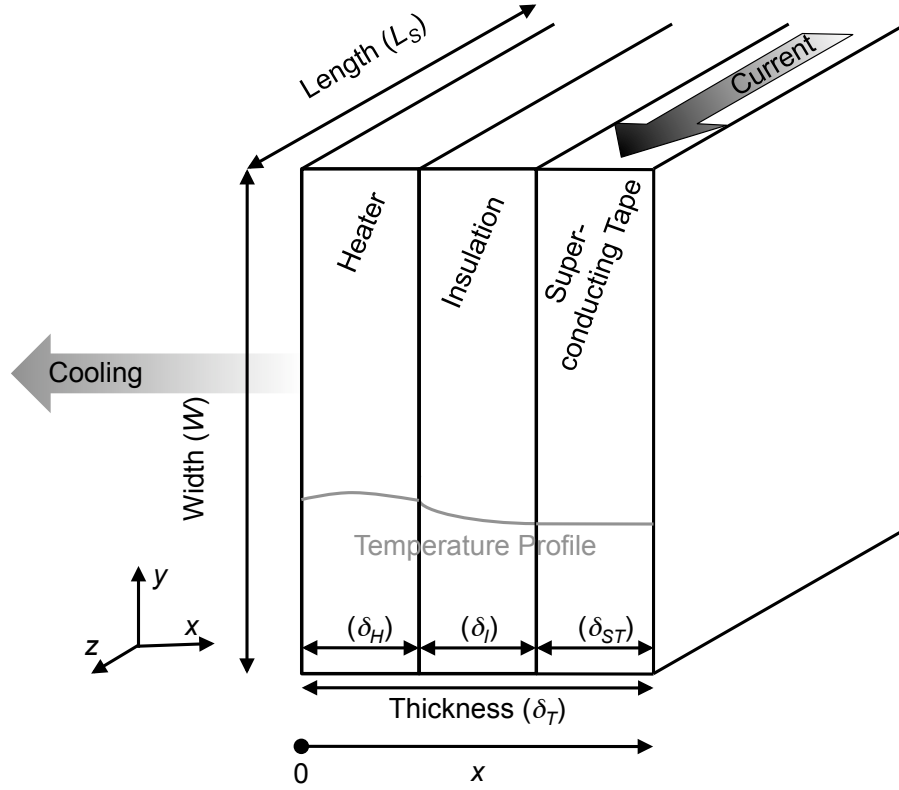


FIGURE 3.3: Physical layout of a superconducting switch. The thermal profile relates to a switch where the heater and superconductor layers have high thermal diffusivity.

sections with high aspect ratios lend themselves well to switches as the transfer area and thus heat transfer between the heater and the superconductor are maximized.

**Insulation considerations of thermally triggered switches** between the heater and the superconductor ideally require the insulation to have low thermal resistance and low heat capacity whilst at the same time being able to withstand the large voltages experienced during a magnet quench. This is difficult to achieve in practice as most practical electrical insulators, such as polyimide, have low thermal conductivity and relatively high specific heat capacity at low temperatures. A contact-less triggering system would remove the requirement for good heat transfer, thus the insulation would only have to satisfy the high voltage electrical insulation requirements. Preliminary experiments on stainless steel clad YBCO switches showed that contact-less triggering could be achieved by inducing an AC voltage across the superconductor layer and causing heating via the induced current [86].



### 3.3 Heat Diffusion in the Switch

#### 3.3.1 Heat Diffusion Equation

The thermal characteristics of switches having the layout described in the previous section (Figure 3.3) only have thermal gradients in the  $x$  direction with  $\frac{\partial T}{\partial y} = 0$  and  $\frac{\partial T}{\partial z} = 0$ . Therefore the resulting transient one dimensional heat diffusion equation is

$$\begin{aligned} \gamma C_p(T(t, x)) \frac{\partial T(t, x)}{\partial t} = & \frac{\partial}{\partial x} \left( k(T(t, x)) \frac{\partial T(t, x)}{\partial x} \right) \\ & + G_{ST}(t, x) \\ & + G_H(t, x), \end{aligned} \quad (3.2a)$$

to which cooling to the surrounds is a boundary condition. The heat generation due to the triggering heater is

$$G_H(t, x) = \begin{cases} G_H(t, x), & 0 < x \leq \delta_H \\ 0, & \delta_H < x \leq \delta_T \end{cases} \quad (3.2b)$$

and is coupled to the heater electrical circuit. Similarly the heat generation due to self heating is

$$G_{ST}(t, x) = \begin{cases} G_{ST}(t, x), & (\delta_T - \delta_{ST}) < x \leq \delta_T \\ 0, & 0 < x \leq (\delta_T - \delta_{ST}) \end{cases} \quad (3.2c)$$

and is coupled to the magnet discharge circuit.

For an arbitrary system that carries a time variant current, non-magneto material properties that are dependent upon temperature, and cooling to constant surroundings, the one dimensional heat balance equation can be written in rectangular cartesian coordinates as shown in Equation 3.2a, adapted from [87]. The heat generation in the superconducting tape ( $G_{ST}(t, x)$ ) in the current sharing regime depends upon the non-linear electric field-current density ( $E$ - $J$ ) characteristics as well as the time variant current and temperature. As the heat generation in heater and superconductor layers depend upon the current that they carry the associated electrical circuits must also be solved. As the switch operates over temperature ranges where there are large changes in material properties; temperature dependent resistivities, thermal conductivities, and heat capacities must be used. For switches that have fast diffusion times a lumped approximation can be used to reduce the PDE to the system of ODEs. The lumped approximation is explained in Section 3.7.

### 3.3.2 Initial and Boundary Conditions of the Heat Diffusion Equation

**The initial conditions** to the heat diffusion equation (Equation 3.2a) when the switch is initially at the temperature of the surrounds are a homogeneous temperature

$$T(t = 0, x) = T_\infty, \quad (3.3a)$$

an initial heat generation in the heater that is

$$G_H(t = 0, x) = \begin{cases} G_{Ho}(x), & 0 < x \leq \delta_H \\ 0, & 0 < x \leq \delta_H, \end{cases} \quad (3.3b)$$

which depends upon the heater's electrical circuit that is described in Section 3.4. As the superconducting tape is initially fully superconducting there is no heat generation,

$$G_{ST}(t = 0, x) = \begin{cases} 0, & (\delta_T - \delta_{ST}) < x \leq \delta_T \\ 0, & 0 < x \leq (\delta_T - \delta_{ST}). \end{cases} \quad (3.3c)$$

**The boundary conditions** are that the outer ( $yz$ ) faces of both the heater and the superconductor are cooled with heat transfer coefficients  $h_1$  and  $h_2$  respectively. This results in boundary conditions for a cooled switch with

$$\begin{aligned} \frac{\partial T(t, x)}{\partial x} &= \frac{-h_1}{k(x)}(T(t, x) - T_\infty) \text{ for } x = 0 \\ \frac{\partial T(t, x)}{\partial x} &= \frac{-h_2}{k(x)}(T(t, x) - T_\infty) \text{ for } x = \delta_T. \end{aligned} \quad (3.4a)$$

For well insulated fast acting switches the switching process is adiabatic ( $h_1 = h_2 = 0$ ) and the boundary conditions are

$$\begin{aligned} \frac{\partial T(t, x)}{\partial x} &= 0 \text{ for } x = 0 \\ \frac{\partial T(t, x)}{\partial x} &= 0 \text{ for } x = \delta_T. \end{aligned} \quad (3.4b)$$

## 3.4 Electrical Circuits

When solving the switching problem the heat diffusion equation must be solved in conjunction with the associated electrical circuits. This is because the heat generation in both the superconductor and heater layers is due to ohmic heating which in turn is due to time dependent currents, temperature dependent resistivity, and in the case of the superconductor the non-linear electric field-current density ( $E$ - $J$ ) characteristic is also temperature dependent.

### 3.4.1 Heater Circuit

In general the heat generation that triggers the switch is the result of a capacitor discharge through the switch's heater (Figure 3.4) as this can provide a fast release of energy.

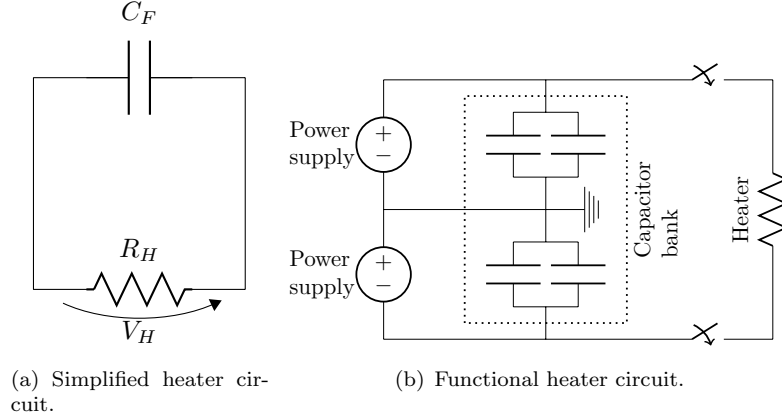


FIGURE 3.4: Circuit diagrams for powering a heater with capacitor discharge. (a) shows the simplified layout for analysis, (b) shows the functional diagram including power supplies to charge the capacitor bank.

It is possible to change the heater energy input by modifying the capacitor discharge with the use of *e.g.* an insulated gate bipolar transistors or multiple thyristors and a separate heater capacitor energy dump. Capacitor discharge powered heaters have demonstrated their effectiveness and reliability and are currently used in the LHC to power the magnet quench heaters [30]. The energy ( $Q_H$ ) stored in a capacitor with a charge voltage  $V_{Ho}$  and capacitance  $C_F$  is

$$Q_H = \frac{1}{2} C_F V_{Ho}^2. \quad (3.5)$$

The standard LHC quench heater power supply consists of a bank of capacitors operating at  $\pm 450$  V with a stored energy of 2.86 kJ [88]. In the superconducting switch application the capacitor's energy is dissipated in the heater that has a resistance

$$R_H(t) = \frac{1}{\int_0^{\delta_H} \frac{W_H}{\rho_H(T(t,x)) L_s} dx}, \quad (3.6)$$

which requires the solution of the heat diffusion equation. The decay of the heater voltage is

$$\frac{dV_H}{dt} = \frac{-V_H(t)}{R_H(t) C_F}, \quad (3.7)$$

which when combined with the heater's resistivity gives a heat generation

$$G_H(t, x) = \frac{E_{Hv}^2}{\rho_H(t, x)}. \quad (3.8)$$

As the capacitor is initially charged to a voltage  $V_{Ho}$  there is an initial electric field  $E_{Hvo}$  and initial heat generation in the heater of

$$G_H(t = 0, x) = \frac{E_{Hvo}^2}{\rho_H(t = 0, x)}. \quad (3.9)$$

### 3.4.2 Magnet Circuit

The heat generation in the superconducting tape ( $G_{ST}(t)$ ) results from the dissipation of the energy stored in the magnet. Therefore the time variant magnet current must necessarily be modeled. This is of particular importance to dump-switches where the magnet energy not only makes up a significant part of the total energy deposited in the switch but it may also be dumped in the current sharing regime where the  $E$ - $J$  characteristics of the superconductor are highly non-linear. During discharge of the magnet the power supply is shorted out and if the line inductances and resistances are negligible then the circuit for the discharge is that shown in Figure 3.5. For bypass-switches there is a real dump resistor, but for dump-switches there is no parallel resistor and so  $R_D = \infty$ . The magnet

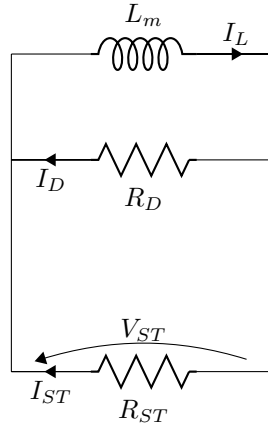


FIGURE 3.5: Magnet circuit diagram during discharge when the power supply is shorted out. Line inductance and resistances are assumed to be zero.

chain has an inductance  $L_m$  and operates at a current  $I_{Lo}$ . This results in a stored energy ( $Q_L$ ) of

$$Q_L = \frac{1}{2} L_m I_{Lo}^2. \quad (3.10)$$

The magnet current will start to decay when a voltage is introduced to the circuit. If there are no line resistances in the circuit this decay will be of the form

$$\frac{dI_L}{dt} = \frac{-V_{ST}}{L_m}, \quad (3.11)$$

where the voltage across the switch ( $V_{ST}$ ), which is the same as both the magnet and dump voltage due to their parallel connection, is

$$V_{ST} = \frac{I_{ST}(t)R_DR_{ST}(T)}{R_D + R_{ST}(T)}. \quad (3.12)$$

The heat generation in the superconducting tape ( $G_{ST}$ ) is thus

$$G_{ST} = J_{ST}(t)E_{ST}(T), \quad (3.13)$$

which in the current sharing regime also takes into account the non-linear  $E$ - $J$  characteristics of the superconductor. A more detailed description of the non-linear heat generation in the current sharing regime is given in Section 3.5. As for  $G_H(t)$ ,  $G_{ST}(t)$  is linked back into the heat diffusion equation (Equation 3.2a).

## 3.5 Heat Generation in the Current Sharing Regime

### 3.5.1 Configuration of Superconducting Composite Conductors

A composite conductor is one which contains both normal conducting and superconducting components in close electrical contact. The normal conducting component is referred to as the matrix and may be a matrix, sheath materials, substrates, or cladding. In such a tape (or wire *etc.*) there exists current sharing between the components above the current sharing temperature ( $T_{cs}$ ) and below the critical temperature ( $T_c$ ). Most useful superconducting materials come in the form of composite tapes and contain both superconducting and normal components. The main role of the matrix is to act as a bypass when the superconductor is no longer fully superconducting and thus limit the heat generation and temperature rise of the conductor. The matrix can also provide mechanical support, facilitate manufacturing, and has an impact on AC losses. In a superconducting tape that is to be used in a switch the matrix would ideally be optimized to allow a short switch without the risk of excessive temperature rise.

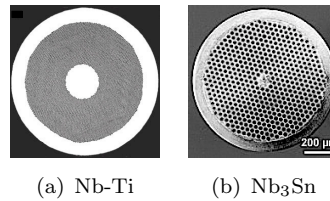


FIGURE 3.6: Cross sections of composite LTS tapes. (a) is Nb-Ti in a Cu matrix (0.8 mm diameter) and (b) is Nb<sub>3</sub>Sn in a Cu matrix (0.8 mm diameter).

Figure 3.6 and Figure 3.7 show the cross sections of LTS and HTS tapes that have metal matrices. The Nb-Ti LTS tape in Figure 3.6(a) has about 3000 filaments of superconductor

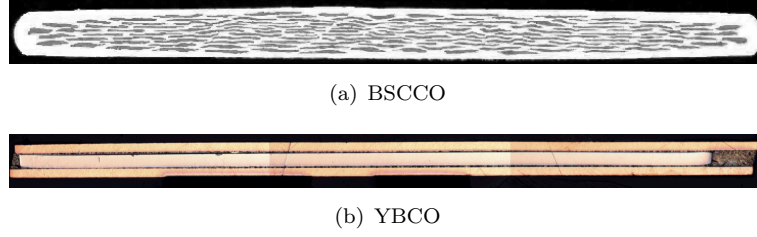


FIGURE 3.7: Cross sections of composite HTS tapes. (a) is multifilamentary Bi-2223 in an Ag matrix tape (4 mm  $\times$  0.22 mm) and (b) is YBCO on a nickel-tungsten substrate with copper cladding (4.3 mm  $\times$  0.2 mm).

in a copper matrix [89]. The Nb<sub>3</sub>Sn LTS tape in Figure 3.6(b) has 504 filaments of Nb<sub>3</sub>Sn in a copper matrix and was produced by the PIT method [90]. The HTS tape in Figure 3.7(a) is a composite tape with 121 filaments of Bi-2223 in a silver matrix produced by the OPIT method [91]. An alternative architecture for HTS tapes is shown in Figure 3.7(b). This has a layered construction of Y-123 film deposited on a Ni-W substrate with Cu cladding. In this case the “matrix” refers to the cladding, substrate, and relevant buffer layers.

### 3.5.2 Heat Generation in LTS Composite Conductors

Most superconducting devices are formed of LTS materials and so operate at a temperature ( $T_{op}$ ) that is close to their critical temperature. Typically Nb-Ti devices operate at 4.2 K but their critical temperature is only  $\approx 9.8$  K. The small temperature difference between  $T_{op}$  and  $T_c$  means that the current sharing temperature range must also be small. Moreover, LTS materials have a sharp superconducting to normal transition. The  $E$ - $J$  relationship for a LTS at a constant temperature below  $T_c$  and with a constant applied field below  $B_c$  is

$$E(J) = \begin{cases} 0 & J < J_c(T) \\ J\rho(T) & J > J_c(T). \end{cases} \quad (3.14)$$

At the critical current density at a given temperature ( $J_c(T)$ ),  $E$  is not defined and can take any intermediate value. This allows current sharing with the superconducting portion carrying  $J_c(T)$ . This would equate to an  $n$ -value approaching infinity if the  $E$ - $J$  characteristic was fit with a power law (see Section 3.5.3 for further details). The approach to heat generation in the current sharing range for LTS materials, as described by Wilson in “Superconducting Magnets” [33], is explained in this section. For superconducting tape that has a total area  $A$ , a matrix resistivity  $\rho_m(T)$ , a superconductor filling factor  $\lambda$ , carries a current  $I_{op}$ , and is operating at a temperature  $T_{op}$ , the current density in the superconductor ( $J_{op}$ ) when the tape is fully superconducting is

$$J_{op} = \frac{I_{op}}{A\lambda}, \quad (3.15)$$

and ohmic heat generation will begin when the temperature reaches  $T_c(J_{op})$ . This temperature is known as the current sharing temperature ( $T_{cs}$ ). For LTS materials the typically linear decrease of the critical current density ( $J_c(T)$ ) with increasing temperature is given by

$$J_c(T) = J_c(T_i) \left( \frac{T_c - T}{T_c - T_i} \right) \quad (3.16)$$

and so the expression for the current sharing temperature is

$$T_{cs} = T_c - (T_c - T_{op}) \left( \frac{J_{op}}{J_c(T_{op})} \right). \quad (3.17)$$

The heat generation, which is averaged over the total cross section, in terms of  $E$  and  $J$  is

$$G = \lambda J_{op} E, \quad (3.18)$$

which within the current sharing regime is generated in both the matrix and the superconductor. In the current sharing regime between  $T_{cs}$  and  $T_c$  the current divides between the matrix and the superconductor with the superconductor developing a resistance known as the flux flow resistance that is due to the motion of flux flow vortices. This flux flow resistance is much greater than the resistance of the matrix and so the superconductor will carry  $J_c(T)$  with the matrix carrying the remainder of  $J_{op}$ , so that the matrix current density ( $J_m(T)$ ) is

$$J_m(T) = \frac{\lambda(J_{op} - J_c(T))}{1 - \lambda}. \quad (3.19)$$

The electric field across the tape can then be determined from Ohm's law,

$$E(T) = \rho_m(T) J_m(T). \quad (3.20)$$

Using Equation 3.19 this can be re-written as

$$E(T) = \frac{\rho_m(T) \lambda (J_{op} - J_c(T))}{1 - \lambda}, \quad (3.21)$$

which when combined with Equation 3.18 yields

$$G(T) = \frac{\rho_m(T) \lambda^2 J_{op} (J_{op} - J_c(T))}{1 - \lambda}. \quad (3.22)$$

This can be rearranged in the form;

$$G(T) = \left( \frac{\lambda^2 \rho_m(T) J_{op}^2}{1 - \lambda} \right) \left( \frac{T - T_{cs}}{T_c - T_{cs}} \right) \quad (3.23)$$

The heat generation at the critical temperature and above when the superconductor is fully normal is

$$G_c(T) = \left( \frac{\lambda^2 \rho_m(T) J_{op}^2}{1 - \lambda} \right) \quad (3.24)$$

and is constant if  $\rho_m$  and  $J_{op}$  are also constant. The heat generation as a function of temperature for an LTS material is

$$G_{ST}(T) = \begin{cases} 0, & T < T_{cs} \\ G_c(T) \left( \frac{T - T_{cs}}{T_c - T_{cs}} \right), & T_{cs} \leq T < T_c \\ G_c(T), & T \geq T_c \end{cases} \quad (3.25)$$

and is shown in Figure 3.8 for the case where  $\rho_m$  and  $J_{op}$  are constant. This approach

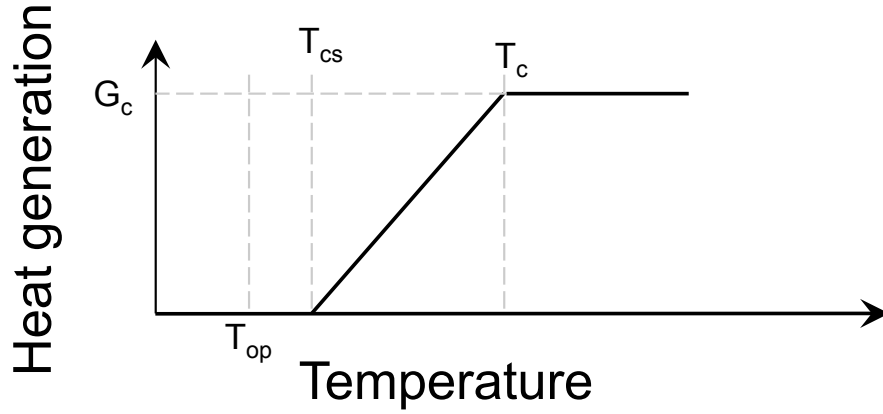


FIGURE 3.8: Heat generation as a function of temperature for LTS materials where there is a narrow current sharing region.  $J_c(T)$  decreases linearly with temperature.  $\rho_m$  and  $J_{op}$  are constant.

has been used to aid the effective design of many LTS devices and is useful for modelling situations where the material has a sharp  $E$ - $J$  characteristic and  $(T_c - T_{op})$  is low. However, it is limited when applied to HTS materials that have a wider current sharing region, a more smeared  $E$ - $J$  characteristic, and where  $(T_c - T_{op})$  may be high, for example  $\approx 105$  K in the case of a BSCCO magnet operating at 4.2 K. The more detailed approach required for these situations is described in the next section.

### 3.5.3 Heat Generation in HTS Composite Conductors

The heat generation in HTS materials is different to that in LTS materials as not only are their  $E$ - $J$  characteristics more smeared, but they can be operated far below  $T_c$  leading to a wide current sharing range. Furthermore, the critical current is not necessarily linear with temperature. In order to calculate the non-linear heat generation in the current sharing



regime the  $E$ - $J$  characteristic of the superconducting to normal transition must first be known. Where the superconductor has a critical current density ( $J_c$ ) defined at an electric field criterion ( $E_c$ ), the  $E$ - $J$  characteristics is typically well described with the power law relationship

$$\frac{E}{E_c} = \left( \frac{J}{J_c(T, B)} \right)^{n(T, B)} \quad (3.26)$$

that was derived by M. N. Wilson and subsequently published by Walters [92]. The exponent  $n(T, B)$  is referred to as the  $n$ -value or transition index. The  $n$ -value typically decreases with increasing applied magnetic field [93]. When measuring the  $J_c$  of HTS materials the electrical field criterion ( $E_c$ ) is usually  $1 \mu\text{V}/\text{cm}$  [94]. Figure 3.9 shows the power law fitted to the superconducting to normal transition of a multifilamentary BSCCO in silver matrix tape operating in pool boiling nitrogen [95]. Using materials

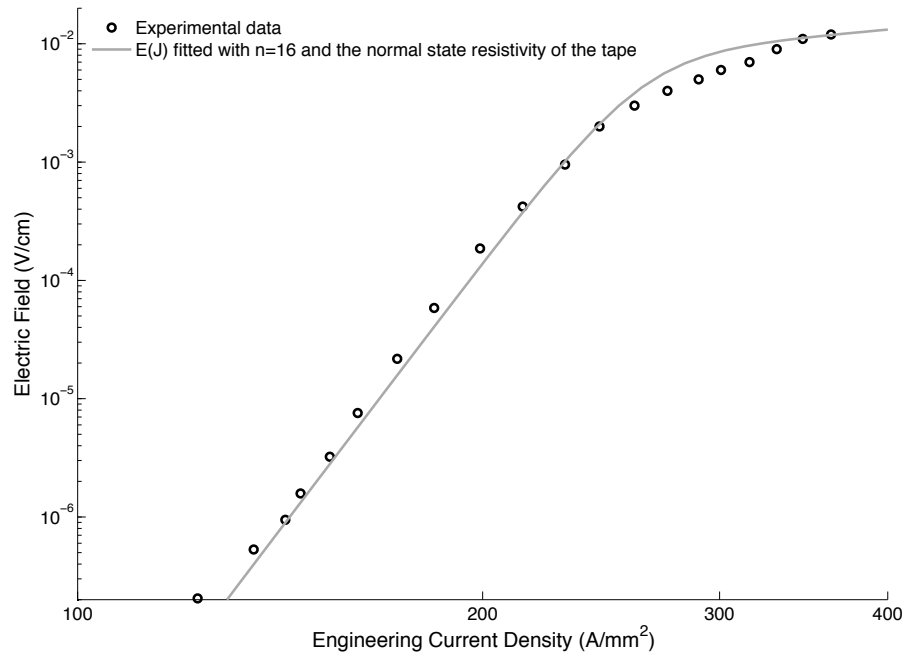


FIGURE 3.9:  $E$ - $J$  characteristics of a multifilamentary BSCCO in silver matrix tape measured in liquid nitrogen.

with higher  $n$ -values means that superconducting switches can have a sharper transition to the normal state. This is beneficial as a high  $n$ -value switch can operate nearer to  $T_{cs}$  with a lower electric field than a low  $n$ -value switch. Further more, above  $T_{cs}$  the high  $n$ -value switch develops a higher electric field at a lower temperature meaning that the magnet discharge begins sooner. Different superconductors have different  $n$ -values which in turn can vary with the applied field, current density, and temperature [96]. Strain can also influence both  $J_c$  and the  $n$ -value [97]. The  $n$ -value for Bi-2212 or Bi-2223 in silver matrix is  $\approx 40$ -60 at 4.2 K [98]. At 77 K the  $n$ -value of Bi-2223 in a silver matrix is  $\approx 20$  [99] and for YBCO on a hastelloy substrate  $\approx 20$  [100]. Typical  $n$ -values of Nb-Ti are in the range 40-120 [101] [98], 20-80 for Nb<sub>3</sub>Sn [97] [102]. Further data on the  $n$ -value can

be found for Bi-2223 in [103] [104], YBCO [105] and MgB<sub>2</sub> [106]. Composite structures also have an associated  $n$ -value, *e.g.* a cable [107], or an HTS coil [108]. The deviation in the  $n$ -value from the single crystal value can also be used as a measure of the quality of a superconductor. A possible but non-standard way to describe the  $E$ - $J$  curve is with an exponential relationship *e.g.* [109] [110]. The critical current can also be defined by a resistivity criterion (*e.g.*  $10^{-8} \Omega\text{cm}$  [111]), the flux flow extrapolation, or the point at which take-off occurs. These criteria could give different values for the critical current but  $E_c$  is the normal standard. If the physical dimensions of the tape are taken into account then the  $E$ - $J$  characteristic becomes the  $V$ - $I$  characteristic.

In a composite tape the components are connected in parallel with the equivalent circuit diagram shown in Figure 3.10. This parallelism means that the electric field ( $E$ ) over

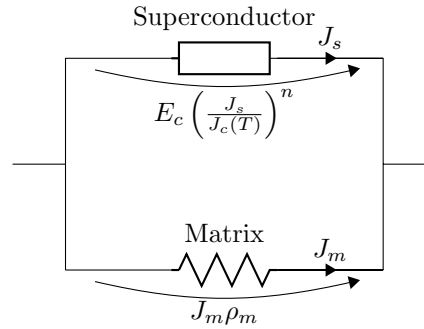


FIGURE 3.10: Current sharing between tape components.

the tape is identical to the electric field across the superconductor ( $E_s$ ) and the matrix ( $E_m$ ). The electric field across the matrix can be calculated from the matrix resistivity ( $\rho_m(T)$ ) and the matrix current density ( $J_m$ ), across the superconductor it is given by the power law relationship Equation 3.26. Equating the two allows the current in each component to be calculated. For superconducting tape that has a total area  $A$ , a matrix resistivity  $\rho_m(T)$ , a superconductor filling factor  $\lambda$ , carries a current  $I_{op}$ , and is operating at a temperature  $T_{op}$ , the current density in the superconductor is

$$J_{op} = \frac{I_{op}}{\lambda A}, \quad (3.27)$$

for when the tape is fully superconducting (see also Section 3.5.2). The operating current is

$$I_{op} = I_s + I_m, \quad (3.28)$$

where initially the tape is fully superconducting and so  $I_m$  is zero. In the current sharing regime the superconductor current is less than the operating current and the superconductor current density is defined as

$$J_s = \frac{I_s}{\lambda A}, \quad (3.29)$$

and the matrix current density as

$$J_m = \frac{I_m}{A(1 - \lambda)}. \quad (3.30)$$

The electric field across the superconductor is

$$E = E_c \left( \frac{J_s}{J_c(T)} \right)^{n(T)} \quad (3.31)$$

and as Ohm's law holds for the matrix that is in parallel with the superconductor,  $E$  can also be calculated from

$$E = J_m \rho_m(T) \quad (3.32)$$

Combing the current densities from each branch with the electric field relationships yields

$$E = E_c \left( \frac{J_{op} - \frac{E(1-\lambda)}{\lambda \rho_m(T)(1-\lambda)}}{J_c(T)} \right)^{n(T)} \quad (3.33)$$

and as  $G = EJ$  the heat generation averaged over the whole cross section of the tape the heat generation is

$$G(T) = \lambda J_{op} E_c \left( \frac{J_{op} - \frac{E(1-\lambda)}{\rho_m(T)\lambda}}{J_c(T)} \right)^{n(T)}. \quad (3.34)$$

Above  $T_c$  the heat generation is determined from the normal state properties of the tape and the electric field giving

$$G = \lambda J_{op} E, \quad (3.35)$$

where

$$E = J_m \rho_m. \quad (3.36)$$

As the superconductor is fully normal most of the current passes through the matrix with very little flowing through the superconductor due to its much higher normal state resistance and so

$$E = \frac{J_{op} \rho_m(T) \lambda L}{1 - \lambda}, \quad (3.37)$$

with the resulting heat generation averaged over the whole cross section

$$G(T) = \frac{\lambda^2 \rho_m(T) J_{op}^2}{1 - \lambda}. \quad (3.38)$$

The heat generation in an HTS composite tape over the whole temperature range with no applied field is

$$G(T) = \begin{cases} \lambda J_{op} E_c \left( \frac{J_{op} - \frac{E_c(1-\lambda)}{\rho_m(T)\lambda}}{J_c(T)} \right)^{n(T)} & T < T_c \\ \frac{\lambda^2 \rho_m(T) J_{op}^2}{1-\lambda} & T \geq T_c. \end{cases} \quad (3.39)$$

Figure 3.11 shows the heat generation as a function of temperature for a stainless steel clad YBCO tape having different  $n$ -values. The tape carries a constant current that has  $T_{cs}$  of 50 K ( $E_c=1 \mu\text{V}/\text{cm}$ ). If the method that uses  $n = \infty$  that was described in Section 3.5.2 is used for HTS materials that have low  $n$ -values and a wide current sharing temperature range then the heat generation in the current sharing regime will be overestimated. This overestimation becomes more significant with decreasing  $n$ -values.

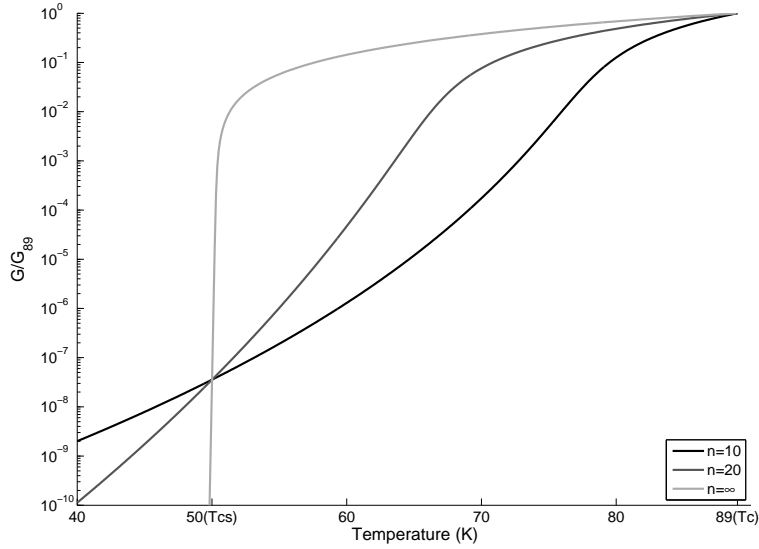


FIGURE 3.11: Heat generation per unit volume ( $G$ ) of a stainless steel clad YBCO tape that has  $T_{cs}$  of 50 K. The heat generation is normalised to the normal state value at  $T_c$  ( $G_{89}$ ).

When a parallel resistance is present, for example an external dump resistor, the magnet current ( $I_L$ ) is shared between the superconductor, the matrix, and the external resistor with equivalent circuit diagram shown in Figure 3.12. As they are in parallel the voltages across the resistor, matrix, and superconductor are identical.

The circuit voltage can be calculated from the dump resistor as

$$V = I_D R_D \quad (3.40)$$

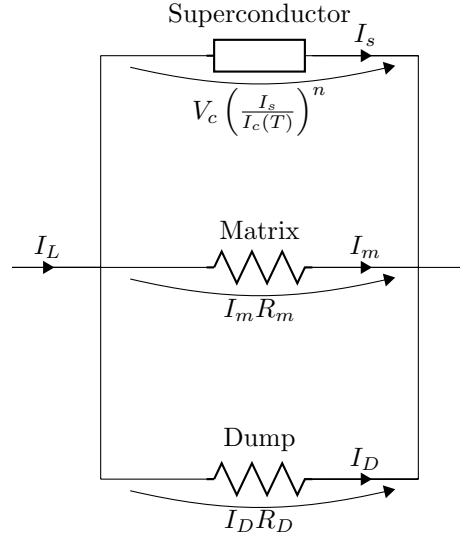


FIGURE 3.12: Current sharing between tape components and a dump resistor.

and similarly for the matrix of the HTS tape giving

$$V = I_m R_m(T). \quad (3.41)$$

The voltage across the superconductor is given by the power law relationship

$$V = V_c \left( \frac{I_s}{I_c(T)} \right)^{n(T)}. \quad (3.42)$$

The current in the superconductor can be determined from the sharing with the dump and matrix to be

$$I_s = I_L(t) - \frac{V}{R_D} - \frac{V}{R_m(T)}, \quad (3.43)$$

which can then be substituted into Equation 3.42 giving

$$V = V_c \left( \frac{I_L(t) - \frac{V}{R_D} - \frac{V}{R_m(T)}}{I_c(T)} \right)^{n(T)}. \quad (3.44)$$

The total electrical power is given by  $I_L V$ , this is averaged across the whole cross section of the tape resulting in a heat generation of

$$G(T) = \frac{I_L V_c}{AL} \left( \frac{I_L - \frac{V}{R_D} - \frac{V}{R_m(T)}}{I_c(T)} \right)^{n(T)} \quad (3.45)$$

As for the case where there is no dump resistor the heat generation above  $T_c$  where  $I_s = 0$  the heat generation can be calculated from standard circuit analysis. The resulting heat

generation in the tape for all temperatures is

$$G(T) = \begin{cases} \frac{I_L V_c}{A L_s} \left( \frac{I_L - \frac{V}{R_D} - \frac{V}{R_m(T)}}{I_c(T)} \right)^n & T < T_c \\ \frac{I_L^2 R_D^2 R_m(T)}{A L_s (R_D + R_m(T))} & T \geq T_c. \end{cases} \quad (3.46)$$

The presence of a parallel dump resistor decreases the heat generation in the tape and has a similar effect to reducing the matrix resistivity. The overall transition will be more smeared if the parallel resistor has a small resistance compared to the resistance of the tape's matrix.

## 3.6 System of Equations for a Superconducting Switch

### 3.6.1 Switch Equations

When an HTS switch that is used to discharge a magnet through a dump resistor there exists a system of switch equations. These equations were described individually in the previous sections but must be combined and solved in order to determine the thermal and electrical switching dynamics and thus the magnet discharge characteristic. The heat diffusion equation for the switch is where the heat generation in the superconducting tape is

$$G_{ST}(T, t) = \begin{cases} \frac{I_L(t) V_c}{W_{ST} \delta_{ST} L_s} \left( \frac{I_L(t) - \frac{V}{R_D} - \frac{V}{R_m(T)}}{I_c(T)} \right)^n & T < T_c \text{ \& } (\delta_T - \delta_S) < x \leq \delta_T \\ \frac{I_L^2(t) R_D^2 R_m(T)}{W_{ST} \delta_{ST} L_s (R_D + R_m(T))} & T > T_c \text{ \& } (\delta_T - \delta_S) < x \leq \delta_T \\ 0 & 0 < x \leq (\delta_T - \delta_S) \end{cases} \quad (3.47a)$$

and in the heater is

$$G_H(T, t) = \begin{cases} \frac{V_H^2(t)}{W_H \delta_H L_S R_H(t)} & 0 < x \leq \delta_H \\ 0 & \delta_H < x \leq \delta_T. \end{cases} \quad (3.47b)$$

The current decay of the magnet circuit has the form

$$\frac{dI_L}{dt} = \frac{-V_{ST}}{L_m}, \quad (3.47c)$$

where the voltage across the superconducting tape is

$$V_{ST} = \begin{cases} V_c \left( \frac{I_{magnet} - \frac{V_{ST}}{R_D} - \frac{V_{ST}}{R_m}}{I_c} \right)^n & T < T_c \text{ \& } (\delta_T - \delta_S) < x \leq \delta_T \\ \frac{I_{magnet}(t) R_D R_m(T)}{(R_D + R_m(T))} & T > T_c \text{ \& } (\delta_T - \delta_S) < x \leq \delta_T. \end{cases} \quad (3.47d)$$

The decay of the capacitor voltage through the heater has the form

$$\frac{dV_H}{dt} = \frac{-V_H}{R_H(t)C_F}. \quad (3.47e)$$

### 3.6.2 Initial and Boundary Conditions for the Switch Equations

The switch equations described above have initial and boundary conditions for the heat diffusion equation that result from the layout of the switch, its operating conditions, and the associated electrical circuits of the heater and magnet.

**Initial conditions** of the switch are as follows. The temperature is homogeneous at that of the surrounds ( $T_\infty$ )

$$T(x, t = 0) = T_\infty. \quad (3.48a)$$

The heater has an initial voltage of

$$V_H(t = 0) = V_{Ho} \quad (3.48b)$$

that results in an initial heater heat generation of

$$G_H(t = 0) = \frac{V_{Ho}^2}{R_H(t = 0)}. \quad (3.48c)$$

The superconducting magnet has an initial current

$$I_L(t = 0) = I_{Lo}, \quad (3.48d)$$

but as the superconducting tape is initially fully superconducting the heat generation

$$G_{ST}(t = 0) = 0. \quad (3.48e)$$

It is useful to note that initially the stored electrical energy in the heater capacitor is

$$Q_H = \frac{1}{2}C_F V_{Ho}^2 \quad (3.48f)$$

and in the magnet is

$$Q_L = \frac{1}{2}L_m I_{Lo}^2. \quad (3.48g)$$

**Boundary conditions** for a cooled switch with heat transfer coefficients  $h_1$  and  $h_2$  on the external heater and superconductor faces respectively are

$$\begin{aligned}\frac{\partial T(t, x)}{\partial x} &= \frac{-h_1}{k(x)}(T(t, x) - T_\infty) \text{ where } t = 0, x = 0 \\ \frac{\partial T(t, x)}{\partial x} &= \frac{-h_2}{k(x)}(T(t, x) - T_\infty) \text{ where } t = 0, x = \delta_T,\end{aligned}\tag{3.49}$$

where if the switch is fast acting and well insulated from the surroundings it can then be modelled as adiabatic during the switching process with  $h_1 = h_2 = 0$ .

### 3.6.3 Possible Solution Methods

In order to obtain the full non-linear temperature distribution through the switch the full partial differential form of the system of switch equations must be solved (Section 3.8). However, if the superconductor and heater layers have high thermal diffusivity (Section 3.7.1), and the diffusion time of the insulation is fast (Section 3.7.1) then it is possible to form a lumped approximation of the system. As for a standard lumped approximation the temperature of the superconductor and heater layers are assumed to be homogenous at  $T_S(t)$  and  $T_H(t)$  respectively. The insulation layer has a thermal gradient  $T_H(t) - T_S(t)$  and so is not lumped. However, if it has a fast diffusion time then it can be assumed to instantly relax into the steady-state profile so  $T_I(x)$  only with  $k_I(T(x))$  and  $C_I(T(x))$ . The enthalpy change of the insulation layer is considered in conjunction with the hotter of the other two layers. The lumped approximation of the system of switch equations is described in Section 3.7.

## 3.7 Approximate Solution of the Switch Equations using a Lumped Model

### 3.7.1 Diffusion Times in the Switch

The approximation of the system of switch equations to a lumped system assumes that the thermal profile in the insulation layer instantly relaxes to its steady state value. This is valid assumption for insulation layers with fast thermal diffusion. In these cases the diffusion time ( $\tau_{\text{diff}}$ ) is

$$\tau_{\text{diff}} = \frac{\delta^2}{\alpha}.\tag{3.50}$$

If the insulation is to be modelled as steady state then the time step in the analysis must be greater than the diffusion time. Figure 3.13 shows the diffusion time against different material thicknesses for polyimide insulation. Whilst superconducting switches are fast



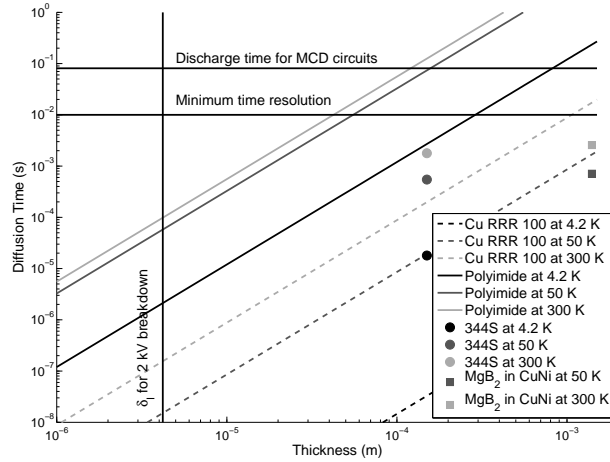


FIGURE 3.13: Diffusion time as a function of thickness for materials used in typical switches.

acting they are slow with respect to the diffusion time. Dump-switches undergo large thermal changes during the extraction of the magnet's energy and so whilst the thermal transients are spread over the whole magnet discharge time. For the fastest discharging LHC circuit, the MCD circuit, the discharge time is 81 ms. Discharge times can be of the order of hundreds of seconds for large circuits such as the main dipoles. The horizontal lines on Figure 3.13 show the MCD discharge time and the required temporal resolution for use with the lumped model. The lumped approximation is more valid the smaller the diffusion time is with respect to the required time step. The vertical line shows the minimum thickness of polyimide for a 2 kV breakdown voltage. The breakdown voltage was based on data for 50  $\mu\text{m}$  Kapton HN tape in air at 23  $^{\circ}\text{C}$  [112].

### 3.7.2 Description of the Lumped Approximation

In its normal form a thermally triggered superconducting switch consists of a heater layer, an insulation layer, and a superconductor layer as described in Section 3.2 and shown in Figure 3.3. The heater and superconductor matrix are metals having high thermal diffusivity. This means that the temperature across these layers can be modeled as a homogeneous value for each layer. Both the heater temperature ( $T_H(t)$ ) and the superconductor temperature ( $T_S(t)$ ) are time variant. The high thermal diffusivity of the superconductor and heater layers mean that  $\frac{dT}{dx} = 0$  in these regions and the partial differential form of the heat diffusion equation can be reduced to two time dependent ordinary differential equations. This simplification can not be applied to the insulation layer as its boundary conditions are  $T_H(t)$  and  $T_S(t)$ , which are not always the same and so a thermal gradient will exist. However, if the insulation layer is thin and has a high thermal diffusivity, heat will diffuse quickly across it and so  $\frac{\partial^2 T}{\partial x^2} = 0$  allowing the insulation to be modelled as steady state.

These simplifications lead to a situation where the thermal profiles in the superconductor and heater are flat, with a linear profile in the insulation layer (Figure 3.14).

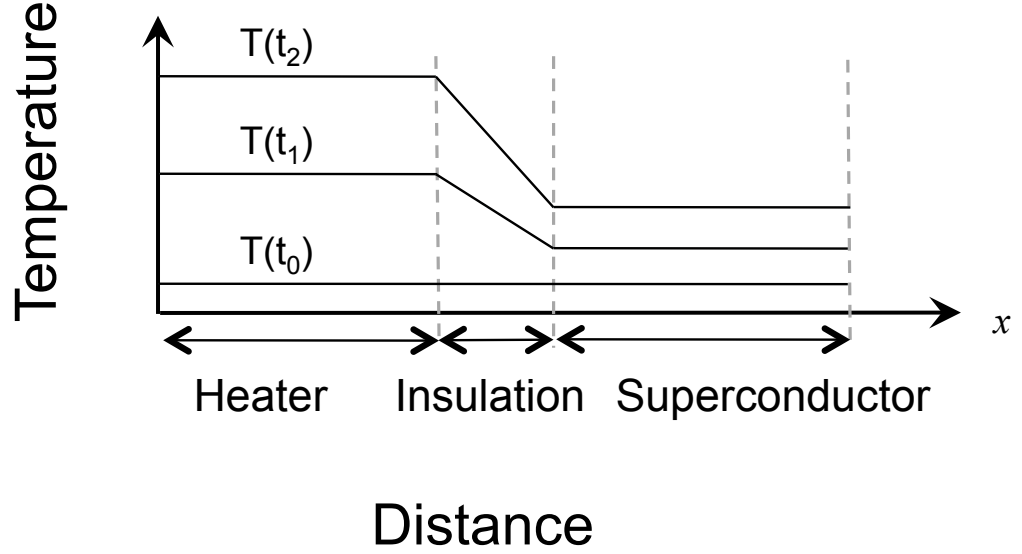


FIGURE 3.14: Sketch of typical switch and thermal profiles within it.

As the change in heat stored in the insulation is significant with respect to the superconductor and heater layers it can not be neglected, but as the layer is treated as steady state the energy required to change its enthalpy must be considered with either the heater or superconductor layer. As heat flows from hot to cold, the heat change in the insulation layer is lumped with the hotter of the two layers. When  $T_H(t) > T_S(t)$  the heat that causes the enthalpy increase in the insulation flows from the heater, when  $T_S(t) > T_H(t)$  it flows from the superconductor (Figure 3.15). A Heaviside step function ( $\Phi(T_S(t), T_H(t))$ ) is used to introduce the rate of change of insulation enthalpy to the relevant layer.

In the lumped approximation the enthalpy change rate equation for the whole switch can be split into two components relating to the two uniform temperature layers that are linked by conduction through the insulation  $Q_{c,I}$ .  $H_H$  is the heater enthalpy,  $H_S$  the superconducting tape enthalpy,  $G_H$  the heat generation in the heater, and  $G_S$  the heat generation in the superconductor. The heat generation in the heater and superconductor layers depends upon the decay of the respective electrical circuits.  $Q_{h,H}$  and  $Q_{h,S}$  are cooling from the heater and superconductor layers to the surrounds. Thus the enthalpy change equation for the heater layer is

$$\frac{dH_H}{dt} = G_H(t) - \Phi(T_H - T_S) \frac{dH_I}{dt} - Q_{c,I} - Q_{h,H} \quad (3.51a)$$

and for the superconductor layer the enthalpy change equation is

$$\frac{dH_S}{dt} = G_S(t) - \Phi(T_S - T_H) \frac{dH_I}{dt} + Q_{c,I} - Q_{h,S}. \quad (3.51b)$$

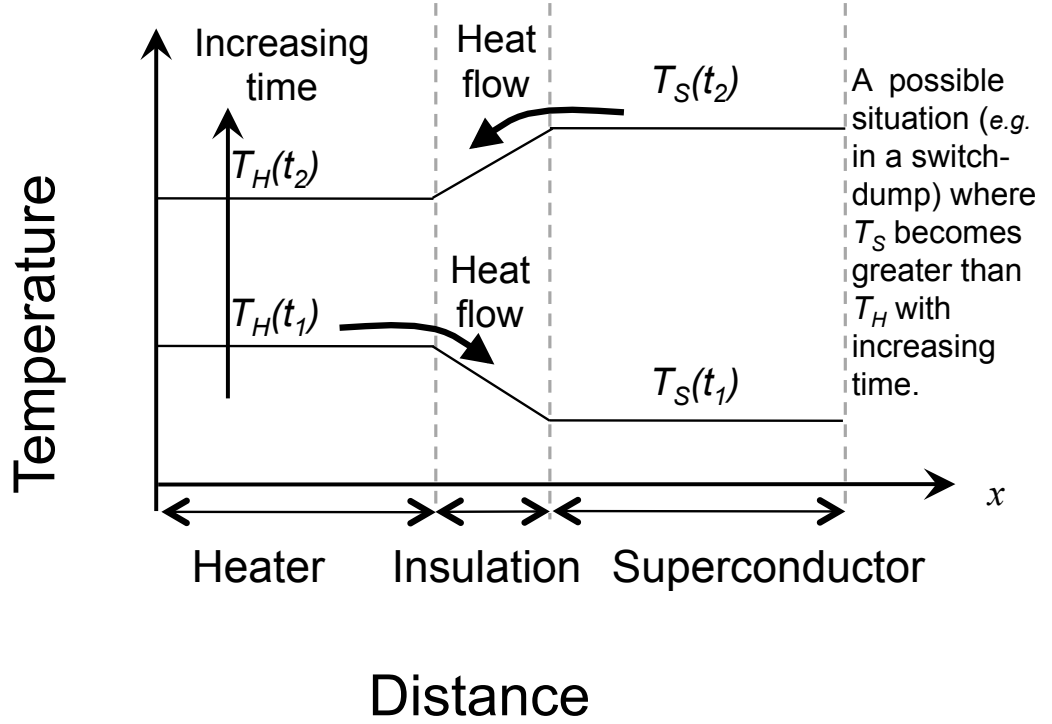


FIGURE 3.15: Heat flow resulting in enthalpy increase of the insulation layer.

### 3.7.2.1 Heat Conduction through the Insulation

The heat conduction through the insulation ( $Q_{c,I}$ ) links the heater and superconductor layers. The lumped approximation assumes that the insulation layer instantaneously adopts a linear temperature profile over which the temperature dependent thermal conductivity of the insulation is integrated along giving

$$\bar{k}_I(t) = \int_{T_S(t)}^{T_H(t)} k_I(T(x,t)) dT, \quad (3.52a)$$

which gives the conduction between the heater and superconductor to be

$$Q_{c,I}(t) = \frac{L_S W_I}{\delta_I} \bar{k}_I(t). \quad (3.52b)$$

$Q_{c,I}(t)$  is positive when the heater is hotter than the superconductor and the heat flows from the heater through the insulation to the superconductor.

### 3.7.2.2 Cooling to the Surrounds

In the lumped approximation the cooling from the external face of layer, which was a boundary condition in the PDE form of the heat diffusion equation, is averaged over the whole cross section of the layer. The heat transfer coefficient from the heater is  $h_1$  and from superconductor layer is  $h_2$ . This leads to the cooling of the heater layer being

$$Q_{h,H}(t) = h_1 W_H L_s (T_H(t) - T_\infty) \quad (3.53a)$$

and of the superconductor layer

$$Q_{h,S}(t) = h_2 W_S L_s (T_S(t) - T_\infty). \quad (3.53b)$$

For well insulated fast acting switches the switching process can be considered to be adiabatic with  $h_1 = h_2 = 0$ .

### 3.7.2.3 Enthalpy Changes in the Switch

Enthalpy in the heater with a temperature profile  $\phi(t)$  is

$$H_H = W_H \delta_H L_S \varrho_H \int_0^{\phi(t)} C_H(T_H(t)) d\phi(t). \quad (3.54a)$$

This can be differentiated with respect to time giving the rate of change in enthalpy for the heater layer at a uniform temperature  $T_H(t)$  of

$$\frac{dH_H}{dt} = W_H \delta_H L_S \varrho_H \frac{dT_H}{dt} C_H(T_H(t)). \quad (3.54b)$$

Enthalpy in the superconducting tape can be similarly calculated as it also has a uniform temperature resulting in an enthalpy of

$$H_S = W_S \delta_S L_S \varrho_S \int_0^{\phi(t)} C_S(T_S(t)) d\phi(t), \quad (3.55a)$$

differentiating with respect to time for the superconductor layer at a uniform temperature  $T_S(t)$  gives a rate of change in enthalpy of

$$\frac{dH_S}{dt} = W_S \delta_S L_S \varrho_S \frac{dT_S}{dt} C_S(T_S(t)). \quad (3.55b)$$

Enthalpy in the Insulation is more complicated to solve, as unlike the heater and superconductor layers the insulation has a thermal gradient due to the temperature difference

between  $T_S$  and  $T_H$ . The insulation layer is assumed to instantly adopt this thermal profile (Section 3.7.1) but the heat required to change the enthalpy of the insulation must still be taken into account in the energy balance. The insulation layer has an instantaneous temperature distribution  $(\phi(x, t))$  and a heat capacity  $C_I(\phi(x, t))$  that is to be integrated with respect to  $T$  and  $x$ . The enthalpy of the insulation  $(H_I(T, x))$  for a given instantaneous temperature profile is

$$H_I(T, x) = W_I L_S \varrho_I \int_0^{\delta_I} \int_0^{T_I(t, x)} C_I(\phi) d\phi dx, \quad (3.56)$$

which is differentiated with respect to time to give

$$\frac{dH_I}{dt} = W_I L_S \varrho_I \frac{\partial}{\partial t} \int_0^{\delta_I} \int_0^{T_I(t, x)} C_I(\phi) d\phi dx, \quad (3.57a)$$

however, this differentiation also allows the equation to be simplified to

$$\frac{dH_I}{dt} = W_I L_S \varrho_I \int_0^{\delta_I} \frac{\partial(T_I(t, x))}{\partial t} C_I(\phi) dx, \quad (3.57b)$$

which is valid for any temperature distribution in the insulation layer. However, the lumped model assumes that the insulation layer instantly adopts a linear temperature distribution

$$T_I(x, t) = T_H(t) - x \left( \frac{T_H(t) - T_S(t)}{\delta_I} \right), \quad (3.57c)$$

which can be substituted into the rate of change of enthalpy relationship to give

$$\frac{dH_I}{dt} = W_I L_S \varrho_I \int_0^{\delta_I} \frac{\partial}{\partial t} \left( T_H(t) - \frac{x}{\delta_I} (T_H(t) - T_S(t)) \right) C_I(T_I(t, x)) dx, \quad (3.57d)$$

then rearranging to group  $\frac{dT_S}{dt}$  and  $\frac{dT_H}{dt}$

$$\begin{aligned} \frac{dH_I}{dt} = & \frac{dT_H}{dt} W_I L_S \varrho_I \int_0^{\delta_I} \left( 1 - \frac{x}{\delta_I} \right) C_I(T_I(x, t)) dx \\ & + \frac{dT_S}{dt} W_I L_S \varrho_I \int_0^{\delta_I} \frac{x}{\delta_I} C_I(T_I(x, t)) dx. \end{aligned} \quad (3.57e)$$

#### 3.7.2.4 Electrical Circuits and Heat Generation

The decay of the heater and magnet circuits are simplified with respect to the partial differential form of the switch equations as  $T_S(t)$  and  $T_H(t)$  are uniform so the resistivity does not need to be integrated over the layer thickness and so

$$R_H = \frac{\rho_H L_s}{W_H \delta_H}, \quad (3.58a)$$

through which the heater capacitor is discharged. This discharge has a voltage decay of the form

$$\frac{dV_H}{dt} = \frac{-V_H(t)}{R_H(t)C_F} \quad (3.58b)$$

that results in a heat generation in the heater of

$$G_H(T_H, t) = \frac{V_H^2(t)}{L_S^2 \rho_H(T_H(t))}. \quad (3.58c)$$

The heat generation in the superconducting tape ( $G_{ST}(t)$ ) is linked to the magnet discharge circuit, which due to the voltage across the superconducting tape ( $V_{ST}$ ) has a decay profile of the form

$$\frac{dI_L}{dt} = \frac{V_{ST}}{-L_m}. \quad (3.59a)$$

Above  $T_c$  the voltage depends upon Ohm's law for the normal state circuit components, below  $T_c$  it also depends upon the power law relationship of the superconductor resulting in a heat generation of

$$G_{ST}(T_S, t) = \begin{cases} \frac{I_L(t)V_c}{W_{ST}\delta_{ST}L_S} \left( \frac{I_L(t) - \frac{V_{ST}}{R_D} - \frac{V_{ST}}{R_m(T_S(t))}}{I_c(T_S)} \right)^n & T_S < T_c \\ \frac{I_L^2(t)R_D^2 R_m(T_S(t))}{W_{ST}\delta_{ST}L_S(R_D + R_m(T_S(t)))} & T_S \geq T_c. \end{cases} \quad (3.59b)$$

### 3.7.3 Switch Equations for the Lumped Approximation

The lumped approximation results in a set of four linked ODEs that describe switching process. One ODE describes the decay of the heater voltage and another the decay of the magnet current. There are further two ODEs to describe the rate of enthalpy change of the superconductor and heater layers, with the enthalpy change rate being switched into the hotter layer by means of a Heaviside step function ( $\Phi(T_S(t), T_H(t))$ ). The differential

equation for the heater layer temperature is

$$\begin{aligned}
\frac{dT_H}{dt} W_H \delta_H L_S \varrho_H C_H(T_H(t)) = & \\
& -\Phi(T_H(t) - T_S(t)) \left( \frac{dT_H}{dt} W_I L_S \varrho_I \int_0^{\delta_I} \left(1 - \frac{x}{\delta_I}\right) C_I(T_I(x, t)) dx \right. \\
& \quad \left. - \frac{dT_S}{dt} W_I L_S \varrho_I \int_0^{\delta_I} \frac{x}{\delta_I} C_I(T_I(x, t)) dx \right) \\
& + \frac{V_H^2(t) \delta_H W_H}{L_S \rho_H(T_H(t))} \\
& - \frac{L_S W_I}{\delta_I} \int_{T_S(t)}^{T_H(t)} k_I(T_I) dT.
\end{aligned} \tag{3.60a}$$

The differential equation for the superconductor layer temperature is

$$\begin{aligned}
\frac{dT_S}{dt} W_S \delta_S L_S \varrho_S C_S(T_S(t)) = & \\
& -(1 - \Phi)(T_S(t) - T_H(t)) \left( \frac{dT_H}{dt} W_I L_S \varrho_I \int_0^{\delta_I} \left(1 - \frac{x}{\delta_I}\right) C_I(T_I(x, t)) dx \right. \\
& \quad \left. - \frac{dT_S}{dt} W_I L_S \varrho_I \int_0^{\delta_I} \frac{x}{\delta_I} C_I(T_I(x, t)) dx \right) \\
& + (I_m(t) + I_S(t)) V_S(T_S(t)) \\
& + \frac{L_S W_I}{\delta_I} \int_{T_S(t)}^{T_H(t)} k_I(T_I) dT.
\end{aligned} \tag{3.60b}$$

The heater voltage decay profile has the form

$$\frac{dV_H}{dt} = \frac{-W_H \delta_H V_H(t) N_p}{\rho_H(T_H(t)) L_S C_F} \tag{3.60c}$$

and the discharge of the magnet has the current decay given by

$$\frac{dI_L}{dt} = \frac{-V_S}{L_m}. \tag{3.60d}$$

This set of equations has initial conditions described in the following section and approximate the partial differential form of the switch equations to lumped system. This lumped model is used in Chapter 5 to optimise the design of switches for specific LHC circuits.

### 3.7.4 Initial Conditions for the Lumped Approximation

Reducing the system of switch equations from the partial form to a lumped approximation mean that the spatial boundary conditions disappear and additionally the initial conditions are not a function of  $x$ . The uniform temperature of the heater layer

$$T_H(t = 0) = T_\infty, \tag{3.61a}$$

which is the same for the superconductor layer

$$T_S(t = 0) = T_\infty. \quad (3.61b)$$

The heater has an initial voltage of

$$V_H(t = 0) = V_{Ho} \quad (3.61c)$$

that results in an initial heater heat generation of

$$G_H(t = 0) = \frac{V_{Ho}^2}{R_H(t = 0)} \quad (3.61d)$$

The superconducting magnet has an initial current

$$I_L(t = 0) = I_{Lo}, \quad (3.61e)$$

but as the superconducting tape is initially fully superconducting the heat generation

$$G_{ST}(t = 0) = 0. \quad (3.61f)$$

It is useful to note that initially the stored electrical energy in the heater capacitor is

$$Q_H = \frac{1}{2} C_F V_{Ho}^2 \quad (3.61g)$$

and in the magnet is

$$Q_L = \frac{1}{2} L_m I_{Lo}^2. \quad (3.61h)$$

### 3.8 Solution of the Switch Equations Using Finite Element and Finite Difference Methods

In some situations where the thermal profiles within the switch depend on both time and distance it is more appropriate to solve the full partial differential form of the heat diffusion equation (Section 3.6) rather than using the lumped approximation. This would be the case in a switch where thick insulation is required in order to withstand high voltages during a very large magnet discharge, for example in the LHC 13 kA circuits. Another case would be if the superconductor or heat layers had low thermal diffusivity, for example when using a bulk BSCCO superconductor. The partial differential form of the heat diffusion equation Equation 3.2a can be used in the thermal-electrical system can be solved by finite element or finite difference methods. The finite difference method



approximates the PDE to a set of ODEs at a specified points in space. In the finite element method the problem is broken down into smaller elements and the solution to the PDE is approximated at each element using a trial function. The solutions of all the elements are combined to give the global solution [113].

### 3.8.1 Solution with a Finite Element Method

It is possible to solve transient coupled thermal-electrical systems by finite element analysis with commercial FEA programs such as ANSYS®. Modelling quenching superconductors with thermal-electrical elements can be done in ANSYS® by modelling the superconducting to normal transition as a sharp change to the normal state at  $T_{cs}$  as the current sharing regime is not fully described by standard ANSYS elements. This method has been used to model the quenching of LTS superconducting coils [114]. The quench characteristics, including the non-linear heat generation in the current sharing regime, of HTS materials can be modelled in ANSYS over a wide range of temperatures using elements that only have thermal properties. This method has been used to model the two dimensional quench characteristics of BSCCO coils with operating temperatures in the range 30-77 K [115]. It is possible to extend the thermal-electrical elements of ANSYS® to include a non-linear resistivity by implementing additional element subroutines. This method has been used to model HTS fault current limiters [116]. For HTS switches where operation in the current share regime is significant it is necessary to model both the thermal and electrical process. For this reason the switch equations were solved by the finite difference method where the current sharing regime could be fully taken into account.

### 3.8.2 Solution with a Finite Difference Method

This system of switch equations was solved numerically on MATLAB® using the finite difference method. The switch equations were one dimensional due to the layout of the switch (Section 3.2) thus simplifying the finite difference analysis. The switch equations are system of one PDE and two ODEs which were solved with MATLAB®'s PDE solver. This solver converts PDEs to ODEs using a second-order accurate spatial discretization method, the resulting ODEs were solved using numerical differentiation formulas [117]. A user defined  $x$ -mesh provides the spatial discretization with a minimum resolution being required to obtain accurate results. The computational cost of the calculation increases strongly with increasing resolution.

The system of thermal and electrical equations can either be solved as a coupled system or sequentially and then iterated. Figure 3.16 shows the flow charts for each procedure. For systems where it is not possible to couple the equations the system must be solved sequentially, with the solution being iterated until convergence, at a high computational

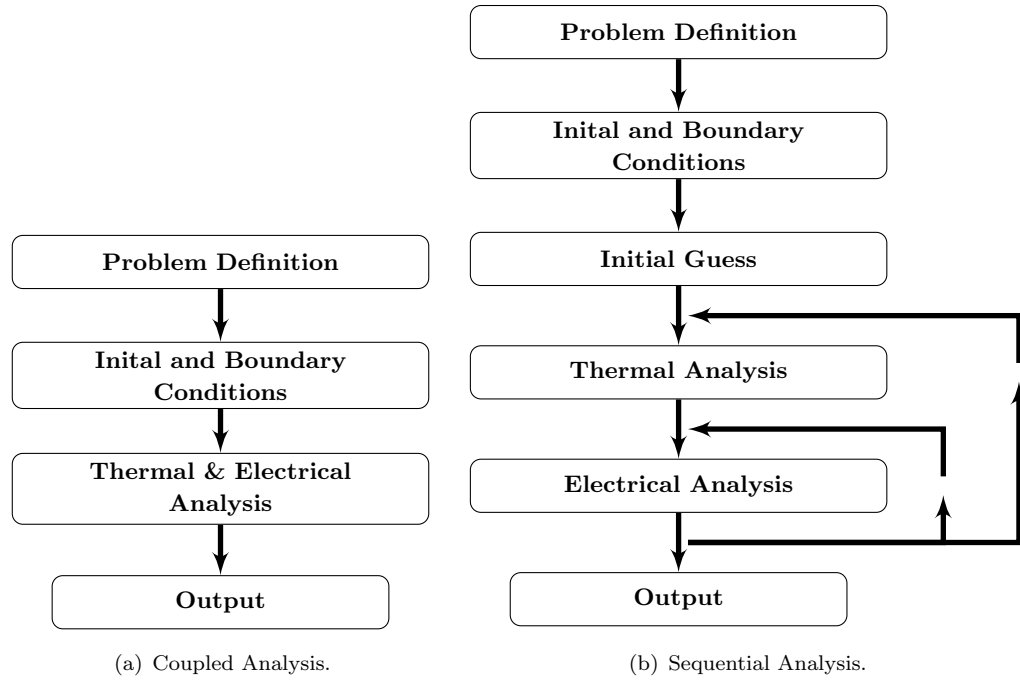


FIGURE 3.16: Flow charts for the solution of the partial differential form of the system of switch equations using either a coupled method (a) or a sequential method (b).

cost. The coupled analysis solves the problem with a lower computational cost and is used to model the switch equations in Chapter 4.

### 3.9 Conclusions

Superconducting switches can be used in magnet discharge circuits as either dump-switches or as bypass-switches (Section 3.1). In the case of a bypass-switch the magnet energy is dissipated in a dump resistor in parallel to the switch and the switching dynamics are dominated by the heater. In dump-switches there is no dump resistor and the magnet energy is dumped in the switch itself. The layout of both types of switch is a superconducting tape separated from a co-wound heater by an insulation layer (Section 3.2). The transition of the switch is triggered by the distributed heater. In the case of the dump-switch the heater layer also acts as a heat sink. Typically the heating power is provided by the discharge of a capacitor through the heater. Analysis of a switching problem requires the solution of the system of switch equations (Section 3.6) that comprises the heat diffusion equation as well as the heater and magnet electrical circuits. The magnet electrical circuit includes the superconducting tape section of the switch where the non-linear  $E$ - $J$  characteristics and heat generation in an HTS material are considered in Section 3.5.

For switches with high thermal diffusivities in the heater and superconductor layer, and fast heat diffusion in the insulation layer the system of switch equations can be approximated as lumped system as described in Section 3.7. Where there is slow heat diffusion through

the insulation the system of switch equations can be solved with partial derivatives as described in Section 3.8. The lumped model has a much lower computational cost than the PDE model and so can be more readily used for efficient optimization of suitable switches. Chapter 5 contains the optimization of switches for specific LHC circuits.

## Chapter 4

# Experimental HTS Switches

## 4.1 Aim of the Experiments

The aim of the experiments is to show that HTS switches can be thermally activated in a short enough time to allow their use in energy extraction circuits. At low temperatures (4.2 K) the specific heat capacity of a material is low so fast switching would be possible; however, there is a high cryogenic cost to depositing the magnet and the heater energies at this temperature. In order to avoid the problems associated with dissipating energy at low temperatures it is expedient to operate energy extraction switches at higher temperatures. The specific heat capacity of most materials increases proportionally to  $T^3$  and so at higher temperatures the heat capacity of the switch will be larger and the diffusion time of the insulation will be longer. Both of these factors contribute to slowing down the transition of the superconducting switch and so it is necessary to demonstrate that fast transitions can be achieved at high temperatures. If fast transitions can be achieved, then HTS switches have the potential to be used in energy extraction circuits.

Operation at 77 K is close to the useful upper operating temperature of HTS devices and is where the high specific heat capacity could lead to slow switching times. For use in particle accelerators, such as the LHC, operating temperatures lower than this but above 4.2 K may also be utilised (see also Section 5.1.1). Potential switch operating temperatures are at 20 K utilising the cold helium gas that has been recovered from the magnet boil off, or at 50 K that is the temperature of the heat exchanger between the HTS part and the resistive part of the LHC current leads. If switches can be shown to operate fast enough at 77 K then the lower heat capacity at 20 K and 50 K means that the switching time will also be fast enough at these temperatures.

Thermal diffusion is slower with thick insulation and at high temperatures. The thermal diffusivity ( $\alpha = \frac{k}{\gamma C_p}$ ) slows down as increasing the temperature from 4.2 K to 77 K increases the specific heat of polyimide by  $\approx 370$  times but the thermal conductivity only increases by  $\approx 12$  times. Low thermal diffusivity increases the diffusion time ( $\tau_{\text{diff}} = \frac{\delta^2}{\alpha}$ ) as does increasing the insulation thickness. The diffusion times of polyimide insulation at 4.2 K and at 77 K is given in Table 4.1 for a thickness ( $\delta$ ) of 20  $\mu\text{m}$  and of 200  $\mu\text{m}$ . When modelling switches that have slow diffusion times (Section 3.7.1), the non-linear temperature gradient through the switch may be significant, in which case the lumped approximation may not be valid and so the full heat diffusion equation should be used.

$T$ (K)	$C_p$ (J/kg/K)	$k$ (mW/m/k)	$\alpha$ (km <sup>2</sup> /s)	$\delta$ ( $\mu\text{m}$ )	$\tau_{\text{diff}}$ (ms)
4.2	0.92	11	8.3	20	0.05
				200	4.8
77	340	125	0.26	20	1.5
				200	153

TABLE 4.1: Thermal diffusion times of different thickness polyimide insulation at 4.2 K and 77 K.

Operating superconducting switches at 77 K restricts the choice of superconductor to either YBCO or BSCCO. YBCO tapes have more stabilization options than BSCCO tapes which are only available in silver or silver alloy matrices. The resistivity of silver at room temperature is  $\approx 1.6 \mu\Omega\text{cm}$ . BSCCO tapes that have a higher resistivity silver-gold alloy matrix are also available and have a room temperature resistivity of  $\approx 5 \mu\Omega\text{cm}$ . This is similar to the resistivity ( $\approx 4 \mu\Omega\text{cm}$ ) of copper clad YBCO from American Superconductor. The resistivity of these YBCO tapes can be increased to  $\approx 23 \mu\Omega\text{cm}$  by replacing the copper with stainless steel cladding. The YBCO based tapes have a nickel-tungsten alloy substrate and the heat capacity of these tapes at room temperature  $\approx 3.3 \text{ J/K/cm}^3$ . This is higher than  $\approx 1.6 \text{ J/K/cm}^3$  of the Ag-Au matrix BSCCO tapes making it more important to test if the YBCO tapes can be made to switch fast enough at high temperatures. As the YBCO tapes use far less silver<sup>1</sup> than the BSCCO tapes they have the potential to be formed into cheaper switches.

Superconducting switches that have a low resistivity matrix are suited for use in dump-switches as a greater length is needed in order to develop the required dump resistance. This longer length means that the enthalpy change from the operating temperature to the maximum allowable temperature is greater than for higher resistivity switches allowing more energy to be dissipated in the switch. Copper clad YBCO was used to make a dump-switch with an  $I_c$  of 45 A at 77 K [55]. For magnet circuits where the energy extraction requirements are smaller, dump-switches that have more resistive matrices could be used. These higher resistivity switches have the advantage that less conductor and lower heater energies are needed. A stainless steel clad YBCO dump-switch with an  $I_c$  of 45 A was also made and tested.

Superconducting switches that have a high resistivity matrix are suited to use in bypass-switches as less length is needed in order to shunt the current into the parallel dump resistor. Stainless steel clad YBCO was used to make a bypass-switch with an  $I_c$  of 57 A [86]. Bypass-switches are suited to systems where it is preferred to dissipate the majority of the magnet energy in a resistor at room temperature. In magnet circuits the stored energy increases with current squared;  $E_M = 0.5LI^2$ . To show the scalability of superconducting bypass-switches to higher currents, four stainless steel clad YBCO switch modules were connected in parallel to form a bypass-switch with an  $I_c$  of 220 A.

---

<sup>1</sup>YBCO based tapes that are  $\approx 4 \text{ mm}$  wide generally have a silver cap layer that is  $\approx 2\text{-}3 \mu\text{m}$  thick ( $\approx 0.01 \text{ mm}^2$  of Ag). BSCCO tapes are about  $4 \text{ mm} \times 0.2 \text{ mm}$ , of which  $\approx 70 \%$  is silver alloy ( $\approx 0.56 \text{ mm}^2$  of Ag).

## 4.2 Design and Manufacture of HTS Switches

### 4.2.1 Dump-Switches Based on YBCO Tape

Two dump-switches were formed of American Superconductor YBCO tapes, one with copper cladding and one with stainless steel cladding. The switches had a critical current of  $\approx 45$  A and used  $\approx 1.75$  m of superconductor. The superconductor was wound into a low inductance bifilar spiral that had a 50 mm soldered joint in the centre (Figure 4.1). A resistance heater was wound between the two legs of the superconductor and polyimide was used to provide insulation between the electrical components. As there was no switch back in the heater it had a non-zero inductance. The switch was wound around a 100 mm diameter stainless steel cylinder that acted as a mechanical support; several layers of insulation isolated the support. The HTS section comprised of two lengths of tape that had slightly different lengths (Table 4.2) in order to offset the attachment of the current leads. The voltage taps, heater current leads, and transport current leads were attached by means of terminals formed of 0.2 mm thick copper. Soldering to the HTS tape was performed at 160 °C with 99.99 % pure indium; this was to avoid damaging the tape as the cladding was attached by solder. The resistance of the HTS to HTS joint was measured at 77 K in self field to be  $213 \text{ n}\Omega/\text{cm}^2$  for YBCO-SS, and  $54.2 \text{ n}\Omega/\text{cm}^2$  for YBCO-Cu.

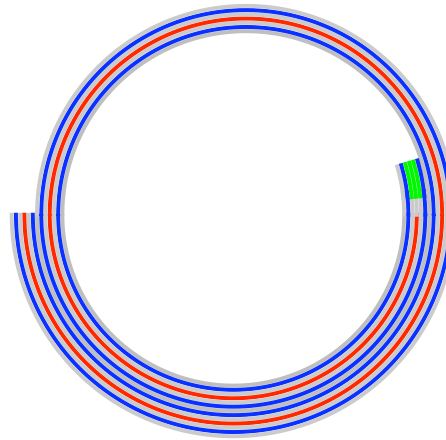


FIGURE 4.1: Sketch of 1.5 turns of a switch (not to scale) showing the non-inductive bifilar HTS winding co-wound with a heater and insulation. The HTS tape is shown in blue, the steel heater in red, and the insulation in grey. The indium solder between the two legs of the superconductor is shown in green. The inner diameter of the switch is about 100 mm.

The heater was a 1.4 m long steel strip of thickness 0.05 mm that was connected to a thyristor triggered capacitor discharge circuit. The heater energy was controlled by setting the capacitor charge voltage. Locating the heater between the two HTS legs meant that a lower heater resistance could be achieved for the same heat capacity as using a longer thinner switch that was wrapped around the outside of both HTS legs. Using a lower resistance heater meant that the capacitor discharge time was also less and so more rapid heating of the switch could be achieved. This shorter heater also avoided a sharp switch

back or soldered joint that would have damaged the thin heater. The heater resistance was measured to be  $351 \text{ m}\Omega/\text{m}$  at  $77 \text{ K}$ , and  $752 \text{ m}\Omega/\text{m}$  at room temperature. The heater coil had an extra turn around the outermost layer of superconductor to reduce cooling from the superconductor to the surrounds. Electrical insulation was provided by  $12.7 \text{ }\mu\text{m}$  thick polyimide between the heater and superconductor, and between turns of the coil. The switch layers were bonded together by epoxy that was a pre-existing  $12.7 \text{ }\mu\text{m}$  thick coating on each side of the polyimide. The epoxy was cured at  $140 \text{ }^\circ\text{C}$  for two hours.

Superconductor	Length (m)	$R$ (300 K) ( $\text{m}\Omega$ )	$I_c$ (77 K) (A)
YBCO Cu - short leg	0.79	33	48
YBCO Cu - long leg	1.01	43	46
YBCO Cu - total	1.8	76	46
YBCO SS - short leg	0.74	262	77
YBCO SS - long leg	0.95	335	45
YBCO SS - total	1.69	597	45

TABLE 4.2: Metrics of YBCO based dump-switches with copper and stainless steel cladding. The total resistance includes the resistance of the HTS-HTS joint.

#### 4.2.2 Bypass-Switches Based on Stainless Steel Clad YBCO

Bypass-switches are required to have a high resistance in order to shunt the current into a parallel dump resistor at room temperature. In order to minimise the amount of conductor and heater energy that is needed, stainless steel clad YBCO was used to form the dump-switches. To avoid the soldered joint in the centre of the switch that was used to switch back the HTS in the dump switches, a centrally located “S” shape was used for the bypass-switches Figure 4.2. This joint-less design was thus fully superconducting at  $77 \text{ K}$ . Similar designs with an “S” shaped switch back have been used in YBCO based fault current limiters [118]; the difference is that in this bypass-switch there is heater co-wound with the HTS. Electrical insulation was provided by a double layer of  $12.7 \text{ }\mu\text{m}$  polyimide insulation; a double layer was used reduce the effect of pin holes. The polyimide was pre-coated with  $12.7 \text{ }\mu\text{m}$  of epoxy on each side and the switch was cured in an oven at  $140 \text{ }^\circ\text{C}$  for two hours. At  $1 \text{ kV}$  the insulation resistance between the heater and HTS tapes was measured to be greater than  $1 \text{ G}\Omega$ . As in the case of the dump-switch, soldering to the HTS tape was performed at  $160 \text{ }^\circ\text{C}$  with 99.99 % pure indium to avoid de-soldering the cladding.

About  $5 \text{ m}$  of superconductor was used for the coil, this gave a room temperature resistance of about  $1.7 \text{ }\Omega$  (Table 4.3). The heater was wound in the same manner as the HTS and so had the same length and a room temperature resistance of  $3.6 \text{ }\Omega$ . The thickness ( $0.05 \text{ mm}$ ) of the heater was the same as for the dump-switch but due to the difference in design the heat capacity and resistance of the heater was increased per length of superconductor. The increase in resistance leads to a longer capacitor discharge time. The heater was powered



No. of Modules	$I_c$ (77 K) (A)	$R_S$ (300 K) ( $\Omega$ )	$R_L$ (m $\Omega$ )	$R_H$ (300 K) ( $\Omega$ )	$R_H$ (77 K) ( $\Omega$ )	$R_{DR}$ (m $\Omega$ )
1	57	1.71	10.4	3.69	1.72	16.5
4	220	0.41	2.62	0.891	0.416	8.4

TABLE 4.3: Metrics of YBCO based bypass-switches with stainless steel cladding. The length of each module is about 5 m.  $R_S$  is the switch resistance,  $R_L$  the total lead resistance,  $R_H$  the heater resistance, and  $R_{DR}$  the resistance of the parallel dump resistor.

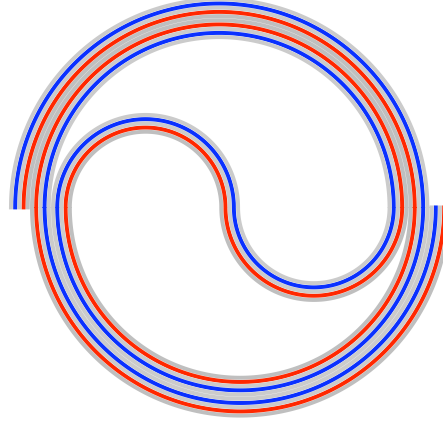


FIGURE 4.2: Sketch of 1.5 turns of a switch (not to scale) showing the non-inductive winding of the HTS, heater, and insulation with the switch back located in the centre of the switch. The HTS is shown in blue, the heater in red, and the insulation in grey. The diameter of the switch is about 100 mm.

by a 1.6 mF capacitor discharge that was controlled by a thyristor. The charge voltage of the capacitor was in the range 100 V to 1 kV, equivalent to energy of the range 8 J to 800 J.

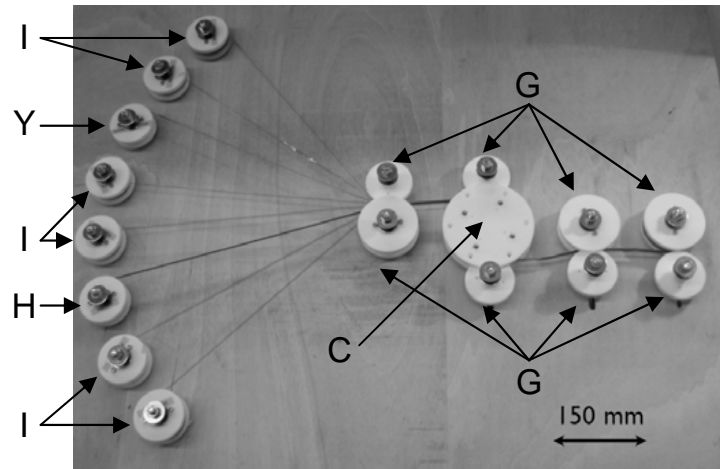


FIGURE 4.3: A machine for assisting with winding the multilayer bypass-switches. I indicates spools of insulation; H, spool of steel tape; Y, spool of YBCO tape; G, guides; C the coil. Friction brakes were mounted on each axle.

To allow scaling of the switch to higher transport current the coil had a modular design.

A single coil had an  $I_c$  of  $\approx 55$  A at 77 K, a length of  $\approx 5$  m, and a resistance of  $\approx 1.7 \Omega$  at room temperature. This single coil was tested as a bypass-switch with a  $16.5 \text{ m}\Omega$  resistor connected in parallel at room temperature. Resistive current leads with a total resistance of  $10.4 \text{ m}\Omega$  connected the HTS switch to the dump resistor. This switch was tested with non-decaying currents of 30 A to 50 A. To test the suitability of HTS switches to higher energy circuits four modules were connected in parallel giving the switch a critical current of 220 A. The parallel connection reduced the switch resistance to  $0.41 \Omega$  at room temperature and reduced the total current lead resistance to  $2.6 \text{ m}\Omega$ . The dump resistor that was connected in parallel was reduced to  $8.4 \text{ m}\Omega$ . The total heater resistance reduced to  $0.9 \Omega$  at room temperature and as the same capacitor circuit was used there was a faster discharge time constant but the amount of energy per unit length was reduced by a quarter.

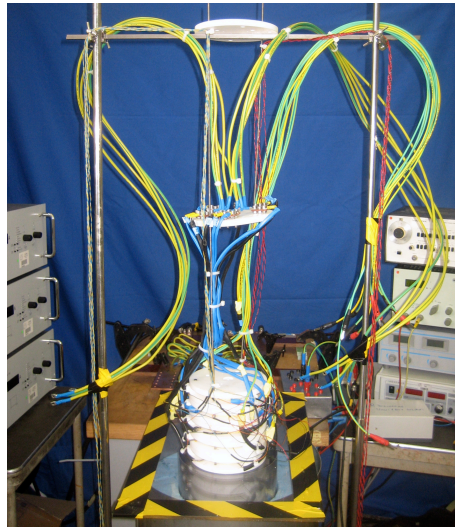


FIGURE 4.4: Photograph of the bypass-switch and test station. The switch is shown centre-bottom. Current leads, heater leads, and instrumentation wires lead up from the switch. The superconductor power supply is on the left, the heater controls are on the right. The cryostat is underneath the switch.

Due to the intricacy of winding all eight elements of the switch concurrently, a total length of  $\approx 40$  m, a purpose-built winding machine was used to provide assistance. The winding machine is shown in Figure 4.3 and also facilitated the manufacture of a number of modules. When using the winding machine half of the material was wound onto a common bobbin. The switch support was then placed between this bobbin and the spools of material; shaped pieces of Teflon supported the “S” shaped switch back. The switch was the rotated drawing in material from both the bobbin and the spools. The minimum bending diameter was limited to 50 mm so as not to damage the tape and friction brakes were mounted on each axle in order to provide a light tension. Soldering to the HTS tape was performed with indium solder and the current leads and heater leads had additional mechanical support where they were attached to the switch. The critical current and resistance of each module was measured individually but the voltage traces during switching were only

recorded across the dump resistor due to restrictions with the data acquisition system. A photograph of the experimental set-up is shown in Figure 4.4. The switch is shown centre-bottom with the current leads, heater leads and instrumentation wires leading upwards. The cryostat into which the switch is lowered is underneath the switch, this was slowly filled with liquid nitrogen once the switch was in place. The superconductor power supply is to the left of the photograph; the heater controls and capacitor charging system are shown on the right. The heater capacitor and the warm dump resistors are hidden behind the switch and cryostat.

### 4.3 Experimental Results of Dump-Switches

Dump-switches utilizing YBCO Cu and YBCO SS were manufactured as described in Section 4.2.1. These switches had a room temperature resistance of  $\approx 75 \text{ m}\Omega$  for the copper clad YBCO and  $\approx 0.6 \text{ }\Omega$  for the stainless steel clad switch. Both switches had a length of  $\approx 1.75 \text{ m}$  and a critical current of  $\approx 45 \text{ A}$  at  $77 \text{ K}$ . The switches were co-wound with a  $1 \text{ }\Omega$  heater that was powered by the discharge of a  $1.6 \text{ mF}$  capacitor.

#### 4.3.1 Heater Dynamics

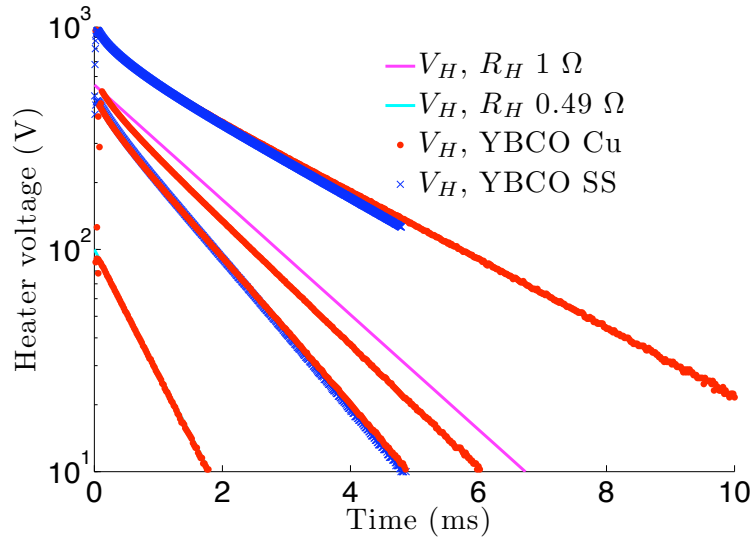


FIGURE 4.5: Heater voltage decays for YBCO dump-switches. Voltage decays are shown for the heater having a constant resistance equivalent to the  $77 \text{ K}$  resistance ( $0.49 \text{ }\Omega$ ) and the  $300 \text{ K}$  resistance ( $1 \text{ }\Omega$ ). Data for the YBCO SS switches was recorded for  $5 \text{ ms}$ .

The switch was triggered without transport current in order to investigate the heater dynamics. The heater voltage decay was not a normal exponential capacitor decay as there was an increase in heater resistance with temperature. The switches were tested with capacitor charge voltages in the range of  $100 \text{ V}$  to  $1 \text{ kV}$ . Figure 4.5 shows the heater voltage decays for these switches. The capacitor decay profiles for the heater at a constant

resistance of  $0.49 \, \Omega$  and at  $1 \, \Omega$  are also shown. These resistances are equivalent to a constant heater temperature of 77 K and 300 K respectively. For low heater energies, the resulting temperature rise is low and the discharge profile is similar to the constant resistance case. For a 100 V capacitor charge voltage, equivalent to an energy of only 8 J, the heater voltage decay is the same as for a  $0.49 \, \Omega$  resistance. This implies that the switch temperature remains constant at 77 K. For a 550 V capacitor charge voltage, equivalent to an energy of 242 J, there is an initially fast decay due to the lower resistance at 77 K. The discharge slows down as the rise in temperature causes the resistance to also rise. Once most of the energy has been discharged the voltage decay has a slope that is steeper than the voltage decay with a  $1 \, \Omega$  resistor implying that the temperature is less than 300 K. The heaters with  $V_{HI}$  of 1 kV also have an initially fast discharge due to the initially low resistance at 77 K but due to the large stored energy (800 J) there is a larger temperature rise causing a larger increase in resistance and a lower rate of voltage decay. The experimental data for all of the test heater decays are shown along with a smoothed spline fit in Figure 4.6.

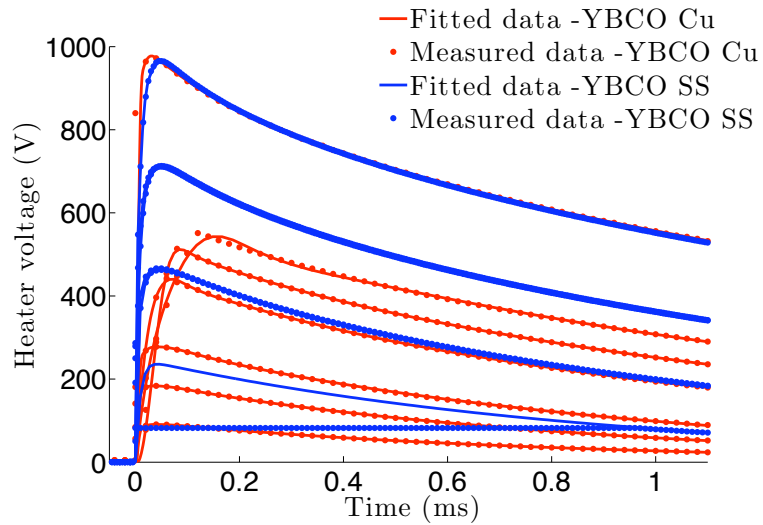


FIGURE 4.6: Measured and fitted heater voltage decays. The fitting was performed with a smoothed spline. The measured voltage of the YBCO SS switch that had a  $V_{HI}$  of 250 V was limited to a maximum of 82 V by the data acquisition system.

**The inductance of the heater** circuit is low but causes a small modification to the voltage characteristics of the heater. This small inductance is due to winding the heater into a spiral without a switch-back; the superconductor with which it is co-wound has switch-back and so has a much lower inductance. This inductance causes the heater voltage to have a non-zero rise time ( $\tau_r$ ) and a lower peak voltage than expected by a purely resistive capacitor decay. The voltage of this series resistor-inductor-capacitor circuit is

$$V_H(t) = V_{HI} \left( e^{\left(\frac{-t}{RC}\right)} - e^{\left(\frac{-tR}{L}\right)} \right). \quad (4.1)$$

With a rise time of

$$\tau_r = \frac{RLC \log(\frac{R^2 C}{L})}{R^2 C - L}. \quad (4.2)$$

The inductance of the heater circuit can be estimated by comparing the heater voltage profile of the experiment with a  $V_{HI}$  of 100 V to Equation 4.1. The  $V_{HI}$  of 100 V results are used for this estimation as due to the low input energy the temperature rise is not significant and so there is a constant heater resistance equivalent to the 77 K value. Figure 4.7 shows the experimental results and the ideal  $RLC$  circuit voltage for a constant heater resistance of  $0.5 \Omega$  and inductances of  $1 \mu\text{H}$ ,  $5 \mu\text{H}$ , and  $10 \mu\text{H}$ . The heater circuit has an inductance of about  $5 \mu\text{H}$ , which gives a rise time of  $44 \mu\text{s}$ .

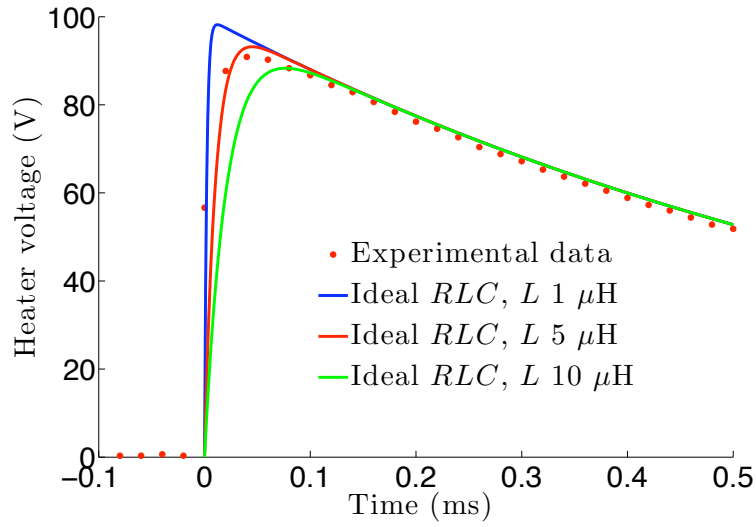


FIGURE 4.7: Measured heater voltage decay compared to an ideal  $RLC$  circuit. Time of zero corresponds to the initiation of the heater voltage rise.

Higher capacitor charge voltage situations, which have a higher energy, deviate from the ideal  $RLC$  circuit that has a constant heater resistance due to the increase in heater resistance with temperature.

**The energy in the heater** circuit is provided by the capacitor that has a capacitance of  $1.6 \text{ mF}$  and a charge voltage from  $100 \text{ V}$  to  $1 \text{ kV}$ . The current in the the heater can be estimated by differentiating the fitted heater voltage;

$$I_H(t) = C \frac{dV_H(t)}{dt}. \quad (4.3)$$

The cumulative energy deposited in the heater ( $E_H$ ) can be estimated by integrating the heater voltage and current;

$$\begin{aligned} E_H(t) &= \int_0^t I_H(t) V_H(t) dt \\ &= \frac{1}{2} C V_H^2(t). \end{aligned} \quad (4.4)$$

The heater energy deposition as a function of time for different capacitor charge voltages is shown in Figure 4.8. The energy stored in the capacitor ( $0.5CV_{HI}^2$ ) is also shown. The same heater circuit and same length of heater are used in both switches and so they have similar energy deposition profiles. The estimation of the total heater energy is generally less than the energy stored in the capacitor. This is due to losses in the rest of the heater circuit and errors in fitting the data which lead to an underestimation of the derivative and so lower estimated voltages. The heaters that have higher capacitor charge voltages discharge slower as the heaters become hotter and more resistive thus increasing the time constant of the capacitor discharge.

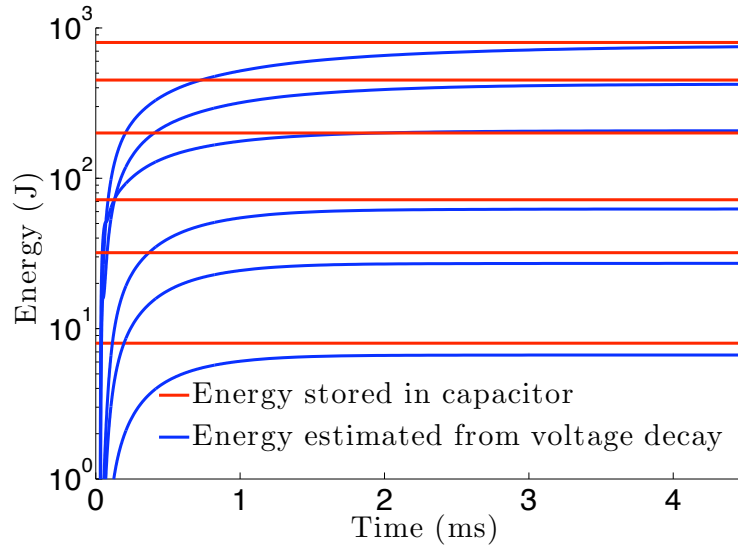


FIGURE 4.8: Heater energy deposition for capacitor charge voltages of 100 V, 200 V, 300 V, 500 V, 750, and 1 kV. The estimated heater energy is calculated from the heater voltage and its differential.

**Voltages induced into the superconductor** are a result of inductively winding the heater with the superconductor. In order to reduce the inductance of the switch the superconductor has a switch-back. As the induced current is in the same direction as the heater current one half of the superconductor has a positive voltage and the other has a negative voltage. If the two legs had the same length the overall induced voltage would be zero. However, the two legs of the switch have different lengths in order to offset the attachment points of the current leads. This leads to there being a non-zero overall voltage that is smaller than in each of the legs. The induced voltages are shown in Figure 4.9 for both copper clad YBCO switches and stainless steel clad YBCO switches. The YBCO SS switches were tested with a higher time resolution than the YBCO Cu switches in order to allow the initial transients to be better observed. Flat spots on the voltage curves are where the data was outside of the scope range.

The voltage induced in the superconductor is proportional to the rate of change of the heater voltage. Due to the non-linear rise and fall of the heater voltage there is a positive maximum voltage induced in the superconductor during ramp up and a negative maximum

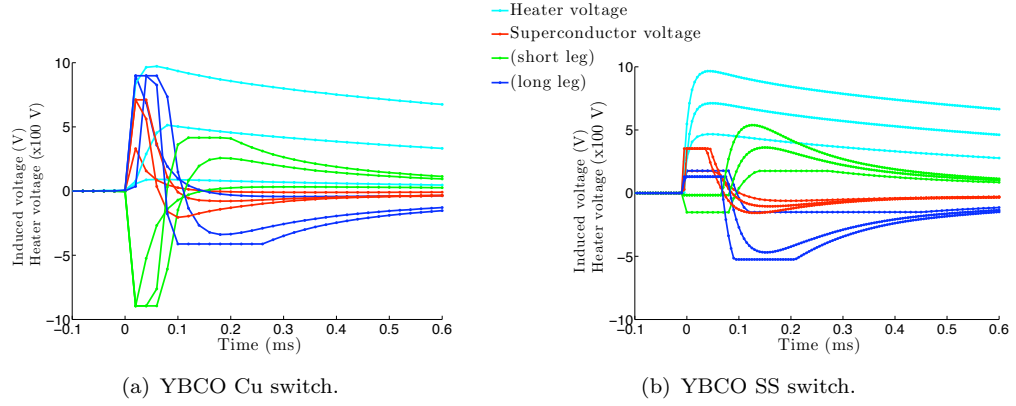


FIGURE 4.9: Voltages induced in the switch by the heater capacitor discharge. Due to the switch-back in the superconductor the short ( $\approx 75$  cm) leg has a voltage in the opposite sense to the heater and the long ( $\approx 100$  cm) leg of the switch. Time zero is the onset of capacitor voltage rise. Flat spots in the voltages are where the voltage is out of range of the acquisition system.

voltage induced in the superconductor during ramp down. During the voltage rise of the capacitor the derivative of the heater voltage is positive and so the voltage induced in the superconductor is also positive. There is reversal in the  $\frac{d^2 V_H}{dt^2}$  during ramp up and so the superconductor voltage will have a maximum. At the peak heater voltage there is zero slope and so the superconductor voltage is zero. During the capacitor discharge the derivative of the heater voltage is negative and so the voltage induced in the superconductor is also negative. As the inductive time constant of the heater circuit is much smaller than the capacitive time constant, the rate of voltage increase is much faster than the rate of voltage decay. The higher  $\frac{dV_H}{dt}$  during ramp up causes there to be a larger voltage induced in the superconductor at times less than the rise time than after the rise time when the capacitor is discharging with a lower  $\frac{dV_H}{dt}$ . As the rise and fall times of an  $RLC$  circuit do not vary with the capacitor charge voltage, the magnitude of  $\frac{dV_H}{dt}$  must increase with increasing  $V_{HI}$ . This causes the voltages induced in the superconductor to be higher when the capacitor charge voltage is also higher. These maximum voltages are shown in Figure 4.10. The increase in heater resistance with temperature slows down the capacitor discharge resulting in a lower  $\frac{dV_H}{dt}$  and induced voltage. The heater circuits with the longest discharge times are in the switches that have high  $V_{HI}$  due to the hotter and more resistive heaters. After  $\approx 0.5$  ms the total induced voltages have decayed to zero. The induced voltages occur on time scales of less than 1 ms and so do not affect the voltage increase due to the warming of the current carrying superconductor.

### 4.3.2 Superconductor Dynamics

The recorded switch voltage is formed of two components, the voltage rise caused by the quenching superconductor and the voltage induced by the heater. The induced voltages were caused by co-winding the heater with the superconductor and occur even when there



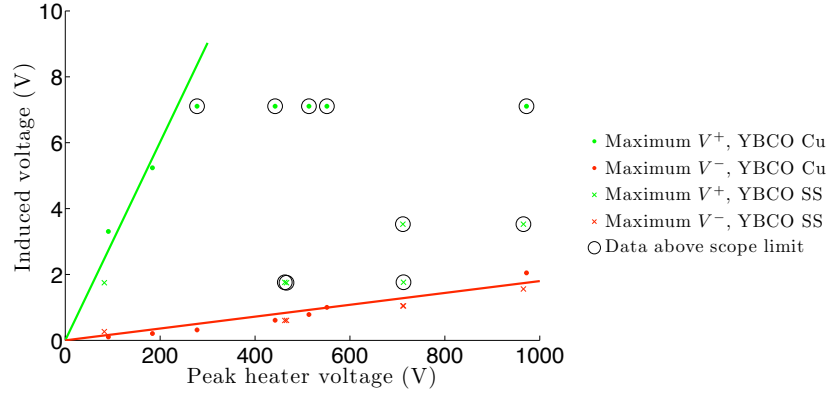


FIGURE 4.10: Induced voltage in the superconductor as a function of the peak heater voltage. The maximum  $V^+$  occurs during the rise of the heater voltage, the maximum  $V^-$  occurs during the discharge of the capacitor.

is no transport current. The heater dynamics and the resulting induced voltages were discussed in the previous section. The voltage rise and the resulting energy dissipation that resulted from warming the superconductor above the fully superconducting state is discussed below.

**The voltage rise of the YBCO Cu** based switch when it was triggered with a 1 kV capacitor discharge is shown in Figure 4.11. The induced voltages decay to zero at around the same time as the voltage begins to rise due to the quenching superconductor. In order to remove the voltage rise that was induced by the heater, the switch was tested with no transport current and the resulting voltages were subtracted from when the switch was triggered with current. The switch was tested three times with current and the data was fit with a smoothed spline, which had the induced voltages removed.

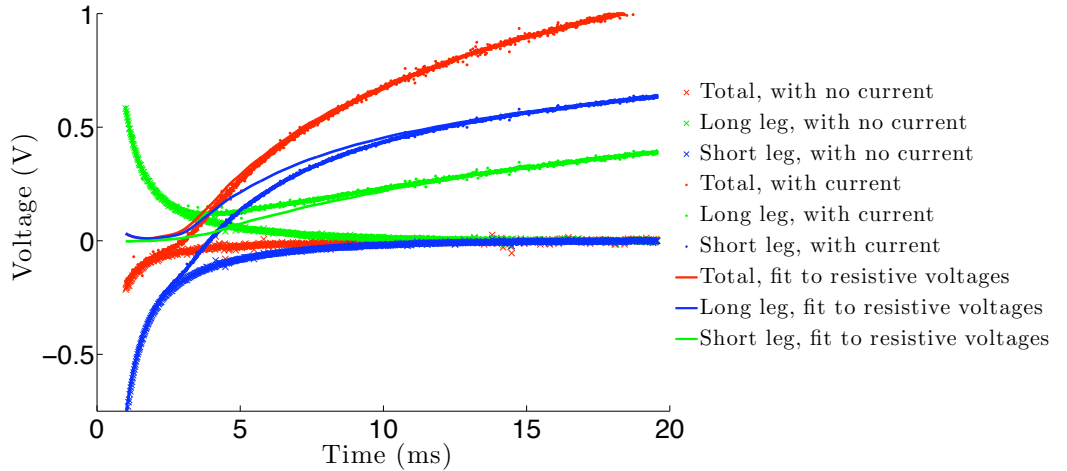


FIGURE 4.11: Voltage traces for the YBCO Cu switch when triggered with a 1 kV capacitor discharge. The applied current was 40 A. When no current was applied there are still voltages induced in the superconductor by the heater. Three experiments were performed and the fit represents the average voltage with the induced voltages subtracted.

Time zero is when the heater voltage begins to rise.



The voltage rise is higher on the longer leg as the increase in length means that it is more resistive. The longer leg also has a marginally lower current sharing temperature, 78.9 K compared to 78.5 K, and so it will develop a slightly higher electric field when in the current sharing region. The total voltage drop is higher than the sum of the two legs due to the soldered joint between the legs that has a resistance of about  $0.28 \mu\Omega$ .

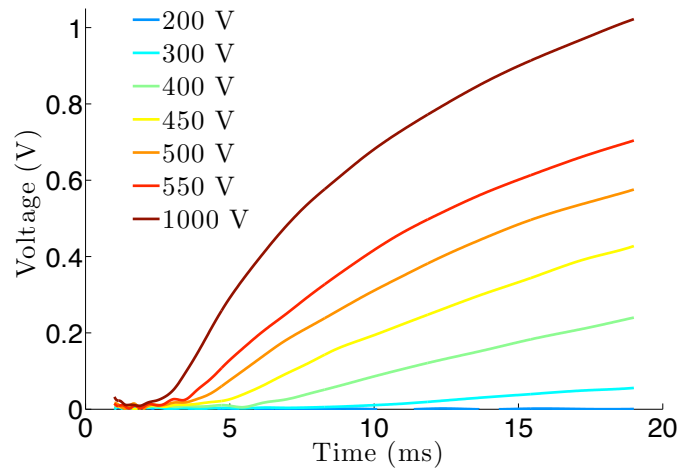


FIGURE 4.12: Voltage traces for the YBCO Cu switch when triggered with a capacitor discharge. The applied current was 40 A. The fit represents the average voltage with the induced voltages subtracted. Time zero is when the heater voltage begins to rise.

The voltage traces for the copper clad switch carrying 40 A when it is triggered with a range of capacitor charge voltages, are shown in Figure 4.12. With capacitor charge voltages of 200 V or less no voltage rise was measured and the switch did not trigger in  $< 20$  ms. Increasing the capacitor charge voltage, and therefore the heater energy, causes both an earlier onset of transition and a higher voltage. This is because the heater gets hotter faster and so there is a greater rate of heat conduction through the insulation. The higher energy means that the switch rises to a higher final temperature where it has a higher resistance.

Within the measured time, about 20 ms, the switch did not become fully normal even when it was triggered with a capacitor charged to 1 kV. If the switch went fully normal then there would have been a voltage drop of 0.56 V/m when carrying 40 A. Due to self heating of the switch the voltage would continue to rise after 20 ms.

**The voltage rise of the YBCO SS** based switch when it was triggered with a 1 kV capacitor discharge is shown in Figure 4.13. As for the copper clad switches described above there is a smoothed spline fit to the experimental data that has the induced voltages removed. The induced voltages were measured by triggering the switch without transport current. In the stainless steel clad switch the difference in voltage between the long leg and the short leg is greater than can be explained by length alone. The reason for the large difference is the much higher critical current of the short leg, 77 A compared to 45 A. This results in the current sharing temperature of the short leg being 82.6 K whereas it is

only 78.3 K in the long leg. The higher current sharing temperature means that it takes longer for the short leg to warm up to the current sharing regime and once in the current sharing regime the voltage drop is lower than for the longer lower  $I_c$  leg. This results in the voltage of the long leg starting to rise at  $\approx 2.5$  ms whereas it does not rise in the short leg until  $\approx 3.5$  ms. After  $\approx 3.75$  ms the power supply tripped and the current reduced.

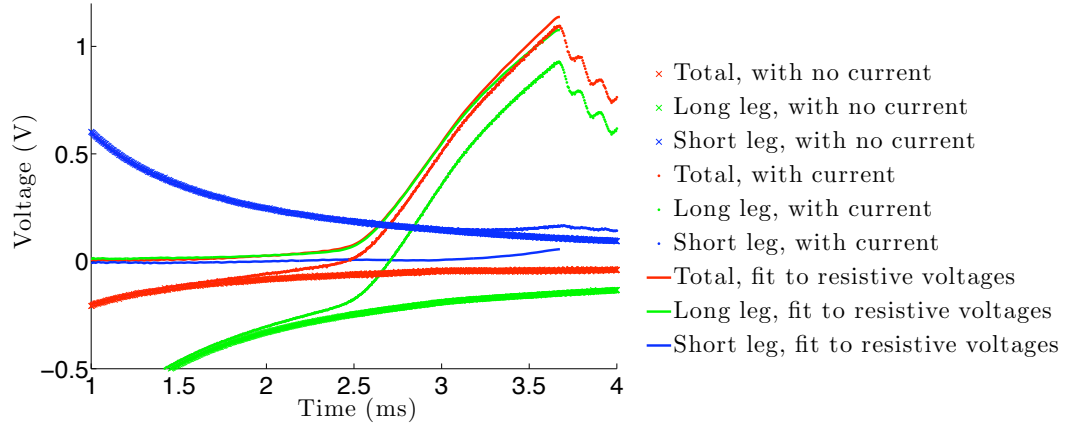


FIGURE 4.13: Voltage traces for the YBCO SS switch when triggered with a 1 kV capacitor discharge. The applied current was 40 A. When no current was applied there are still voltages induced in the superconductor by the heater. The fit represents the voltage with the induced voltages subtracted. Time zero is when the heater voltage begins to rise. After about 3.75 ms the power supply tripped and the current reduced.

Figure 4.14 shows the voltage rise of the stainless steel clad YBCO based switch when it was carrying a range of transport currents and it had a range of capacitor charge voltages. Capacitor charge voltages of 100 V did not cause the switch to trigger even when the transport current was  $\approx 90\%$  of  $I_c$  as not enough energy was input into the switch to cause the superconductor to quench. The final time of the YBCO SS based switches is less than for the copper clad switches due to the higher resistance giving higher voltages that caused the power supply to trip and also a smaller time step meaning that the final recorded time was less. If the whole switch had quenched the switch would have developed a voltage of  $\approx 4.5$  V/m, but as this was not achieved the implication is that the switch did not fully quench and the energy was only dissipated in the lower voltage current sharing regime. Increasing the capacitor charge voltage leads to fast switching times as the heater gets hotter faster leading to faster heat transfer through the insulation. Increasing the transport current reduces the switching time as the temperature margin is also lowered so less energy is needed to be input into the switch before self heating begins.

**The energy dissipated in the superconductor** can be calculated from the resistive voltage increase and the known transport current that always flows through the superconducting tape as these switches are dump-switches. The cumulative energy dissipated in the switch can be calculated by integrating the voltage and current;

$$E(t) = \int_0^t I_{op} V(t) dt. \quad (4.5)$$

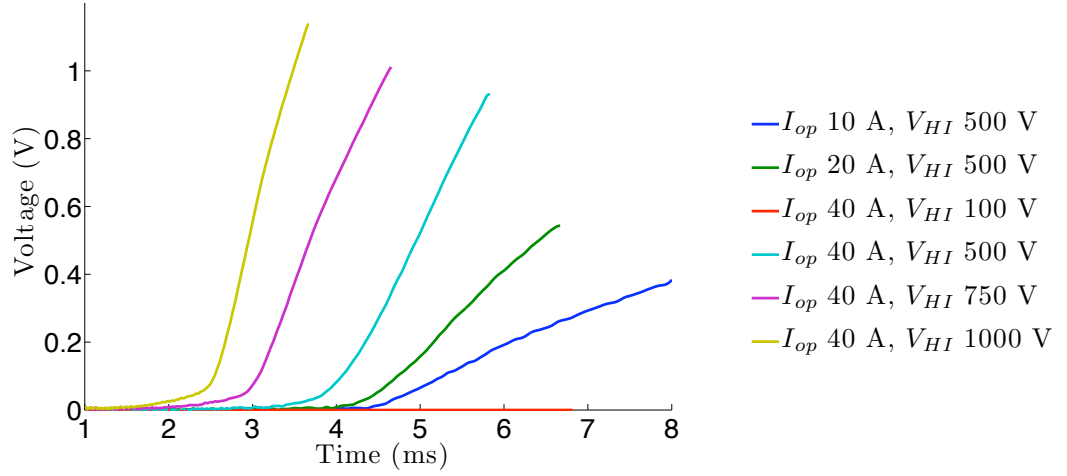


FIGURE 4.14: Voltage evolution for the YBCO based dump-switches with a constant operating current.

Figure 4.15 shows the cumulative energy dissipation in YBCO based switches that have either copper or stainless steel cladding. The copper clad switch had an  $I_{op}$  of 40 A, the stainless steel clad had  $I_{op}$  of 10 A, 20 A, or 40 A. The switches were triggered with capacitors that had charge voltages from 100 V to 1 kV. For both switches increasing the capacitor charge voltage means that in a given time more energy is dissipated in the switch. This is because the switch gets hotter and thus more resistive yet the transport current does not decay leading to high switch powers. The stainless steel clad switch starts to dissipate energy before the copper clad switch due to its faster voltage rise that results from its higher normal state resistivity. In total the copper clad YBCO switches dissipate more energy than the stainless steel clad YBCO switches as the lower resistance means that the voltage is also lower and so the power supply does not trip. In a dump-switch where the limit is the final temperature of the switch then these two switches could dissipate about the same energy as they have the same enthalpy. However, if the same dump resistance was required then the length of the copper clad switch would be greater and so the enthalpy change to the final temperature would also be greater and so the switch could dissipate more energy. In the experiments, both switches had the about the same final voltage ( $\approx 1$  V) and therefore resistance when they were transporting 40 A and were triggered with a 1 kV capacitor discharge. The stainless steel clad switch reached this voltage in 3.5 ms and the copper clad switch in 18.2 ms. In this time the copper clad switch dissipated  $\approx 400$  mJ whereas the stainless steel clad switch only dissipated  $\approx 25$  mJ.

**The superconductor temperature** can be estimated from the  $V - I$  characteristics of the tape. For these dump switches that have a constant current the voltage-temperature relationships are shown in Figure 4.16 Above the critical temperature, the determination of the superconductor temperature depends upon the normal state resistivity of the tape. Beneath the critical temperature, where the superconductor is in the current-sharing regime, the voltage-temperature relationship depends on the non-linear  $V - I$  characteristics of the superconductor. When the superconductor is fully superconducting, the voltage is zero for

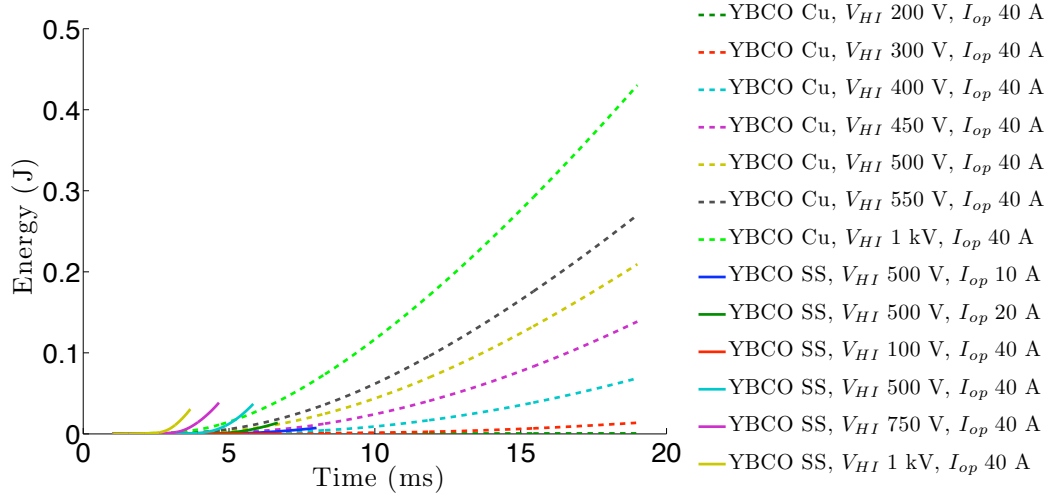


FIGURE 4.15: Energy dissipated in YBCO dump switches that were triggered by a capacitor that was charged to a voltage  $V_{HI}$ . The switch length was about 1.75 m and the transport current ( $I_{op}$ ) was constant.

all temperatures and so the temperature can not be estimated from the measured voltage. These switches were triggered by a 500 V capacitor discharge that provided 200 J. This energy would be enough to heat up the YBCO Cu switch to  $\approx 125$  K and the YBCO SS switch to 135 K. Due to heat loss to the surrounds, including the support, extra insulation, and the coolant, the actual temperature rise is less than this.

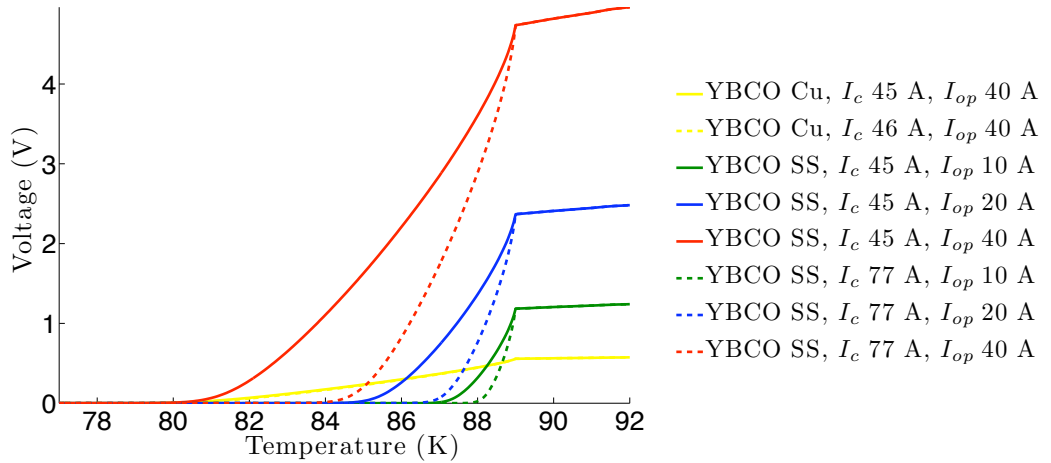


FIGURE 4.16: Voltage as a function of temperature of YBCO based tapes that have different critical currents and carry different transport currents.

The current sharing temperature depends on both the critical current of the tape and the transport current of the switch. The experimental switches had non-homogenous critical currents and were tested at different transport currents resulting in a range of current sharing temperatures (Table 4.4). When the switch had a temperature around or below this temperature, the estimation of temperature from voltage is not valid. The estimated temperature rise of YBCO based switches with either stainless steel cladding or copper

cladding are shown in Figure 4.17. The temperature is estimated for each leg due to the differences in critical current; variations in critical current along the leg itself cause an uncertainty in the estimation. The long YBCO SS leg has the lowest temperature margin due to its low critical current and so the temperature rise is recorded first on this leg. The critical current of the short YBCO SS leg is higher and so the temperature margin is also higher. This means that the temperature rise is not recorded until the estimation is greater than 83.5 K. Due to the high normal state resistivity of the stainless steel clad YBCO it has a faster rate of temperature rise than the YBCO Cu as the high electrical power is also higher. The temperature margin of the two YBCO Cu legs are about the same and so the estimated temperature rises should also be similar. The difference in the estimated temperature could be due to a non-homogenous critical current along the leg length causing part of the superconductor to be in the current sharing regime and part of the tape to be fully superconducting, this would lead to an error in the estimation of the temperature. Despite the distributed heater and low thermal resistivity between the legs, due to the thin layer of insulation, small temperature gradients could exist in the switch due to increased local heating in areas with a low critical current.

Superconductor	$I_c(77\text{ K})$ (A)	$I_{op}$ (A)	$T_{cs}$ (K)
YBCO Cu	48	40	78.9
	46	40	78.5
		10	86.2
	45	20	83.5
YBCO SS		40	78.3
		10	87.4
	77	20	85.7
		40	82.6

TABLE 4.4: Superconducting properties of the tested YBCO based dump-switches.

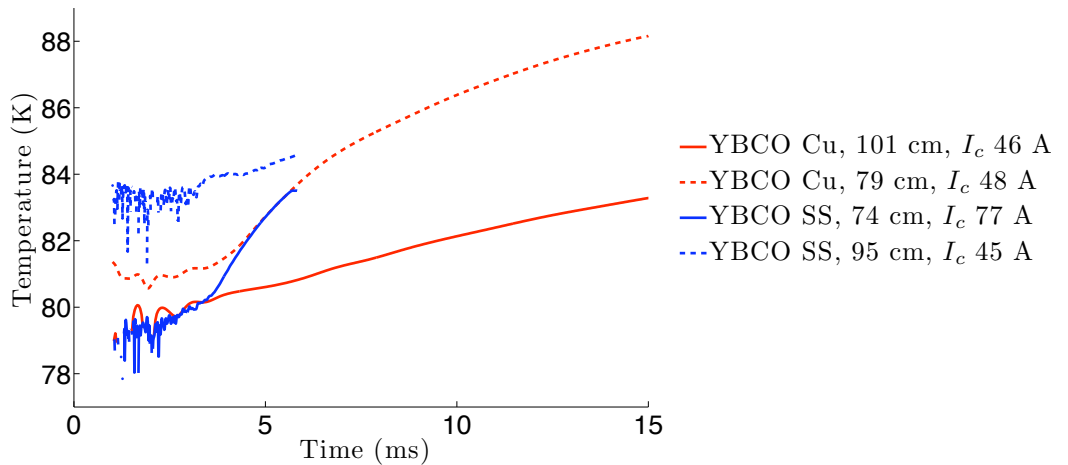


FIGURE 4.17: Estimated temperatures of YBCO based switches that transport 40 A and are triggered by a 500 V capacitor discharge. Temperature estimations around or below  $T_{cs}$  are not valid due to the zero resistance of the superconductor.

**The switching time** of these dump-switches is defined as the time taken from the initiation of the rise in the heater voltage to when the switch has a dump resistance equivalent to  $10\text{ m}\Omega$ . The voltage traces for the copper clad switch were shown in Figure 4.12 and for the stainless steel clad switch in Figure 4.14. The switching times for both switches when they carried  $40\text{ A}$  and were triggered with capacitor charge voltages from  $300\text{ V}$  to  $1\text{ kV}$ , are shown in Figure 4.18. The capacitor had an energy in the range  $70\text{--}800\text{ J}$ . The switch based on stainless steel clad YBCO switched faster than the copper clad version as its higher normal state resistivity meant that a lower temperature rise was needed in order to achieve the required dump resistance. The higher resistivity also made up for the higher  $T_{cs}$  of the short leg. If both legs had a critical current of  $45\text{ A}$  then the switching time would be less as the voltage would be developed along the whole tape at lower temperatures. The switching time is inversely proportional to the heater energy. The minimum energy that causes the switch to transition is the energy that is required to raise the temperature of the switch into the current sharing regime where self heating occurs. Whilst only  $\approx 5\text{ J}$  are required to raise this switch design to the current sharing temperature, the experimental switch was cooled and about ten times the heater energy was required to make up for that lost to the surrounds and to the support. The minimum switching time depends on the rate of heat conduction through the insulation. This is limited by the diffusion time of the insulation; for  $12\text{ }\mu\text{m}$  of polyimide the diffusion time is about  $1\text{ ms}$ . The experimental switch has a minimum switching time higher than this,  $\approx 2.5\text{ ms}$ , due to extra thermal resistance caused by the epoxy that joins the layers together and the non-zero temperature rise time of the heater.

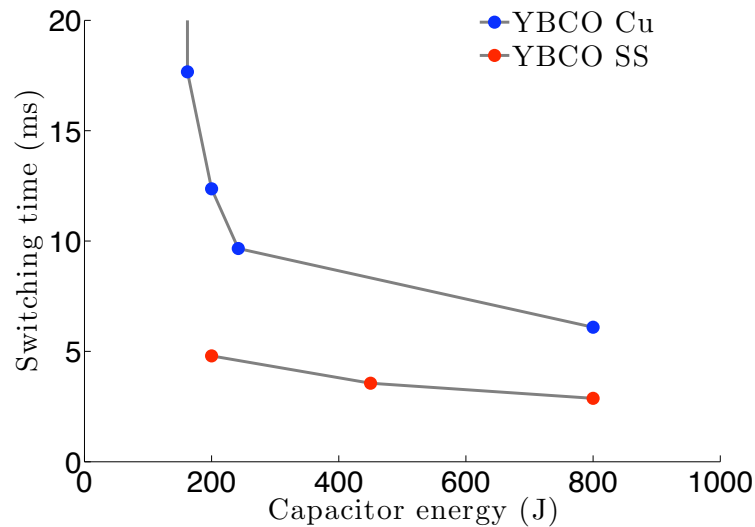


FIGURE 4.18: Switching time as a function of capacitor energy for YBCO Cu and YBCO SS based dump-switches that transport  $40\text{ A}$ .

Reducing the transport current causes an increase in the current sharing temperature and thus an increase in the temperature rise that the switch must undergo for a voltage to be developed. For the same input heater energy this will result in a slower switching time. The effect of the transport current on the switching time on an YBCO SS based dump-switch

that is triggered with a 500 V (200 J) capacitor discharge is shown in Figure 4.19. As the transport current tends to zero the current sharing temperature tends to the critical temperature and the switching time tends to a maximum; in this case  $\approx 4.75$  ms. The decrease in switching time with increasing current is dependent on the decrease in the critical current with temperature. As the transport current is increased the switching time decreases as the temperature margin is reduced. Increasing the transport current also means that there will be greater self heating once the switch is resistive, further decreasing the switching time.

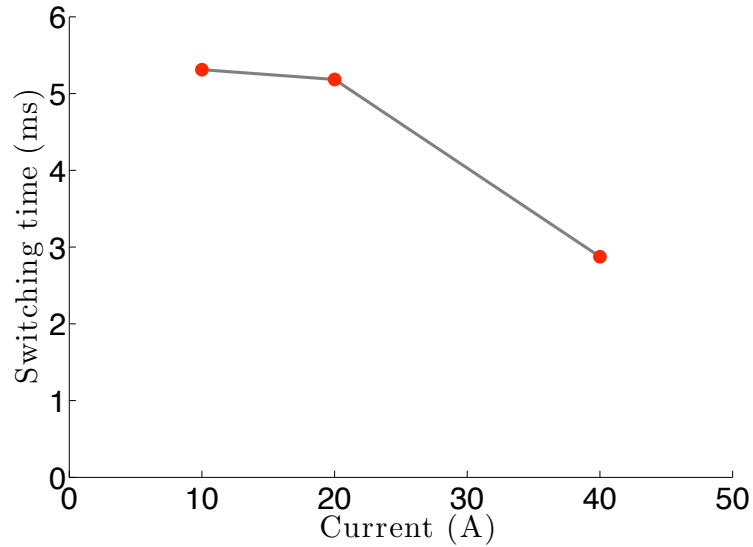


FIGURE 4.19: Switching time as a function of transport current for YBCO SS based dump-switches that are triggered with a 500 V (200 J) capacitor discharge.

### 4.3.3 Conclusions from Experiments on Dump-Switches

Dump switches that were formed of both stainless steel clad YBCO and of copper clad YBCO were tested in liquid nitrogen. The switches had a length of  $\approx 1.75$  m and a critical current of  $\approx 45$  A. The switches were triggered with a capacitor discharge that was charged in the range 100 V to 1 kV; an energy of 8 J to 800 J. Switching times of less than 5 ms were observed for both switches when the heater energy was greater than 200 J. The switching time was defined as the time taken from the rise in voltage of the heater until the switch had a resistance of 10 m $\Omega$ . The fast switching time was achieved by using a thin (12.7  $\mu\text{m}$ ) layer of polyimide insulation between the heater and the superconductor; epoxy was used to bond the superconductor to the polyimide to the insulation. The stainless steel clad YBCO switch had a slightly faster switching time than the copper clad version as its higher resistivity meant that it reached the required dump resistance at a lower temperature and there was greater self heating in the superconductor. The lower resistivity of the copper clad YBCO switch meant that it could dissipate more energy than the YBCO SS switch for the same upper voltage limit or temperature rise. Large variations in the critical current of the YBCO SS based switch meant that not all of the switch quenched at the same

time and the dump resistance was lower than if the switch had a homogenous critical current. Poor homogeneity in the critical current leads to poor switching characteristics and the potential for local hotspots. For a given dump resistance, copper clad YBCO shows the potential to be used where more energy must be dumped whereas stainless steel clad YBCO switches show potential to be used as lower energy dumps, these would require less conductor and a lower heater energy.

## 4.4 Experimental Results of Bypass-Switches

Bypass-switches formed of stainless steel clad YBCO were manufactured and tested as described in Section 4.2.2. About 5 m of superconductor was used per coil, giving a room temperature resistance of  $\approx 1.7 \Omega$  with a critical current of  $\approx 55$  A. The HTS switches had a modular design and four modules were connected in parallel to give a switch with a critical current of 220 A and a room temperature resistance of  $\approx 0.4 \Omega$ . The switches were tested in liquid nitrogen and had a warm dump resistor connected in parallel ( $16.5 \text{ m}\Omega$  for a single module,  $8.4 \text{ m}\Omega$  for four modules). The switch was triggered by a capacitor discharge through a heater co-wound with the superconductor. The capacitor had a charge voltage of up to 1 kV, equivalent to an energy of 800 J, and the heaters were also connected in parallel.

### 4.4.1 Heater Dynamics

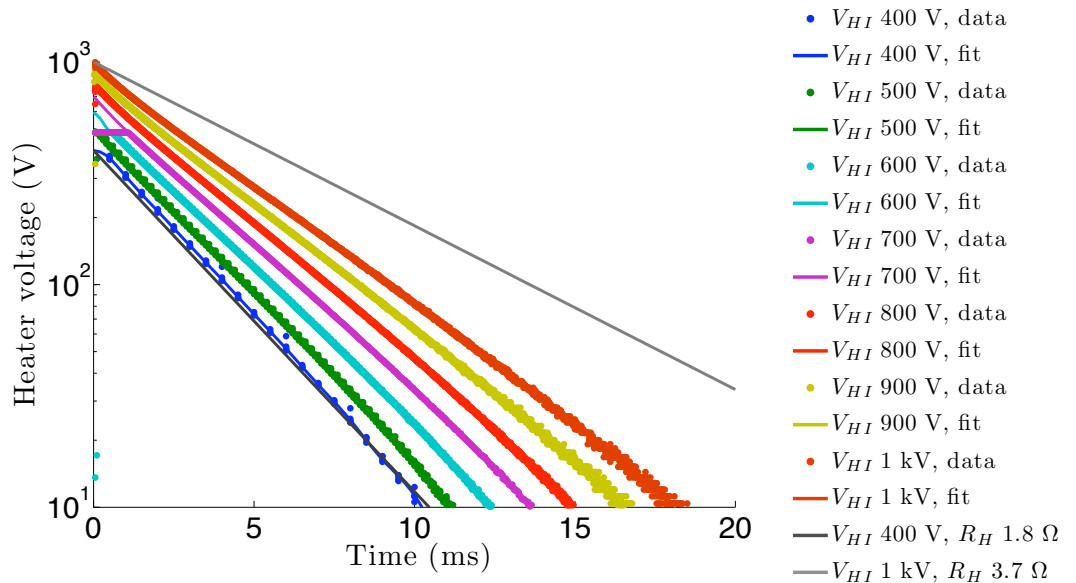


FIGURE 4.20: Heater voltage decays for stainless steel clad YBCO based bypass-switches. The fit is a smoothed spline to the average of a number (2-5) of tests. Voltage decays are also shown for the heater having a constant resistance equivalent to the 77 K resistance ( $1.8 \Omega$ ) and the 300 K resistance ( $3.7 \Omega$ ). The recorded voltage for  $V_{HI}$  of 500 V, 600 V, and 700 V saturated at 480 V. The data and fit are generally coincident.



The bypass-switch was initially triggered without transport current in order to investigate the heater dynamics. Figure 4.20 shows the heater voltage decay for a bypass-switch formed of one coil of stainless steel clad YBCO. As for the dump-switch, the heater voltage decay was not a normal exponential capacitor decay as there was an increase in heater resistance with temperature. The increase in resistance was less than for the dump-switch as the longer length and thicker insulation meant that the thermal mass was higher and so the final temperature was lower for the same input heater energy. The capacitor decay profiles for the heater at a constant resistance of  $1.8\ \Omega$  and at  $3.7\ \Omega$  are also shown. These resistances are equivalent to the heater having a constant temperature of 77 K and 300 K respectively. For low heater energies, the resulting temperature rise is low and the discharge profile is similar to the constant resistance case. For a 400 V capacitor charge voltage the heater voltage decay is the similar to that of the  $1.8\ \Omega$  resistance, implying that the switch temperature did not rise much above 77 K. For a 1 kV capacitor charge voltage the slope of the discharge is gentler than the  $1.8\ \Omega$  case but steeper than the  $3.7\ \Omega$  case implying that the heater temperature has increased from 77 K but has not reached 300 K. The experimental data for a number of tests were fitted with smoothed splines, the average for each capacitor charge voltage is shown in Figure 4.20.

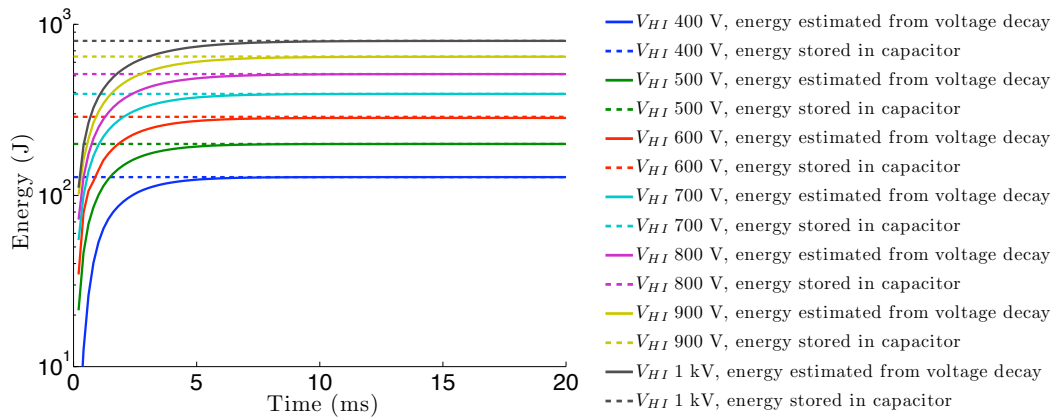


FIGURE 4.21: Heater energy deposition. The estimated heater energy is calculated from the heater voltage decay, the energy stored in the capacitor is calculated from the charge voltage of the capacitor.

Due to the switch-back in the center of the heater the inductance of the heater in the bypass-switch is lower than that of the dump-switch. This leads to a faster heater voltage rise time and as the length is better matched to the length of the superconductor there are lower induced voltages. The energy deposited in the heater can be calculated as a function of time from the voltage decay ( $\frac{1}{2}CV^2(t)$ ). As the capacitor discharges its energy is deposited in the heater causing the switch to heat up. The increasing energy deposition in the heater is shown in Figure 4.21, where the energy stored in the capacitor is also shown. The majority of the energy has been deposited within 5 ms to 10 ms with the higher energy switches having a slower discharge time due to the increased heater resistance at higher temperatures.

#### 4.4.2 Switching Dynamics with a Single Coil Bypass-Switch

The voltage of the system was measured across the dump resistor and is the voltage of energy extraction. There is an initial voltage even when the switch is fully superconducting due to the resistance of the current leads that are in series with the switch. The total resistance of the current leads is  $10.4 \text{ m}\Omega$  and as they are in parallel with a  $16.5 \text{ m}\Omega$  dump resistor the total resistance is  $6.4 \text{ m}\Omega$ . The voltage traces for the system when there is a constant operating current of 40 A and of 50 A are shown in Figure 4.22. A smoothed spline was fit to a number of test runs. At times less than 5 ms there were some voltages induced in the switch due to the heater capacitor discharge.

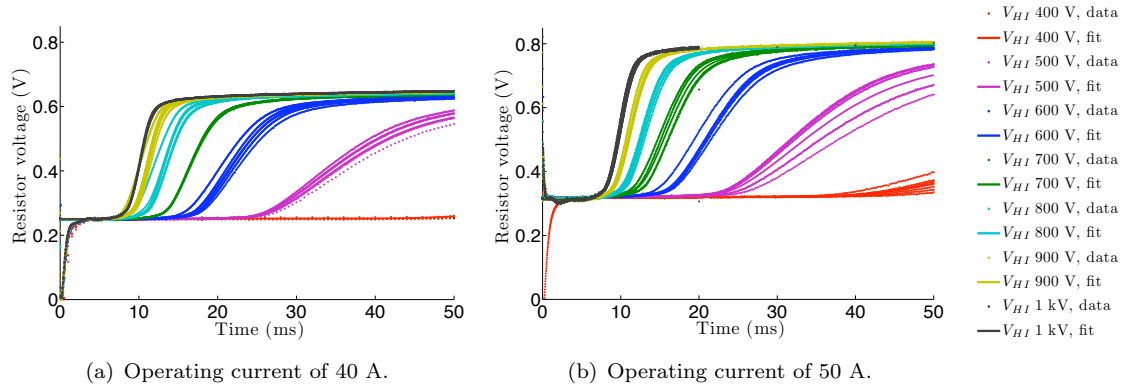


FIGURE 4.22: Voltages measured across the dump resistor for a one coil bypass-switch formed of stainless steel clad YBCO. The data is from a number of experiments and the fit is a smoothed spline of the average.

Higher heater energies cause a faster voltage rise due to the more rapid heating of the heater and thus higher heat conduction through the insulation. The lower current sharing temperature of the higher operating current switch means that it has a faster initiation of voltage rise. However, as the current bypass the switch once it starts to develop a voltage the operating current has less of an effect on the switching characteristics than it does for the dump-switch. At low capacitor charge voltages, below 600 V (288 J), there is not enough heat energy input into the switch to cause a full transition. Self heating due to the transport current is low as the current bypass the switch in the parallel resistor. As the switch is cooled it will recover back to the superconducting state.

**The current distribution** between the switch and the dump resistor is shown in Figure 4.23. As the switch is initially superconducting most of the current flows through the switch; however, some current flows through the dump resistor due to the resistive current leads. The critical current decreases with increasing temperature and so above the current sharing temperature more current will flow in the matrix and parallel dump resistor. As the critical current approaches zero most of the current will flow in the dump resistor with only a small amount flowing in the much more resistive switch. The small amount of current flowing through the switch will cause self heating and help balance heat lost to the

coolant. A decrease in temperature would also cause a decrease in the switch resistance but an increase in the self heating due to the increased current flow.

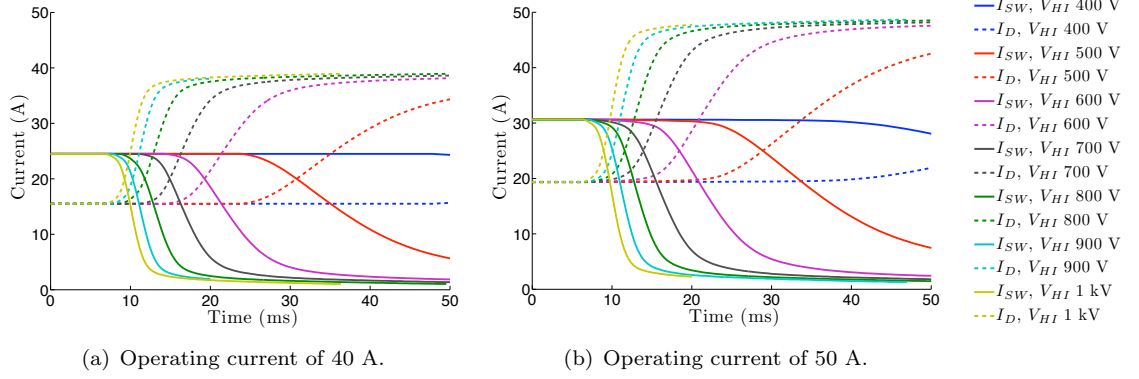


FIGURE 4.23: Current in a stainless steel clad YBCO bypass-switch.  $I_{SW}$  is the current in the switch,  $I_D$  is the current in the parallel dump resistor. The operating current ( $I_{op}$ ) does not decay with time.

**The evolution of the dump resistance** is shown in Figure 4.24. As mentioned at the start of this section the initial resistance of the system is  $6.4 \text{ m}\Omega$  due to the resistive current leads ( $10 \text{ m}\Omega$ ) connected in parallel to the dump resistor. As the switch warms up the total dump resistance increases due to the non-linear  $VI$  characteristics of the superconducting switch. Once the switch has warmed to the critical temperature the dump resistance is dominated by the parallel resistor. Increasing the temperature above the critical temperature has less of an affect on the dump resistance as the rate of change of resistance with temperature is less steep. The increase in dump resistance due to heating of the fully normal switch appears as a gradual resistance rise after the kink in the graph.

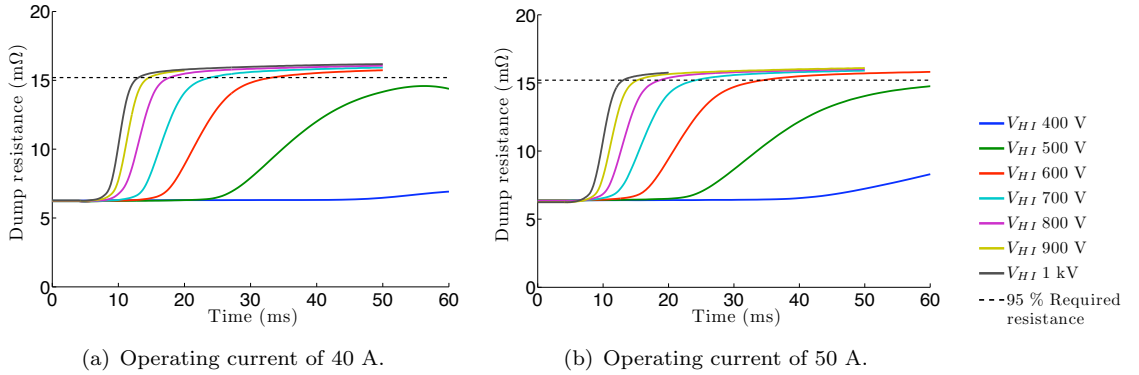


FIGURE 4.24: Dump resistance of an YBCO bypass-switch with a room temperature resistance of  $3.7 \text{ }\Omega$  connected in parallel with a  $16.5 \text{ m}\Omega$  dump resistor.

In this particular case the required dump resistance was  $16 \text{ m}\Omega$  that can be achieved by warming a  $5 \text{ m}$  long stainless steel clad YBCO switch to just above  $T_c$  with a parallel connected dump resistor of  $16.5 \text{ m}\Omega$ . Whilst the onset of voltage rise occurs as soon as the switch is no longer fully superconducting, the switching time is defined as the time taken for 95 % of the total dump resistance to be developed. At this point most of the energy

dissipation is occurring in the dump resistor as the switch is almost completely bypassed. When there was insufficient heater energy the switch resistance decreases as the switch re-cools and the critical current increases with the falling switch temperature.

**The switch temperature** can be estimated from the non-linear  $VI$  characteristics of the superconductor, the constant operating current, and the known resistances of the matrix, dump resistor, and current leads. The estimation of switch temperature is shown in Figure 4.25. When the switch is fully superconducting the switch temperature can not be estimated as there is a zero switch voltage for a wide range of temperatures. Similarly the temperature estimation is not valid around or below the current sharing temperature as the low voltage ( $1 \mu\text{V}/\text{cm}$  at  $T_{cs}$ ) is below the resolution of the data recorder. Above  $T_c$  when the switch is fully normal the total dump resistance is dominated by the lower resistance of the parallel dump. This means that even large increases in temperature of the switch will only cause a small increase in the voltage and so the temperature estimation of the switch is less accurate above  $T_c$ . The higher heater energies, up to 800 J that is provided by a capacitor that discharges within 20 ms, coupled to the thin insulation cause the switch to rise from  $T_{cs}$  to  $T_c$  in about 10 ms. The self heating of the switch is less significant in the temperature rise as the current is shunted into the parallel resistor thus reducing joule heating in the switch. The switches that have a low heater energy (128 J and 200 J) warm up more when the transport current is higher due to the higher self heating. The re-cooling of the low heater energy switches begins in less than 100 ms and so these heater energies are not suitable for triggering bypass-switches.

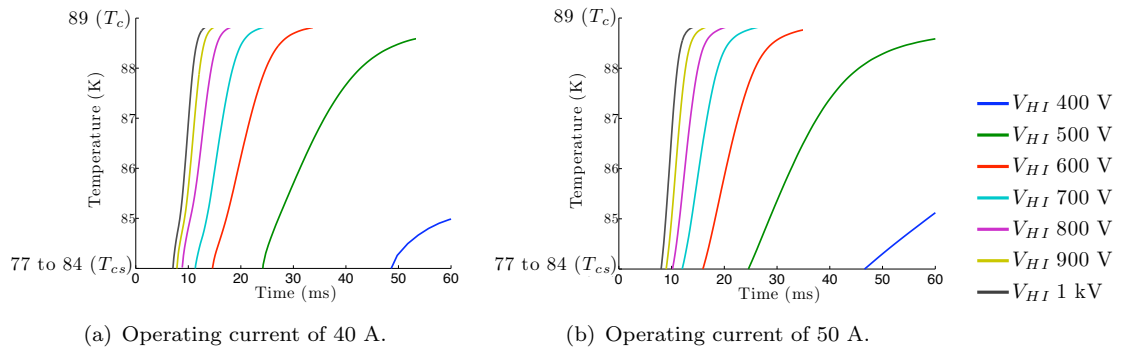


FIGURE 4.25: Estimated temperature rise of a bypass-switch based on stainless steel clad YBCO. The temperature is estimated from the non-linear  $V - I$  characteristics of the superconductor, the operating current, and the resistances of the matrix, dump resistor, and current leads. Temperature estimation not valid below  $T_{cs}$  where there is a zero voltage. Above  $T_c$  temperature estimation is less accurate as even large changes in temperature will only have a small effect on the voltage across the dump resistor.

**The recovery** of the cooled switches over times longer than the initial transition is shown in Figure 4.26. Voltage traces are shown for the switch when it is triggered with a 1 kV (800 J) capacitor discharge when carrying 50 A, and for when the switch is triggered with a 400 V (128 J) capacitor discharge when carrying 40 A. Three tests were performed on the low current switch and nine tests were performed on the higher energy switch. More

tests were needed to provide good time resolution during switching and also to cover a wide temperature range at a lower resolution.

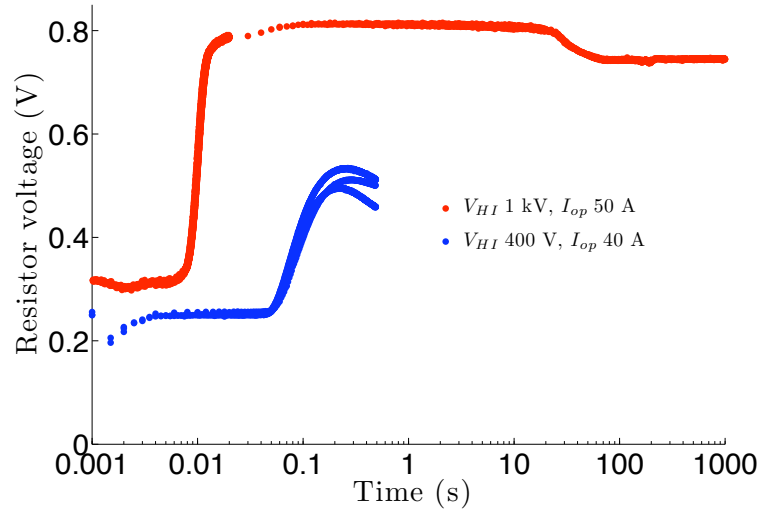


FIGURE 4.26: Dump resistor voltages after switching. With an  $I_{op}$  of 50 A and a  $V_{HI}$  of 1 kV (800 J) the switch remains resistive after triggering. With an  $I_{op}$  of 40 A and a  $V_{HI}$  of 400 V (128 J) the switch does not fully trigger and starts to recover in less than 1 s.

The low energy does not fully quench and starts to recover in less than 1 s; this heater energy is not sufficient to trigger the switch and allow effective energy dissipation. The higher energy and current switch develops a higher system voltage sooner and faster due to the higher heater power and transport current. The switch becomes fully normal within 20 ms and then remains fully normal for the next 20 s. During this time the voltage is  $\approx 0.81$  V, the current is 50 A, and so about 810 J is dissipated, primarily in the dedicated dump resistor. The dump resistor was mounted on a large air cooled copper heat sink in order to limit its temperature rise. Between 20 s and 70 s the system voltage decreases to  $\approx 0.7$  V as the switch cools down. The system voltage remained stable until 1000 s at which point the test was terminated and about 37 kJ had been dissipated. The system voltage did not continue to decrease as the decrease in switch temperature and switch resistance was limited by the increase in self heating of the switch due to more current flowing the now lower resistance switch.

The estimated temperature of the switch is shown in Figure 4.27. The switch has a fast temperature rise to around 175 K in less than a second due to the 800 J capacitor being discharged in the heater and diffusing through the insulation. After the heating has ended the switch cools down over the next ten to twenty seconds. Once the switch re-cooled to around  $T_c$  the temperature stabilised as the self heating of the current flowing balanced the cooling. The thermal resistance ( $R_k = \frac{dx}{kA}$ ) of the switch insulation can be estimated from the energy balance. The system voltage is 0.75 V so  $\approx 45$  A is flowing through the 16.5 m $\Omega$  dump resistor and 5 A through the switch. The voltage drop across the 10 m $\Omega$  current leads is  $\approx 50$  mV so the voltage drop across the switch is 693 mV. The self heating of the switch is about 3.5 W, as the switch is stable this must balance the cooling to the

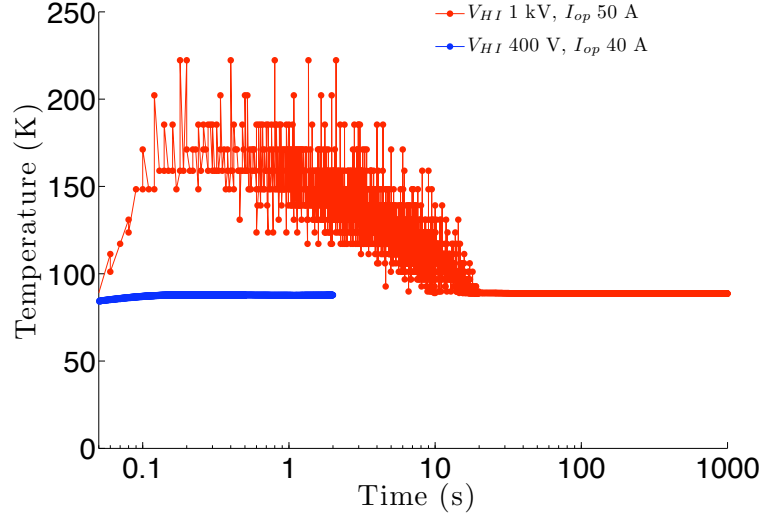


FIGURE 4.27: Estimated temperature of the switch.

liquid nitrogen at 77 K, with a  $\Delta T$  of  $\approx 12$  K. The thermal resistance of the insulation is approximately 3.4 K/W.

**The switching time** is defined as the time taken for the dump resistance to rise to 95 % of the required value of 16 m $\Omega$ . Time zero is the start of the heater voltage rise. Figure 4.28 shows the switching time as a function of the heater energy for single coil bypass-switches formed of stainless steel clad YBCO. Whilst the onset of voltage rise occurs sooner in the higher current switch due to the lower current sharing temperature, the time taken for 95 % of the dump resistance to be developed is the same as the current is shunted into the parallel resistor. At high capacitor charge voltages the self heating caused by the small amount of current flowing through the switch is not significant compared to the higher heater energy. However, for heater energies of less than 288 J the extra self heating when the operating current is 50 A means that the switch will trigger, whereas it will not at lower currents. The switching time is inversely proportional to the heater energy. The minimum energy that will trigger the switch is higher than for a dump-switch as it is not sufficient to heat the switch to the current sharing temperature as the current will bypass the switch in the parallel resistor. The heater energy must be high enough to heat the switch to  $T_c$  where the required dump resistance is developed and the the heat generation is not a function of the temperature dependent critical current. The switching time also tends to a minimum with increasing heater energy as due to the time taken for the heat to diffuse through the insulation and for the switch to warm from the operating temperature to the critical temperature. Whilst the switch will trigger with heater energies above 288 J using heater energies of 100 J/m or more will give switching times of less than 20 ms making giving comparable switching times to mechanical dump switches. Reducing the switching time to less than 10 ms would require over 160 J/m or a different switch design with a faster acting heater.

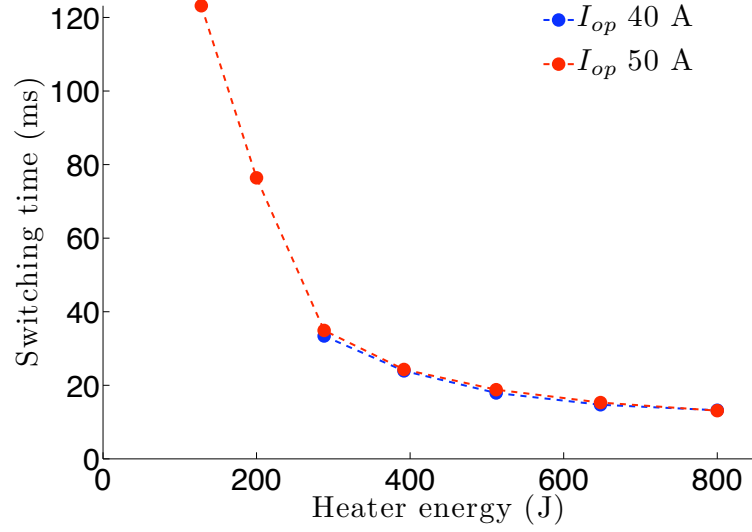


FIGURE 4.28: Switching time of a single coil YBCO based bypass-switch. The switching time is defined as the time taken to reach 95 % of the required dump resistance ( $16 \text{ m}\Omega$ ). When carrying 40 A the switch did not switch when triggered with heater energies of 128 J or 200 J.

#### 4.4.3 Switching Dynamics with a Multi-Module Bypass-Switch

Four bypass-switch modules were connected in parallel to give a bypass-switch with a critical current of 217 A. The parallel connection meant that the switch resistance was reduced to  $410 \text{ m}\Omega$  and the resistance of the current leads to  $2.6 \text{ m}\Omega$ . The switch heaters were also connected in parallel resulting in a decrease in the total heater resistance to  $890 \text{ m}\Omega$ . This decreases the capacitor discharge time constant by a quarter but also reduces the energy deposited in the switch by a quarter. With a charge voltage of 1 kV the heater energy that is deposited in the switch is  $\approx 40 \text{ J/m}$ , equivalent to the single module switch being triggered with a  $V_{HI}$  of 500 V. At this energy level the single module switch only just triggered when transporting 50 A and did not trigger when carrying 40 A, for this reason the multi-module switch is expected to be on the threshold of triggering.

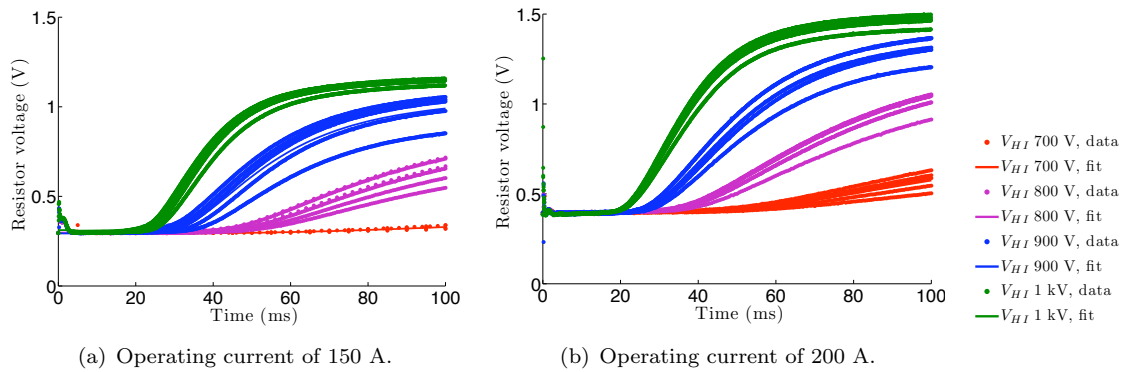


FIGURE 4.29: Voltages measured across the dump resistor for a four module bypass-switch formed of stainless steel clad YBCO. The data is from a number of experiments and the fit is a smoothed spline of the average.



The voltage evolution of the multi-module switch is shown in Figure 4.29 for operating currents of 150 A and 200 A. The onset of voltage rise occurs at about the same time as the single coil switch with the same heater energy per unit length. The voltage evolution has a similar profile to the single module switch with the initial voltage drop is due to the resistive current leads. When triggered with 40 J/m the switch does not go fully normal; the voltage when the switch is just above is expected to be 1.2 V for  $I_{op}$  of 150 A and 1.6 V for  $I_{op}$  of 200 A. The single module switch fully triggered with a sub 20 ms switching time when the heater energy was greater than 100 J/m so the multi-coil switch should trigger with a heater energy of  $\approx 2$  kJ. This would require the capacitor charge voltage to be increased to 1.6 kV, this would require a higher rated capacitor. The energy could also be increased by increasing the capacitance. The discharge time would remain the same as for the single module switch as the increase in capacitance is the same as the decrease in resistance.

**The current distribution** between the four switch modules and the parallel dump resistor is shown in Figure 4.30. The initial current flowing through the dump is due to the presence of the resistive current leads. As insufficient heater energy was input into the switch it did not fully quench and so some current still flowed in the switch after triggering. The self heating of the switch is low as the current is bypassed into the parallel resistor and when the switch does not fully quench some current is still carried by the superconductor. Less than 1 J/m was deposited in the superconductor during switching, this is low compared to the 40 J/m for a  $V_{HI}$  of 1 kV and the 20 J/m for a  $V_{HI}$  of 700 V.

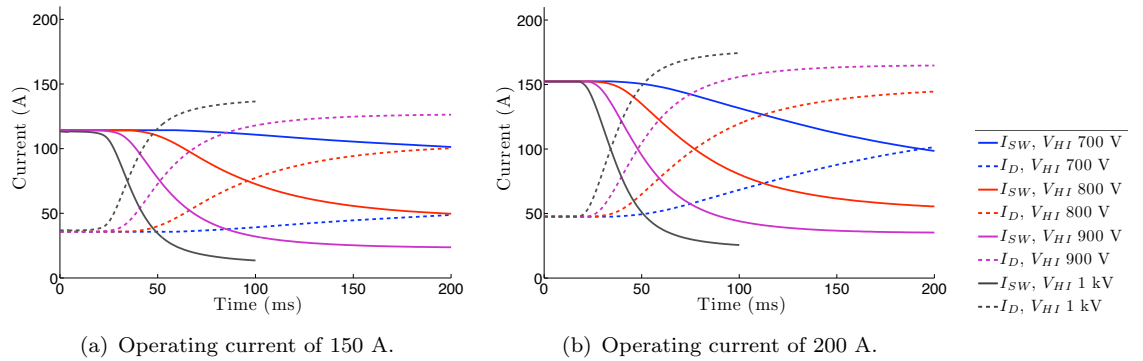


FIGURE 4.30: Current in a stainless steel clad YBCO bypass-switch.  $I_{SW}$  is the current in the switch,  $I_D$  is the current in the parallel dump resistor. The operating current ( $I_{op}$ ) does not decay with time.

**The switch temperature** is shown in Figure 4.31 and was estimated in the same way as for the single coil switch. As before the temperature estimation below the current sharing temperature or above the critical temperature is not valid. For the high energy switches the temperature rises rapidly from 77 K to between 88 K and 89 K. The temperature rise is more rapid than for the single module bypass switch with the same heater energy per length due to the faster capacitor discharge with the lower total heater resistance. The switches do not rise above 89 K as the heater energy was too low.



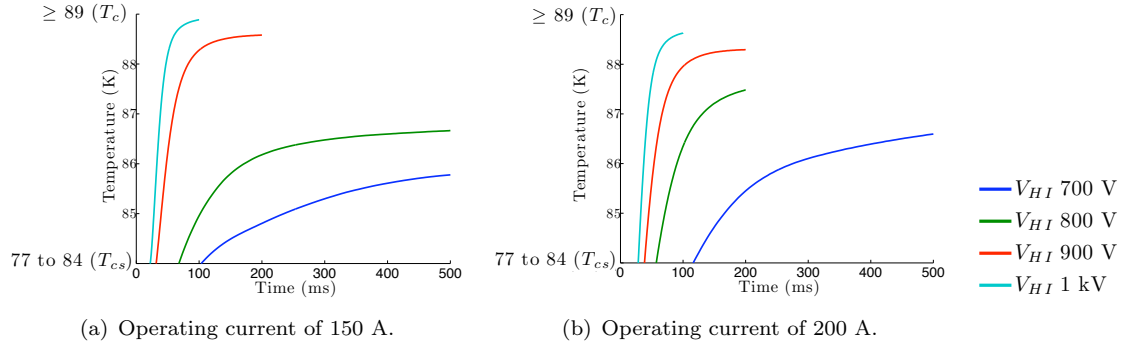


FIGURE 4.31: Estimated temperature rise of a bypass-switch based on stainless steel clad YBCO. The temperature is estimated from the non-linear V-I characteristics of the superconductor, the operating current, and the resistances of the matrix, dump resistor, and current leads. Temperature estimation not valid below  $T_{cs}$  where there is a zero voltage. Above  $T_c$  temperature estimation is less accurate as even large changes in temperature will only have a small effect on the voltage across the dump resistor.

When triggered with a lower heater energy the switch has a initially fast temperature rise due to heating by the heater. The temperature rise slows down once the heat has been transferred from the heater and the heating of the switch is due to the much lower self heating component. As the switch becomes hotter the critical current decreases and the matrix resistance increases and so more current flows through the bypass causing the self heating of the switch to decrease.

**The evolution of the dump resistance** is shown in Figure 4.32. The total dump resistance when fully quenched is less than for the single module switch as a less resistive parallel dump resistor that had a higher current rating was used. The full resistance was not developed as the heater energy was less than the 100 J/m required to fully trigger the switch in less than 20 ms. The resistance did not rise significantly after the heater capacitor discharge as the energy provided by the self heating was less than 1 J/m and the switch was cooled.

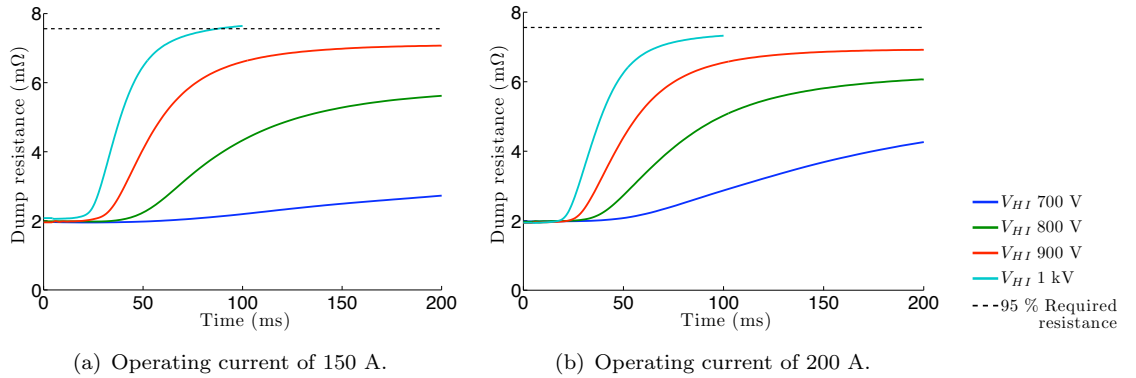


FIGURE 4.32: Dump resistance of an YBCO bypass-switch with a room temperature resistance of 410 mΩ connected in parallel with a 8.4 mΩ dump resistor. The initial resistance is due to the current leads that had a resistance of 2.6 mΩ.

**The switching time** is the time taken for the dump resistance to rise to 95 % of the required value of 8 m $\Omega$ . With a heater energy of 40 J/m, a  $V_{HI}$  of 1 kV, the switching time was 88 ms, which is comparable to the 76 ms for the single module switch. At heater energies less than 40 J/m the multi-module switch did not switch. A total heater energy of 2 kJ would be required to achieve switching times of less than 20 ms.

#### 4.4.4 Conclusions from Experiments on Bypass-Switches

Bypass-switches formed of stainless steel clad YBCO were shown to be able to be used for dissipating energy in an external dump resistor. The switches were tested in liquid nitrogen and had resistive current leads connecting them to a dump resistor at room temperature. The switches had a critical current of  $\approx 55$  A per module and the power supply current was kept constant. The required length in relation to the parallel dump resistor of these single module bypass-switches was 0.3 m/m $\Omega$ . The switches were thermally activated by discharging a capacitor through a steel heater that was co-wound with the superconductor. To achieve switching times of less than 20 ms, which are comparable to mechanical switches, heater energies of 100 J/m are required. Reducing the switching time to less than 10 ms would require heater energies of over 160 J/m. The system was shown to maintain the required dump resistance for long time periods (up to 1000 s) when sufficient heater energy was used to fully trigger the switch. The switch was latched into the resistive state by self heating due to the portion of current that did not get shunted into the dump resistor. These bypass-switches can be operated in parallel to allow operation with higher current circuits. The single module, which has a length of 5 m, can be used as a reference design to scale the design to different currents or for use with other parallel dump resistors ( $R_{DR}$ ). For the same fraction of current bypassing the switch, the required length is

$$L_{\text{NEW}} = L_{\text{REF}} \left( \frac{I_{\text{NEW}}}{I_{\text{REF}}} \right)^2 \left( \frac{R_{DR, \text{NEW}}}{R_{DR, \text{REF}}} \right). \quad (4.6)$$

Similar switching times can be achieved if the same heater energy per length of switch is used. A doubling of the transport current with the same dump resistor requires quadrupling of the switch length and also of the heater energy.

## 4.5 Modelling of HTS Switches Operating at 77 K

### 4.5.1 Heater Dynamics

The heater voltage decay for the dump-switch when there is no transport current in the superconductor is shown in Figure 4.33. For a capacitor charge voltage of 100 V, equivalent to an energy of 8 J, there is not a significant temperature rise of the switch and the heater decay is similar to both the constant temperature case and the experimental results

Section 4.3.1. When the heater energy is increased to 200 J ( $V_{HI}$  of 500 V) the modelled voltage decay is again similar to the experimental results implying that the temperature rise of the model is similar to that of the experiment. For higher heater energies of 800 J ( $V_{HI}$  of 1 kV) there is a deviation between the model and the experimental results. When modelled with the normal heater resistance, the model initially has the same heater decay as the the experimental results. However, the modelled heater has a faster discharge time implying that the heater resistance is less than that of the experiment. Increasing the resistance of the modelled heater by 1.5 times increases the discharge time of the capacitor and is closer to the experiments at times greater than  $\approx 5$  ms. The implication of this is that at a high heater energies the model under-predicts the temperature rise of the switch leading to a colder less resistive heater with a faster discharge time. This increase in under-prediction could be due to reduced cooling due to the higher heater energy and greater temperature rise causing a change in the cooling regime to film boiling that has a higher thermal resistance. Another possibility is the uncertainty in the heater resistivity away from the measured values at 77 K and 300 K; the maximum temperature of the heater was predicted to be  $\approx 420$  K.

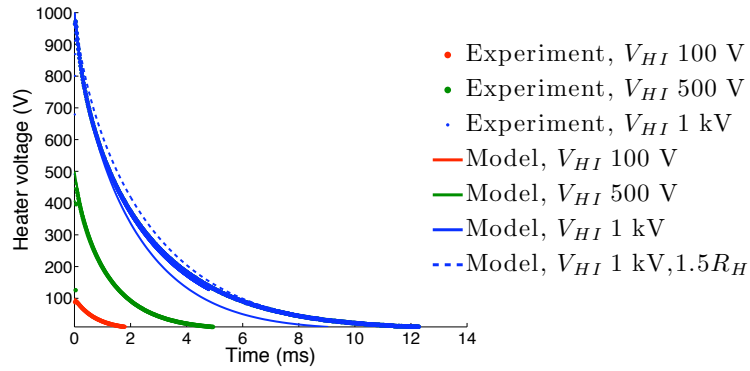


FIGURE 4.33: Measured and modelled heater voltage decays for the single coil dump-switch when there is no transport current. The model with a  $V_{HI}$  of 1 kV was calculated for the normal heater resistance and also for an increased resistance ( $1.5R_H$ ). The model and experiment are coincident for  $V_{HI}$  100 V and 500 V.

The modelled and experimental heater decays of the single coil bypass-switch are shown in Figure 4.34. There is generally good agreement between the modelled heater decays and the experimental results (Section 4.4.1). Unlike the dump-switch there does not appear to be an underestimation of the temperature for higher heater energies. This is due to the higher heat capacity of the bypass-switch, which is longer and has thicker insulation, limiting the overall temperature rise so the cooling regime remains more constant and the temperature range of the material data is not exceeded.

#### 4.5.2 Sensitivity of Switching Characteristics to Critical Surface

The switching characteristics predicted by the model are sensitive to the critical surface of the superconductor between  $T_{op}$  and  $T_c$ . The model is based on the heat diffusion equation

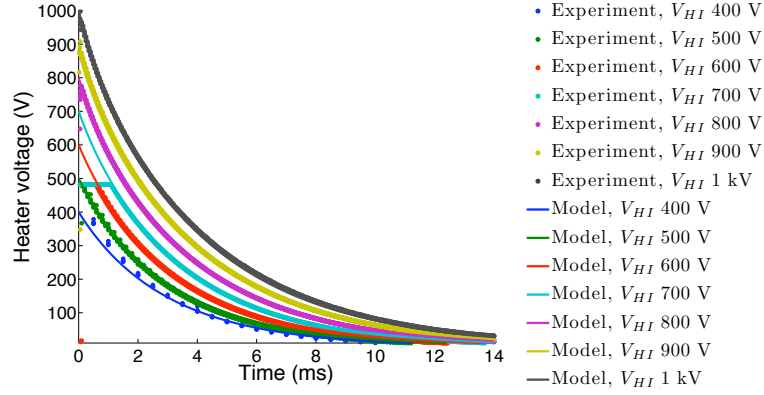


FIGURE 4.34: Measured and modelled heater voltage decays for the single coil bypass-switch when there is no transport current. The recorded voltage for  $V_{HI}$  of 500 V, 600 V, and 700 V saturated at 480 V.

and so the temperature of the superconductor is used in the determination of the voltage by means of an assumed voltage-temperature characteristic. This characteristic is dependent upon the resistivity of the matrix, the transport current, the  $J_c(T)$  characteristic, and the  $n(T)$  characteristic (Section 3.6). The decrease in critical current density with increasing temperature is given by

$$J_c(T) = a \left(1 - \frac{T}{T_c}\right)^\alpha \quad (4.7)$$

and that the temperature dependent  $n$ -value is

$$n(T) = n(0) \left(1 - \frac{T}{T_c}\right)^{\frac{1}{2}} + n(T_c). \quad (4.8)$$

Small variations in the assumed profiles can have a large affect on the predict voltage of the switch for a given temperature. Figure 4.35 shows the voltage-temperature characteristics for the YBCO based dump-switches for different fitting parameters of the critical surface and  $n$ -value.

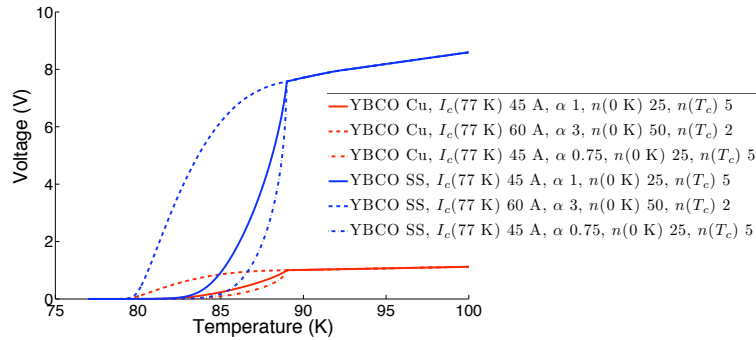


FIGURE 4.35: Voltage-temperature characteristics of YBCO based dump-switches for different fitting parameters of the critical surface and  $n$ -value. The transport current is 40 A, the length of the stainless steel clad YBCO switch is 1.7 m and of the copper clad YBCO switch 1.87 m.

Above  $T_c$  variations in the voltage-temperature characteristics are dependent upon variations in the resistance in the switch and are much smaller than below  $T_c$  where the  $V - T$  characteristics are highly non-linear. For this reason there is a large uncertainty associated with predicting the voltage characteristic of a superconducting switch when it is in the current sharing regime.

### 4.5.3 Comparison of Experimental YBCO Based Dump-Switches to the Model

The modelled and experimental voltage increases of the copper clad YBCO dump-switch is shown in Figure 4.36 and for the stainless steel clad dump-switch in Figure 4.37. In both cases the model predicts the voltage rise of the switch to occur about 2 ms to 3 ms faster than that observed in the experiments. In addition to this the predicted rate of voltage rise is also faster.

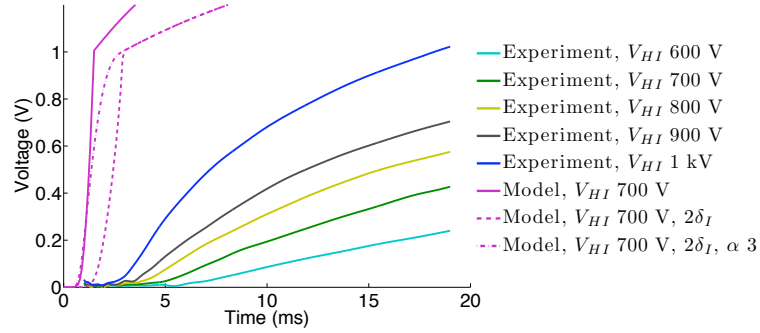


FIGURE 4.36: Measured and predicted voltage rises of a copper clad YBCO dump switch that transports 40 A and operates in liquid nitrogen. Modelled results are shown for the experimental switch configuration, with twice the thickness of insulation, and with a more rapid decrease of  $I_c$  with temperature ( $\alpha$  of 3).

There are two main reasons for difference between the model and the experiment. The first is an underestimation of the thermal resistance between the heater and the superconductor and the second is the uncertainty in the voltage-temperature characteristics (Section 4.5.2). The insulation in the experimental switches was a single layer of  $12.7 \mu\text{m}$  polyimide that had the same thickness of epoxy on each face; the modelled switches had the same arrangement using the standard material properties. In the experimental switch likely that there is a higher thermal contact resistance between the layers that results in a lower rate of heat conduction than predict by the model. This results in the superconductor warming up more slowly and thus a delay in the onset of the voltage rise. This problem would be compounded by any voids between the layers.

The delay in onset of voltage rise also has a strong dependance on  $V - T$  characteristics. This is compounded by the poor homogeneity of the critical current in the switches. In the stainless steel clad YBCO switch the critical current varied from 45 A to 77 A at different points along its length when tested at 77 K. This poor homogeneity in  $I_c$  implies that

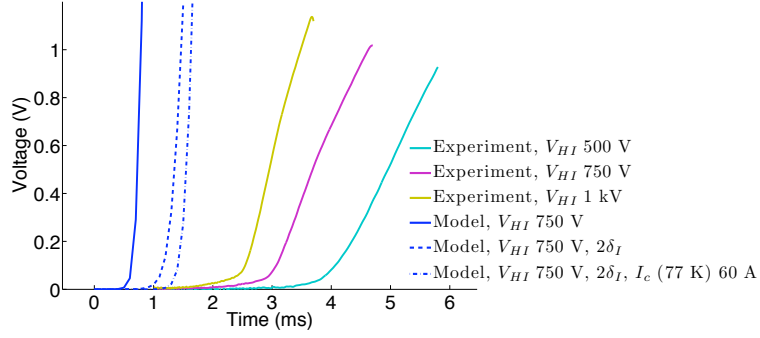


FIGURE 4.37: Measured and predicted voltage rises of a stainless steel clad YBCO dump switch that transports 40 A and operates in liquid nitrogen. Modelled results are shown for the experimental switch configuration, with twice the thickness of insulation, and with a higher  $I_c$ .

there is probably also a large variation in the  $n$ -value. Furthermore the critical surface between  $T_{op}$  and  $T_c$  was not measured and variations in this region will also have a large effect on the quenching switch. As the power supply in the experiments tripped before the switches reached a temperature above  $T_c$  it was not possible to perform a comparison using the higher confidence resistive  $V - T$  characteristics of the switch. Due to the large uncertainty in the voltage-temperature characteristics of these dump-switches there is a corresponding uncertainty in comparing the model and the experimental switches that remained below  $T_c$  during the test.

#### 4.5.4 Comparison of Experimental YBCO Based Bypass-Switches to the Model

The stainless steel clad YBCO bypass-switch was connected in parallel to a 16.5 m $\Omega$  dump resistor with current leads that had a resistance of 10.4 m $\Omega$ . As the total dump resistance was limited by the parallel resistor the superconductor could become fully normal without tripping the power supply. This allows the modelled and experimental switches to be compared independently of the non-linear voltage-temperature characteristics of the switch in the current sharing regime.

Figure 4.38 shows the experimental and modelled results. The shape of the voltage rise below  $T_c$  is dependent upon the non-linear  $V - T$  characteristics in which there is a high degree of uncertainty. However, above  $T_c$  the voltage calculated from the modelled temperature has less uncertainty as the normal  $V - I$  characteristics of the superconductor are well known. Comparing the point at which the superconductor is almost fully normal, 95 % of the required resistance, it can be seen that the model predicts to fast a switching time. This is due to an overestimation of the thermal conductivity of the insulation layer. In the experimental switch extra thermal resistance may exist due to contact resistance between the layers. Reducing the thermal conductivity to about half of the expected value, to allow for contact resistance in the model, yields a better fit to the experiments.

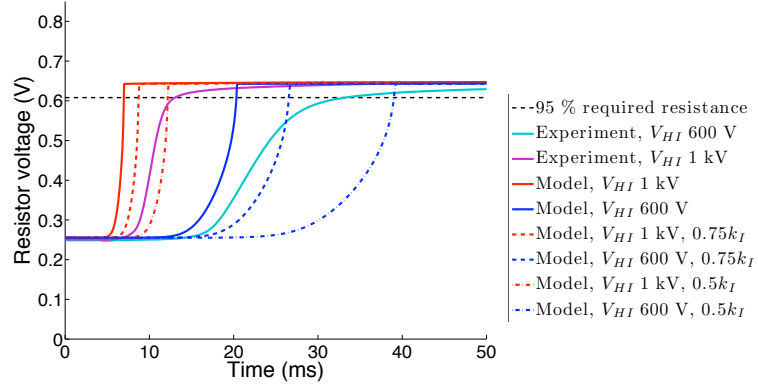


FIGURE 4.38: Measured and predicted voltage rise of a stainless steel clad YBCO bypass-switch that transports 40 A and operates in liquid nitrogen. Modelled results are shown for the experimental switch configuration, with twice the thickness of insulation, and with a higher  $I_c$ .

However, the voltage growth is still different due to uncertainty in the  $V-T$  characteristics of the switch.

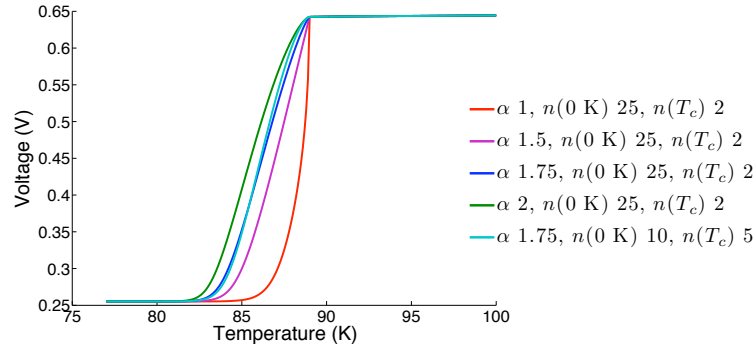


FIGURE 4.39: Voltage-temperature of a stainless steel clad YBCO bypass-switch that transports 40 A. The parallel dump resistor is  $16.5 \text{ m}\Omega$  and the current leads have a total resistance of  $10.4 \text{ m}\Omega$ . The  $I_c$  at 77 K is 57 A.

**The voltage-temperature characteristics** of the YBCO based bypass-switch with a parallel dump resistor and resistive current leads is shown in Figure 4.39. As for the dump-switch (Section 4.5.2), the assumed critical surface leads to a sharp discontinuity in the  $V-T$  characteristics at  $T_c$ . This sharp transition is dependent upon the shape of the  $J_c(T)$  characteristics. For non-linear of YBCO  $\alpha$  is normally less than  $\approx 3$  [119], [120]. An increase in  $\alpha$  leads to a smoother transition at  $T_c$ , more similar to the experimental results. A reduction in the  $n$ -value at low temperatures causes a delay in the growth of the voltage due to the less sharp superconducting to normal transition.

Figure 4.40 shows the effect of a different  $V-T$  characteristic on the modelled switch results. As described above the thermal conductivity of the insulation layer was reduced by a half to compensate for contact resistance between the layers of insulation. With a smoother  $V-T$  characteristic the modelled voltage rise is more similar to the experimental results. Measuring the critical surface in the range 77 K to 89 K would allow a better

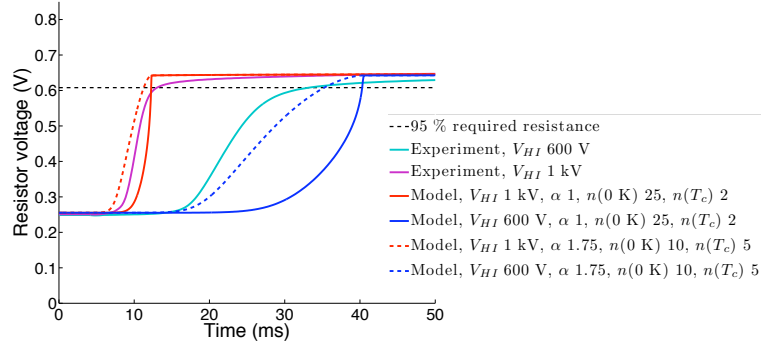


FIGURE 4.40: Measured and predicted voltage rise of a stainless steel clad YBCO bypass-switch that transports 40 A and operates in liquid nitrogen. Modelled results are shown for different  $J_c(T)$  and  $n(T)$  characteristics, the thermal conductivity of the insulation was reduced to allow for contact resistance between the layers.

prediction and a closer examination of the thermal effects, such as insulation or cooling, that also effect the transition. A further complication is inhomogeneity in the critical current of the superconductor; the critical current of the tape used for the bypass-switches varied from 40 A to 70 A, for this switch the  $I_c$  was 57 A.

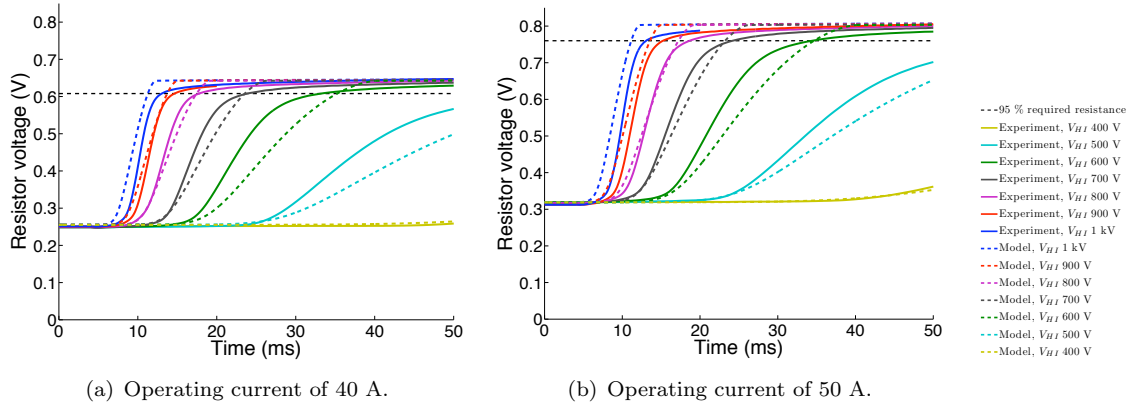


FIGURE 4.41: Measured and predicted voltage rises of a stainless steel clad YBCO bypass-switch that operates in liquid nitrogen. The modelled results use  $\alpha$  of 1.75,  $n(0\text{ K})$  of 10,  $n(T_c)$  of 5, and the thermal conductivity of the insulation is half of the theoretical value to account for thermal contact resistance between the layers.

**The switching characteristics** of the bypass-switch over a range of heater triggering energies are shown in Figure 4.41. The model more closely resembles the measurements for triggering energies above about 500 J, equivalent to a  $V_{HI}$  of 800 V. This is because the faster temperature rise of the switch leads to sharper increase in voltage and so uncertainties in the voltage-temperature characteristic have less of an effect. At lower heater energies the onset of voltage rise and the time to achieve 95 % of the required dump resistance are similar for the model and the experiment, but the shape of the voltage curve between these two points differs. The greatest difference is below  $T_c$  and is due to the uncertainty in the  $J_c(T)$  and  $n(T)$  in this region.



**Switching times of the experiment and the model** are shown in Figure 4.42. The switching time is the time taken for the total dump resistance to grow to 95 % of the required value. With a smoother  $V - T$  characteristic and an allowance for contact resistance between the layers there is a good agreement between the predicted and measured switching times.

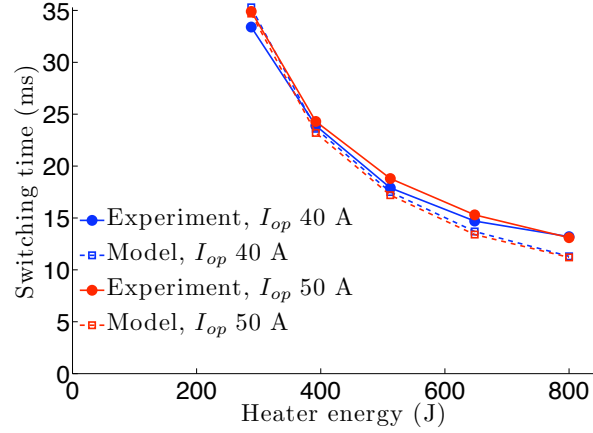


FIGURE 4.42: Switching times for the experimental and modelled stainless steel clad YBCO bypass-switch.

#### 4.5.5 Modelled Switching Characteristics with Cooling

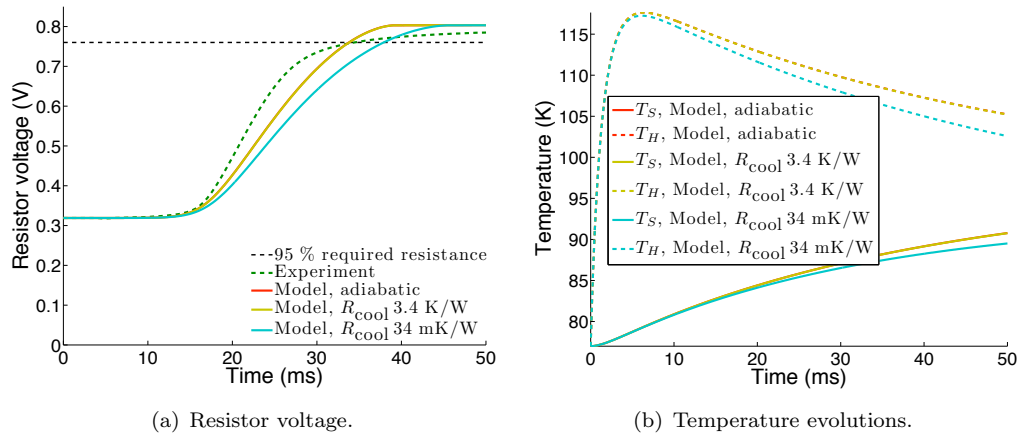


FIGURE 4.43: Comparison between the experimental results and the modelled switch with different levels of cooling. Cooling is shown for an adiabatic switch, a switch with a thermal resistance ( $R_{\text{cool}}$ ) of 3.4 K/W, and with  $R_{\text{cool}}$  of 3.4 mK/W.

The modelled switches that were compared to the experiment were adiabatic even though the experimental switch was cooled in liquid nitrogen. The effective thermal resistance ( $R_{\text{cool}}$ ) from the switch to the surrounds was estimated to be 3.4 K/W at 77 K (Section 4.4). Figure 4.43 shows the effect of different levels of cooling on the switching characteristics; the cooling levels were an adiabatic switch, cooling to match the experimental switch at 77 K, and cooling 100 times higher than the experimental switch. Over the first 50 ms,

the duration of the analysis, there was seen to be no difference between the thermal or electrical profiles of the adiabatic or  $R_{\text{cool}}$  3.4 K/W switch. This shows that the adiabatic assumption is valid for modelling the initial transition of these switches. If the cooling is increased a hundred times then the onset of voltage increase remains the same but there is a more gradual transition due to the heat loss to the surrounds causing a delay in the switching time by  $\approx 5$  ms.

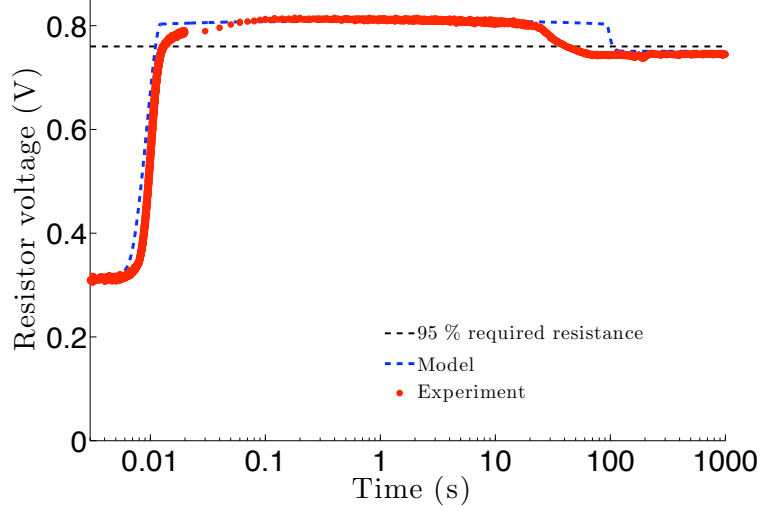


FIGURE 4.44: Dump resistor voltages after switching with an  $I_{op}$  of 50 A and a  $V_{HI}$  of 1 kV (800 J). The modelled switch has cooling to the surrounds through a thermal resistance of 3.4 K/W. The voltage drop at 95 % of the required resistance is also shown.

Over longer time periods, greater than 10 s, the adiabatic assumption is not valid as the switch will slowly cool back down to  $T_c$ . Figure 4.44 shows the modelled and experimental voltage profiles of cooled switches for 1000 s. Both the modelled and experimental switches show a step decrease in the voltage once the switch has cooled to just below  $T_c$ . At this point the current flowing resistively in the switch is sufficient to balance out the cooling and the switch neither warms nor cools further. The step decrease of the experimental switch is smoother due to the smoother voltage-temperature characteristics. The decrease in voltage happens sooner for the experimental switch than for the prediction. One reason for this is that the model uses a constant  $R_{\text{cool}}$  equivalent to the 77 K value, in reality the thermal resistance is temperature dependent due to the increase in thermal conductivity of the insulation at higher temperatures. The use of a constant value of  $R_{\text{cool}}$  leads to an underestimation of the cooling at higher temperatures and thus an overestimation of the time taken for the switch to cool to the lower resistance state.

#### 4.5.6 Switching Characteristics Calculated with the PDE Model

The switching characteristics so far in this section had been modelled using the lumped approximation. This is suitable for use in switches where there is fast thermal diffusion through the insulation (Section 3.7.1). This bypass-switch has 76.2  $\mu\text{m}$  of insulation

between the superconductor and the heater and  $152 \mu\text{m}$  of insulation between similar layers. In addition to this the thermal conductivity of the insulation was reduced to take into consideration contact resistance between the layers. This means that this switch configuration is on the border of what can be modelled with the lumped approximation.

Figure 4.45 shows the predicted thermal profiles of the experimental bypass-switch when modelled with the lumped approximation and with the PDE model. The PDE had a varying  $x$ -mesh spacing; 25 linearly spaced points were used in the insulation layers that had high  $\frac{d^2T}{dx^2}$ , the heater and superconductor layers had 20 logarithmically spaced points with a higher density close to the material boundary where  $\frac{d^2T}{dx^2}$  is higher. The lumped approximation matches the PDE model well in the heater and superconductor layers, as well as in the insulation between them. However, in the thicker insulation between similar layers there is a large difference between the two models. The slower diffusion into the insulation of the PDE model means that the heater temperature rises faster to a peak temperature  $\approx 10$  K higher than that calculated with the lumped approximation. Despite the difference in heater temperatures, the predicted superconductor temperature remains about the same for both models.

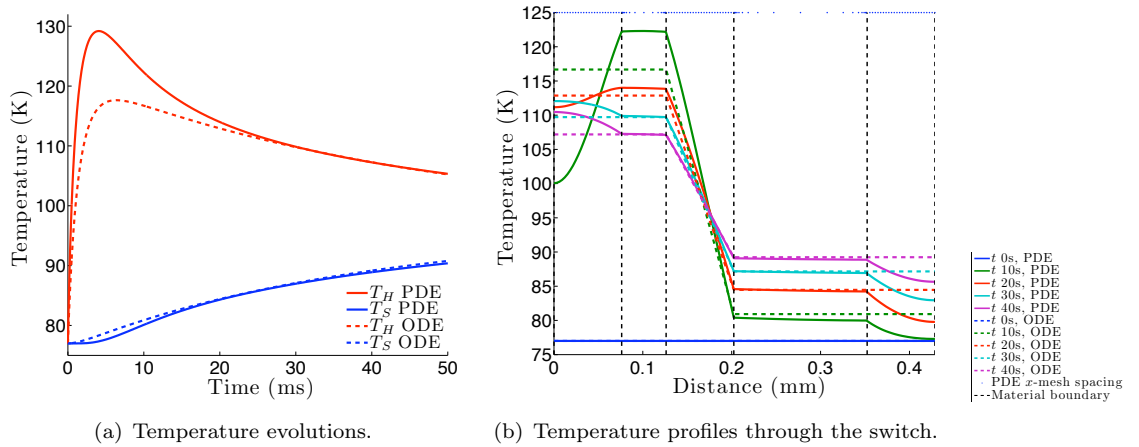


FIGURE 4.45: Switch temperature calculates with the lumped approximation and the PDE form of the heat diffusion equation for the stainless steel clad YBCO bypass-switch with  $I_{op}$  of 50 A and  $V_{HI}$  of 600 V.

Figure 4.46 shows the predicted voltage traces with the two models; the experimental results are shown for comparison. The predicted voltages are similar as the predicted superconductor temperatures were similar and the same voltage-temperature characteristics were used for both models. The ODE model predicts a slightly faster ( $< 1$  ms) switching time than the PDE model due to the insulation layers instantly adopting a linear thermal profile. Both switches have about the same switching time as the experimental switch. The similarity in switching characteristics means that the lumped approximation is valid for this switching situation.

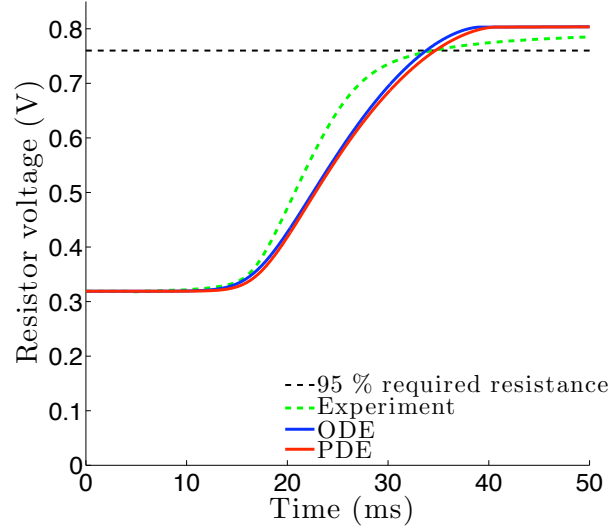


FIGURE 4.46: Voltage evolution calculated with the lumped approximation and the PDE form of the heat diffusion equation for the stainless steel clad YBCO bypass-switch with  $I_{op}$  of 50 A and  $V_{HI}$  of 600 V.

## 4.6 Summary of Experimental HTS Switches

HTS switches of both the dump-switch and bypass-switch type were tested in liquid nitrogen. The dump-switches were formed of YBCO that had either copper cladding or stainless steel cladding, the bypass-switches were formed of stainless steel clad YBCO. Switching times comparable to those obtained with mechanical switches ( $\approx 15$  ms) can be achieved with of both bypass-switches and dump-switches provided that enough heater energy is deposited fast enough. For these experimental switches this was  $\approx 100$  J/m that was provided by discharging a 1.6 mF capacitor through the heater. The lumped approximation could be used to model the switches even when the thermal conductivity was lowered to allow for contact resistance between the layers. The largest source of variation between the model and the measurements is the uncertainty in the voltage-temperature characteristics of the switch below  $T_c$ .

Future experiments should use temperature sensors embedded within the switch to allow the temperature to be measured directly during switching. Small thermocouples that have a fast response time could be used. Additionally the voltage-temperature characteristics of the superconductor that is used in the switch should be measured to allow more accurate modelling beneath  $T_c$ . The power supply used in these experiments was a constant current source that could only provide a low DC voltage. To allow the switch to be investigated in a decaying current circuit a superconducting magnet could be discharged by the switch. However, the cost of this may be prohibitive so a power supply that can mimic an inductive load could be used instead.

## Chapter 5

# Design and Optimisation of HTS Switches for Magnet Circuits

## 5.1 Superconducting Switches for Discharging Energy from Magnet Circuits

Superconducting switches allow alternative energy extraction schemes (Section 3.1) that may have advantages over existing schemes. In the LHC, for example, effective energy extraction is provided for a wide range of magnets by switching a dump resistor into the circuit. For high stored energies of up to 1.3 GJ, extraction is provided by a mechanical switch and a warm dump resistor [4]. Mechanical DC circuit breakers are large, costly, and provide only limited lifetime. This is especially the case for higher currents where arcing and erosion can be significant. In order for the LHC breakers to withstand over 300 switching cycles, tungsten-silver alloy contacts were specially developed as conventional copper contacts would have required replacing after less than 100 cycles- about five months of LHC operation [6]. For this reason it would be beneficial to use a contact-free switch.

Superconducting switches might first find an application in cases such as those of the LHC 600 A circuits because this magnet current can be carried by a small number of HTS tapes. For YBCO based switches as few as five tapes would be sufficient to carry the magnet current safely at 50 K. HTS switches appear to be less suitable for the high current (13 kA) circuits of the LHC as many tapes would be required to be operated in parallel in order to carry the magnet current due to their relatively low critical current [44]. For example, YBCO based switches would require over fifty tapes to carry the 13 kA magnet current at 50 K. The resulting large conductor cross section means that kilometers of conductor would be required in order to develop a usable resistance. The rapid advance in HTS materials, including in  $\text{MgB}_2$ , means that switches may become suitable for high current circuits in the future. However, magnet circuits such as those of the LHC MCD<sup>1</sup> correctors are rated at a maximum of 600 A and have a relatively modest maximum stored energy, 5.5 kJ. These may be suitable candidates for protection with superconducting switches. The MCD magnet circuits are currently discharged with mechanical switches and dump resistors. The details of these circuits are given in Table 5.1; the details of the 13 kA LHC MB magnet circuit and other 600 A circuits are also included for comparison [3].

Magnet Type	Inductance (mH)	$I_{\text{nom}}$ (A)	$I_{\text{max}}$ (A)	No. of Circuits	Energy (kJ)	$R_D$ (m $\Omega$ )	$\tau_{LR}$ (s)
MCD	30.8	550	600	16	5.5	700	0.044
MCS	123.2	550	600	16	22.2	700	0.18
MS	432	550	600	32	77.8	150	0.62
MB	15 400	11 810	13 000	8	1.3e6	150	103

TABLE 5.1: Parameters of selected LHC magnet circuits.  $I_{\text{nom}}$  is the nominal current of the circuit,  $I_{\text{max}}$  is the maximum current of the power convertor, and  $\tau_{LR}$  is the time constant of the magnet decay through the dump resistance ( $R_D$ ). The stored energy is evaluated at the maximum current level.

<sup>1</sup>Naming conventions of the LHC magnets: MCD- magnet corrector decapole, MB- magnet bending (dipole), MS- magnet sextupole, and MCS- magnet corrector sextupole.

**The operating temperature** of superconducting switches for the LHC magnet circuits is dependent upon the cooling that is available in the LHC machine. These LHC magnets are powered by circuits that contain hybrid current leads that transport the magnet current from 4.2 K to 300 K [81]. These leads have an HTS section between 4.2 K and 50 K and a resistive copper section between 50 K and 300 K. The LHC also has a thermal screen at 50 K to 75 K. If a superconducting switch is to be integrated into these circuits then operation at 50 K is a possible choice as the switch can then utilise the available cooling and also allow the existing designs of the HTS and resistive sections of the hybrid current leads to be used. Operation at 50 K means that the parallel connected safety lead that is required by the bypass-switch may only operate between 50 K and 300 K and so the heat leak is less than if the switch were operated at lower temperatures. Alternatively the safety lead could also protect the HTS part of the lead during energy extraction.

A proposal for the LHC upgrade is the replacement of some Nb-Ti bus-bars with  $\text{MgB}_2$  links [121]. This means that the temperature of the interface between the bus-bar and HTS section of the hybrid current leads would be at about 20 K. Extending the length of the  $\text{MgB}_2$  based bus-bar allows the current leads to be relocated in the lower radiation environment of the side caverns. In addition to this there is 20 K helium gas available in the LHC and in this case there would also be the possibility of running the switch at about 20 K. Operating superconducting switches at 20 K would have benefits over 50 K operation. Fewer tapes would be required to carry the magnet current due to the increase in critical current with decreasing temperature. Less heater energy per length would be required to warm the switch from  $T_{op}$  to  $T_{cs}$  as the specific heat capacity is lower at 20 K than at 50 K. Magnesium diboride based tapes, which are cheaper than YBCO based tapes, could also be used as the switch superconductor. However, a longer length of switch may be needed if the required dump resistance is also to be developed at lower temperatures due to the reduction in normal state resistivity at lower temperatures.

### 5.1.1 Description of Existing Magnet Circuits in which Superconducting Switches could be Used

In order to put this study into superconducting switches on a realistic footing, examples of real LHC magnet systems are considered. The LHC MCD magnet circuits consist of 16 chains of 77 corrector magnets that have a maximum current rating of 600 A. Each chain has a total circuit inductance of 30.8 mH and a maximum stored energy of 5.5 kJ [3]. In the event of a problem in the circuit the magnet energy is dissipated in a  $0.7 \Omega$  resistor that is at room temperature. This resistor is normally bypassed through a normally closed mechanical breaker that opens in  $\approx 15$  ms leading to 95 % of the magnet energy being discharged in 80.9 ms after the initiation of switch opening. Figure 5.1 shows the existing MCD magnet circuit layout and Figure 5.2 the modelled energy extraction profile for the existing circuit.

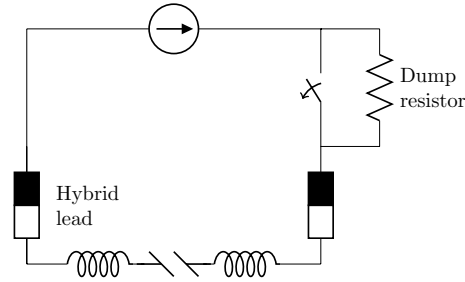


FIGURE 5.1: Circuit diagram for energy extraction in the LHC MCD magnet circuits.

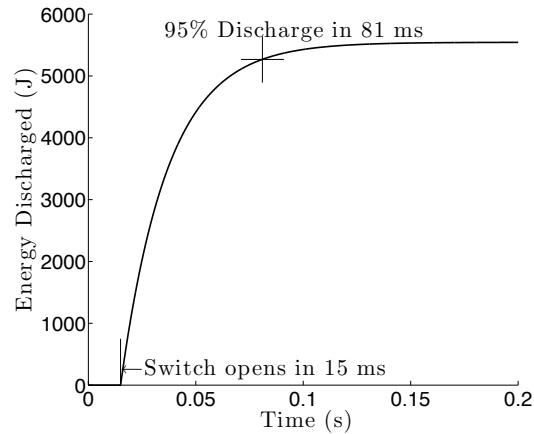


FIGURE 5.2: Energy discharge profile for the LHC MCD magnet circuits operating at the maximum current of 600 A (nominal current is 550 A).

## 5.1.2 Application of Superconducting Switches to Typical Magnet Circuits

### 5.1.2.1 Energy Extraction Using a Superconducting Bypass-Switch

The mechanical bypass-switch in the LHC MCD magnet circuits could be replaced with a superconducting bypass-switch. The gradual transition of a superconducting switch means that it has the potential to reduce the peak voltage during energy extraction whilst still meeting the magnet energy dissipation requirements. The advantages and disadvantages of such a superconducting bypass-switch are described in Section 3.1. In the LHC MCD magnets the operating temperature of a superconducting switch could be at either 50 K or 20 K for the reasons described at the start of Section 5.1. The circuit diagrams for energy extraction from the LHC MCD magnet circuits with superconducting bypass-switches operating at both 50 K and 20 K are shown in Figure 5.3.

To ensure that a large fraction of the magnet energy is dissipated in the dedicated dump resistor the switch resistance needs to be larger than the dump resistance so that the switch is effectively bypassed. For example, a switch resistance of twenty times the resistance of the dump resistor will result in over 95 % of the magnet energy being dissipated in the dump resistor (Equation 3.1). Operation at 20 K requires shorter switches as fewer tapes



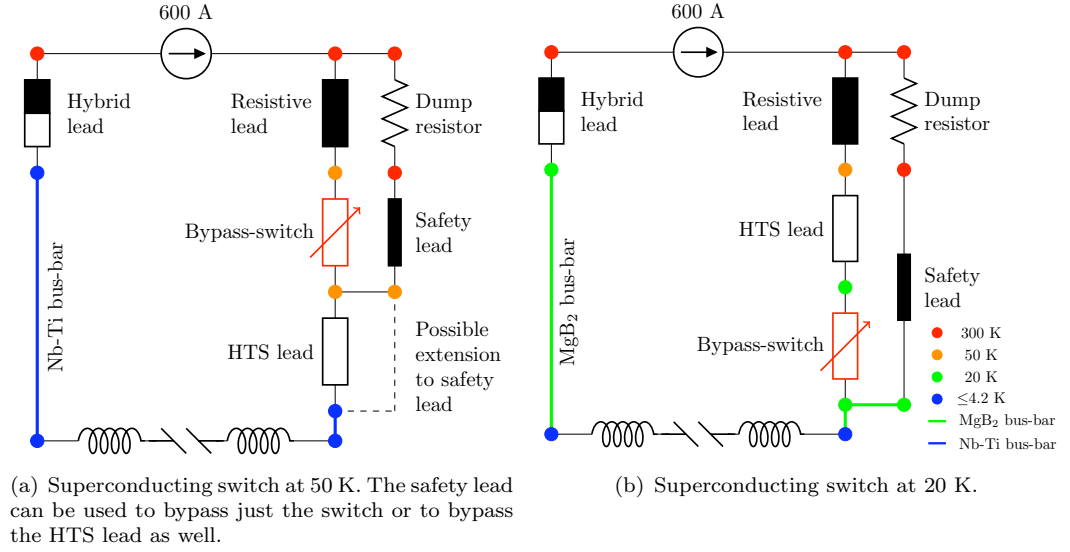


FIGURE 5.3: Magnet circuit layout with a superconducting bypass-switch, safety lead, and warm dump resistor. (a) is for when the bypass-switch operates at 50 K and there is a Nb-Ti bus-bar, (b) for when the switch operates at 20 K and there is a MgB<sub>2</sub> bus-bar.

are needed to carry the 600 A magnet current due to the higher critical current at this lower temperature. The required switch length when the switch resistance is developed just above  $T_c$  is given in Table 5.2 for MgB<sub>2</sub> and YBCO based switches when there is a  $0.7 \Omega$  dump resistor. If the switch resistance was developed at higher temperatures then less conductor would be required due to the higher resistivity of the tape. However, more heater energy would be required to warm the switch to this higher temperature.

$T_{op}$ (K)	YBCO based switch		MgB <sub>2</sub> based switch	
	No. of tapes	$L$ (total) (m)	No. of tapes	$L$ (total) (m)
20	2	465	1	425
50	3	1 046	-	-

TABLE 5.2: Required conductor length for superconducting bypass-switches to dissipate over 95 % of the magnet energy in a  $0.7 \Omega$  dump resistor. The operating current is 600 A and the stored energy is 5.5 kJ. Lengths are given for switches formed of stainless steel clad YBCO, which was produced by American Superconductor, and also MgB<sub>2</sub> in 70%(70%Cu-30%Ni), 11%Nb matrix, which was produced by Columbus.

### 5.1.2.2 Energy Extraction Using a Superconducting Dump-Switch

Superconducting dump-switches have simpler energy extraction schemes than bypass-switch based circuits as there is no dump resistor. As for superconducting bypass-switches, potential operating temperatures for dump-switches in the LHC 600 A circuits are 50 K and 20 K (Section 5.1). The circuit diagrams for energy extraction from the LHC MCD magnet circuits with superconducting dump-switches operating at both 50 K and 20 K are shown in Figure 5.4.

Superconducting dump-switches have the potential to reduce the peak voltage during energy extraction, meet the magnet energy discharge requirements, and require less length and less heater energy than superconducting bypass-switches. The required length of superconductor for a dump-switch that develops the dump resistance of  $0.7 \, \Omega$  at a temperature just above  $T_c$  is given in Table 5.3. Developing the dump resistance at higher temperatures will reduce the required conductor length but may increase the required heater energy. The advantages and disadvantages of such a superconducting dump-switch are described in Section 3.1.

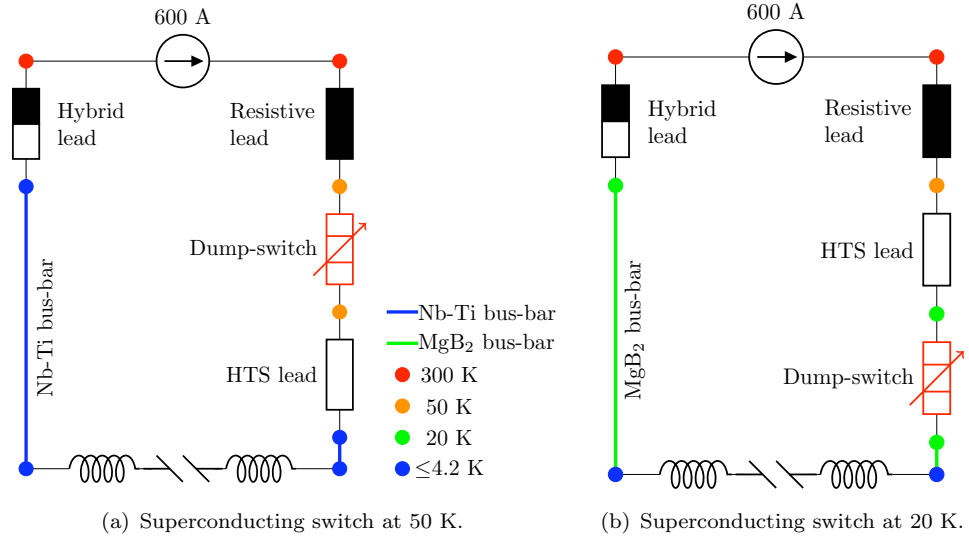


FIGURE 5.4: Magnet circuit layout when the energy is dissipated in a superconducting dump-switch. (a) is for when the dump-switch operates at 50 K and there is a Nb-Ti bus-bar, (b) for when the switch operates at 20 K and there is a  $\text{MgB}_2$  bus-bar.

$T_{op}$ (K)	YBCO based switch		$\text{MgB}_2$ based switch	
	No. of tapes	$L$ (total) (m)	No. of tapes	$L$ (total) (m)
20	2	24	1	21
50	3	52	-	-

TABLE 5.3: Required conductor length for superconducting dump-switches that have  $0.7 \, \Omega$  dump resistance just above  $T_c$ . Lengths are given for switches formed of stainless steel clad YBCO produced by American Superconductor and also  $\text{MgB}_2$  in a 70%(70%Cu-30%Ni), 11%Nb matrix produced by Columbus.

### 5.1.2.3 Cooling of a Superconducting Switch

Superconducting switches are suited to be operated adiabatically as the heater energy must just be sufficient to trigger the switch. If the switch was cooled then more heater energy may be required to make up for the heat loss to the surroundings. Overheating of an adiabatic switch can be avoided by ensuring that there is sufficient thermal mass to absorb the energy from the magnet and the heater. A potential switch configuration is a

spiral bifilar winding of the heater and superconductor. In such designs the diffusion time from the center of the switch to the surroundings would be slow relative to the switching time and so the switch is effectively adiabatic. Cooling between the layers, like that used in fault current limiters [26], is less well suited to energy extraction switches as the switch must not recover as the current decreases. In fault current limiters the superconductor is required to quickly recover once the current decrease to acceptable levels.

The experimental switches (Chapter 4) were tested in pool boiling nitrogen with  $\approx 100 \mu\text{m}$  of insulation between the switch and the cryogen. In these experiments fast switching times were recorded and the cooling was not seen to play a large part over the switching time scales.

In order to prevent the heat from being conducted out of the switch and into the current leads or bus-bars, quench stoppers could be added at the interconnect. These quench stoppers could be copper blocks that have a sufficiently high thermal mass and low electrical resistance to arrest the propagation of quench along the conductor. Similar blocks are used at the interconnection between the HTS part of the LHC current leads and the LTS bus-bar [122]. For recovery to the normal state when the magnet chain is re-powered the switch could be re-cooled by conduction or via controlled helium gas flow.

## 5.2 Design and Characteristics of HTS Switches

A possible application of a superconducting switches is to use YBCO based switches in, for example, the LHC MCD magnet circuits. Other potential LHC magnet circuits, operating temperatures, and choice of superconductor were described Section 5.1.2. This section describes the discharge characteristics of switches that are based stainless steel clad YBCO and operate at 50 K. In this analysis it is assumed that switches have heaters which instantly heat up to an initial heater temperature ( $T_{HI}$ ). This is equivalent to a fast capacitor discharge circuit. This approach allows decoupling of the heater electrical circuit in order to investigate the design parameters of the switch. Switches that have capacitor discharge powered heaters are also examined to investigate the interplay of the heater circuit and magnet circuit. The discharge characteristics of both dump-switches and bypass-switches are compared to the existing discharge characteristics to assess their suitability for energy extraction. The existing discharge characteristics are modelled by switching a  $0.7 \Omega$  dump resistor into the circuit at 15 ms.

### 5.2.1 Configuration of YBCO Based Switches

Thermally activated superconducting switches, whether of the bypass-switch type or dump-switch type, contain a length of superconducting tape that has a heater distributed along its length. There is an insulation layer between the two separate electrical components,

as shown in Figure 5.5. The physical layout of superconducting switches was described in more detail in Section 3.2. The choice of materials and size of the switch depend upon the required magnet discharge characteristics and the switch's operating conditions. The properties of different materials that may find use in superconducting switches are described in detail in Chapter 2. The properties of the materials that are used in this YBCO based switch are reproduced in this section in the form used for the modelling of the switches.

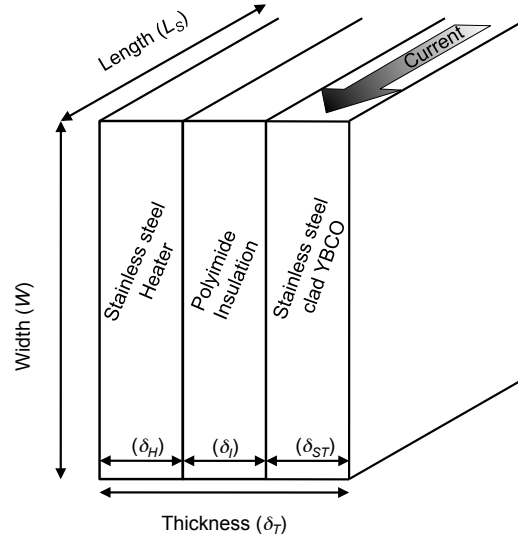


FIGURE 5.5: Physical layout of a superconducting switch based on stainless steel clad YBCO.

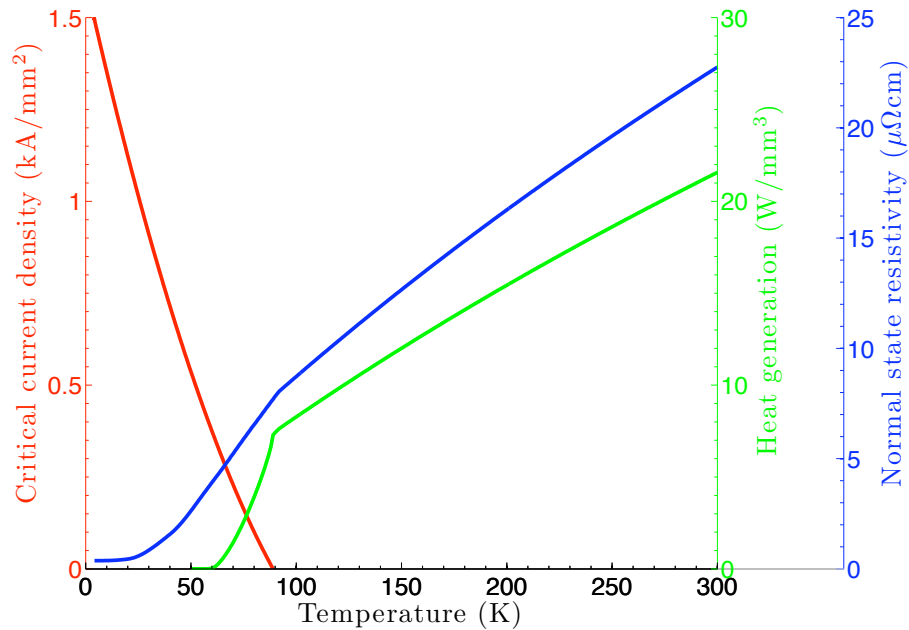


FIGURE 5.6: Superconducting properties for stainless steel clad YBCO produced by American Superconductor. Shown are the engineering critical current density (measured at CERN), the heat generation when the tape is carrying 200 A, and the normal state resistivity (measured at the University of Southampton).

**The superconductor layer** is stainless steel clad YBCO as it has a high normal state resistivity and can operate at 50 K temperatures. Tapes of copper clad YBCO and BSCCO in a silver alloy matrix are currently more widely used than the stainless clad YBCO but their low normal state resistivity means that prohibitively long lengths would be required to develop the required resistance. Stainless steel clad YBCO can be considered to have a fast diffusion time (Section 3.7.1) and so the lumped approximation can be used for this layer. The density ( $\gamma$ ), width ( $W$ ), thickness ( $\delta$ ), superconductor filling factor ( $\lambda$ ), and the critical temperature ( $T_c$ ) are given in Table 5.4 [44]. The  $n$ -value is a function of temperature and is 25 at 77 K, falling to 5 at  $T_c$ . For operation at 50 K, three tapes are required to be used in parallel giving the switch a critical current of 660 A. The resistivity, critical current density, and heat generation are shown in Figure 5.6. The temperature dependent and integrated values of specific heat capacity and thermal conductivity are shown in Figure 5.7. The full range of material properties are given in Chapter 2.

Superconductor	$W$ (mm)	$\delta$ (mm)	$\gamma$ (kg/m <sup>3</sup> )	$\lambda$ (%)	$T_c$ (K)
YBCO	4.33	0.15	8518	$\approx 0.67$	89

TABLE 5.4: Properties of stainless steel clad YBCO tape produced by American Superconductor.

**The heater layer** is a standard resistance heater that in the switches instantly heats to an initial temperature of  $T_{HI}$ . The material used for the heater is stainless steel as it has high resistivity and is suitable for use in a cryogenic environment. In order to provide uniform heating to the superconductor, the heater has the same length and width as the superconductor. A heater thickness of 0.05 mm is used. The heater layer also has a fast diffusion time and so the lumped approximation is valid for this layer. The temperature dependent and integrated values of specific heat capacity and thermal conductivity for stainless steel 304 are shown in Figure 5.7.

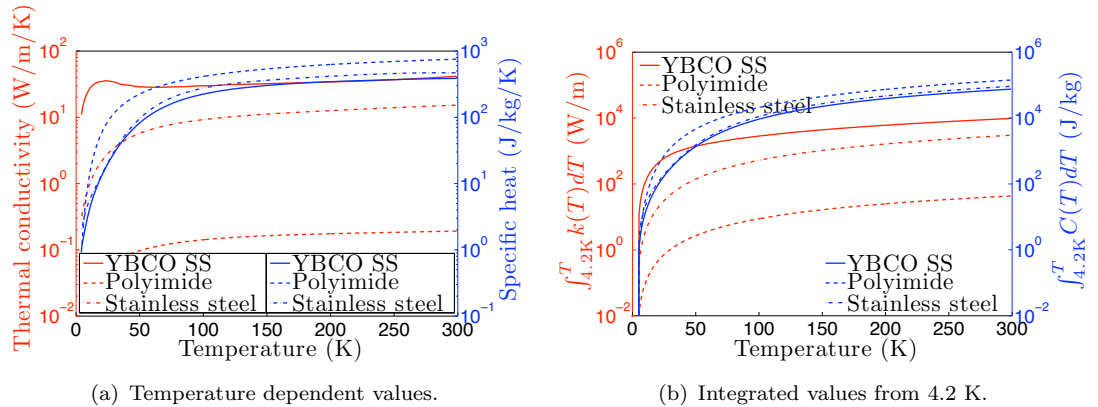


FIGURE 5.7: Thermal conductivity and specific heat capacity of materials used in the stainless steel clad YBCO (YBCO SS) based switch. (a) shows the temperature values and (b) the integrated values from 4.2 K. The YBCO tape was produced by American Superconductor.

**The insulation layer** between the superconductor and heater is required to provide good electrical insulation and to have high thermal diffusivity. Polyimide insulation was chosen for these switches as it provides good electrical insulation and is suitable for use in a cryogenic environment. Its flexible tape form means that it is well suited to switches that are wound into coils. An insulation thickness of  $76.2\ \mu\text{m}$  is used to provide a practical level of insulation [112]. A thickness of  $5\ \mu\text{m}$  could theoretically provide adequate electrical insulation, but in practice this could easily suffer from damage. The  $76.2\ \mu\text{m}$  insulation thickness could be built up from 3 layers of  $25.4\ \mu\text{m}$  thickness to reduce the chance of pin holes degrading the insulation. However, multiple layers of insulation would also increase the complexity of manufacturing the switch. This thickness of polyimide is on the limit of what can be effectively modelled with the lumped approximation (Section 3.7.1). The temperature dependent and integrated values of specific heat capacity and thermal conductivity are shown for both epoxy and polyimide in Figure 5.7. A commercial polyimide insulation that is widely used is Kapton<sup>TM</sup> from DuPont<sup>TM</sup> [112] that is commonly available in  $25.4\ \mu\text{m}$  and  $12.7\ \mu\text{m}$  thicknesses.

### 5.2.2 Discharge Characteristics of the MCD Magnets when Using a YBCO Based Bypass-Switch

Energy extraction from the MCD magnet chain was modelled with the superconducting bypass-switch based scheme described in Section 5.1.2.1. This bypass-switch operated at 50 K and had the design described in Section 5.2.1. This design is a switch that is not optimised and has a heater that instantaneously warms to 300 K. The initial heater approximation is valid when the heater is powered by a fast capacitor discharge as discussed in Section 5.3.11. The discharge characteristics are shown in Figure 5.8. A log time scale is used to show the switching characteristics at early time scales as well as the final state of the switch when all of the magnet energy has been dissipated. Time zero is where the heater instantly rises to its initial temperature. The modelled discharge characteristics of the existing mechanical switch are also shown for comparison. In the LHC MCD circuits a  $0.7\ \Omega$  dump resistor is switched into the circuit after 15 ms; this results in a peak voltage of 420 V. The magnet chain then has an exponential decay with 95 % of the energy being dissipated in 81 ms.

The top pane of Figure 5.8 shows the temperature evolution of the heater and superconductor layers. The large initial temperature gradient between the heater at 300 K and the superconductor at 50 K results in high heat transfer from the heater, through the insulation, to the superconductor. This causes the superconductor to rapidly warm and it reaches its  $T_{cs}$  (200 A) of 55 K about 1 ms later. As the current bypass the switch the current sharing temperature will increase due to the  $J_c(T)$  characteristics. The heat generation in the current sharing regime is insignificant compared to the heat that is provided by the heater as only a small portion of the magnet energy is dissipated in the switch

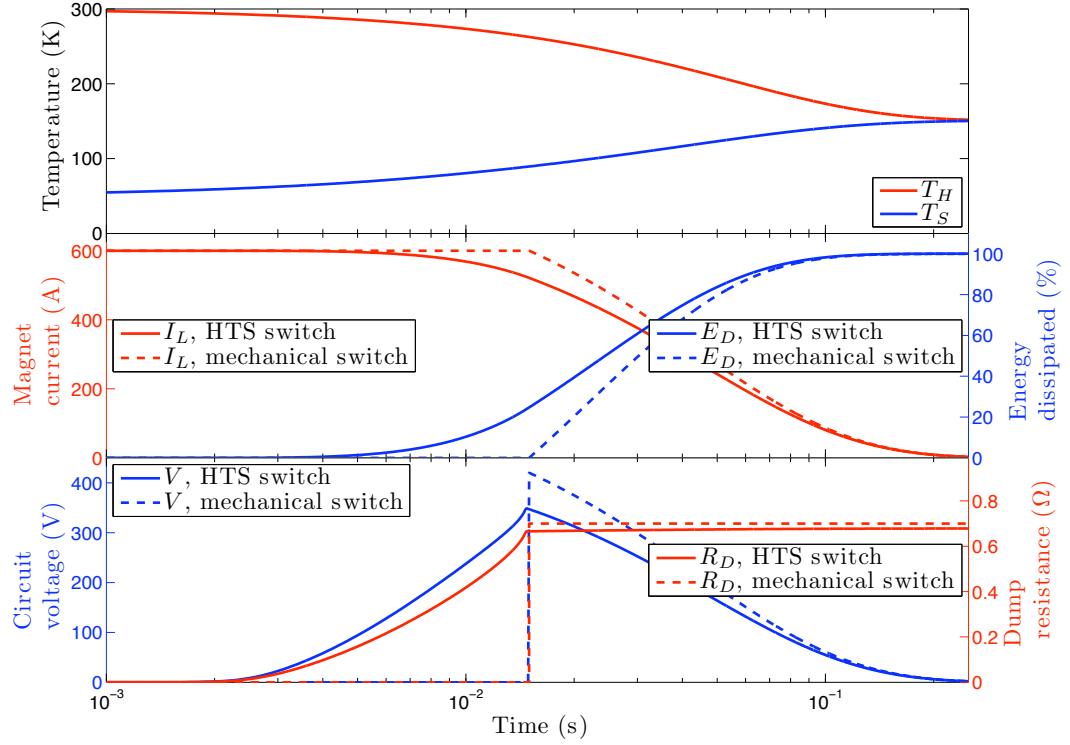


FIGURE 5.8: Switching characteristics of a HTS bypass-switch. The top pane shows the thermal histories of the heater ( $T_H$ ) and superconductor ( $T_S$ ). The middle pane shows the magnet current ( $I_L$ ) decay and energy dissipated ( $E_D$ ) for the HTS bypass-switch and for a mechanical switch, both with a  $0.7 \Omega$  dump resistor. The bottom pane shows the circuit voltage ( $V$ ) and the dump resistance ( $R_D$ ) for the two systems. Time zero is when the heater temperature instantly rises to  $T_{HI}$ .

itself due to the parallel connected dump resistor. In 3 ms the dump resistance grows to  $83 \text{ m}\Omega$  with a superconductor temperature of 62 K, this causes the circuit voltage to rise to 50 V (lower pane) and the magnet current to decay by 1 A (middle pane). After 11 ms  $T_S$  has increased to 82 K with a corresponding switch resistance of  $1.84 \Omega$ ; the total dump resistance is  $0.5 \Omega$  due to the presence of the  $0.7 \Omega$  resistor in parallel. The increase in resistance results in the magnet current decaying to 550 A

The superconductor reaches its  $T_c$  of 89 K after about 15 ms, with 27 % of the magnet being discharged whilst the superconductor is still in the current sharing regime. At just above  $T_c$  the dump resistance of the HTS bypass-switch system has reached  $0.66 \Omega$  and has reduced the magnet current to 513 A. The peak voltage with HTS bypass-switch was 341 V, at which point 93 % of the current was flowing in the dump resistor. The dump resistance of the HTS bypass-switch system gradually increases from  $0.66 \Omega$  to  $0.68 \Omega$  due to warming of the fully normal superconductor. After 15 ms the magnet current has a close to exponential decay due to the almost constant dump resistance. The HTS switch system has a slightly slower decay rate than the mechanical-switch system due to its lower dump resistance. However, the magnet is discharged sooner due to the earlier onset of energy dissipation with 95 % of the energy being dissipated after 76 ms compared to 81 ms for the existing setup. The heat flow within the switch is always from the heater to the

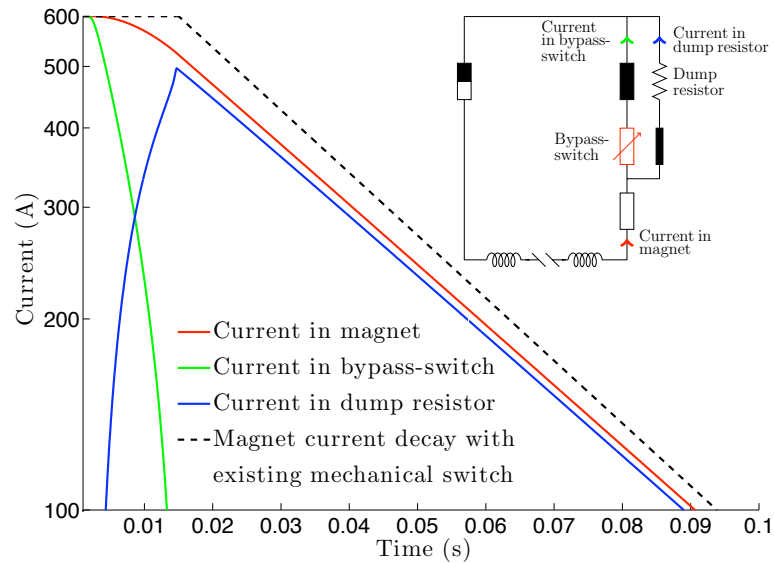


FIGURE 5.9: Currents in the magnet, switch, and dump resistor during energy extraction with a superconducting bypass-switch and with the existing mechanical bypass-switch. Inset is the circuit diagram of the energy extraction scheme; the power converter is bypassed during energy extraction.

superconductor, with the temperatures equalizing to 151 K at a time greater than 0.235 s. At this time the magnet current has decayed to 4 A and over 99.9 % of the magnet energy has been dissipated.

This HTS bypass-switch, which was not optimised, discharged the magnet in about the same time and with a slightly lower peak voltage than the mechanical switch system (Figure 5.8). However, the switch required a long length of conductor (1 km - Table 5.2) and a large amount of heater energy (189 kJ), both of which are too large to be practical. One of the purposes of a bypass-switch is to dissipate the magnet energy at warm in a dedicated dump resistor. The heater energy required for this HTS bypass-switch (189 kJ) is 35 times higher than the energy stored in the relatively low energy MCD magnet circuits (5.5 kJ). The reason for such a large required length and energy is that the switch must develop a high resistance to shunt the current into the dump resistor. If the switch only had to develop the dump resistance then the length could be reduced by  $\approx 20$  times with a corresponding decrease in heater energy. As dump-switches have no parallel resistor they have these reduced length and energy requirements. The discharge characteristics of such a dump-switch are described in the next section.

### 5.2.3 Discharge Characteristics of the MCD Magnets when Using an YBCO Based Dump-Switch

A reduction in length and heater energy can be achieved by dissipating the magnet energy in a dump-switch as the switch must only develop a dump resistance of  $0.7 \Omega$ . The dump-switch based energy extraction scheme for the MCD magnet circuits is described



in Section 5.1.2.2. This dump-switch that is operated at 50 K has a design described in Section 5.2.1. This design is for a switch that is not optimised and has a heater that instantaneously warms to 300 K. Developing this resistance at just above  $T_c$  requires a dump-switch that is 53 m long; this requires 9.45 kJ of heater energy. As the magnet energy is also dissipated in the switch, a total of 15 kJ of energy is deposited in the dump-switch. This is 12.6 times less than the heater energy that was deposited in the corresponding bypass-switch. The discharge characteristics obtained with both the dump-switch and the existing mechanical switch are shown in Figure 5.10.

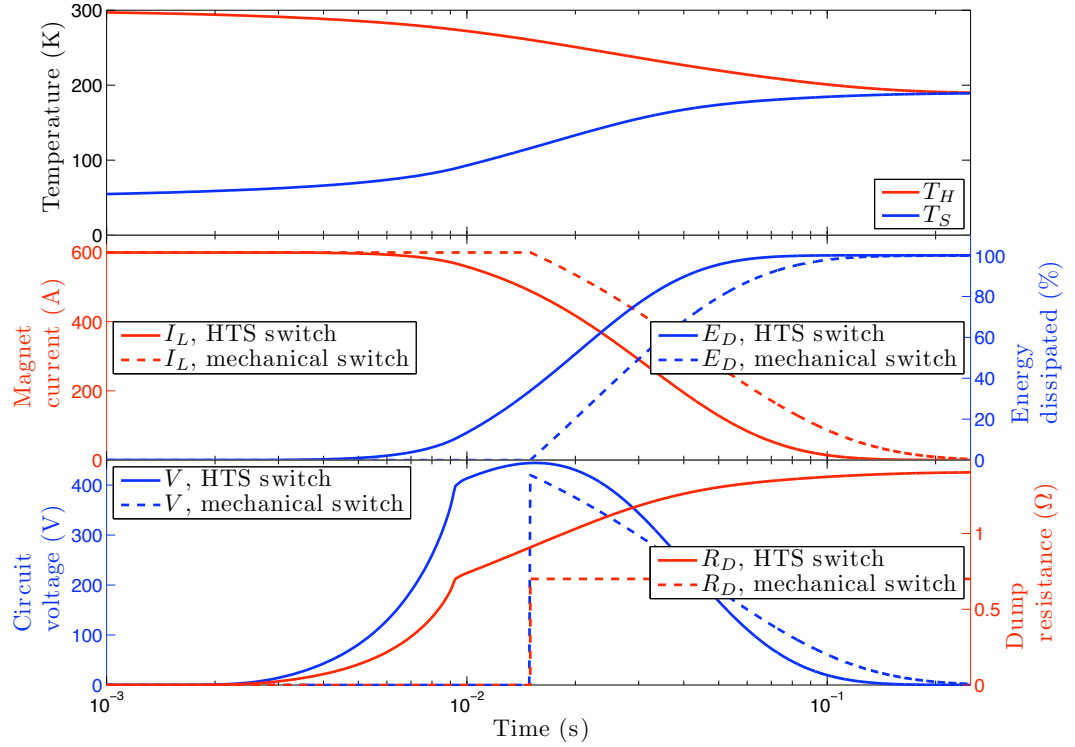


FIGURE 5.10: Switching characteristics of a HTS dump-switch. The top pane shows the thermal histories of the heater ( $T_H$ ) and superconductor ( $T_S$ ). The middle pane shows the magnet current ( $I_L$ ) decay and energy dissipated ( $E_D$ ) for the HTS dump-switch and for a mechanical switch with a  $0.7 \Omega$  dump resistor. The bottom pane shows the circuit voltage ( $V$ ) and the dump resistance ( $R_D$ ) for the two systems.

The top pane of Figure 5.10 shows the temperature history of the switch. The switch operates at 50 K and in this case the heater instantly warms to 300 K with an associated linear temperature gradient across the insulation layer. Due to this large temperature gradient heat from the heater flows to the superconductor, which begins to warm and reaches  $T_{cs}$  of 55 K about 1.1 ms later. The heat generation in the current sharing regime contributes to the heating of the superconductor that would otherwise have slowed down due to the reduction in heat conduction through the insulation due the reducing temperature difference between the heater and the superconductor. In the current sharing regime the superconducting tape develops a voltage (lower pane of Figure 5.10) and the magnet begins to discharge (middle pane) with the energy being dissipated in the dump-switch. The heat generation and circuit voltage continue to grow with the superconductor

reaching its  $T_c$  of 89 K after about 9 ms, with  $\approx 10\%$  of the magnet energy having being dissipated in the current sharing regime. The mechanical switch has an opening time of 15 ms, at which point a  $0.7\ \Omega$  dump resistor is instantly switched into the circuit causing the magnet to start to discharge with the resulting peak circuit voltage being 420 V. By this time the dump-switch, which is now fully normal with an HTS temperature of 116 K, has dissipated 34 % of the magnet energy and reduced the magnet current by  $\approx 112$  A, with a peak circuit voltage of 444 V. This dump-switch with a resistance of  $0.7\ \Omega$  at  $T_c$  discharges the magnet much faster than an equivalent mechanical bypass-switch system; 95 % of the magnet's energy was discharged in 49 ms, compared to 81 ms obtained with the mechanical switch system. The peak circuit voltage is only marginally higher, 444 V compared to 420 V. In this design of dump-switch the heat always flows from the heater to the superconductor and so the heater never acts as a heat sink. After 235 ms all of the magnet has been discharged and the temperature within the switch is uniform at 189 K.

This non-optimised superconducting dump-switch comes close to matching the magnet discharge profile obtained with the mechanical switch and dump resistor system. Furthermore, it required twenty times less length of superconductor and heater energy than the equivalent superconducting bypass-switch. In order to achieve the required magnet discharge characteristics, the length of conductor needs to be refined to reduce the peak voltage. The length and initial heater energy can be optimised to give a dump-switch with low heater energy requirements. This switch model features an instantaneous heater that resulted in high thermal gradients across the insulation; there is scope for optimising the heater to reduce these internal thermal gradients.

#### 5.2.4 Application of HTS Switches to Magnet Circuits such as MCD, Bypass- or Dump- Type?

Superconducting dump-switches and superconducting bypass-switches can meet the energy extraction requirements of the MCD circuits. Superconducting dump-switches can achieve this with practical lengths of superconductor and practical heater energies; superconducting bypass-switches are not practical due to the long lengths of superconductor and high heater energies that they require. A superconducting bypass-switch for the LHC MCD magnet circuits that operates at 50 K, requires 1046 m of superconductor and an input heater energy of 189 kJ, much higher than the 5.5 kJ of magnet circuit energy that is to be dissipated. Superconducting bypass-switches may be more suited to high energy circuits that require bypass switches and energy extraction at warm due to the larger magnet energies involved; for example the 1.3 GJ LHC main dipole circuits. Superconducting dump-switches require less length and less heater energy and are suitable for low and medium energy circuits. The optimisation of dump-switches is discussed in the following section.

### 5.3 Optimisation of HTS Dump-Switches for 600 A Magnet Circuits Similar to MCD

The starting design of the switch to be optimised is the same design as the above initial heater temperature switches, with each design aspect then being considered in turn. The superconductor layer is stainless steel clad YBCO, there is a stainless steel heater layer that instantly warms to an initial temperature, and there is 76.2  $\mu\text{m}$  of polyimide insulation. The operating temperature is 50 K and 3 tapes are used in parallel.

#### 5.3.1 Required Magnet Discharge Characteristics

Before optimising a dump-switch for energy extraction it is necessary to consider what are the required magnet discharge characteristics. Any energy extraction scheme is a compromise between quickly reducing the magnet current so that a quenching magnet does not overheat, yet still having a low enough  $\frac{dI_L}{dt}$  so that the discharge voltage does not exceed the allowable limits. The LHC existing energy extraction schemes achieve this compromise and so any proposed system must be equal to or better than the existing system, with the decaying magnet current never higher than that obtained with mechanical switch.

The peak circuit voltage should not be greater than the peak circuit voltage obtained with the mechanical switch so that the existing magnet insulation can be used. A superconducting switch may also allow a reduction in the peak circuit voltage due to the non-linear resistance and a faster initiation of current decay leading to a more gradual transition and lower  $\frac{dI_L}{dt}$ .

It is not sufficient to simply set an arbitrarily high threshold, such as 95 %, of the energy to be discharged in the same time as the existing mechanical switch and warm dump system. The reason for this is that it is conceivable to have a dump-switch that is initially too slow to act but then rapidly achieves a high resistance ( $> 0.7 \Omega$ ). Such a switch could be made to discharge 95 % of the magnet energy in the required time, but at times less than the 95 % threshold the magnet current would be higher than in the existing system. This could result in unacceptable temperature rise in a quenching magnet.

The required magnet discharge characteristics are such that:

- The current in a discharging magnet must never be higher than that obtained with the existing mechanical switch and dump resistor at any given time.
- The peak circuit voltage must not be higher than that obtained with the existing mechanical switch and dump resistor, and should be minimised with respect to alternate dump-switch designs.

### 5.3.2 Minimisation of Switch Length that Meets the Discharge Requirements

The thermal characteristics of bypass-switches and of dump-switches are similar during the initial switching phase, before significant magnet energy dissipation, as both switches have the same switch layout and receive the same heater energy per unit length. The switching characteristics are different in the dumping phase. The electrical characteristics are different as the dump resistance of the dump-switch system has a strong dependence on temperature. The temperature dependence of the dump resistance of the bypass-switch system is less due to the presence of a parallel resistor that limits the overall resistance growth. The thermal characteristics are also different as the superconducting tape in the dump-switch receives much more magnet energy than in the bypass-switch.

The simplified dump-switch model described in Section 5.2.3 did not meet the magnet discharge requirements as it developed too high a resistance causing a fast magnet decay rate and a high peak voltage ( $\approx 440$  V). The bypass-switch did not have this high peak voltage as the resistance was limited by the parallel dump resistor. Reducing the dump resistance of the dump-switch would lower the magnet decay rate and the peak voltage. The resistance can be reduced by reducing the length of the dump-switch. The thermal profiles of dump-switches having different lengths are shown in Figure 5.11.

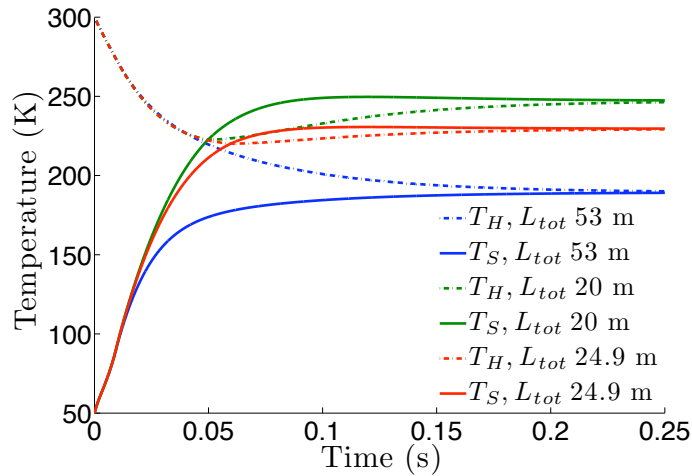


FIGURE 5.11: Effect of changing the length on the thermal profiles of a superconducting dump-switch.

Decreasing the total length ( $L_{tot}$ ) of conductor does not change the initial thermal profiles (Figure 5.11) as this regime is dominated by the heater and insulation, which is the same per unit length for each design. The thermal profiles diverge after  $\approx 16$  ms due to the deposited magnet energy per unit length being different for the three switch designs. The shorter switches receive more magnet energy per unit length and so have a correspondingly higher final temperature. This increase in temperature means that the superconductor temperature exceeds that of the heater and so the direction of heat flow is reversed and the heater acts as a heat sink.

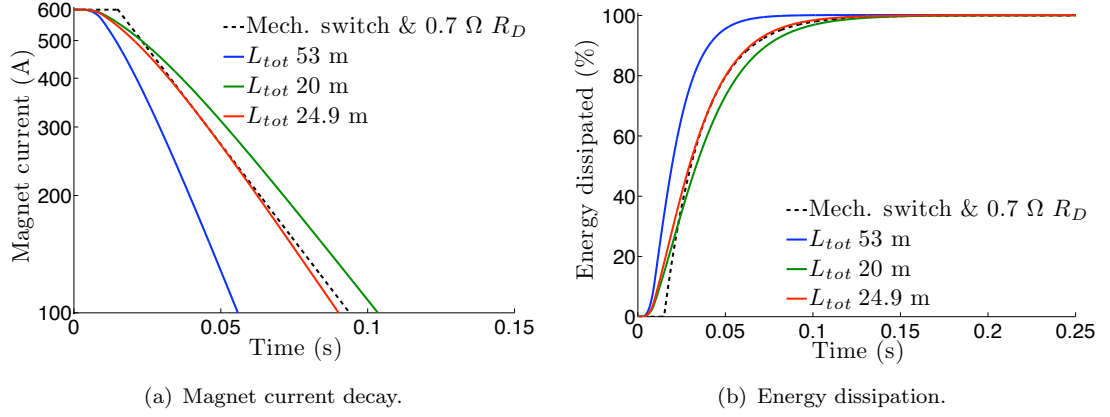


FIGURE 5.12: Effect of changing the length on the current decay (a) and on the energy dissipation (b).

Decreasing the switch length to 20 m and 24.9 m results in the switching characteristics shown in Figure 5.12. The magnet current decay with these shorter designs of switch start at about the same time ( $\approx 5$  ms) as the same insulation and heater is used, but the subsequent decay rate is slower due to the shorter lengths decreasing the resistance. The  $L_{tot}$  of 20 m is too short a switch as the current decay is so slow that after 24 ms the magnet current is always greater than that obtained with the mechanical switch setup and so the magnet discharge requirements are not met. The  $L_{tot}$  of 24.9 m has a magnet current decay rate that is slower than the dump-switch having a resistance of  $0.7 \Omega$  at  $T_c$  ( $L_{tot}$  53 m), but as the current decay starts earlier the current is never more than that obtained with the existing setup and so the magnet decay requirements are met.

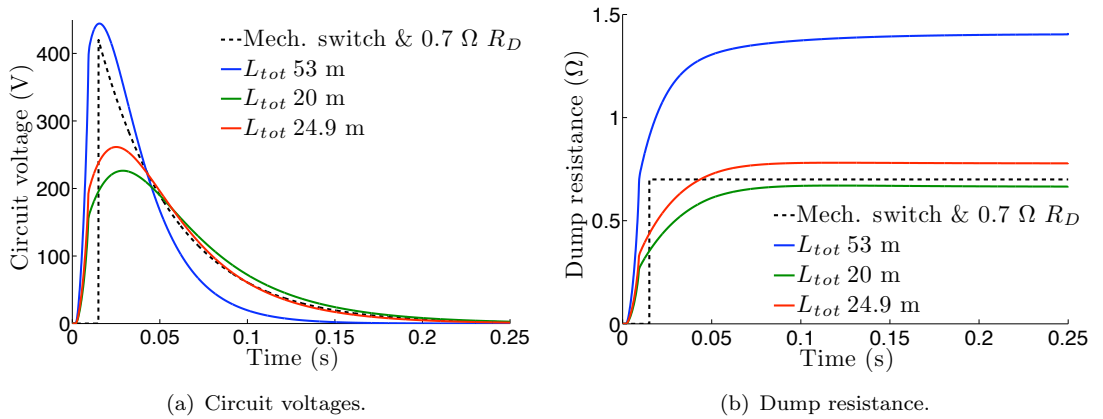


FIGURE 5.13: Effect of changing the switch length on the circuit voltage (a) and on the dump resistance (b).

The peak circuit voltages (Figure 5.13) of the shorter designs are lower than that obtained with the mechanical switch, but the longest switch has a peak voltage that is slightly higher and so does not meet the magnet discharge requirements. Comparing the magnet decay of the superconducting dump-switches and the mechanical switch shows that a slower dump-switch could be used and this would result in a lower peak voltage. The minimum length

of switch is the one that results in the magnet decay current criterion being met with the minimum voltage.

A switch total length of 24.9 m (three tapes of 8.3 m) is the minimum length that meets the magnet discharge requirement for these operating conditions. The discharge current criterion is met and the peak circuit voltage is also minimised. However, this length is only the minimum for these operating conditions and will change as the design parameters are changed.

### 5.3.3 Performance Metrics for Superconducting Switches

The previous section (Section 5.3.2) showed that length of a dump-switch is not a free parameter as it must be refined in order for the switch to meet the magnet discharge requirements. Switch length is a performance metric of a superconducting switch, but it is not the only one as superconducting switches are complex devices that can have their performance defined in multiple ways. In order to compare the performance of superconducting switches that allow the correct magnet discharge but have different design parameters it is necessary to define the performance metrics for superconducting switches. These metrics are described in turn below and are in addition to the magnet discharge requirements detailed in Section 5.3.1.

The time when the magnet discharge is considered to be finished ( $\tau_F$ ) is set to be the same for all switches in order to allow comparison of the final state of different switches. This final time is defined as five times the magnet decay time constant ( $\frac{L}{R}$ ) of the existing extraction system plus the opening time of the mechanical switch.  $\tau_F$  represents the time at which the magnet current has decayed by over 99 % of the original value in the existing mechanical bypass-switch setup. For the MCD magnet circuits  $\tau_F = 235$  ms, at which point the bypass-switch has a temperature of 151 K, the magnet current has decayed to 4 A, and over 99.9 % of the magnet energy has been dissipated.

**Heater energy** ( $E_H$ ), should be minimised in order to reduce the energy being deposited at cold, limit the temperature rise and thermal gradients in the switch, and to allow a smaller capacitor bank to be utilized. Where the heater is powered by a capacitor discharge circuit the heater energy is equal to the stored energy in the capacitor, where switches with instantaneous heaters are used the energy is due to the enthalpy change from raising the heater from the operating temperature to the initial heater temperature ( $T_{HI}$ ).

**Total length** ( $L_{tot}$ ) of the conductor is the switch length multiplied by the number of strands. The switch length is optimised for a given set of design parameters in order to meet the required magnet discharge characteristics, but different inputs result in different optimum lengths. The total length should be minimised in order to have a smaller, lower mass switch and also to decrease the cost of the switch.

**Peak voltage** ( $V_{max}$ ) of the magnet circuit during energy extraction, which is required to be never more than the existing, should also be minimised in order to reduce the insulation requirements and chance of arcing in the magnet circuit. The existing mechanical switch based energy extraction schemes have a fixed dump resistance and the peak voltage occurs at the moment that this is switched into the circuit. For the LHC MCD magnet circuits  $V_{max}$  is 420 V. However, superconducting switches develop the dump resistance more gradually and so the magnet current will have already started to decay before the maximum resistance is attained, potentially resulting in a lower peak voltage. As the rate of decay of magnet current and the maximum dump resistance depend on the design of the superconducting switch it is possible to minimise the peak magnet circuit voltage.

**Maximum difference in temperature** ( $|T_H - T_S|_{max}$ ) in the switch between the heater and superconductor layers should be minimised to reduce the internal thermal gradients and thus stresses in the switch. For switches where the heater instantly warms up the maximum difference tends to be  $(T_{HI} - T_{SI})$  but for capacitor discharge powered heaters the maximum temperature difference may occur later.

**Average difference in temperature** ( $\overline{\Delta T}$ ) in the switch between the heater and superconductor evaluated between time equal to zero and  $\tau_F$ ;

$$\overline{\Delta T} = \frac{1}{\tau_F} \int_0^{\tau_F} |T_H - T_S| dt. \quad (5.1)$$

Time zero is when the capacitor discharge begins, or when the heater instantly warms up to  $T_{HI}$ .

**Final temperature of the switch** ( $T_F$ ) is the average temperature of the heater and superconductor layers at  $\tau_F$ . The final temperature of the switch ( $T_F$ ) should be below 300 K to avoid overheating but should also be minimised to prevent high thermal gradients within the system that the switch is integrated into as these could lead to damage due to thermal stresses. A high final temperature also increases the cryogenic cost of switching and the subsequent re-cooling of the switch.

In summary the performance metrics of a superconducting switch, which should all be minimised, are:

1. Heater energy,  $E_H$ .
2. Total length,  $L_{tot}$ .
3. Peak voltage of the magnet circuit,  $V_{max}$ .
4. Maximum temperature difference,  $|T_H - T_S|_{max}$ .
5. Average temperature difference,  $\overline{\Delta T}$ .
6. Final temperature,  $T_F$ .

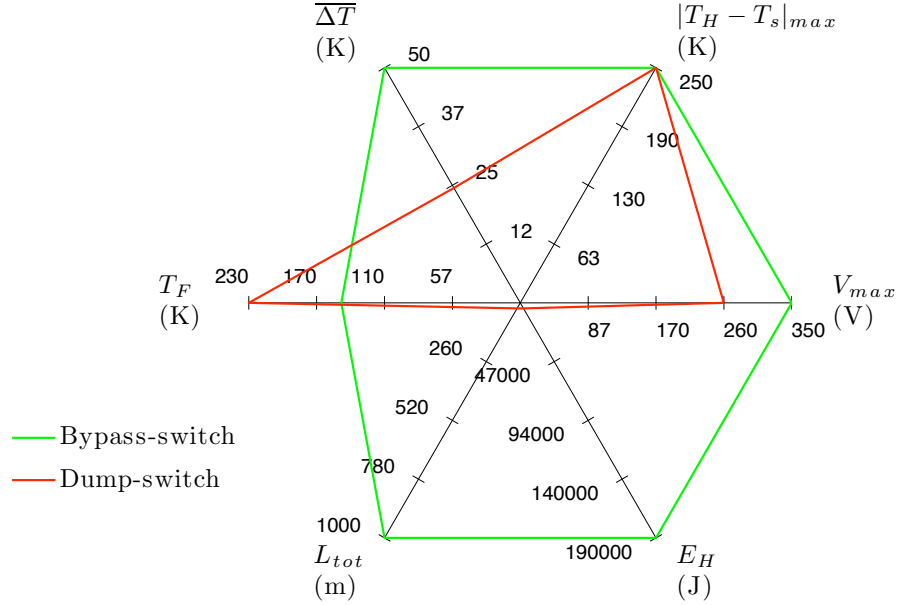


FIGURE 5.14: Star plot showing the performance metrics of superconducting bypass and dump switches that use stainless steel clad YBCO, operate at 50 K and have a heater that instantly warms to 300 K. A smaller enclosed area represents a better performing switch.

**Star plots** can be used to provide a graphical representation of the performance metrics described above. In a star plot for switch performance there are six axes corresponding to the six performance metrics. The distance along each axis represents the magnitude of the metric. For all of the chosen performance metrics smaller values represent higher performances and a smaller enclosed area may represent a better performing switch. A star plot of the performance of a superconducting bypass-switch and of a superconducting dump-switch are shown in Figure 5.14. The superconducting bypass-switch operates at 50 K, has an initial heater temperature of 300 K, uses 1046 m of stainless steel clad YBCO, and was described in Section 5.2.2. The superconducting dump-switch also operates at 50 K with an initial temperature of 300 K but as there is no parallel dump resistor only 24.9 m of stainless steel clad YBCO are needed. This switch was described in Section 5.3.2. The star plot clearly shows that the dump-switch out performs the bypass-switch in all performance metrics except for the final temperature, which is higher due to the magnet energy being dumped in the shorter switch. However, the final temperature is still acceptable. As these switches have the same initial heater temperature of 300 K, they also have the same  $|T_H - T_S|_{max}$  that occurs at time equal to zero. The star plot also makes apparent the difference in required length and energy that were part of the reason for discarding the use of superconducting bypass-switches; this was described in Section 5.2.4. Switches that have performance metrics closer to the center of the star are better switches. However, there is often a compromise as the reduction in one indicator may result in the increase in another. For example, a smaller  $|T_H - T_S|_{max}$  means that conduction through the insulation is less



and so a longer switch is required to achieve the required discharge characteristics. For the cases considered, the superconducting dump-switch clearly has a smaller area and thus better performance than the bypass-switch; performance scores based upon the star plot area can be used to compare switches where it may not be immediately apparent as to which design is better.

**Area score** is defined as  $\frac{1}{\text{area}}$  of the star plot and so higher values represent better performing switches. The area score will indicate the performance of a single switch or allow comparison of switches having different parameters based on the absolute area of the star plot. Figure 5.15 shows area scores from the above star plot ( Figure 5.14) for the superconducting bypass-switch described in Section 5.2.2 and the superconducting dump-switch described in Section 5.3.2. The area score is much higher for the dump-switch than for the bypass-switch. This is due to the large star plot area of the bypass-switch that results from the long lengths and high energies that are required. One problem with using absolute area is that performance metrics that have high values (*e.g.*  $E_H$ ) with respect to the others can distort the score and so it would be possible for a better performing switch to be penalised for having a heater energy that was only relatively only slightly more than other switches but the magnitude of the increase dominates the star plot area. For this reason it is advantageous to use relative areas when comparing sets of switches.

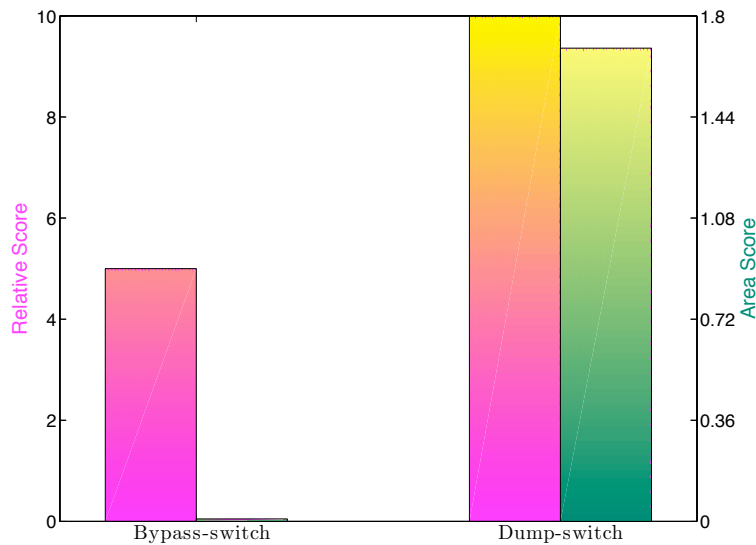


FIGURE 5.15: Relative and area scores for superconducting bypass and dump switches. Relative scores are read on the left axis; area scores are read from the right axis.

Higher performing switches have higher scores and are a lighter colour at the top

**Relative score** is used for comparing different switches and is related to the area score, but the area is scaled relative to the other switches. For each performance metric, the values are scaled between 1 and 2 with 1 representing the minimum value and 2 the maximum value. Scaling the minimum to 1 rather than the 0 prevents the existence of false zero areas, which would occur if a switch was the best performer in all but one of the categories. The inverse of the enclosed area of the star chart with these relative

dimensions is then calculated. To improve readability the scores are scaled to the best switch having a value of 10. Figure 5.15 shows relative scores calculated from scaling the above star plot (Figure 5.14). The relative scores indicate that the dump-switch is still the better performing switch but the relative score of the bypass-switch is now more significant to reflect that in one case,  $(T_F)$ , it out performs the dump-switch and in another,  $|T_S - T_H|_{max}$ , it performs equally well.

When comparing the performance of the switches a more complete description of performance is gained if both the relative and area scores are used in-conjunction with the star plot. For the examples chosen, in a comparison of the bypass-switch and the dump-switch both the relative and area scores show that the dump-switch has a higher performance and the star plot shows that it out performs the bypass-switch on all of the performance indicators except the final temperature, which is 230 K compared to 152 K for the bypass-switch.

### 5.3.4 Heater Energy

In order achieve fast thermal diffusion through the insulation the initial heater temperature for the above switches was set to 300 K. However, a  $T_{HI}$  of 300 K is not ideal as it requires a high input heater energy ( $\approx 4.5$  kJ) and also leads to high internal thermal gradients that can stress the switch. Therefore switches with a high  $T_{HI}$  perform badly on the  $E_H$ ,  $|T_H - T_S|_{max}$ , and  $\overline{\Delta T}$  performance metrics. Reducing the initial heater temperature will reduce the thermal gradients and may also reduce the required heater energy. If a lower  $T_{HI}$  is used then the thermal diffusion will be slower leading to a delay in an onset of magnet current decay. This requires a longer and thus more resistive switch to be used in order to meet the magnet discharge requirements.

**Reducing the initial heater temperature** to a lower temperature of 200 K will result in the thermal profiles shown in Figure 5.16. Lowering  $T_{HI}$  requires the length to be re-optimised in order to meet the magnet circuit discharge requirements, the new required total length for  $T_{HI}$  of 200 K is an increase to 34.5 m from 24.9 m. The temperature traces of a switch with too long a length (39 m) and too short a length (30 m) are also shown, as is the  $T_{HI}$  300 K design with a length of 24.9 m. The thermal profiles of the three  $T_{HI}$  200 K switches are very similar up to  $\approx 30$  ms as they have the same heater energy per unit length and the same heat conduction per unit length through the insulation. However, the heat deposited in the switch due to the discharge of the magnet is greater per unit length for the under length switch and so it has a higher final temperature; the over length switch receives less magnet energy per unit length and so it has a lower final temperature. On all three  $T_{HI}$  200 K switches the kink in the rise in superconductor temperature at  $\approx 13$  ms that is due to the dissipation of magnet energy is more noticeable than in the  $T_{HI}$  300 K designs as the magnet energy is more significant with respect to the heater energy. The

heater layer in the  $T_{HI}$  200 K switches also starts to acts as a heat sink earlier (40 ms) than the  $T_{HI}$  300 K design (62 ms).

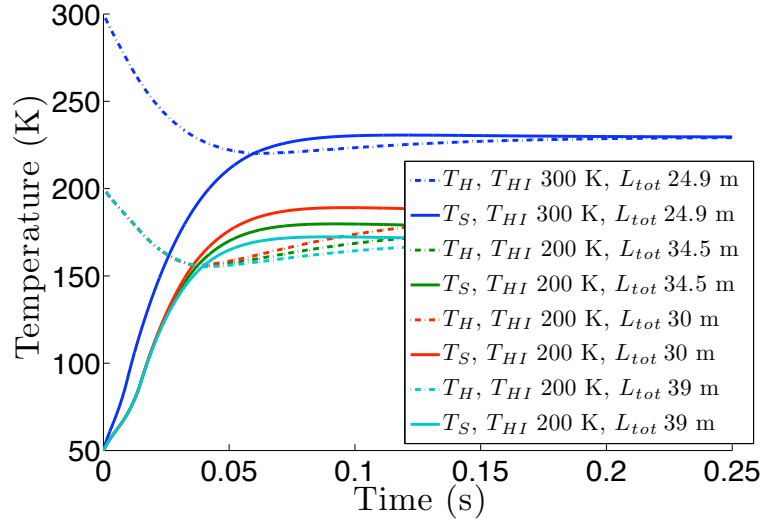


FIGURE 5.16: Effect of changing the initial heater temperature on the thermal profiles of a superconducting dump-switch.

The lower initial heater temperature means that there is less initial heat conduction through the insulation and so the time to reach  $T_{cs}$  is longer for the  $T_{HI}$  200 K switches than the  $T_{HI}$  300 K ones. This causes a corresponding delay in the onset of magnet current decay as shown in Figure 5.17(a). Due to the similar initial thermal profiles of the  $T_{HI}$  200 K switches their magnet current decays start at the same time. However, as they have different lengths they develop different resistances and so after initiation the resulting magnet decays are also different. The longest, most resistive, switch has the fastest decay and dumps the magnet energy faster than the optimised length  $T_{HI}$  300 K design. The shortest, least resistance, switch has the slowest magnet discharge and between  $\approx 20$  ms and  $\approx 65$  ms it is too slow and has decreased the magnet current by less than the existing mechanical switch based system. However, the resistance of this under-length switch continues to grow, speeding up the rate of magnet decay. This increase in resistance means that after 65 ms the magnet current is lower than in the existing setup and the magnet is discharged in a shorter time. The optimum length switch never has a current greater than that obtained with the existing setup and also discharges the magnet faster than the optimised  $T_{HI}$  300 K design. These different rates of magnet current decay result in different peak voltages.

The voltage traces during energy extraction are shown in Figure 5.17(b). All of the switches, even with non-optimum lengths and fast magnet discharge times, have lower peak voltages than that obtained with the existing mechanical switch. Until  $\approx 15$  ms the  $T_{HI}$  200 K switches have similar circuit voltages that are less than that obtained with the faster initiating  $T_{HI}$  300 K switch. After this time the rate of voltage increase decreases as a function of switch length and thus resistance. The longest, most resistive, switch has the highest peak voltage, the optimised length switch the next highest, and the under-length

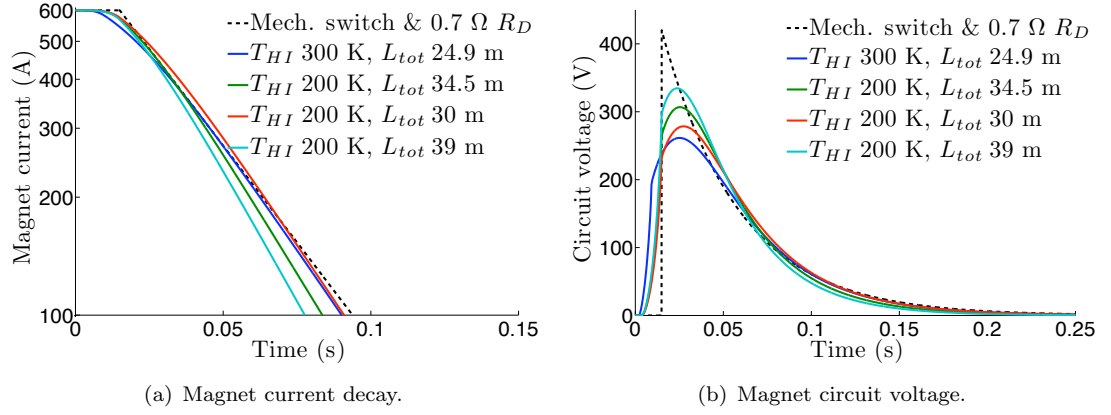


FIGURE 5.17: Effect of changing the length on the current decay (a) and on the circuit voltage (b).

switch lower still. The shorter switches have lower resistances that cause slower rates of magnet decay that lead to lower peak voltages. The  $T_{HI}$  300 K design, which has the shortest length, has the lowest peak voltage due to its more gradual current decay as a result of its earlier discharge initiation and lower resistance.

**Switch length as a function of  $T_{HI}$**  is set by the refining of the length for a given  $T_{HI}$  so that the superconducting dump-switch meets the magnet discharge requirements (Section 5.3.2). The switching characteristics of switches with a range of initial heater temperatures are described below, with Figure 5.18 showing the thermal profiles. The overall shapes of the curves are similar, with the  $T_{HI}$  160 K design having a more pronounced kink in the rise of the superconductor and the  $T_{HI}$  220 K design having more heat transfer from the superconductor to the heater. The higher  $(T_{HI} - T_{SI})$  of the  $T_{HI}$  220 K design gives it the highest rate of heat conduction through the insulation layer with a corresponding faster initial rate of temperature rise of the superconductor layer.  $T_{cs}$  is reached in  $\approx 2$  ms and  $T_c$  in  $\approx 13$  ms, compared to  $\approx 3$  ms and  $\approx 16$  ms for the  $T_{HI}$  185 K switch. Between 10 ms to 20 ms there is a kink caused by the magnet energy accelerating the temperature rise of the superconductor layer. This is more noticeable in the  $T_{HI}$  160 K design than the higher  $T_{HI}$  designs due to its initially lower rate of temperature rise that results from the lower initial heat conduction through the insulation.

The faster initial temperature rise of the  $T_{HI}$  220 K switch means that it has a shorter delay to the onset of magnet current decay than the other two switches; this is shown in Figure 5.19(a). This delay is  $\approx 6$  ms for the  $T_{HI}$  220 K switch and  $\approx 8$  ms for the other two. This longer delay means that the lower  $T_{HI}$  switches must more rapidly dissipate the magnet energy (Figure 5.19(a)) in order to meet the magnet current decay requirements. This fast current decay is achieved by increasing the resistance of the dump by means of increasing the switch length. This has the disadvantage that once fully normal the longer switches have a high resistance, which gives a fast discharge and leads to a high peak voltage. The faster initiation of magnet current decay of the  $T_{HI}$  220 K switch means that

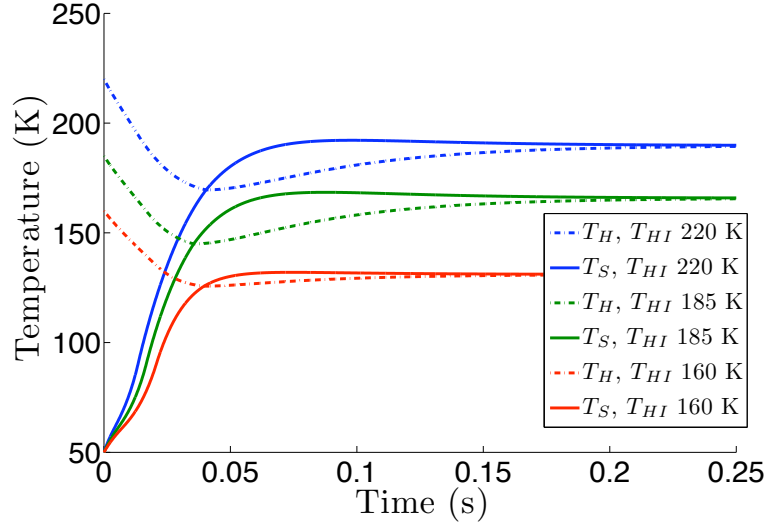


FIGURE 5.18: Effect of changing the initial heater temperature on the thermal profiles of a superconducting dump-switch.

it does not need to have as high a rate of  $\frac{dI_L}{dt}$  and so can have a smaller resistance and thus shorter length.

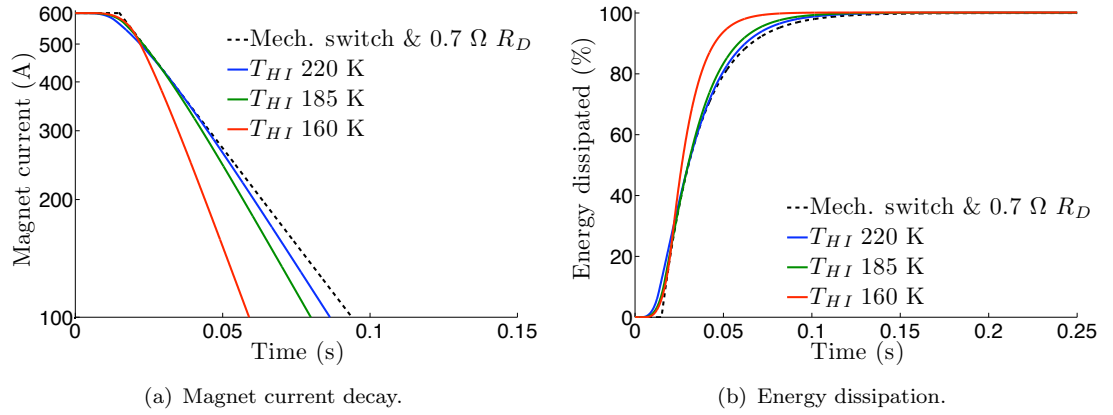


FIGURE 5.19: Effect of changing the initial heater temperature on the current decay (a) and on the energy dissipation (b).

The short delay in onset of magnet current decay and lower  $\frac{dI_L}{dt}$  of the  $T_{HI}$  220 K switch gives it the lowest peak voltage, as shown in Figure 5.20(a). The other two switches have the same initial voltage profile until  $\approx 16$  ms at which time the  $\frac{dV}{dt}$  of the  $T_{HI}$  185 K switch starts to reduce reaching its peak of 330 V after 25 ms. At the same time the  $T_{HI}$  160 K switch has a peak of 530 V, 110 V more than that obtained with the existing setup. The growth in resistance of the switches, shown in Figure 5.20(b), follows a similar pattern with the  $T_{HI}$  220 K switch starting earlier and having a more gradual resistance rise than the lower  $T_{HI}$  switches that have similar initial resistance growths. The longer length of the  $T_{HI}$  160 K switch means that despite its lowest final temperature it has the highest final resistance.

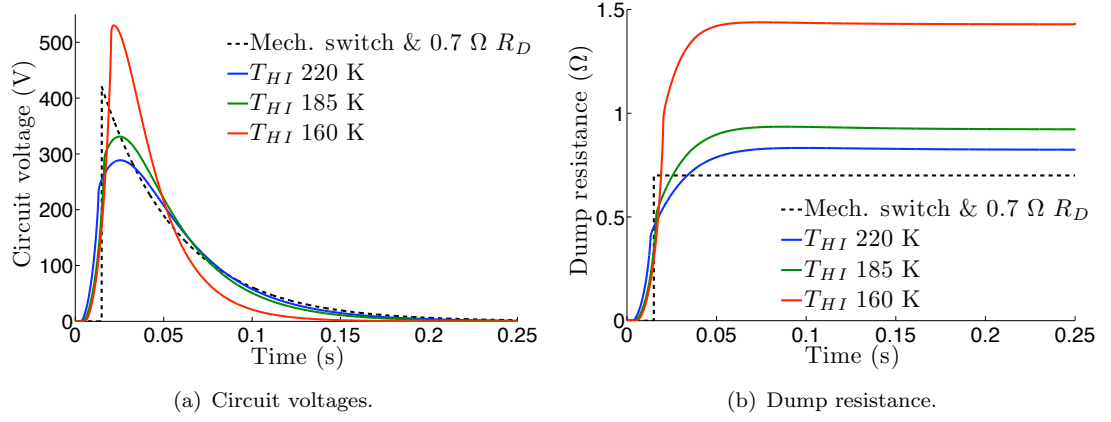


FIGURE 5.20: Effect of changing the initial heater temperature on the circuit voltage (a) and on the dump resistance (b).

Figure 5.21 shows the required switch length as a function of the initial heater temperature. The same figure also shows the required heater energy and  $\overline{\Delta T}$ . The long lengths required by switches with a  $T_{HI}$  of less than 168 K give high resistances that result in peak voltages greater than that obtained with a mechanical switch and dump resistor. As the input heater energy is proportional to the length of the switch but inversely proportional to  $T_{HI}$  there exists a minimum input heater energy. The relationship between  $T_{HI}$  and the required heater energy is shown in Figure 5.21 where the upper bound of 300 K is the maximum allowable temperature. The minimum input heater energy of 3.1 kJ occurs with a  $T_{HI}$  of 185 K and a total switch length of 39 m.  $T_{HI}$  of 185 K is the minimum heater energy switch, a  $T_{HI}$  of 220 K uses a higher energy but shorter length design, and a  $T_{HI}$  of 160 K also requires higher energy but has lower internal thermal gradients. Reducing  $T_{HI}$  to 185 K reduces the required heater energy to about two thirds of the  $T_{HI}$  300 K design.

The performance metrics of different initial heater temperatures switches are shown in Figure 5.22. The  $T_{HI}$  185 K design requires the lowest heater energy, has thermal gradients and a final temperature close to the minimum, requires a middling length, and yields a voltage  $\approx 100$  V less than that obtained with the mechanical switch and dump resistor. The  $T_{HI}$  220 K design gives the benefits of a short conductor length and low peak voltage, but this comes at the expense of a higher heater energy, high thermal gradients, and a high final temperature. The lowest initial heater temperature design gives the lowest thermal gradients and final temperature, but also requires the longest length, high heater energy, and gives the highest peak voltage. The  $T_{HI}$  300 K design allows the least amount of conductor to be used and gives the lowest peak voltage, but it requires the highest heater energy and results in the highest thermal gradients and final temperature.

Figure 5.22 shows the performance of switches having different initial heater temperatures in the form of a star plot. Figure 5.23 shows the performance scores of the switches based upon the enclosed area of the star plot (see Section 5.3.3 for details of scoring). If the

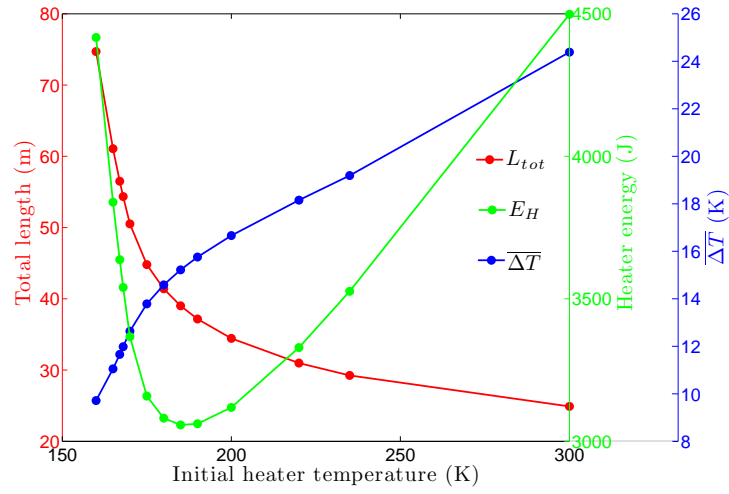


FIGURE 5.21: Required total switch length, total heater energy, and  $\Delta \bar{T}$  for switches where the heater is instantly warmed to an initial heater temperature. Circles represent results of analyses.

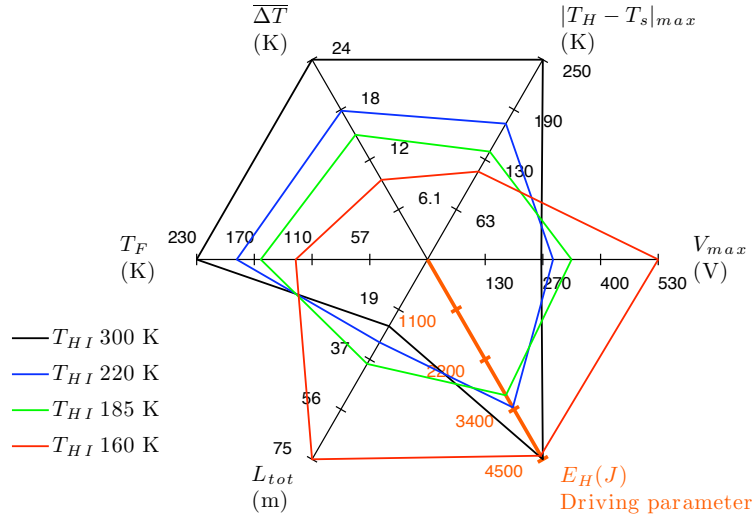


FIGURE 5.22: Star plot of the performance of superconducting dump-switches with different initial heater temperatures.

relative score is used then the  $T_{HI}$  185 K is best,  $T_{HI}$  300 K the worst, with the  $T_{HI}$  220 K just better than the  $T_{HI}$  160 K one. This is because even though the  $T_{HI}$  300 K design is the best performer in two categories, it is the worst performer in the other four. The lowest initial heater temperature design is the best in three categories but the worst in two. The minimum energy design is only the best performer in one category but crucially is almost the best in two categories and never the worst. This results in it being the best compromise between the different performance indicators out of the four switches. If the area score is used then the  $T_{HI}$  220 K switch has the best performance with the  $T_{HI}$  185 K design a close second, and the  $T_{HI}$  design 160 K much worse. However, the strong performance of the  $T_{HI}$  220 K design is due to the interplay between length and heater

energy giving it a smaller absolute area even though its area relative to the  $T_{HI}$  185 K design is larger.

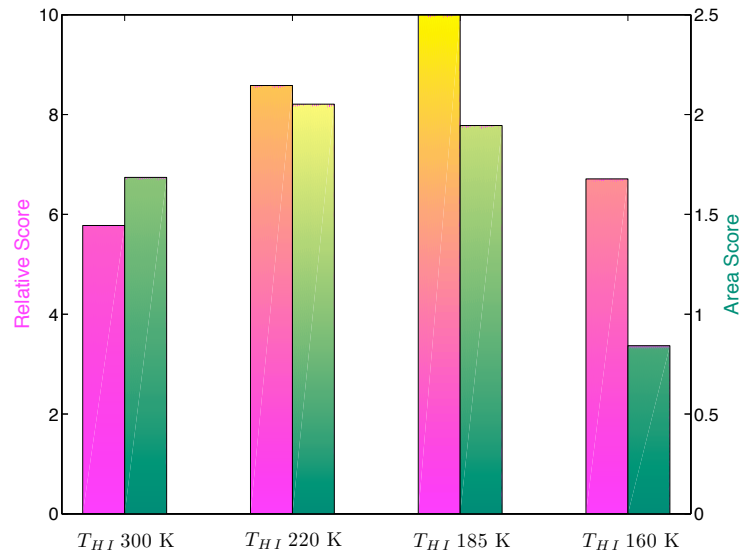


FIGURE 5.23: Effect of changing the initial heater temperature on the performance of a superconducting dump-switch.

Out of the four switch designs the best choice is the  $T_{HI}$  185 K design as it requires the least heater energy design, has low internal thermal gradients, and a low final temperature, without requiring too long a length or giving too high a peak voltage. However, it may be beneficial to operate the switch at a non-minimum heater energy, *e.g.* with a  $T_{HI}$  of 220 K, in order to reduce the required amount of superconductor and the peak voltage.

### 5.3.5 Operating Temperature

The operating temperature of a superconducting switch depends upon the system into which it is integrated. For superconducting switches in the LHC potential operating temperatures are 50 K or 20 K as discussed in Section 5.1. The previous sections investigated the minimum heater for HTS switches operating at 50 K. Operating at 20 K would allow the use of  $MgB_2$  as the switch superconductor and may also have benefits for YBCO based switches. This includes the use of shorter switch lengths due to less tapes being needed to carry the magnet current as a result of the higher critical current at low temperatures.

**An YBCO based switch operated at 20 K** needs 23 m of stainless steel clad superconductor to achieve a dump resistance of  $0.7 \Omega$  at just above  $T_c$ . This about half that required by a similar switch operated at 50 K and is a result of one less tape being required to carry the magnet current. The superconducting properties for operation at 50 K and at 20 K are shown in Table 5.5. A switch that uses 23 m of stainless steel clad YBCO and operates at 20 K will have the switching characteristics shown in Figure 5.24.



$T_{op}$ (K)	No. of Tapes	$I_c$ (A)	$T_{cs}$ (K)
20	2	978	42
50	3	701	55

TABLE 5.5: Properties of superconducting switches based on stainless steel clad YBCO over a range of operating temperatures with a magnet current of 600 A.

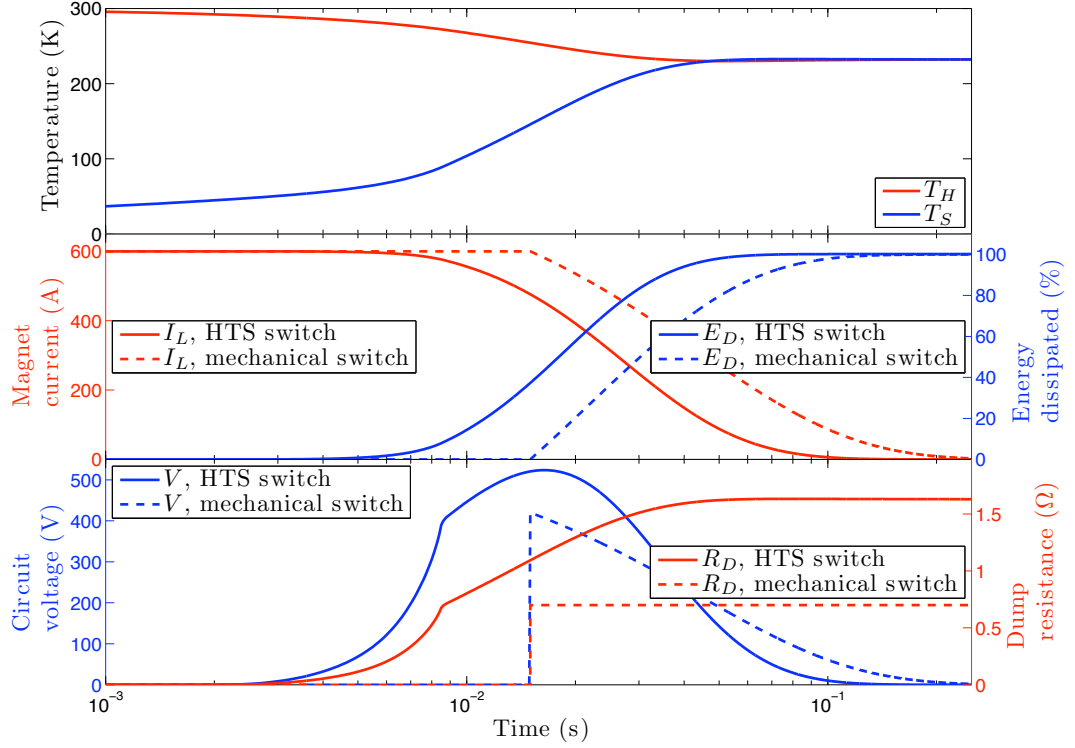


FIGURE 5.24: Switching characteristics of a stainless steel clad YBCO dump-switch that operates at 20 K, has a  $T_{HI}$  of 300 K, and develops a dump resistance of 0.7  $\Omega$  at just above  $T_c$ .

The initial rate of temperature increase of the superconductor layer is faster than for switches operated at 50 K as there is more heat conduction through the insulation due to the higher temperature gradient. The lower specific heat capacity at low temperatures also allows the superconductor temperature to rise more quickly. The faster temperature rise coupled with the lower temperature margin (3.5 K at  $T_{op}$  20 K compared to 5 K at  $T_{op}$  50 K) means that the switch enters the current sharing regime sooner and so there is shorter delay until the onset magnet current decay. This delay, of  $\approx 0.5$  ms, is much less than the 15 ms opening time of the mechanical switch and by the time the mechanical switch opens this dump-switch has dissipated  $\approx 30$  % of the magnet's energy. This dump-switch was designed to have a dump resistance of 0.7  $\Omega$  at  $T_c$ , however, the heater energy required for a  $T_{HI}$  of 300 K and the 5.5 kJ of magnet energy means that the switch heats up to  $\approx 225$  K resulting in a dump resistance of 1.6  $\Omega$ . This higher dump resistance and shorter time to initiation of magnet current decay leads to the dump-switch discharging the magnet faster than in the existing setup. The higher rate of magnet current decay also

leads to high voltages during energy extraction with the peak voltage being 100 V higher than that allowed. The length of this dump-switch is too long and it must be refined in order to meet the magnet discharge requirements.

**Refinement of length for  $T_{op}$  of 20 K** is required, as it is for any parameter change (Section 5.3.2), in order to find the switch length that results in the magnet discharge requirements being met. The required length of conductor for a switch that has an initial heater temperature of 300 K and the configuration described Section 5.2, is unacceptable as the maximum temperature is over 300 K. This is because a short length is required and so the deposited magnet energy per unit length is high enough to over heat the dump-switch. To avoid this overheating the heater energy must be reduced; in this switch case this is achieved by using a lower initial heater temperature. Reducing the heater energy also means that the required switch length is longer, therefore the magnet energy per unit length that is dissipated is also reduced. Reducing  $T_{HI}$  to 200 K results in a switch that meets the magnet discharge requirements when it has a length of 11 m. The maximum temperature of this switch is 305 K, just above the 300 K limit. Switches with lower initial heat temperatures that have the required switch length will also have maximum temperatures less than the 300 K limit.

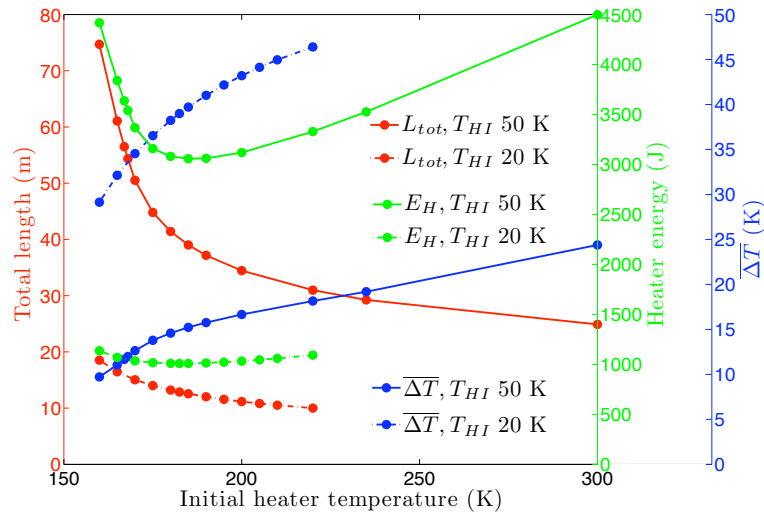


FIGURE 5.25: Required total switch length, total heater energy, and  $\Delta\bar{T}$  for switches operating at 20 K and at 50 K where the heater is instantly warmed to an initial heater temperature. Circles represent results of analyses.

**Switch length as a function of  $T_{HI}$  for  $T_{op}$  of 20 K** may allow a reduction in the required heater energy as it did for switches operating at 50 K (Section 5.3.4). The required switch length, heater energy, and  $\Delta\bar{T}$  for stainless steel clad YBCO switches operating at 20 K are shown in Figure 5.25. The results from operation at 50 K are shown for comparison. Reducing  $T_{op}$  to 20 K approximately halves the required length of conductor. This shorter length results in the required heater energy being reduced by over two thirds. The shorter required length means that the magnet energy per unit length increases and so the initial heater temperatures can also not be as high or else the total energy per length

may cause the switch to overheat. The sensitivity of the heater energy to the initial heater temperature is less at  $T_{op}$  of 20 K than  $T_{op}$  of 50 K due to the limited upper  $T_{HI}$  of low temperature operation and the less steep rise in required length with decreasing  $T_{HI}$ . The minimum heater energy occurs at similar  $T_{HI}$  for both operating temperatures, 185 K for  $T_{op}$  of 50 K and 182.5 K for  $T_{op}$  of 20 K, but the shorter length, 12.8 m compared to 39 m, means that even though the temperature rise is more the heater energy has been reduced from 3 kJ to 1 kJ. The thermal gradients within the switch are much higher for low temperature operation due to the high initial temperature gradients and also the increased temperature rise of the superconductor layer due to the greater magnet energy per unit length that is deposited.

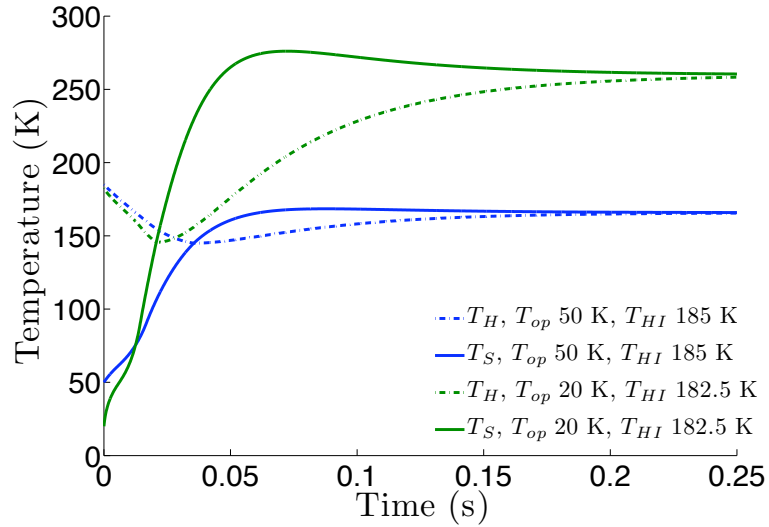


FIGURE 5.26: Thermal profiles of YBCO based dump-switches operating at 20 K and at 50 K.

The thermal profiles of the minimum energy switches that operate at 50 K and 20 K are shown in Figure 5.26. The faster temperature rise of the switch operating at 20 K is due to the greater heat conduction through the insulation as a result of the higher thermal gradients and the lower specific heat capacity of the switch at lower temperatures. At about 8 ms the magnet current decay (Figure 5.27(a)) for both switches begins causing the superconductor temperature rise of the two switches to speed up. This kink at about 10 ms to 15 ms is more pronounced for the lower operating temperature switch as it has a shorter length and so receives more magnet energy per unit length.

At 12.5 ms the superconductor temperature of the  $T_{op}$  20 K switch equals that of the  $T_{op}$  50 K switch at 75 K. The  $T_{op}$  20 K design reaches  $T_c$  after 14 ms and the  $T_{op}$  50 K design after 16 ms. The magnet energy that was dissipated in the current sharing regime was 5 % and 10 % respectively (Figure 5.27(b)). The superconductor temperature of the  $T_{op}$  20 K switch continues to grow rapidly equalling that of the heater after 21 ms and at 147 K. The regime of the  $T_{op}$  20 K switch where the heater acts as a heat sink occurs over a wider temperature range and has a greater temperature difference than for the  $T_{op}$  50 K switch. Despite the increased use of the heater as a heat sink the lower operating temperature

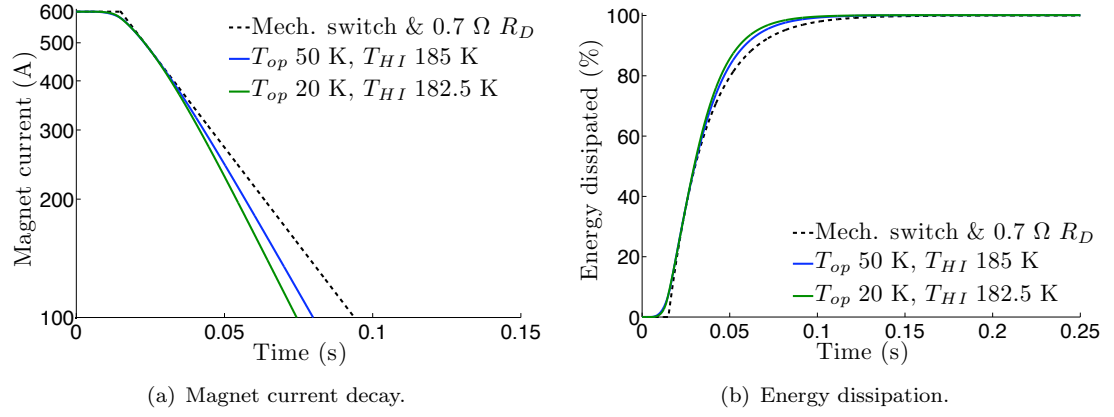


FIGURE 5.27: Effect of reducing the operating temperature on the current decay (a) and on the energy dissipation (b).

switch has a higher final temperature, 260 K compared to 166 K, due to the shorter length and the higher energy that is deposited per unit length. This higher temperature and lower number of strands mean that even though the length is less the dump resistance is higher (Figure 5.28(b)). This higher resistance leads to a higher magnet current decay and also to a higher peak voltage of 347 V compared to 331 V (Figure 5.28(a)) but both peak voltages are lower than the 420 V obtained by the existing mechanical switch. Both switches meet the magnet discharge requirements, the  $T_{op}$  20 K switch with a shorter length and lower energy and the  $T_{op}$  50 K switch with a lower final temperature and smaller internal temperature gradients.

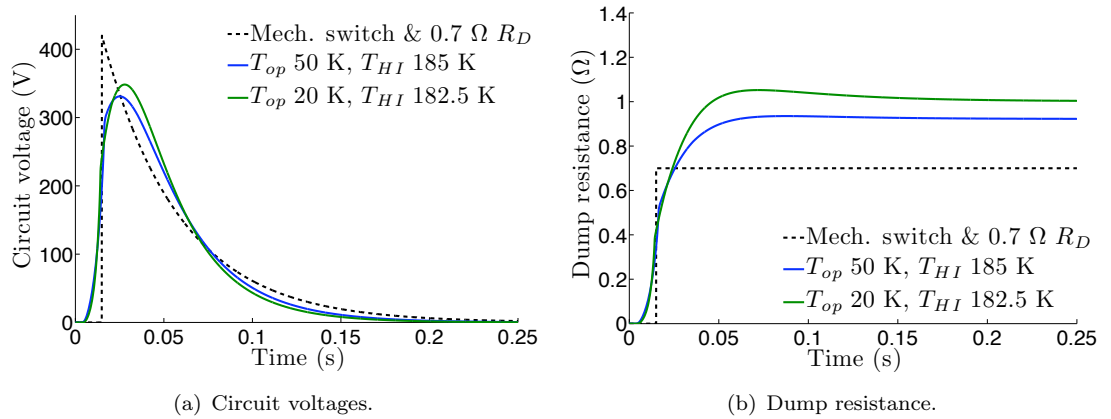


FIGURE 5.28: Effect of reducing the operating temperature on the circuit voltage (a) and on the dump resistance (b).

**Performance metrics for different operating temperatures** dump-switches are shown in a star plot (Figure 5.29) for minimum energy switches operating at 20 K and at 50 K. The performance of a dump-switch that operates at 50 K and has an initial heater temperature of 300 K (described in Section 5.3.4) is also shown for comparison. This switch that has the shortest length possible for operation at 50 K still requires more length than the minimum energy switch that operates at 20 K. The peak voltage is also less than the

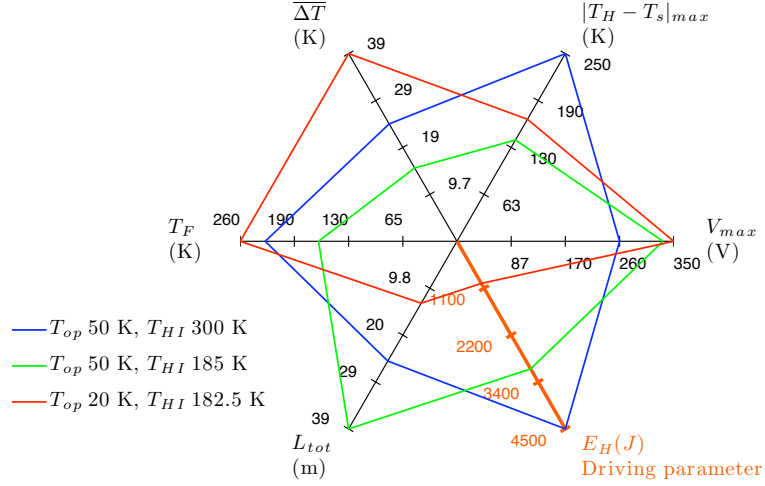


FIGURE 5.29: Star plot of the performance metrics of superconducting dump-switches with different operating temperatures.

other two but all three have a peak voltage less than that obtained with the mechanical switch and meet the magnet discharge requirements. As well as having the shortest length the  $T_{op}$  of 20 K design also requires the least energy. The required heater energy of this switch is only 18 % of that of the magnet energy, whereas the minimum energy design that operates at 50 K requires a heater energy that is 55 % of that of the magnet energy. Operating at 50 K results in the lowest final temperature and the smallest temperature gradients – both  $\Delta \bar{T}$  and  $|T_H - T_S|_{max}$ . This results in a switch that has lower internal stresses during operation.

In order to account for the extra cost of providing the heater energy at a lower operating temperature an equivalent heater energy ( $\overline{E_H}$ ) is defined as

$$\overline{E_H} = \frac{E_H}{T_{op}}. \quad (5.2)$$

The equivalent heater energies for the above minimum heater energy switches are given in Table 5.6. If the  $\overline{E_H}$  is used as the performance metric instead of  $E_H$  then the performance of the switch operating at 50 K becomes closer to that of the one operating at 20 K.

$T_{op}$ (K)	$E_H$ (J)	$\overline{E_H}$ (J/K)
20	1009	50.5
50	3057	61.1

TABLE 5.6: Heater energy ( $E_H$ ) and equivalent heater energy ( $\overline{E_H}$ ) delivered at the operating temperature for minimum energy switches formed of stainless steel clad YBCO.

The minimum energy switch that operates at 50 K has the best relative score as it is the best performer in the three thermal gradient performance metrics. The minimum energy switch that operates at 20 K has the best area score due to the low required heater energy and length. It is also the best performer in these two metrics giving the switch

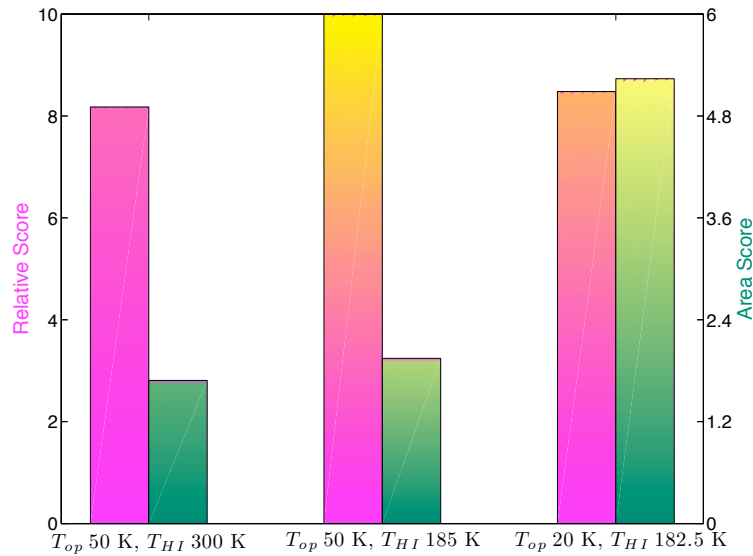


FIGURE 5.30: Effect of changing the operating temperature on the performance metrics of superconducting dump-switches.

a good relative score. Both minimum energy designs have better performance scores than the switch that is operated at 50 K with an initial heater temperature of 300 K. If both operating temperatures are potential choices due to the extension of the bus-bar (Section 5.1) then the choice between the two minimum energy designs would be decided by whether a shorter lower energy switch is more suited to use in the LHC than a longer higher energy but lower thermal gradient design. Due to the much higher heater energy it is more likely the lower operating temperature switch would be used if it can be made to be robust enough to withstand the thermal stresses.

### 5.3.6 Choice of Superconductor

Operation at a lower temperature of 20 K allows  $\text{MgB}_2$  to be used as the superconductor in the switch.  $\text{MgB}_2$  based superconductors are cheaper and available in longer continuous lengths than YBCO based superconductors. The higher critical current of  $\text{MgB}_2$  tapes than YBCO based tapes means that fewer tapes need to be connected in parallel to carry the magnet current at this temperature. This lower number of tapes means that a shorter length of  $\text{MgB}_2$  is needed and that the  $\text{MgB}_2$  operates closer to  $T_{cs}$  due to the smaller current margin.

$\text{MgB}_2$  is available with a variety of stabilisation including a resistive cupronickel matrix and also with a less resistive matrix containing copper stabilization as well as nickel and iron. An alternative YBCO tape with copper cladding is also investigated. Superconductors with less resistive matrices maybe of interest when operated at 20 K as the reduction in the required switch length for low temperature use may offset the increase in length

required by the decrease in resistivity. Such switches may have lower internal thermal gradients and lower peak voltages but may require more heater energy.

Super-conductor	Matrix	No. of Tapes	$I_c$ (A)	$T_{cs}$ (K)	$T_c$ (K)	$L_{T_c}$ (m)
MgB <sub>2</sub>	Cu-Ni	1	693	23.5	39	22.2
MgB <sub>2</sub>	Cu	1	827	26.6	39	141
YBCO	SS	2	978	41.4	89	53.2
YBCO	Cu	2	1000	44	89	452

TABLE 5.7: Properties of dump-switches that operate at 20 K with a magnet current of 600 A.  $L_{T_c}$  is the length required for a dump resistance of  $0.7 \Omega$  at  $T_c$ .

Table 5.7 shows the properties of superconductors for use in dump-switches that operate at 20 K. The critical current and  $T_{cs}$  of the MgB<sub>2</sub> with a resistive cupronickel matrix is less than the one with copper stabilization as it has a smaller area of superconductor. The less resistive tape also contains nickel and iron in its matrix in addition to the copper. The critical current and  $T_{cs}$  of the copper clad YBCO is more than the stainless steel clad YBCO as cladding. Both YBCO tapes have nickel-tungsten substrate and several buffer layers, one of which is silver. The length ( $L_{T_c}$ ) presented in the table is the length required for a dump resistance of  $0.7 \Omega$  at  $T_c$ . As with all switch designs the length needs to be refined in order to meet the magnet discharge requirements.

This refinement is described in Section 5.3.2 and will result in shorter lengths of switches being required. The required length as a function of  $T_{HI}$  for switches formed of the four materials can be investigated to determine the length that requires the least heater energy for dump-switches based on each material.

**Dump-switches with resistive matrices** have a required length as a function of  $T_{HI}$  as shown in Figure 5.31. These two switches operate at 20 K with one switch using stainless steel clad YBCO and the other MgB<sub>2</sub> in a cupronickel matrix. Operating the stainless steel clad YBCO switch at 20 K was described in Section 5.31. Changing the superconductor to MgB<sub>2</sub> leads to a reduction in the required length of switch. This is due to fewer tapes being required to be connected in parallel to carry the magnet current. The minimum heater energy is also reduced from 1 kJ to 0.025 kJ. This is due to the decrease in length and also the reduction in initial heater temperature from 182.5 K to 87.5 K.

The MgB<sub>2</sub> based switch is more sensitive to the initial heater temperature than the YBCO based switch. For reducing  $T_{HI}$  the required switch length increases steeply in order to develop the required resistance. However, the short lengths required by higher initial heater temperatures mean that the magnet energy that is dissipated per unit length is high and so the maximum temperature of the switch will exceed 300 K if  $T_{HI}$  exceeds 92 K. The thermal gradients within the switch are comparable for both materials. Reducing the matrix resistivity may result in a switch that is less sensitive to the initial heater

temperature and has a lower final temperature as longer lengths of conductor would be required to meet the magnet discharge requirements.

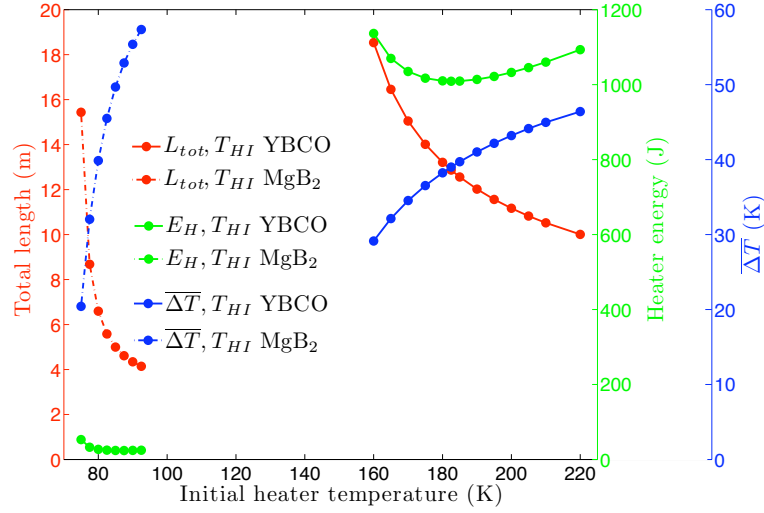


FIGURE 5.31: Required total switch length, total heater energy, and  $\overline{\Delta T}$  for  $\text{MgB}_2$  and YBCO based switches that have resistive matrices and operate at 20 K. Circles represent results of analyses.

**MgB<sub>2</sub> based switches using a less resistive matrix** that contains copper have a required length as a function of  $T_{HI}$  as shown in Figure 5.32. The required length of switch must be increased about ten times compared to the switch with a cupronickel matrix due to the lower resistance. This longer switch length means that higher heater energies are required. The minimum heater energy switch with a copper stabilisation requires 860 J of heater energy to warm up 107 m of switch to an initial heater temperature of 72.5 K. The minimum heater energy switch with a cupronickel matrix requires 24 J of heater energy to warm up 4.6 m of switch to an initial heater temperature of 87.5 K.

The copper stabilised switch has much lower internal gradients than the shorter cupronickel based switch;  $\overline{\Delta T}$  is reduced from 50 K to 5 K resulting in a switch that experiences lower thermal stresses. The sensitivity of thermal gradients to the initial heater temperature is also less for the less resistive switch. This is due to the longer lengths meaning that the magnet energy that is dissipated per unit length is also less and plays a correspondingly smaller role in the heating of the switch. The less resistive  $\text{MgB}_2$  switch requires  $\approx 150$  J less than a stainless steel clad YBCO switch operating at the same temperature; however, the required length is about 100 m more.

**YBCO based switches with less resistive matrices** may also result in switches that have lower internal thermal gradients than stainless steel clad YBCO ones (Figure 5.33). Copper clad YBCO switches have a much lower resistivity than stainless steel clad ones and so the length must be increased from  $\approx 20$  m to over 200 m. Unlike the other three materials that are under consideration, the copper clad YBCO switches have a minimum heater energy that occurs with a  $T_{HI}$  above 300 K. This is unacceptable as it exceeds the allowable temperature of the switch. The lowest heater energy and shortest length of



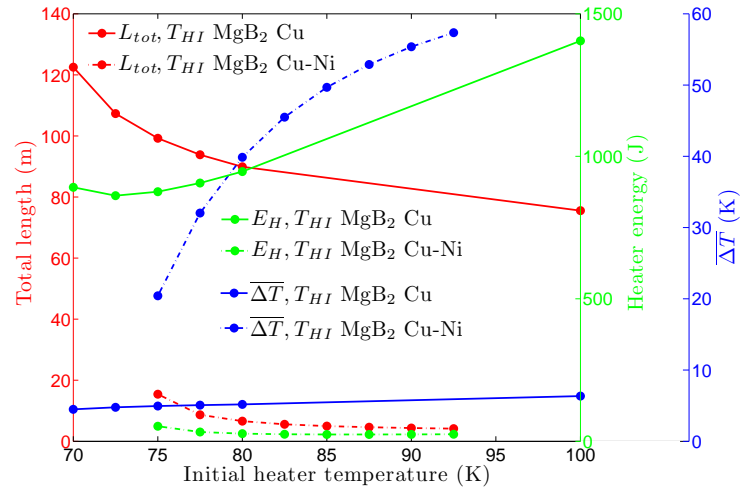


FIGURE 5.32: Required total switch length, total heater energy, and  $\overline{\Delta T}$  for MgB<sub>2</sub> switches that operate at 20 K. Circles represent results of analyses.

switch that can be used is when  $T_{HI}$ , which is also the maximum temperature, is 300 K. This minimum heater energy is 36 kJ, which is about six and a half times that stored in the magnet. Due to the high initial heater temperature the internal temperature gradients are greater than that obtained with the stainless steel clad YBCO switch that requires a  $T_{HI}$  of only 187.5 K.

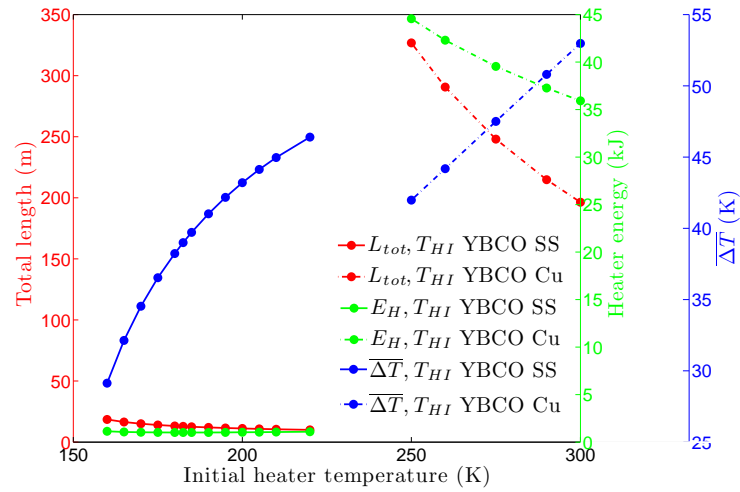


FIGURE 5.33: Required total switch length, total heater energy, and  $\overline{\Delta T}$  for YBCO switches that operate at 20 K. Circles represent results of analyses.

**Switching characteristics** of different superconductor based dump-switches that require a minimum heater energy when operating at 20 K are described below. Figure 5.34 shows the thermal profiles of switches that utilise stainless steel clad YBCO, copper clad YBCO, MgB<sub>2</sub> in a cupronickel matrix, and MgB<sub>2</sub> with copper stabilisation. For about the first 10 ms the thermal profiles of the superconductor layer are the same for each type

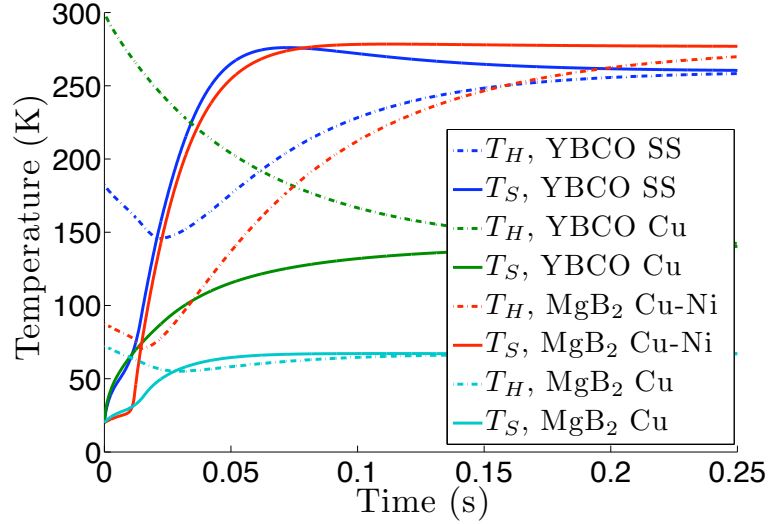


FIGURE 5.34: Thermal profiles dump-switches that utilize different superconducting tapes and have  $T_{op}$  of 20 K.

of superconductor irrespective of the resistivity of the matrix as the heat capacities are similar. The superconductor temperature of YBCO based switches rises faster than the  $MgB_2$  based switches as the heat conduction through the insulation is higher due to the higher heater temperatures and greater transfer area. The thermal profiles diverge from one another after  $\approx 10$  ms when the magnet current starts to decay (Figure 5.35(a)) and the magnet energy begins to be dissipated in the switch (Figure 5.35(b)). The magnet current decay for the copper clad YBCO switch actually starts at around 5 ms but as the length of switch is so long (200 m) and the heater energy so high (36 kJ) the magnet energy per unit length is insignificant compared to the heater and so the magnet discharge does not affect the thermal profiles.

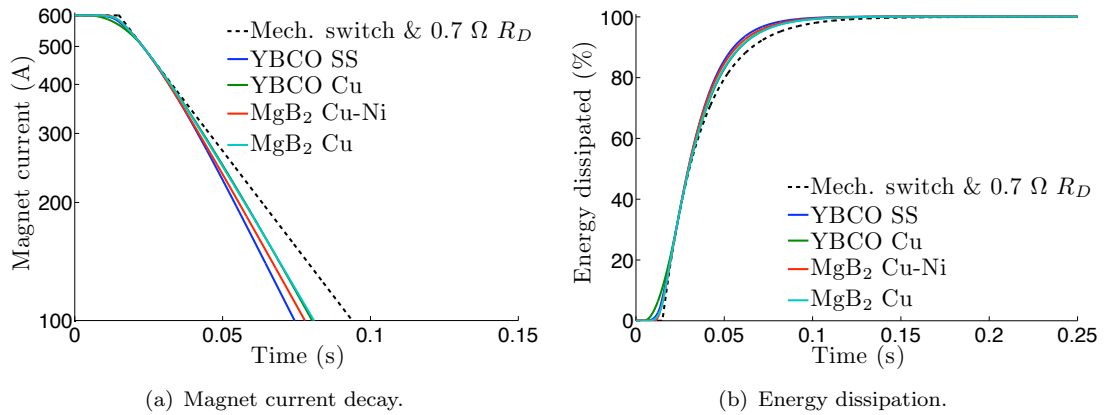


FIGURE 5.35: Effect of utilizing different superconducting tapes on the current decay (a) and on the energy dissipation (b). The Cu stabilised tapes have almost identical current decays.

After 10 ms the superconductor temperatures of the two switches with the more resistive matrices rise steeply as their shorter lengths, 4.6 m for the  $MgB_2$  switch and 13 m for the

YBCO switch, mean that the magnet energy per unit length is significant. The kink in superconductor temperature rise is less noticeable in the copper stabilised YBCO tape as the longer length (107 m) means that the magnet energy has less influence on the thermal profiles. It is still significant as the magnet energy is larger than the 862 J of heater energy.

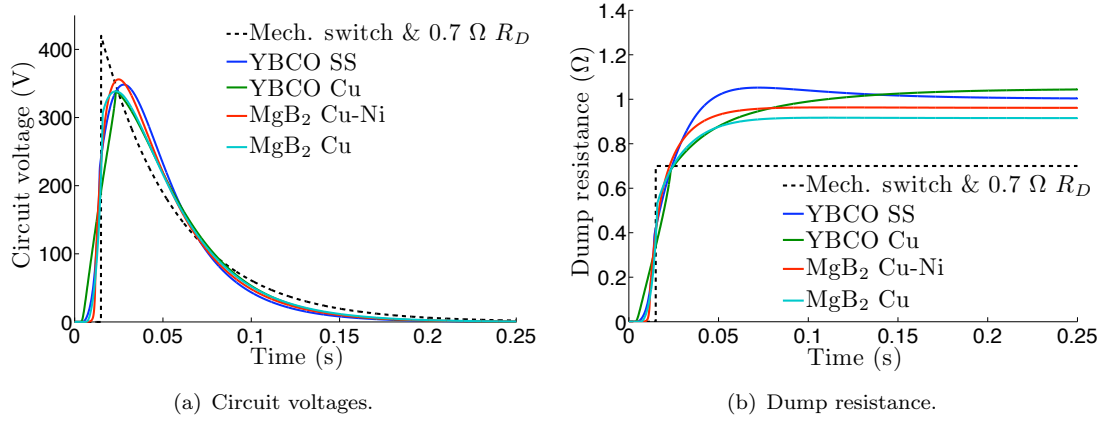


FIGURE 5.36: Effect of utilizing different superconducting tapes on the circuit voltage (a) and on the dump resistance (b).

The stainless steel clad YBCO switch and MgB<sub>2</sub> in a Cu-Ni matrix switch have similar and final temperatures of 260 K and 270 K respectively due to their short lengths. They also have high internal thermal gradients with the heater acting as a heat sink for the majority of the dumping process. The copper stabilised MgB<sub>2</sub> switch has the lowest final temperature of 67 K and also the lowest thermal gradients. The copper clad YBCO switch is dominated by heat energy from the heater and the direction of heat flow does not reverse at any point during energy dissipation. The peak voltages (Figure 5.36(a)) are all  $\approx 345$  V, lower than the 420 V obtained with the existing mechanical switch, due to the similar resistance profiles (Figure 5.36(b)) giving similar rates of magnet current decay.

**Performance metrics for switches with different conductors** are shown as a star plot in Figure 5.37. Copper clad YBCO is removed from the comparison as its required heater energy of 36 kJ, 6.5 times the magnet energy, is too high to be practical. In addition to this it requires the longest length (200 m) of superconductor and has  $\overline{\Delta T}$  and  $|T_H - T_S|_{max}$  due to its  $T_{HI}$  of 300 K. The copper stabilised MgB<sub>2</sub> switch requires 110 m of conductor, much more than the resistive matrix switches, but requires less heater energy (862 J compared to 1010 J) than the stainless steel clad YBCO switch that only uses 13 m of conductor. This lower required heater energy is due to the lower  $T_{HI}$  of 72.5 K compared to a  $T_{HI}$  of 182.5 K for the YBCO switch. This low initial heater temperature and long length means that the copper stabilised MgB<sub>2</sub> switch also has the lowest final temperature, maximum temperature difference, and  $\overline{\Delta T}$ . The cupronickel matrix MgB<sub>2</sub> switch represents the opposite case to the less resistive MgB<sub>2</sub> switch. It requires a minimal length of 4.6 m and the lowest heater energy of the three of 24 J. As a result of this short length the magnet energy that is deposited per unit length is high and so this switch has

the highest final temperature and  $\overline{\Delta T}$ . It does not have the highest  $|T_H - T_S|_{max}$  due to the higher initial heater temperature requirement of the stainless steel clad YBCO switch. The YBCO switch does not perform as well as the  $\text{MgB}_2$  switches as it requires a high heater energy but also has high thermal gradients and a high final temperature. The peak voltages of the three switches are similar and at  $\approx 345$  V they are below the 420 V limit.

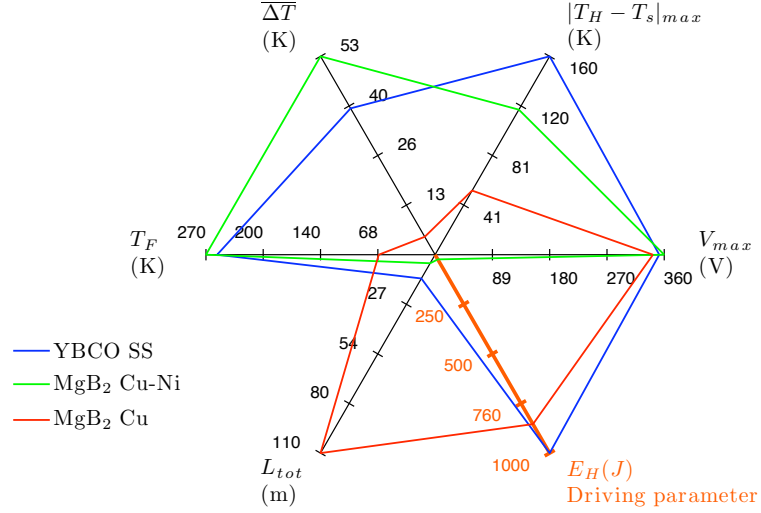


FIGURE 5.37: Star plot of the performance of superconducting dump-switches that utilize different superconducting tapes.

The performance scores of the three switches are shown in Figure 5.38. As described above the stainless steel clad YBCO switch is the worst performer of the three when it is operated at 20 K. Based upon the relative score the copper stabilised  $\text{MgB}_2$  switch is the best performer as it has the best metrics in four of the six categories. However, its long length and high heater energy give it a poor area score. With this measure the Cu-Ni matrix  $\text{MgB}_2$  switch is the best performer due to its low energy and length requirements. The most suitable switch for operation at 20 K would be a  $\text{MgB}_2$  based switch. The choice of matrix material would depend upon whether it is more desirable to have a switch with low internal thermal gradients and final temperature, or a switch that requires a short length and low heater energy.

### 5.3.7 Number of Tapes and Tape Width

Operating at a given temperature requires the use of a minimum number of strands in order to carry the magnet current with sufficient temperature and current margins. Increasing the number of tapes is the same as increasing the width of the tape but as most superconductors are only available in fixed widths whole numbers of tapes must be used. Coated conductor YBCO tapes are available in different widths and so it is possible to have greater control over the switch properties. Increasing the number of tapes (or width) leads to larger temperature and current margins, a higher thermal mass per length, and a lower resistance per length. Increasing the thermal mass maybe advantageous for high

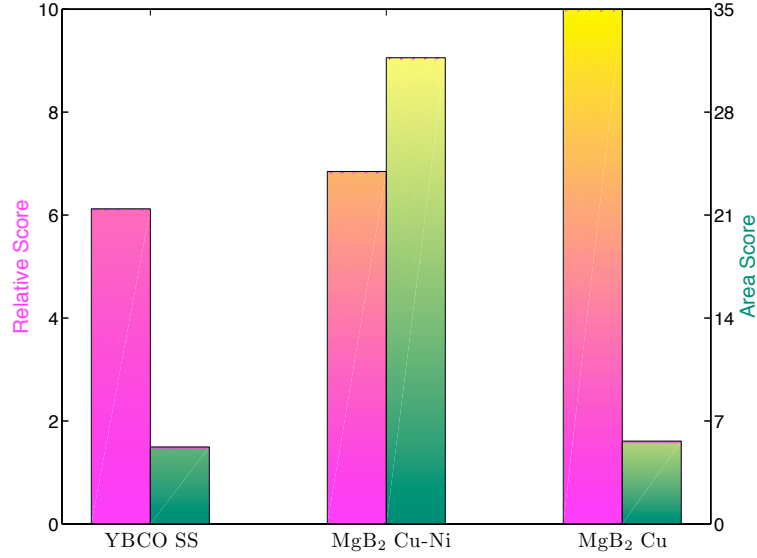


FIGURE 5.38: Effect of utilizing different superconducting tapes on the performance of a superconducting dump-switch.

energy circuits and for short dump-switches as it has the potential to lower the thermal gradients and final temperature. The increase in margin delays the onset of energy dissipation and so more heater energy per unit length is required to speed up the transition. As the resistance per length decreases, longer lengths are required in order to achieve the required dump resistance. These longer lengths may also require greater heater energy. The required lengths as a function of  $T_{HI}$  for switches formed of MgB<sub>2</sub> in a Cu-Ni matrix and also of stainless steel clad YBCO are shown in Figure 5.39. At 20 K the MgB<sub>2</sub> switch can carry the magnet current with one tape, but it has high thermal gradients so an alternative, higher thermal mass, design using two tapes is investigated. Two tapes of YBCO are required to carry the magnet current at this temperature; a design with a tape width equivalent to 2.5 tapes is investigated to attempt to reduce the thermal gradients and the final temperature of the switch. The total length is reduced compared to separate tapes as it is a wider single tape.

The thermal profiles of the four minimum energy switch designs are shown in Figure 5.40. The temperature gradients and final temperature of both the YBCO and MgB<sub>2</sub> switches are reduced by increasing the number of strands (and width). The thermal mass increases as the width of the switch is increased and the length must also be increased in order to raise the dump resistance back to the required level so that the magnet discharge requirements are met. This compounded increase in thermal mass leads to the decrease in thermal gradients and final temperature even though the heater energy must be higher in order to trigger the switch.

Increasing the MgB<sub>2</sub> based switch to two strands results in a faster initial superconductor temperature rise due to increased thermal conduction through the insulation that results from the increased temperature gradient and increased heat transfer area. This effect is

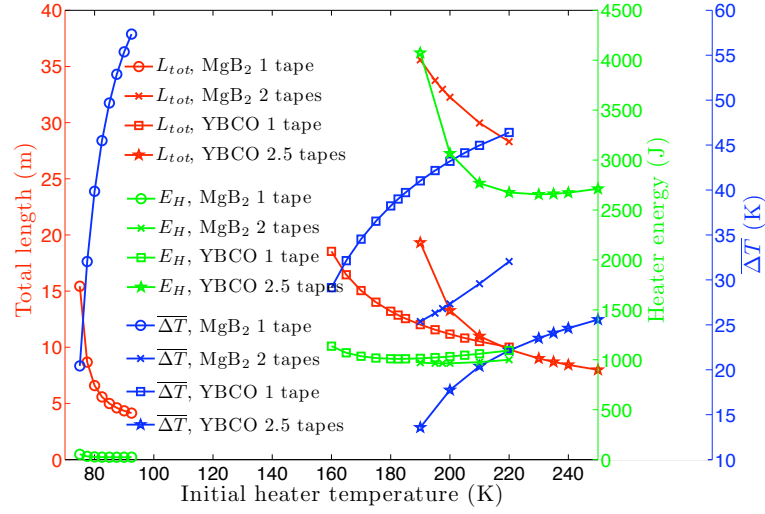


FIGURE 5.39: Required total switch length, total heater energy, and  $\overline{\Delta T}$  for  $\text{MgB}_2$  in Cu-Ni matrix switches and stainless steel clad YBCO switches that operate at 20 K. Markers represent results of analyses.

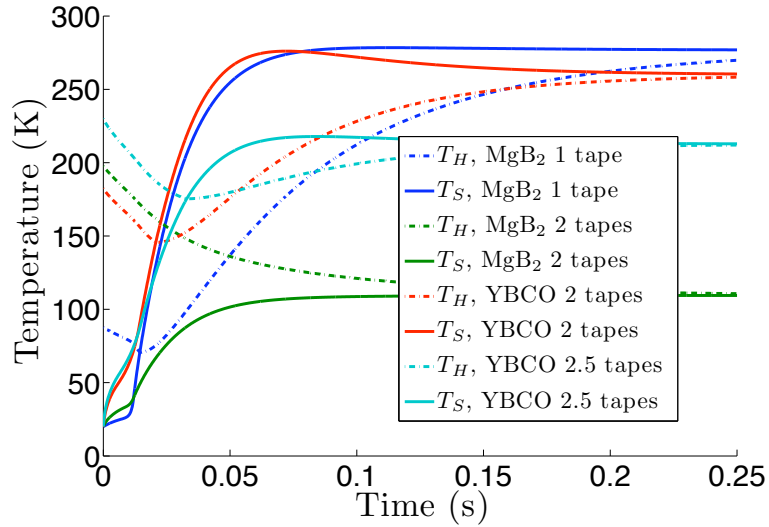


FIGURE 5.40: Thermal profiles of dump-switches that utilize different numbers of superconducting tapes.

less noticeable for the YBCO based switch as the initial heater temperature and transfer area are increased by a smaller amount due to the finer control over the width of the tape.

The large increase in thermal mass of the two strand  $\text{MgB}_2$  switch lowers the final temperature from 273 K to 110 K. The thermal gradients are also reduced but due to the higher initial temperature and reduced temperature rise of the superconductor layer the heat flow does not reverse and the heater layer does not act as a heat sink. Increasing the thermal mass of the YBCO based switch allows the final temperature to be reduced from 217 K to 167 K. The finer control of the width that is possible with the coated conductor YBCO tapes allows the heater layer to act as a heat sink.

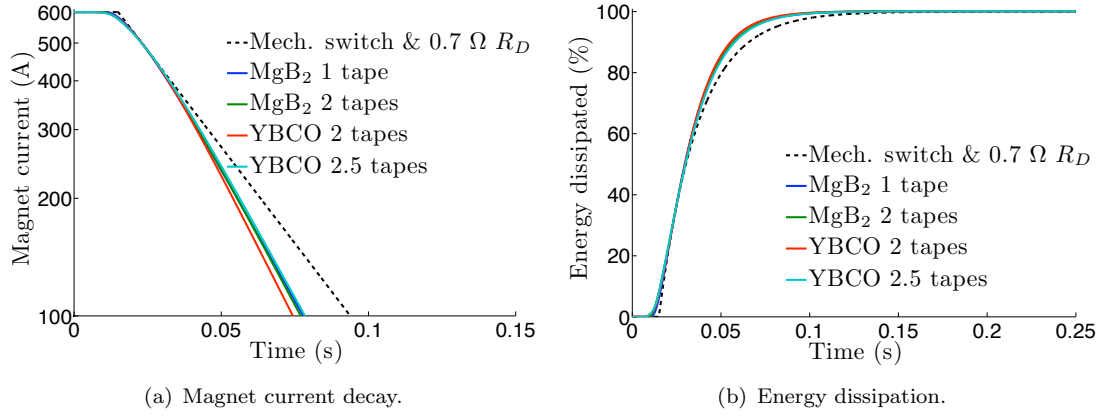


FIGURE 5.41: Effect of utilizing different numbers of superconducting tapes on the current decay (a) and on the energy dissipation (b). The current decay with 2 tapes of YBCO is slightly faster than with the other switches.

The current decay (Figure 5.41(a)), energy dissipation (Figure 5.41(b)), and voltage (Figure 5.42(a)) of the circuit during discharge are similar for all four switches. This is because the different lengths of the switches means that even though the thermal profiles are different the resistance growths (Figure 5.42(b)) are similar.

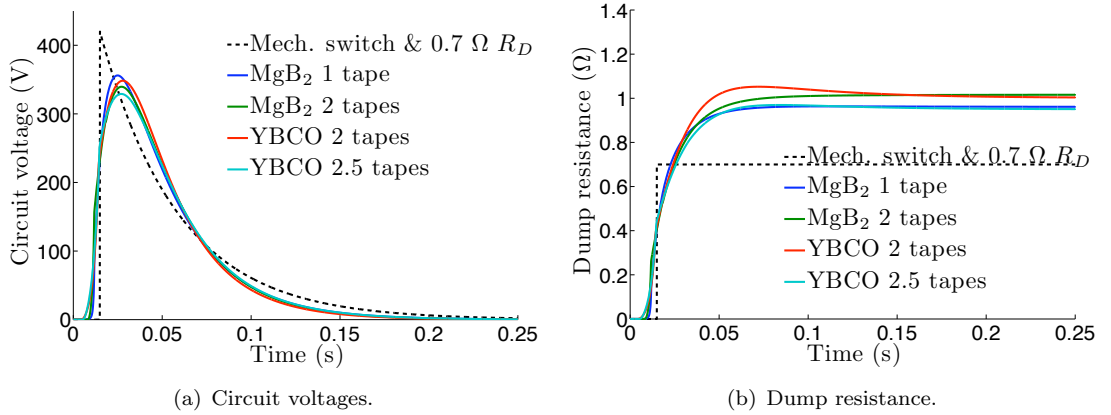


FIGURE 5.42: Effect of utilizing different numbers of superconducting tapes on the circuit voltage (a) and on the dump resistance (b).

A star plot of the performance metrics is shown in Figure 5.43. Increasing the width of the YBCO based switch resulted in a lowering of  $\overline{\Delta T}$  to the least of the four switch designs but the higher required  $T_{HI}$  means that it has the highest  $|T_H - T_S|_{max}$  of the four. Increasing the number of strands of the MgB<sub>2</sub> switch also decreases  $\overline{\Delta T}$  but increases  $|T_H - T_S|_{max}$  for the same reason as the YBCO switch. In both cases increasing the width reduces the final temperature. The peak voltages are the same for all four switches but the wider switches give slightly lower peak voltages than the narrower and shorter ones. Increasing the width increases the required length and also increases the required heater energy as not only is the thermal mass increased but the initial heater temperature must also be increased. For the MgB<sub>2</sub> based switch doubling the number of tapes results in an increase

in heater energy from 24 J to 964 J, about the level required by the normal width YBCO switch. Increasing the width of the YBCO switch means that the heater energy must be increased to 2655 J, which is about half of the energy stored in the MCD magnet chain.

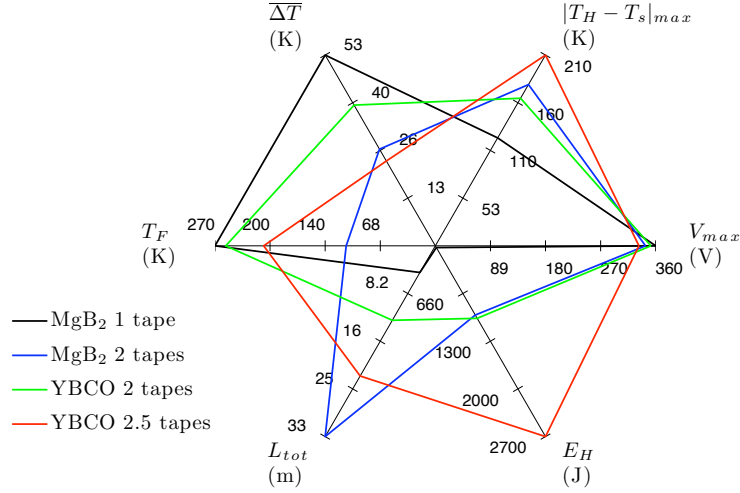


FIGURE 5.43: Star plot of the performance of superconducting dump-switches that utilize different numbers of tapes.

The performance scores of the four switches are shown in Figure 5.44. In this star plot the length of the increased width YBCO switch is scaled by 2.5 times in order to allow comparison with the standard width YBCO tapes. The single strand MgB<sub>2</sub> switch has the best area score due to its low required length and heater energy. It is also the second best in terms of the relative score as it is the best performer in three of the six performance metrics. The two strand MgB<sub>2</sub> switch has the best relative score as it is the best performer in two metrics, the middling in three, and only the worst in one- required length. It also has the second best area score. Irrespective of width the YBCO based switches perform equally well in this situation as the advantages of a high thermal mass, *i.e.* a lower thermal gradients and a lower final temperature, are outweighed by the disadvantages of longer lengths and higher required energy.

### 5.3.8 Superconducting Tape Critical Current Density

The critical current of HTS tapes is being continually improved and SuperPower already produce YBCO tapes with critical currents at 77 K from 80 A to 110 A [57], this is an increase of  $\approx 50\%$  over the 60 A tapes used in the previous analyses. An increase in the critical current density of a superconducting tape may be beneficial as it may allow fewer tapes to carry the magnet current. This reduction in area would mean that less length would be required in order to develop the required dump resistance. Increasing the critical current density is most suitable for YBCO switches as several tapes are required to carry the magnet current. It is even more beneficial for copper clad YBCO switches due to the low resistivity of the tape. For MgB<sub>2</sub> switches that only require one tape to



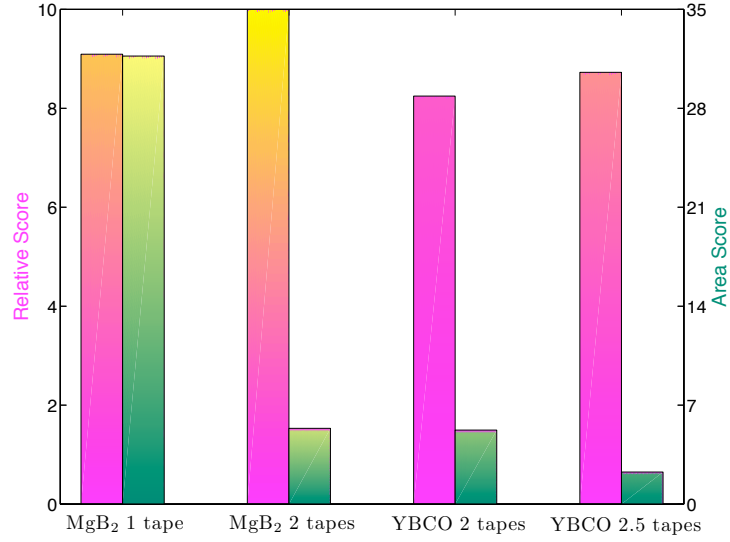


FIGURE 5.44: Effect of utilizing different numbers of tapes on the performance of a superconducting dump-switch.

carry the magnet current increasing the critical current density may not be beneficial as the increases in current margin may mean that an increase in switch length is required in order to offset the delay in initiation of the magnet current decay caused by the increased temperature margin.

Increasing the critical current of stainless steel clad YBCO tapes by 50 % means that the temperature and current margins increase if the same number of tapes are used. Alternatively the number of tapes can be reduced from three to two as fewer tapes are required to carry the 600 A magnet current at 50 K. This means that the length that is needed to meet the discharge requirements is also reduced. The required heater energy is reduced as both the length and the initial heater temperature are reduced. However, increasing the critical current and not reducing the number of tapes means that more heater energy is needed in order to overcome the delay due to the higher temperature margin. The parameters of minimum heater energy switches having different critical current densities are shown in Table 5.8. The thermal profiles of these three switches are shown in Figure 5.45.

$I_c$ /tape (A)	No. of tapes	$T_{cs}$ (K)	$T_{HI}$ (K)	$L_{tot}$ (m)	$E_H$ (J)	$\overline{\Delta T}$ (K)
234	3	54.6	185	39.0	3057	15.2
350	3	64.5	239	34.6	4296	18.7
350	2	54.6	170	12.6	837	39.7

TABLE 5.8: Parameters of minimum energy YBCO switches that have different critical current densities and which operate at 50 K.

Initially the three switches have similar superconductor temperature rises as they have the same insulation configuration and similar heat conduction through the insulation. The higher critical current switch requires the greatest initial heater temperature in order

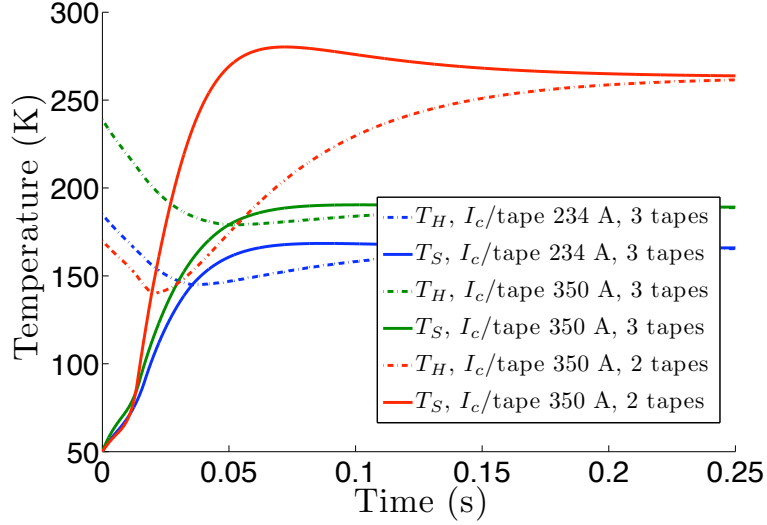


FIGURE 5.45: Effect of changing the critical current density on the thermal profiles of a stainless steel clad dump-switch. Increasing the critical current density by 50 % allows one less tape to carry the magnet current at 50 K.

to overcome the larger temperature margin. At about 10 ms there is a kink in the superconductor temperature rise as the magnet energy begins to be deposited in the switch. The switch with fewer tapes, which is possible due to the higher critical current density, has a much steeper temperature rise as it has a shorter length and so the deposited magnet energy per length is higher. The critical temperature is reached after  $\approx 15$  ms for all switches with  $\approx 10$  % of the magnet energy being discharged whilst they are in the current sharing regime. The greater magnet energy per length that is dumped in the two tape switch means that it has higher internal thermal gradients and a higher final temperature of 263 K compared to 165 K for the switch that requires three tapes and a longer length but has the same critical current. The higher temperature rise results in a higher dump resistance of  $0.99 \Omega$  compared to  $0.93 \Omega$  for the three tape switches. This higher resistance leads to higher peak voltage of 345 V compared to 331 V for the three tape switch with the same critical current due to the higher rate of magnet current decay. The higher critical current switch has the lowest peak voltage of 320 V as it has the lowest rate of magnet current decay.

A star plot of the performance metrics of the three switches is shown in Figure 5.46. The performance of dump-switches that operate at 20 K and are formed of stainless steel clad YBCO and also of  $\text{MgB}_2$  in a Cu-Ni matrix are shown for comparison. To take into consideration the cost of providing the heater energies at different operating temperatures  $\overline{E_H} = \frac{E_H}{T_{op}}$  is used as the heater energy performance metric. Increasing the critical current density of an YBCO based switch that operates at 50 K allows a reduction in the length and heater energy to the levels used for 20 K operation, but as  $T_{op}$  is higher the  $\overline{E_H}$  score is improved. The  $\text{MgB}_2$  has the best  $\overline{E_H}$  score as even though it operates at 20 K its required length and energy are much lower than the YBCO based switches. Increasing the critical current density and reducing the length and number of tapes increased the final

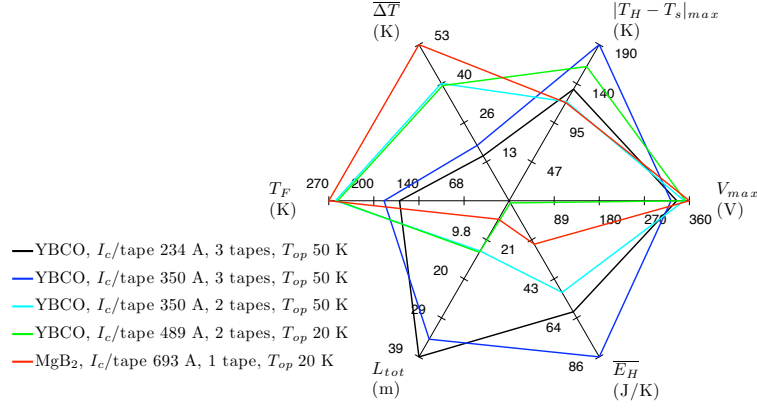


FIGURE 5.46: Star plot of the performance metrics of superconducting dump-switches with different critical current densities.

temperature and  $\Delta T$  of the switch as the heat capacity was decreased and the magnet energy per unit length that was deposited was increased. The peak voltages of all five switches are below the 420 V obtained with the existing mechanical switch. The YBCO switch that operates with three tapes with a high critical current density has the lowest peak voltage as it has the lowest rate of magnet current decay. Increasing the critical current density and reducing the number of tapes results in a more resistive switch that has a higher rate of current decay and so the peak voltage increases from 320 V to 345 V, this is comparable to the peak voltage obtained by operating an YBCO based switch at 20 K (348 V). The MgB<sub>2</sub> based switch has the highest peak voltage (356 V) as it has the fastest current decay rate.

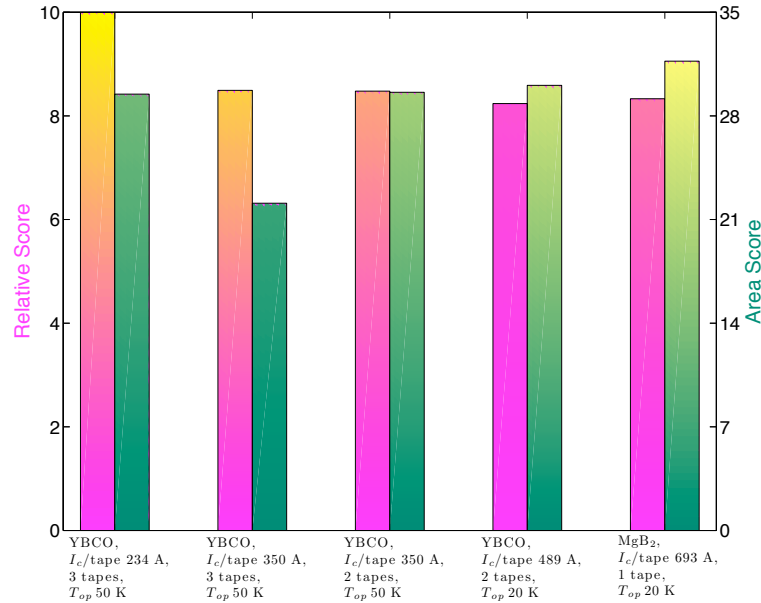


FIGURE 5.47: Effect of changing the critical current densities on the performance metrics of superconducting dump-switches.

Figure 5.47 shows the performance scores of the five switches. The switch with three tapes of YBCO that has a low critical current density has the best relative score as it

is the best performer in two out of the six metrics, the second best in another two, but also the worst in two. The switch with three tapes of YBCO and a high critical current density is also a good performer due to its low thermal gradients and low peak voltage. Both three tape switches have poor area scores due to their long lengths and high heater energies. Increasing the critical current density and reducing the number of tapes results in a switch that performs less well due to the higher thermal gradients. However, its area score is better due to the reduction in length and heater energy. The  $\text{MgB}_2$  switch is a good alternative design and it has the highest area score due to its short required length and low  $\overline{E_H}$  even though it operates at 20 K. Its relative score suffers as it has the highest final temperature and  $\overline{\Delta T}$ .

### 5.3.9 Normal State Resistance of the Superconducting Tape

Altering the normal state resistance of the superconducting tape used in a switch may be beneficial as it allows the switch length to be controlled. Decreasing the resistivity means that a longer length is needed to achieve the correct dump resistance. This increases the heat capacity and reduces the deposited magnet energy per unit length thereby reducing the temperature gradients and final temperature. It may be beneficial to use a lower normal state resistivity superconducting tape to reduce high thermal gradients or to reduce high final temperatures or both. Conversely, in some situations it may be beneficial to use a superconducting tape with a higher normal state resistivity so that a shorter length is needed, thereby reducing the both the amount superconductor and the required heater energy.

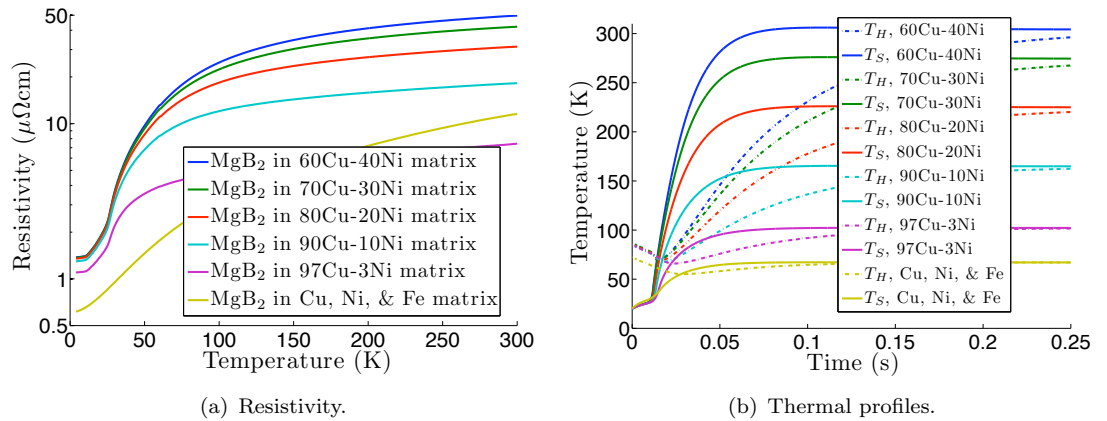


FIGURE 5.48:  $\text{MgB}_2$  based tapes can have different cupronickel matrices. (a) shows the resistivities of such tapes and (b) shows the thermal profiles of dump-switches based on these tapes.

**The normal state resistivity of  $\text{MgB}_2$  tapes** can be adjusted by changing the alloy of the cupronickel matrix or by changing the volume fraction of the copper stabilisation. Altering the alloy has a large effect on resistivity but only a small effect on the heat capacity as the heat capacities of cupronickel alloys are similar. The  $\text{MgB}_2$  dump-switches

that were discussed in Section 5.3.6 have a 70Cu-30Ni matrix and to use the least amount of heater energy require lengths of around 5 m. This leads to high thermal gradients and high final temperatures, problems that would be exacerbated if higher energy magnet circuits were to be protected with such dump switches. It may be possible to reduce the thermal gradients and final temperature by reducing the nickel content of the cupronickel matrix. The resistivities of MgB<sub>2</sub> tapes (Chapter 2) that have a range of cupronickel matrices are shown in Figure 5.48(a) and take into account the MgB<sub>2</sub> and niobium sheaths. The thermal profiles of dump-switches formed of MgB<sub>2</sub> in cupronickel matrices are shown in Figure 5.48(b). The switch that uses a Cu, Ni, & Fe matrix tape is discussed in Section 5.3.6 where the discharge characteristics are also shown. The length of these switches is set so that the magnet discharge requirements are met and the minimum heater energy is used. The required lengths to meet the magnet discharge requirements with the minimum heater energy are shown in Table 5.9.

Superconductor Matrix	$\rho$ (300 K) ( $\mu\Omega$ cm)	RRR ( $\frac{\rho_{300}}{\rho_{4.2}}$ )	$L_{tot}$ (m)	$T_{HI}$ (K)	$E_H$ (J)
60Cu-40Ni	50	36	4.0	86	20
70Cu-30Ni	42	31	4.7	87	24
80Cu-20Ni	31	23	6.5	86	32
90Cu-10Ni	18	14	12	85	56
97Cu-3Ni	7.4	6.8	33	85	159
Cu, Ni, & Fe	12	19	107	72	862

TABLE 5.9: Parameters of MgB<sub>2</sub> based dump-switches that have different matrix compositions. The lengths are set to meet the discharge requirements for the minimum heater energy. The Cu, Ni, & Fe matrix tape has a larger area than the cupronickel alloy tapes.

The initial heater temperature for all five cupronickel matrix switches are similar as they have the same insulation and similar specific heat capacities. This leads to the thermal switches being similar for about the first 10 ms. At this point the magnet chain starts to discharge with the current decay profiles shown in Figure 5.49(a). The higher resistivity switches have a shorter length and so the magnet energy that is deposited per unit length is greater than that of the lower resistivity and longer switches. The high amount of magnet energy that is dissipated per unit length leads to a rapid temperature rise to high temperatures; about 300 K for the most resistive switch. All of the switches have a pronounced kink in the superconductor temperature rise when the magnet starts to discharge as the magnet energy (5.5 kJ) is much larger than the heater energy, which is <160 J for any of the cupronickel matrix switches. The copper stabilised switch has the lowest final temperature as its longer length means that there is less energy deposited per unit length. The initial energy dissipation profiles (Figure 5.49(b)) are similar as due to the required length giving similar discharge profiles in order to meet the magnet discharge requirements. After 25 ms all of the switches have dissipated 37 % of the magnet energy.

After 25 ms the dump-resistances (Figure 5.50(b)) developed by the switches start to diverge due to the difference in length, resistivity, and temperature. The higher temperature

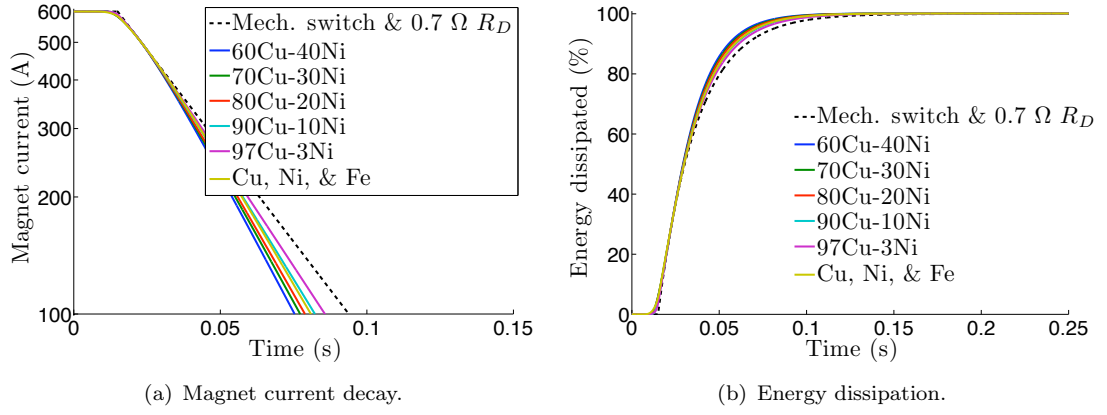


FIGURE 5.49: Effect of using  $\text{MgB}_2$  based dump-switches that have different matrix compositions on the current decay (a) and on the energy dissipation (b).

and resistivity of the switches with high nickel content matrices counteract their shorter lengths and these switches develop the highest dump resistances. The high dump resistance of the switch that has a 60Cu-40Ni matrix means that after 25 ms it has the fastest magnet current decay. The 97Cu-3Ni matrix switch has the slowest decay due to its lower dump resistance. Despite the difference in final dump resistance and magnet current decay rate the peak voltages (Figure 5.50(a)) during energy extraction are between 352 V and 360 V for the cupronickel matrix tapes. The copper stabilised tape has a peak voltage of 369 V.

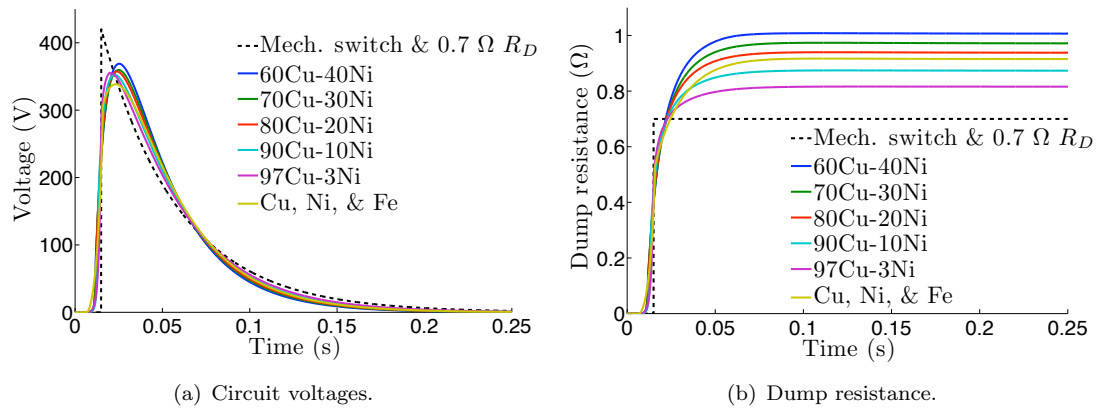


FIGURE 5.50: Effect of using  $\text{MgB}_2$  based dump-switches that have different matrix compositions on the circuit voltage (a) and on the dump resistance (b).

A star plot of the change in performance metrics that result from changing the matrix resistivity is shown in Figure 5.51. Reducing the matrix resistivity reduces the final temperature, the average temperature gradient, and the maximum temperature gradient. The maximum temperature difference for the 97Cu-3Ni matrix switch and for the 90Cu-10Ni matrix switch are the same as they have the same initial heater and superconductor temperatures. All of the switches have about the same peak voltage that is lower than the 420 V obtained with the mechanical switch. Decreasing the matrix resistivity leads to

longer switches and higher heater energies being required. The lowest resistivity switch requires about three times as much length and heater energy as the second lowest resistivity switch. The switch that uses a  $\text{MgB}_2$  tape with a Cu, Ni, and Fe matrix has the lowest thermal gradients and final temperature. This switch requires the most amount of superconductor (107 m) and the highest heater energy (862 J); the switch with the next highest requirements, which has a 97Cu-3Ni matrix, only requires 33 m and 159 J. The long lengths required by the copper stabilised tape means that it is not suited to these magnet circuits.

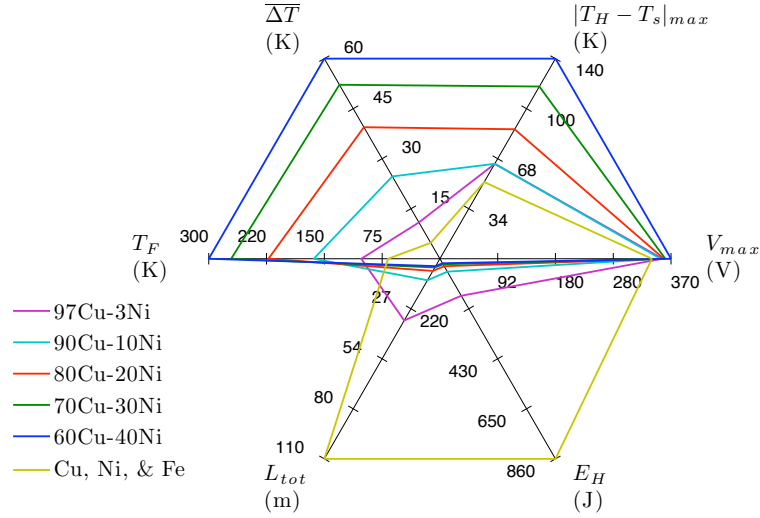


FIGURE 5.51: Star plot of the performance metrics of  $\text{MgB}_2$  based dump-switches that have different matrix compositions.

There is a non-linear relationship between resistivity and the required length and also resistivity and the required heater energy; these relationships are shown in Figure 5.52. As the resistivity is increased the required length decreases in order to meet the required dump resistance. This decrease in length causes a decrease in thermal mass and so the required heater energy also decreases. The relationship is non-linear as the lower resistivity switches have lower final temperatures and so the switching and dumping regime occurs at a temperature range where the RRR causes a larger decrease in resistivity than at 300 K.

The performance scores of the six switches are shown in Figure 5.53. Changing the matrix to 97Cu-3Ni gives a switch with the highest relative performance score but a low area score. Using a 90Cu-30Ni matrix gives a switch with the second best relative performance score and the best area score as the reduction in resistivity leads to low thermal gradients and final temperature for only a modest increase in length and heater energy. The copper stabilised switch has a good relative score as it has the lowest thermal gradients and final temperature but the long lengths and high heater energies that it requires means that it has the worst area score. The high thermal gradients and final temperature of the 60Cu-40Ni switch means that it performs poorly even though it requires the shortest length and least amount of heater energy.

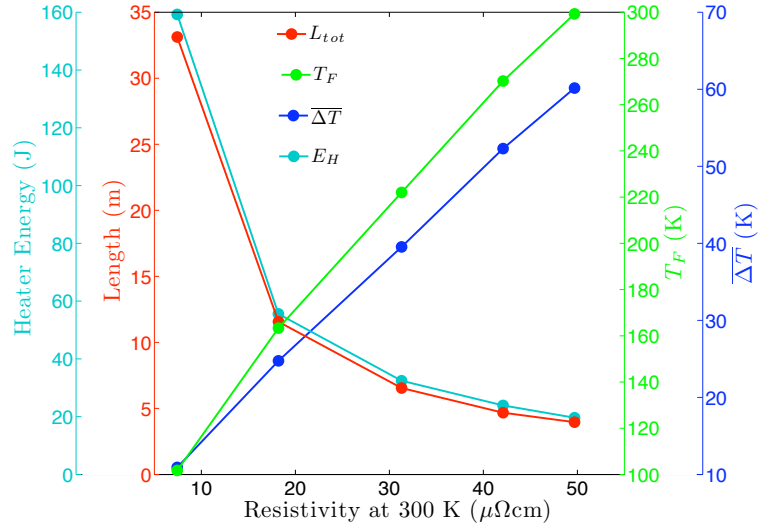


FIGURE 5.52: Effect of changing the matrix resistivity on the required length and heater energy of  $\text{MgB}_2$  based dump-switches.

The optimal switch for this situation utilises a  $\text{MgB}_2$  tape that has a 90Cu-10Ni matrix. This tape has a resistivity of  $18 \mu\Omega\text{cm}$  (300 K) and tapes with a lower resistivity than this, including  $\text{MgB}_2$  tapes with a 97Cu-3Ni matrix or with a copper stabilised matrix, require increasingly longer lengths and greater heater energies for decreasingly smaller thermal gradients. The problem is compounded for the Cu, Ni, and Fe matrix tape as it also has a larger area giving it a higher resistance per length. The larger area and length increase the heat capacity thereby requiring a heater energy about fifteen times that of the optimal design.

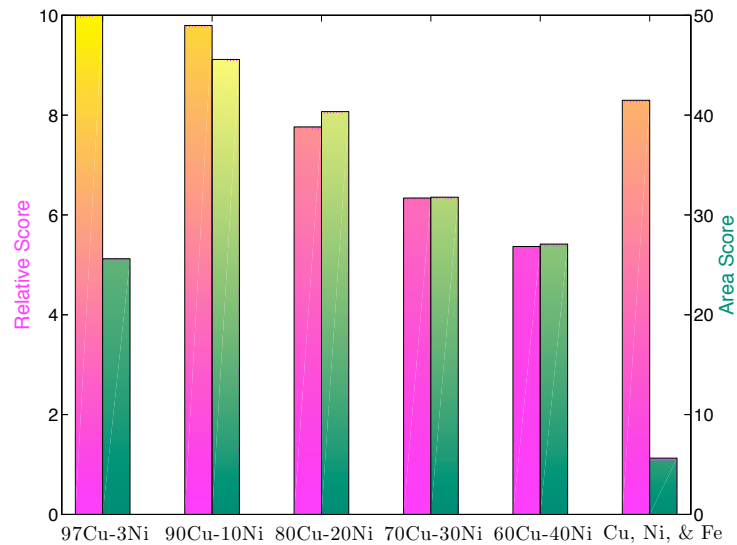


FIGURE 5.53: Performance scores of  $\text{MgB}_2$  based dump-switches with different matrix compositions.

**The normal state resistance of YBCO tapes** can be adjusted by applying a different thickness of copper stabilization or by using a different stabilization material. Second



generation HTS tapes are generally formed by depositing YBCO on a resistive substrate and then applying a stabilisation layer. The substrate is generally hastelloy, a Ni-W alloy, with a thickness of  $50\text{ }\mu\text{m}$  to  $100\text{ }\mu\text{m}$ . This substrate then has a number of buffer layers applied upon which the YBCO is deposited. The number and type of buffer layers depends on the deposition process; typically  $1\text{ }\mu\text{m}$  to  $5\text{ }\mu\text{m}$  of YBCO are deposited. A silver cap layer, which has a thickness of about  $2\text{ }\mu\text{m}$  to  $3\text{ }\mu\text{m}$ , is applied to the YBCO to provide electrical stabilization. Extra stabilization can be added to the tape to achieve the desired thermal and mechanical properties.

For American Superconductor tapes  $50\text{ }\mu\text{m}$  of low conductivity copper cladding is soldered to both faces of the tape [25]. Higher resistance versions are also available with about  $35\text{ }\mu\text{m}$  stainless steel replacing the copper cladding. In both cases the Hastelloy substrate is  $75\text{ }\mu\text{m}$  thick. A comparison of copper clad YBCO switches and stainless steel clad YBCO switches is described in Section 5.3.6. The low resistivity of these copper clad tapes meant that they required lengths of over  $450\text{ m}$  and heater energies of over  $80\text{ kJ}$  and so were not practical for the  $5.5\text{ kJ}$  MCD circuits.

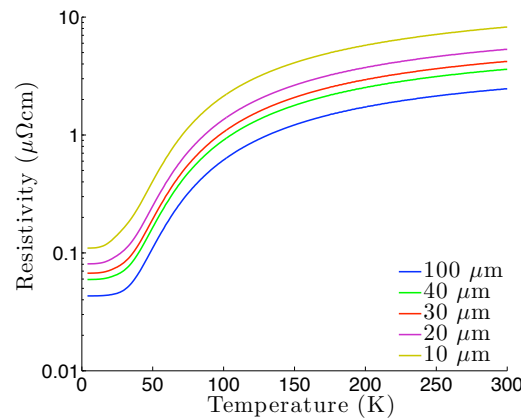


FIGURE 5.54: Normal state resistivity of YBCO tape with different thicknesses of copper stabilisation on a  $50\text{ }\mu\text{m}$  Hastelloy substrate and a  $2\text{ }\mu\text{m}$  silver layer.

SuperPower tapes have higher conductivity copper electro-deposited on the whole tape; the thickness of this deposited layer is controllable. The total thickness is in the range  $1\text{ }\mu\text{m}$  to  $40\text{ }\mu\text{m}$  [58]. In all cases the Hastelloy substrate is  $50\text{ }\mu\text{m}$  thick. Reducing the thickness of the copper stabilization will increase the resistivity and reduce the thermal conductivity and thermal mass of the tape. This will result in a switch where a shorter length is required to meet the dump resistance and less heater energy is needed to trigger the switch. Due to the lower thermal mass of the switch the final temperature will be higher. The normal state resistivity of copper stabilised YBCO tapes are shown in Figure 5.54. Switches based on YBCO tapes that have low resistivities may be more beneficial to higher energy circuits where higher heater energies are more acceptable and the longer length and thermal mass are needed to absorb the heater energy without the switch overheating.

Table 5.10 shows the effect of changing the copper thickness on the resistivity of the YBCO based tape. Reducing the copper thickness results in an increase in the resistivity

<b>Copper thickness</b>	$\rho$ (300 K) ( $\mu\Omega\text{cm}$ )	RRR ( $\frac{\rho_{300}}{\rho_{4.2}}$ )	$L_{tot}$ (m)	$T_{HI}$ (K)	$E_H$ (kJ)
100 $\mu\text{m}$ Cu	2.5	57	602	286	95
80 $\mu\text{m}$ Cu	2.7	58	482	256	63
60 $\mu\text{m}$ Cu	3.0	59	352	228	38
40 $\mu\text{m}$ Cu	3.6	61	222	197	18
30 $\mu\text{m}$ Cu	4.2	62	157	180	11
25 $\mu\text{m}$ Cu	4.7	64	124	171	7.8
20 $\mu\text{m}$ Cu	5.3	66	92	161	5.1
10 $\mu\text{m}$ Cu	8.2	75	35	137	1.4
5 $\mu\text{m}$ Cu	13	88	14	120	0.4

TABLE 5.10: Parameters of HTS dump-switches that operate at 50 K and use YBCO tape with deposited copper (RRR 50) stabilisation. The tapes also contain a 50  $\mu\text{m}$  Hastelloy substrate and a 2  $\mu\text{m}$  Ag (RRR 100) layer. Three tapes are needed to carry the magnet current and the lengths are set to meet the discharge requirements for the minimum heater energy.

of the tape as the Hastelloy substrate dominates the resistivity at high temperatures. The RRR of the tape increases with decreasing thickness as the low temperature resistivity is dominated by the thin (2  $\mu\text{m}$ ) silver layer that has a RRR of 100. The resistance per length of the tape increases as both the resistivity increases and the area decreases. This table also shows the required length for the switch to meet the discharge requirements for the minimum heater energy.

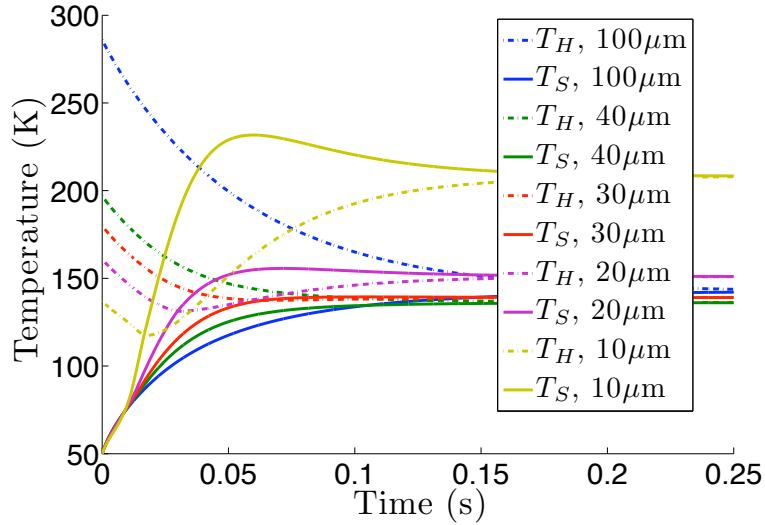


FIGURE 5.55: Thermal profiles of YBCO based dump-switches that have different thicknesses of copper stabilisation.

Reducing the copper thickness means that less length is required to achieve the correct dump resistance and less heater energy is required to trigger the switch. Reducing the copper thickness also reduces the thermal mass of the switch and so the maximum temperature in the switch increases. The thermal profiles for YBCO based switches with a range of thicknesses of copper stabilisation are shown in Figure 5.55. The low resistivity

of tape with 100  $\mu\text{m}$  of copper stabilisation means that a long length of tape is needed in order to develop the required dump resistance. This means that the amount of magnet energy that is deposited per unit length is low and so a high heater energy ( $T_{HI}$  286 K) is needed to drive the transition. This high initial temperature means that the switch has high thermal gradients and the heat flow is always from the heater to the superconductor with the heater never acting as a heat sink. Reducing the copper thickness to 10  $\mu\text{m}$  increases the resistivity so that seventeen times less length is needed. In this case the initial heater temperature (137 K) must just trigger the transition. The short length means that the amount of magnet energy that is deposited per unit length is high. When the magnet discharge begins there is a pronounced kink in the superconductor temperature rise and a subsequent rapid increase in temperature to a high final temperature. This switch also has high thermal gradients but in this case the heat flows from the superconductor to the heater that acts as a heat sink to limit the overall temperature rise. Copper thicknesses of around 20  $\mu\text{m}$  to 30  $\mu\text{m}$  allow the thermal gradients to be minimised without using a large heater energy or resulting in a high final temperature.

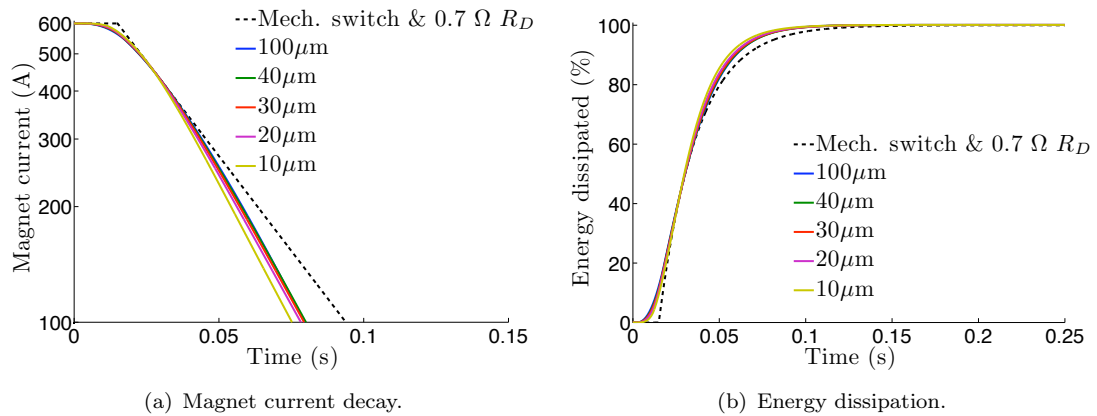


FIGURE 5.56: Effect of using different thicknesses of copper stabilisation on YBCO based dump-switches on the current decay (a) and on the energy dissipation (b). The switch with 10  $\mu\text{m}$  of Cu stabilisation has a slightly fast current decay than the other switches.

Copper thicknesses from 10  $\mu\text{m}$  to 100  $\mu\text{m}$  result in switches that have similar magnet current decay profiles (Figure 5.56(a)) and energy dissipation curves (Figure 5.56(b)). These curves are similar as the lengths are set to meet the magnet discharge requirements. The switches have similar peak voltages (Figure 5.57(a)). The peak voltages increase with increasing resistivity due to the higher rate of magnet current decay. The more resistive tapes require a shorter length to develop the required dump resistance. The rate of increase of dump resistance (Figure 5.57(b)) is similar for all of the switches. The higher resistivity switches have lower initial heater temperatures and so the initial rate of heat conduction through the insulation is less resulting in a more gradual initial development of the dump resistance. The subsequent faster rate of superconductor temperature rise caused by the discharging magnet leads to a faster rate of increase of the dump resistance. After about 0.06 s the dump resistance of the switch that has 10  $\mu\text{m}$  of copper decreases

as the superconductor temperature is lowered by heat flowing into the heater. The dump resistance of the switch that uses  $100\ \mu\text{m}$  of copper continues to grow to become the highest resistance switch due to the long length of superconductor that is used and the large heater energy continuing to warm the superconductor after the magnet decay has finished.

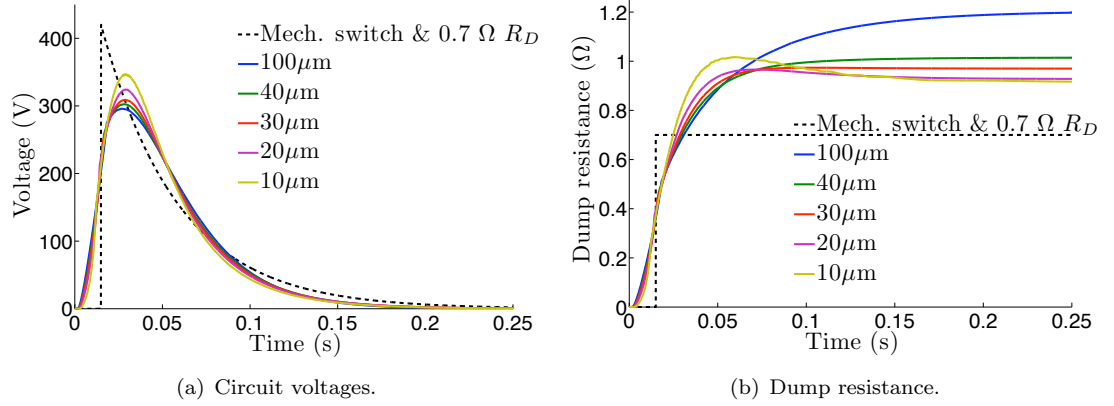


FIGURE 5.57: Effect of using different thicknesses of copper stabilisation on YBCO based dump-switches on the circuit voltage (a) and on the dump resistance (b).

Figure 5.58 shows the effect of the copper thickness on the final temperature, average temperature gradient, heater energy, and total length. Using less resistive YBCO based tapes that have a thick layer ( $> 50\ \mu\text{m}$ ) of copper stabilisation means that long switch lengths are required in order to develop the required dump resistance. This long length means that the magnet energy that is dissipated per unit length is low and so the heater must provide enough energy to drive the transition. The long length of switch means that the heater energy is also high. This large amount of heater energy is provided by a high initial heater temperature and so the average and maximum temperature gradients within the switch are also high. The final temperature is low ( $\approx 150\ \text{K}$ ) as the long length and high thermal mass of the switch limits the temperature rise. Reducing the copper thickness increases the resistivity of the tape and so shorter lengths can be used. This results in decreasing length, heater energy, and thermal gradients. There is a minimum in the average thermal gradient when  $25\ \mu\text{m}$  of copper is used. Reducing the copper thickness ( $< 15\ \mu\text{m}$ ) to less than this results in an increase in the average thermal gradient as the increased resistivity means that shorter lengths are needed and so the magnet energy that is deposited per unit length increases. This causes the superconductor to heat rapidly and the heater acts as a heat sink. The short length and low thermal mass of these switches means that the final temperature is also high, exceeding  $300\ \text{K}$  if only  $5\ \mu\text{m}$  of copper is used. Despite their high final temperature and high thermal gradients switches that only have thin copper layers may have benefits as they only require short lengths and low heater energies.

A star plot of the performance metrics of switches that use YBCO tapes with a range of copper thicknesses is shown in Figure 5.59. Using YBCO with thick copper stabilisation

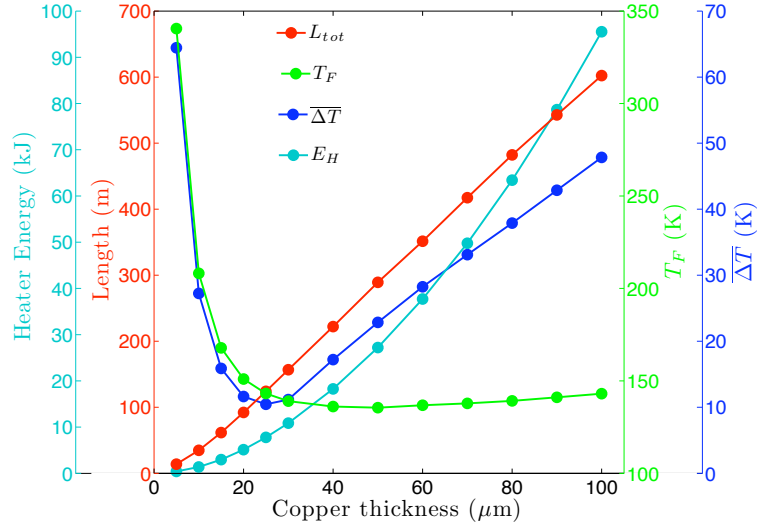


FIGURE 5.58: Effect of the thickness of the copper stabilization on the performance parameters of YBCO based dump-switches.

results in a poorly performing switch as the long length that is need requires a high heater energy that in turn leads to high thermal gradients. Decreasing the copper thickness increases the resistivity allowing shorter lengths and lower heater energies to be used. The thermal gradients are also reduced to a minimum that is achieved with  $25 \mu\text{m}$  of copper stabilisation. Below this thickness the length and heater energy continue to decrease but the thermal gradients and final temperature will increase rapidly. The peak voltage increases with decreasing copper thickness but is always less than the peak voltage obtained with the mechanical switch.

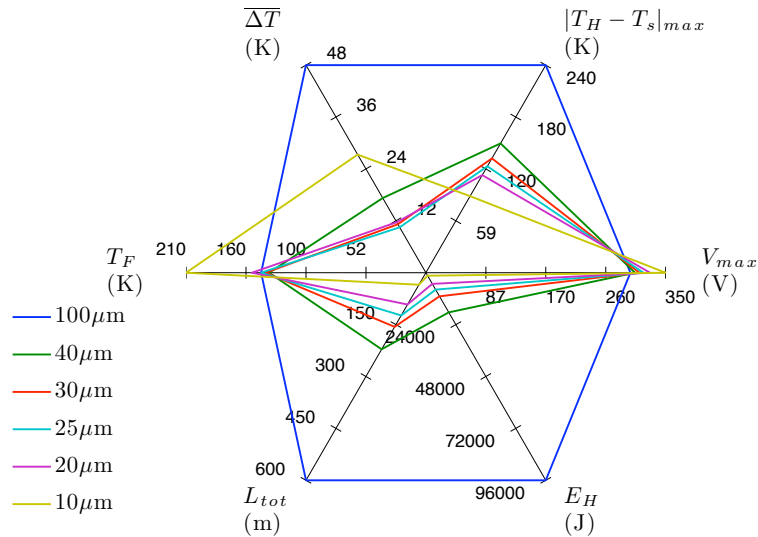


FIGURE 5.59: Star plot of the performance metrics of YBCO based dump-switches that have different matrix compositions.

Figure 5.60 shows the performance scores of switches that use YBCO tapes with a range of copper thicknesses. The best performing switch has a copper thicknesses of  $25 \mu\text{m}$ . This

also corresponds to the minimum in the average thermal gradient. Switches with similar copper thickness also perform well. Decreasing copper thickness improves the area score due primarily to the reduction in heater energy that has a high magnitude compared to the other performance scores. Thus the shortest highest resistivity switch has the best area score but a poor relative score. The optimal copper thickness is  $25\text{ }\mu\text{m}$ , this can be increased up to  $30\text{ }\mu\text{m}$  to reduce the final temperature at the expense of length and energy, or it can be reduced down to  $20\text{ }\mu\text{m}$  to reduce the length and energy at the expense of the thermal gradients and final temperature.

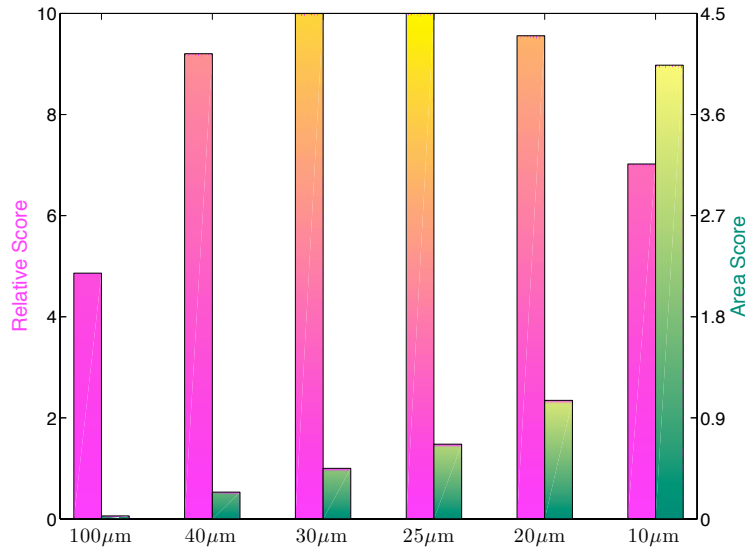


FIGURE 5.60: Performance scores of YBCO based dump-switches with different matrix compositions.

### 5.3.10 Insulation Thickness

Insulation thickness is a design parameter that when reduced will improve the performance of the switch by reducing the thermal resistance between the superconductor and heater. This will lead to faster heat diffusion that requires a shorter optimum length, less heater energy and lower thermal gradients. There will be a higher final temperature due to the reduced thermal mass of the switch. Whilst the switching dynamics will be improved by reducing the insulation thickness this is not always practical. The required thickness of insulation will be set as a function of the magnet circuit, heater voltage, and the operating environment. The thickness and number of layers must be sufficient to prevent arcing and also to lessen the affect of pin holes. When analysing a switch the diffusion time of the insulation must also be considered in order to confirm the validity of the lumped approximation. The switches considered so far have used an insulation thickness of  $76.2\text{ }\mu\text{m}$  as this can provide sufficient electrical insulation without slowing down the thermal dynamics of the switch too much. The diffusion time is on the limit of what can be analysed with the lumped approximation but comparison with the PDE solution

(Figure 5.61) shows that it is still valid. The switch design is that of the stainless steel clad YBCO based switch with a tape length of 8.3 m (total length 24.9 m). The switching characteristics obtained with the lumped approximation that is based on a set of ODEs is similar to the solution that is obtained with the full PDE analysis. However, at early times there is a delay in the ODE solution with respect to the PDE solution, this is due to the thermal diffusion time being on the limit of what can reasonably modeled with the lumped approximation.

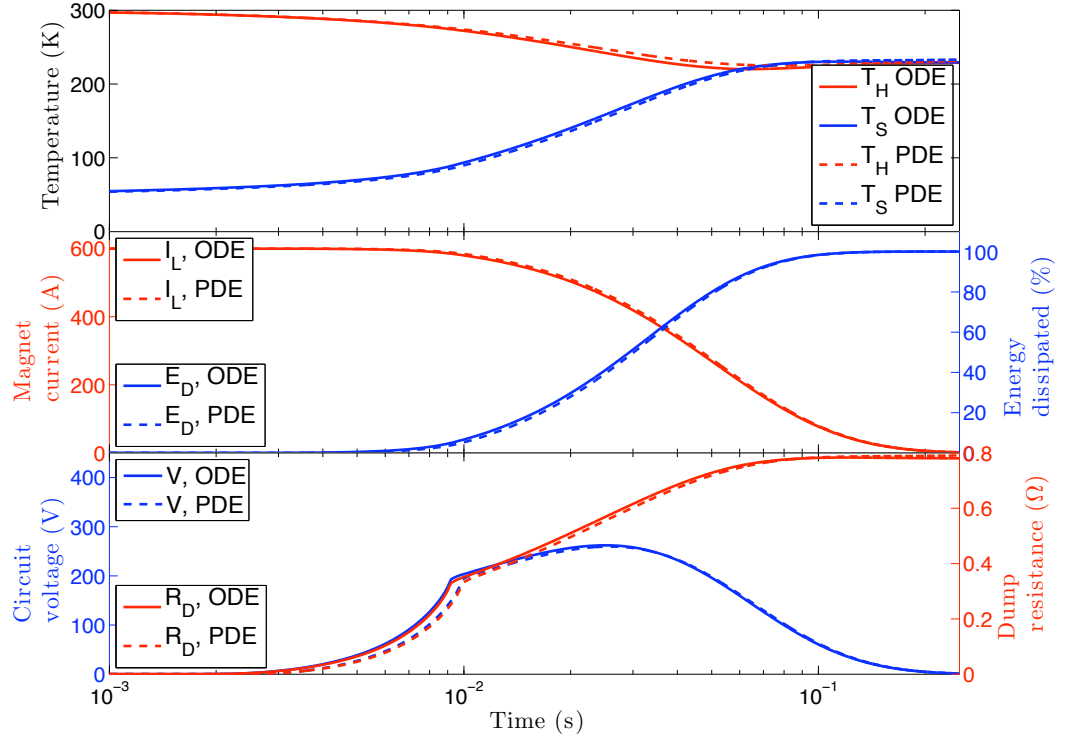


FIGURE 5.61: Switching characteristics of a switch with  $76.2 \mu\text{m}$  of insulation when analysed with the lumped approximation (ODE) and also the PDE solution.

To investigate the benefit of using a switch that has thinner insulation the switch was modelled using the lumped approximation with  $50.8 \mu\text{m}$  and  $25.4 \mu\text{m}$  of polyimide insulation and compared to the previous  $76.2 \mu\text{m}$  based results. In each case the initial heater temperature was 300 K and the switch length was optimised to meet the magnet discharge requirements. The required total length with  $25.4 \mu\text{m}$  was 20.6 m and with  $50.8 \mu\text{m}$  it was 22.6 m. The reduction in length leads to a much reduced required heater energy and a lower peak magnet circuit voltage. The maximum temperature difference between the heater and superconductor layers remain the same as in these switches it represents the difference between the initial heater and initial superconductor temperatures that are the same in each case. The reduction in switch heat capacity by reduction of length and insulation thickness means that even though the input energy is less the final temperature is higher for switches that have thinner insulation layers.

The thermal profiles of the three switch designs are shown in Figure 5.62. In all cases the heat initially flows from the heater to the superconductor with this happening significantly

faster in the  $25.4\ \mu\text{m}$  of insulation switch than in the other two. The result of this is that the heater layer starts to act as a heat sink after 28 ms, compared to 44 ms for the  $50.8\ \mu\text{m}$  insulation and 61 ms for the  $76.2\ \mu\text{m}$  insulation.

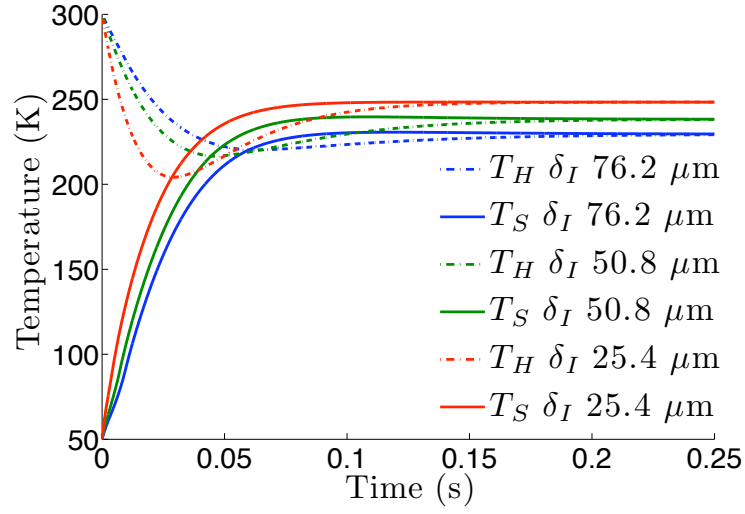


FIGURE 5.62: Effect of changing insulation thickness on the thermal profiles of a superconducting stainless steel clad YBCO dump-switch that operates at 50 K and has a  $T_{HI}$  of 185 K.

The faster temperature rise of the superconductor with a reduction in insulation thickness leads to an earlier initiation of magnet current decay (Figure 5.63(a)) and a correspondingly earlier initiation of magnet energy dissipation (Figure 5.63(b)). As the three switches all have their lengths optimised to meet the magnet energy requirements they all touch the magnet decay that is obtained with the existing setup. Despite the earlier initiation of current decay of the thin insulation switch it is the last one to touch the existing current decay line and then closely follows the existing decay profile. The thickest insulation switch has the longest delay in initiation of energy dissipation but due to the longer length and resistance has the fastest rate of magnet current decay.

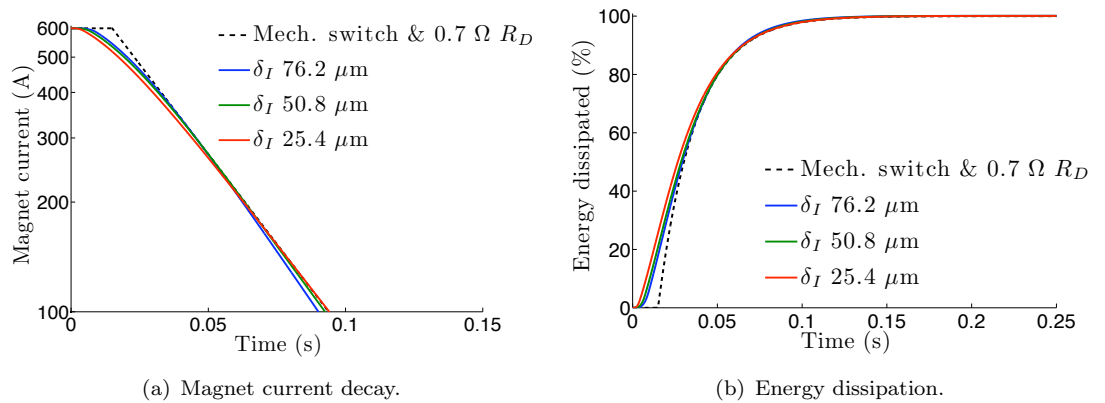


FIGURE 5.63: Effect of changing insulation thickness on the current decay (a) and on the energy dissipation (b).



The faster rate of magnet current decay with increasing insulation thickness leads to higher peak voltages (Figure 5.64(a)). This faster decay is required in order that the switch meets the magnet discharge requirements and is achieved by increasing the length of the switch, which increases the resistance (Figure 5.64(b)). All peak voltages attained with the superconducting dump-switches (250 V to 260 V) are significantly less than the 420 V peak obtained with the mechanical switch. Reducing the insulation thickness results in a lower final resistance of the switch, in the case of 25.4  $\mu\text{m}$  thickness this is less than the existing 0.7  $\Omega$  external dump, but the energy dissipation requirements are still met due to the earlier resistance growth.

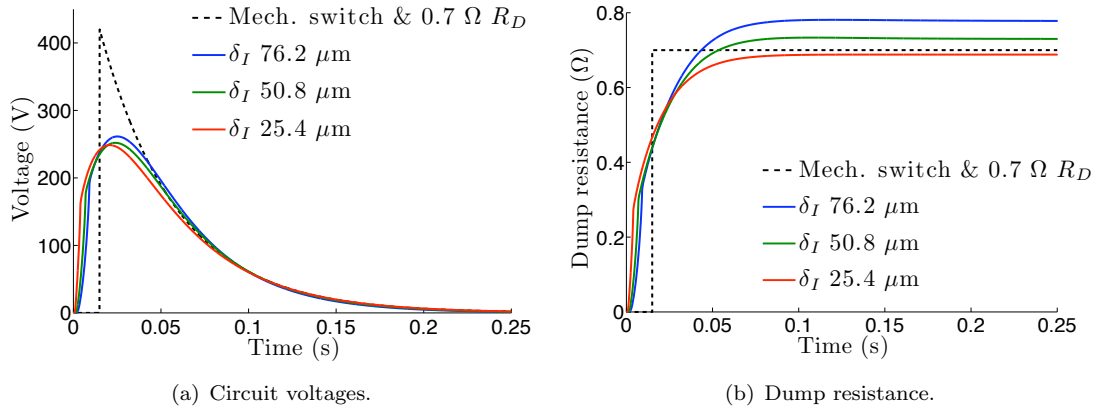


FIGURE 5.64: Effect of changing insulation thickness on the circuit voltage (a) and on the dump resistance (b).

Switches that utilise less length of conductor and lower heater energies can be achieved by using thinner thicknesses of insulation. Such switches will also result in lower magnet circuit voltages. For high inductance magnets where there is a greater stored energy and a higher discharge voltage thicker insulation is more beneficial as it can withstand higher voltages in a helium gas environment. This also has the added advantage of lowering the final temperature of the switch, preventing overheating of dump-switches that are used in high magnet energy circuits.

### 5.3.11 Heater Dynamics with a Capacitor Discharge Powered Heater

The switches considered in the previous sections were switches that had heaters that instantly heated up to an initial heater temperature,  $T_{HI}$ . This is equivalent to a switching situation where the decay of the heater capacitor circuit is much faster than that of the magnet decay circuit. The discharge time constant of the magnet circuit that has an inductance of  $L_m$ , is given by

$$\tau_M^{\text{mech}} = \frac{L_m}{R_D} + \tau_{ms}, \quad (5.3)$$

where  $R_D$  is the dump resistance that is switched into the circuit by a mechanical switch that closes with a delay of  $\tau_{ms}$ . The discharge time constant of the capacitor ( $C$ ) that powers the heater can be estimated using the heater resistance ( $R_H$ ) at the operating temperature ( $T_{op}$ ) to be

$$\tau_H^{\text{est}} = R_H(T_{op})C. \quad (5.4)$$

For cases where the voltage decay is known the discharge time constant of the heater can be calculated as

$$\tau_H^{\text{calc}} = t \left( V_H = \frac{V_{HI}}{e^1} \right), \quad (5.5)$$

where  $V_{HI}$  is the capacitor charge voltage. This method takes into account the temperature dependent resistivity of the heater.

### 5.3.11.1 Heater Dynamics when Operating at 50 K

A stainless steel clad YBCO dump-switch that operates at 50 K (Section 5.3.5) requires a total length of 39 m to meet the magnet discharge requirements when its stainless steel heater has an initial temperature of 186 K. This initial heater temperature results in the minimum heater energy for this switching situation.

Heater material	$L_{tot}$ (m)	$T_{HI}$ (K)	$E_H$ (kJ)	$\overline{\Delta T}$ (K)	$\rho_H(300 \text{ K})$ ( $\mu\Omega\text{cm}$ )	$R_H(T_{op})$ ( $\Omega$ )	$\tau_H^{\text{est}}$ (ms)	$\tau_H^{\text{calc}}$ (ms)
Stainless Steel	38.6	186	3.06	15.2	73	9.9	60.8	66.8
Cu (RRR 100)	37.9	188	3.15	15.6	1.7	0.011	0.072	0.9

TABLE 5.11: Parameters of YBCO based dump-switches operating at 50 K that have 50  $\mu\text{m}$  thick heaters. Three tapes are required to carry the magnet current at 50 K. The magnet circuit discharge time constant ( $\tau_M^{\text{mech}}$ ) is 58.7 ms

Replacing this initial heater temperature switch with one that has a capacitor discharge powered heater results in a heater that is too slow as the time constant of the capacitor discharge is longer than the magnet discharge time constant (Table 5.11). The capacitor for this heater has the same energy as the  $T_{HI}$  186 K switch and the charge voltage is 1 kV. In order to speed up the switching time the heater must heat up faster; this requires a faster capacitor discharge circuit. Reducing the resistance of the heater would allow a faster discharge. Using the same physical dimensions but replacing the stainless steel heater with a copper heater will reduce the capacitor discharge time constant to less than 1 ms. The thermal mass does not change significantly as the heat capacities are similar; at room temperature the heat capacity of stainless steel is only about 6 % more than that of copper.

The thermal profiles of these four switches are shown in Figure 5.65. The final temperatures of the four switches are about the same as the energy input into the system is similar for

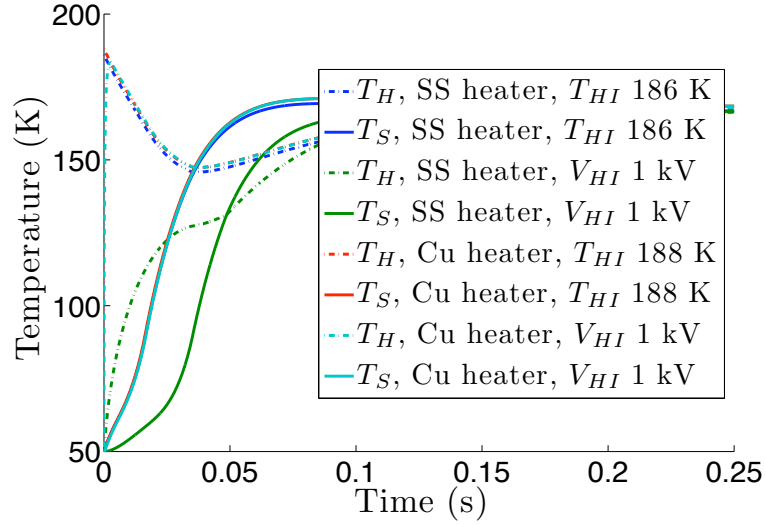


FIGURE 5.65: Thermal profiles of YBCO based dump-switches that have different heater materials. The SS heater with a  $V_{HI}$  of 1 kV is slower than the rest.

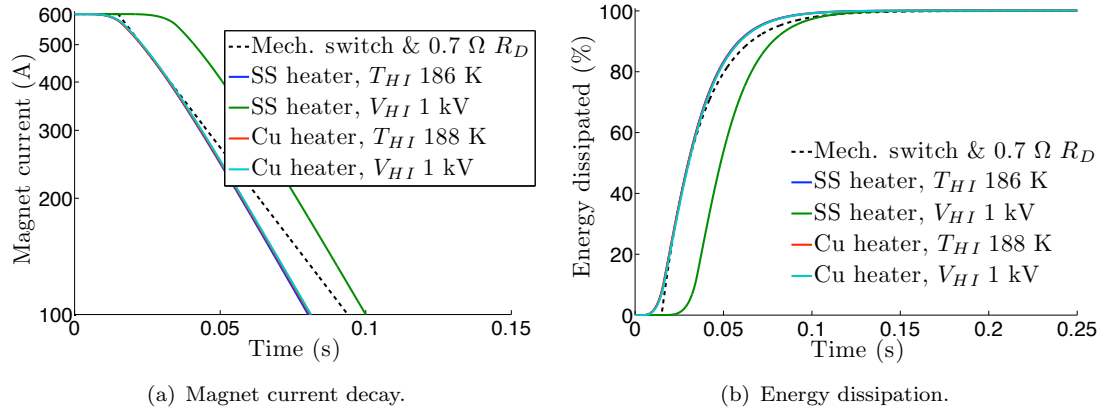


FIGURE 5.66: Effect of using different heater materials in YBCO based dump-switches on the current decay (a) and on the energy dissipation (b). The SS heater with a  $V_{HI}$  of 1 kV is slower than the rest.

each case and the thermal masses are also similar. The thermal profiles of the heater and superconductor of the stainless steel heater switch are different to the initial heater temperature switch due to the slower deposition of heater energy. The copper heater switch has thermal profiles that are similar to the initial heater temperature switch as the capacitor's energy is deposited in the heater within few milliseconds. The more gradual rise in temperature of the switch with a stainless steel heater leads to reduced thermal gradients.

The switches that have heaters which are powered by a capacitor discharge have similar shape but delayed current decay (Figure 5.66(a)) and energy deposition (Figure 5.66(b)) profiles to the switch. Similarly the voltage profiles (Figure 5.67(a)) and dump resistance profiles (Figure 5.67(b)) all have a similar shape but for the slower acting stainless steel heater they are delayed by  $\approx 20$  ms. This delay occurs due to the slower heating due

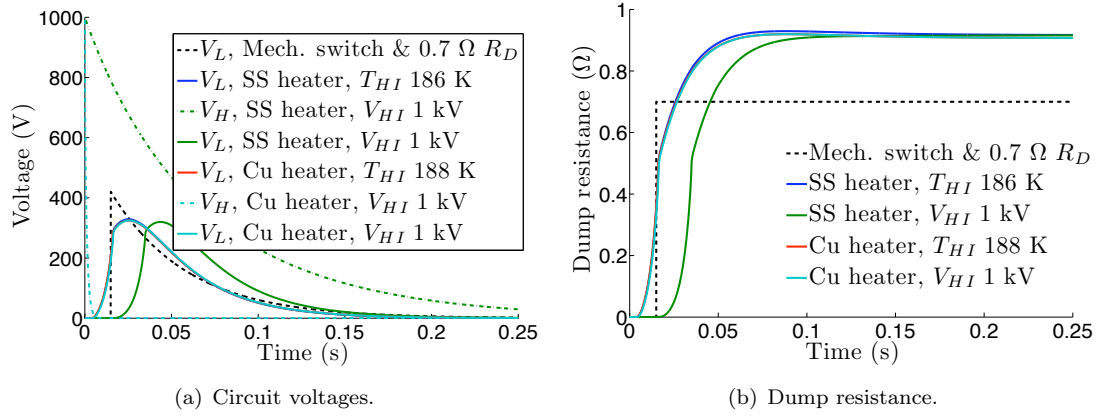


FIGURE 5.67: Effect of using different heater materials in YBCO based dump-switches on the circuit voltage (a) and on the dump resistance (b). The SS heater with a  $V_{HI}$  of 1 kV is slower than the rest.

to the slower capacitor discharge that results from the higher resistivity. The capacitor discharge powered switches that have stainless steel heaters do not meet the magnet discharge requirements (Section 5.3.1) as the slow heating of the superconductor means that the current decay is slower than that obtained with the mechanical switch and dump resistor. This slower temperature rise means that at time less than the discharge time constant the heater temperature is lower than that obtained with the  $T_{HI}$  switch. This leads to a lower temperature gradient and a lower rate of conduction through the insulation and so an increase in heater energy is needed. The faster acting copper heater requires less additional heater energy as it warms up faster and so the initial heat conduction is similar to that of the initial heater temperature switch. The required increase in heater energy as a function of capacitor charge voltage is shown in Figure 5.68.

The required heater energy and heater discharge time constant of stainless steel clad YBCO based switches that operate at 50 K (Figure 5.68) increase with decreasing capacitor charge voltage. The corresponding values for the initial heater temperature switches are given in Table 5.11. The capacitance is also shown as reducing the voltage may result in capacitances that are too large to be practical. In these switches three tapes are used in parallel so the area is increased and the resistance per length decreased. However, longer switches are required and the net result is an increase in heater resistance. If a stainless steel heater is used then the point at which the required heater energy starts to rise rapidly is  $\approx 7$  kV. This would lead to demanding electrical insulation requirements. The use of a copper heater decreases the resistance speeding up the capacitor discharge. In this case the point at which the heater energy rises rapidly is  $\approx 1$  kV. The average thermal gradients remain approximately constant irrespective of the capacitor charge voltage as the reduction in the initial temperature gradient is offset by the increase in heater energy that causes an overheating of the heater.

Switches that operate at 50 K have relatively high heater resistances due to the increase

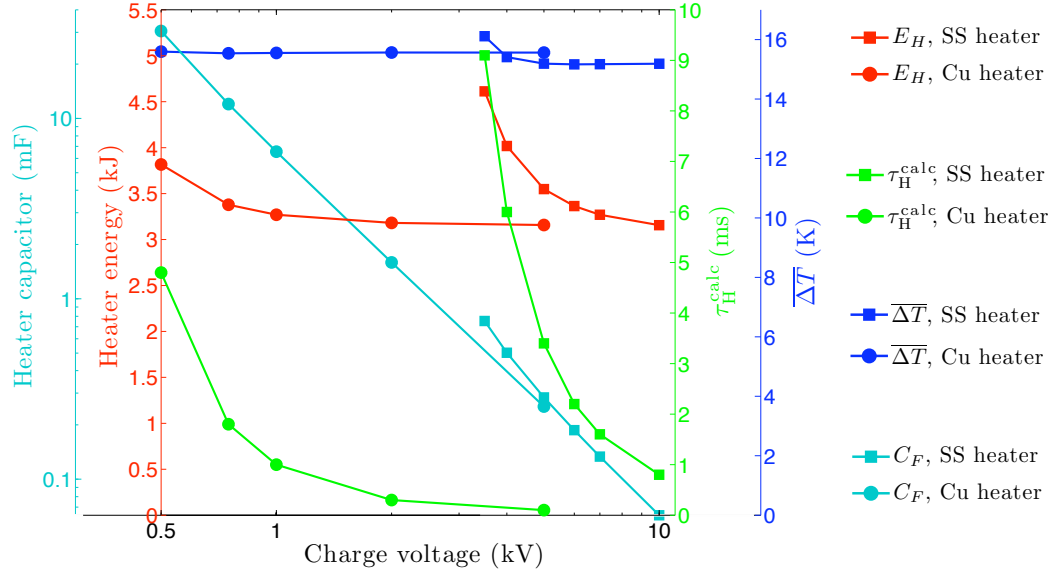


FIGURE 5.68: Required heater energy and heater capacitance, and the resulting average thermal gradient and heater discharge time constant for YBCO based dump-switches operating at 50 K. Results for a switch with a copper heater and also one with a stainless steel heater.

in heater resistivity with temperature and the increasing required switch length with temperature. The increased specific heat capacity and longer length mean that higher heater energies are required to trigger switches operating at 50 K. Both of these factors result in slow heater capacitor discharges. This problem may be exacerbated in higher magnet energy circuits if longer lengths are required to absorb the magnet energy. In order for the heater to act fast enough the heater resistivity must be decreased or else high capacitor charge voltages must be used. The use of copper heaters when operating at 50 K is necessary to allow capacitor charge voltages of 1 kV to trigger the switch. This is a reduction from the  $> 5$  kV that is required by stainless steel heaters.

### 5.3.11.2 Heater Dynamics when Operating at 20 K

A  $\text{MgB}_2$  in a 70Cu-30Ni matrix based dump-switch that operates at 20 K requires the lengths and heater energies given in Table 5.12. When such a switch has a 50  $\mu\text{m}$  thick stainless steel heater that is powered by a capacitor that has a charge voltage of 1 kV the discharge time constant ( $\tau_H^{\text{est}}$ ) is 1.6 ms. This is faster than the YBCO based switches that have stainless steel heaters as although the heater resistance at  $T_{op}$  is greater (33.2  $\Omega$  compared to 9.9  $\Omega$ ) the capacitance is lower (0.048 mF compared to 6.1 mF) due to the lower heater energy requirement. The discharge time constant of the  $\text{MgB}_2$  based switch's heater is much faster than the 58.7 ms discharge time constant of the magnet and so stainless steel heaters that have  $V_{HI}$  of 1 kV can be used with  $\text{MgB}_2$  switches. If a copper instead of stainless steel for the heater then the resistance and discharge time are significantly decreased. This may allow lower capacitor charge voltages to be used.

S'conductor material	Matrix material	Heater material	$T_{HI}$ (K)	$L_{tot}$ (m)	$E_H$ (J)	$T_F$ (K)	$\overline{\Delta T}$ (K)	$R_H(T_{op})$ ( $\Omega$ )	$\tau_H^{est}$ (ms)
MgB <sub>2</sub>	70Cu-30Ni	SS	87	4.7	24	226	51	33.2	1.6
		Cu	87	4.6	26	272	53	0.01	0.0005
	Cu	SS	72	107	862	67	4.8	294	506
		Cu	72	108	924	67	4.9	0.092	0.17
YBCO	SS	SS	253	11.2	1554	42	297	8.059	25
		Cu	258	10.9	1571	302	41	0.0024	0.0077

TABLE 5.12: Parameters of dump-switches operating at 20 K that have 50  $\mu\text{m}$  thick heaters powered by a 1 kV that provides the same energy as the  $T_{HI}$  switch. The magnet circuit discharge time constant ( $\tau_M^{mech}$ ) is 58.7 ms. The YBCO has an  $I_c$  of 90 A at 77 K and two tapes are required to carry the 600 A magnet current at 20 K. The MgB<sub>2</sub> switches only require one tape.

The capacitor charge voltage can be adjusted so that the heater capacitor has the required switch triggering energy without the long discharge time constants that would result from large capacitance capacitors. A MgB<sub>2</sub> in 70Cu-30Ni matrix based dump-switch that has a stainless steel heater and operates at 20 K (Section 5.3.5) requires a total length of 4.7 m to meet the magnet discharge requirements when the initial heater temperature is 87 K. This initial heater temperature results in the minimum heater energy for this switch situation, which is 23.9 J. For a switch that is triggered by a capacitor discharge, the heater energy is the energy stored in the capacitor,  $E_H = \frac{1}{2}CV^2$ . When the switch is triggered by a capacitor discharge powered heater the heater energy needs to be increased in order to make up for the initially lower thermal gradient. For fast capacitor discharges the capacitance should be as small as possible in order to have small capacitor discharge time constants, however, this leads to high capacitor charge voltages. Reducing the resistance of the heater would also lead to a faster discharge.

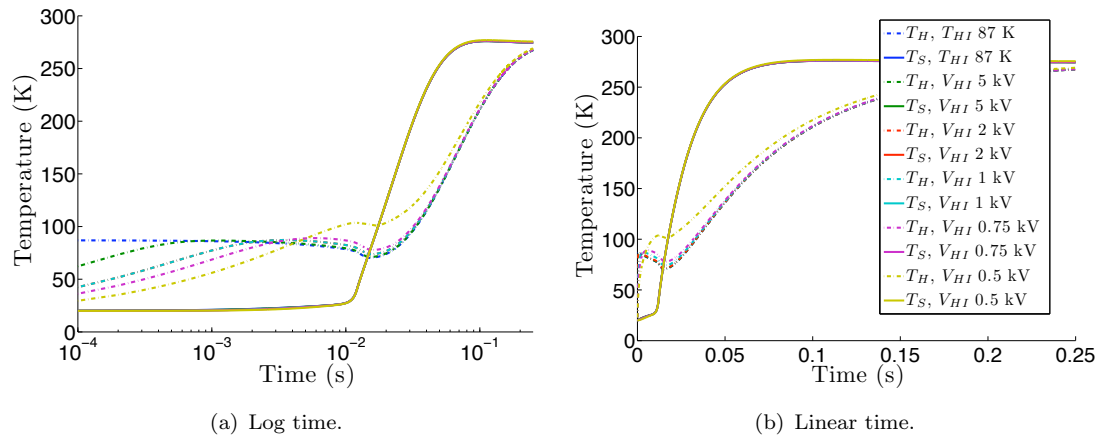


FIGURE 5.69: Thermal profiles for dump-switches that have capacitor discharge powered heaters with different charge voltages. A log time scale (a) is used to show the differences at early times and a linear time scale (b) to show differences at later times. The legend is the same for both figures.

The thermal profiles of MgB<sub>2</sub> based dump switches that have capacitor discharge powered

heaters are shown on a log time scale in Figure 5.69(a) and on a linear time scale in Figure 5.69(b). The log time scale is used to show differences at early times that are predominately due to the heater discharge profile and the linear time scale is used to show the similarities at later times that are predominately due to the slower magnet discharge. For capacitors with a charge voltage over  $\approx 750$  V the thermal profiles are similar to that obtained with the initial heater temperature for times greater than 10 ms. For lower voltages the high capacitance and thus slower capacitor discharge means that the profiles are different. As the charge voltage is increased the thermal profiles become more similar at earlier times with a charge voltage of 5 kV having similar temperature profiles from 1 ms onwards.

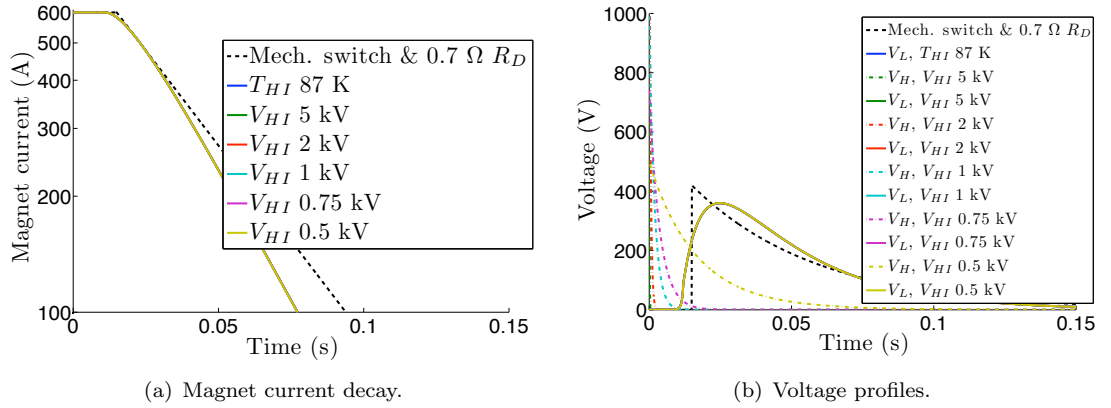


FIGURE 5.70: Effect of utilizing different heater capacitor charge voltages on the current decay (a) and on the voltage decays (b).  $V_L$  is the magnet circuit voltage and  $V_H$  the heater circuit voltage.

The similar thermal profiles during the magnet discharge mean that the switches have similar magnet current decay profiles (Figure 5.70(a)) and magnet discharge voltages (Figure 5.70(b)). The increase in capacitance of the heater that is necessary for low charge voltages leads to longer capacitor discharge times. The capacitance must be increased further still due to the low temperature difference between the heater and superconductor at early times. This low temperature difference means that the thermal gradients within the switch decrease with decreasing capacitor charge voltage. The dependance of the heater energy, capacitance, average thermal gradient, and heater discharge time constant ( $\tau_H^{\text{calc}}$ ) on the capacitor charge voltage are shown in Figure 5.71. Switches that operate at 20 K and are formed of MgB<sub>2</sub> can be triggered with either stainless steel or copper heaters of thickness 50  $\mu\text{m}$  if the capacitor charge voltage is 1 kV. The use of copper heaters allows lower charge voltages to be used. However, reducing  $V_{HI}$  necessitates an increase in the capacitance; a  $V_{HI}$  of 100 V would require a capacitance of 5 mF.

The heater capacitor discharge time constant ( $\tau_H^{\text{est}}$ , Table 5.12) of dump-switches that operate at 20 K show that in general copper heaters are required if the capacitor charge voltage is 1 kV. Short switches, such as those formed of MgB<sub>2</sub> in a 70Cu-30Ni matrix, can be triggered with stainless steel heaters as they have fast capacitor discharge times



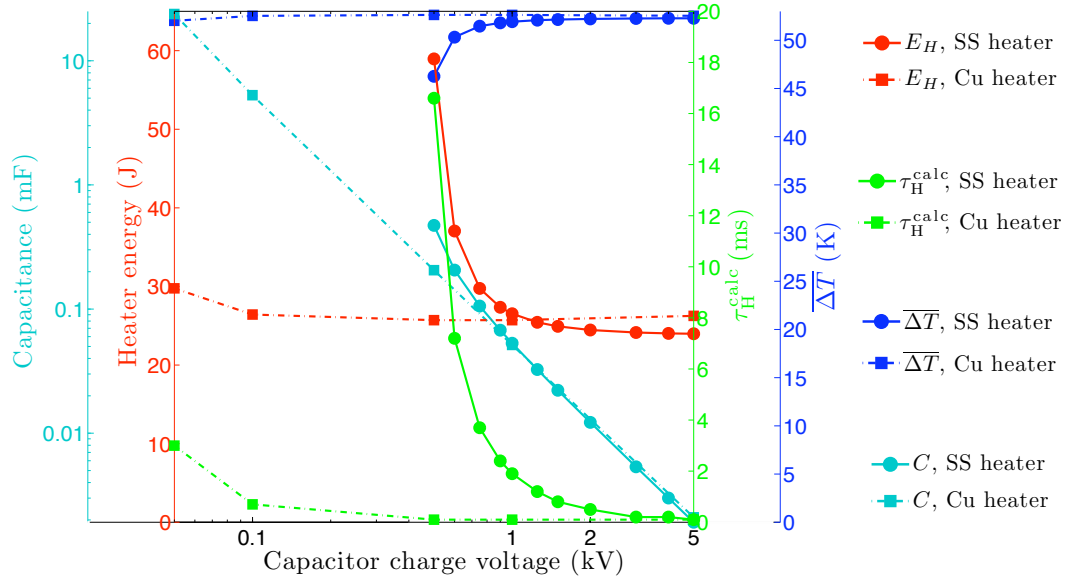


FIGURE 5.71: Required heater energy and capacitance, and the resulting heater discharge time and average thermal gradients for  $\text{MgB}_2$  based dump-switches that have  $50 \mu\text{m}$  thick heaters formed of either stainless steel or copper as a function of  $V_{HI}$ .

due to the low required energy and thus capacitance and also a low, for stainless steel, heater resistance. A comparison between the effect of capacitor charge voltage on  $\text{MgB}_2$  in 70Cu-30Ni matrix with a stainless steel heater and a copper heater is shown in Figure 5.71. Stainless steel heaters are less well suited to  $\text{MgB}_2$  with a copper stabilized and YBCO with stainless steel cladding as high capacitor charge voltage ( $\gg 1 \text{ kV}$ ) would be required in order to reduce the capacitor discharge time constant to an acceptable level. Switches formed of these materials are best used with copper heaters. The effect of capacitor charge voltage on such switches are shown in Figure 5.72. The final temperature does not significantly increase with increasing heater energy as the energy deposited in the switch is mainly from the 5.5 kJ magnet circuit. Switches that have a low final temperature have more potential to be used for higher energy magnet circuits.

### 5.3.11.3 Effect of Heater Thickness on Heater Dynamics

In the previous section the discharge time constant of the heater was reduced by increasing the capacitor charge voltage. This allowed the required energy to be provided with a lower capacitance; reducing the capacitance reduces the discharge time. It is also possible to reduce the capacitor discharge time by reducing the resistance of the heater. Reducing the resistivity by decreasing the resistivity was discussed in the previous section where stainless steel and copper heaters were compared. Increasing the thickness of the heater will also reduce its resistance and may reduce the time taken to the capacitor discharge. Increasing the thickness also increases the thermal mass of the heater and may result in more heater energy being required to trigger the switch. For the same  $V_{HI}$  a greater capacitance will be



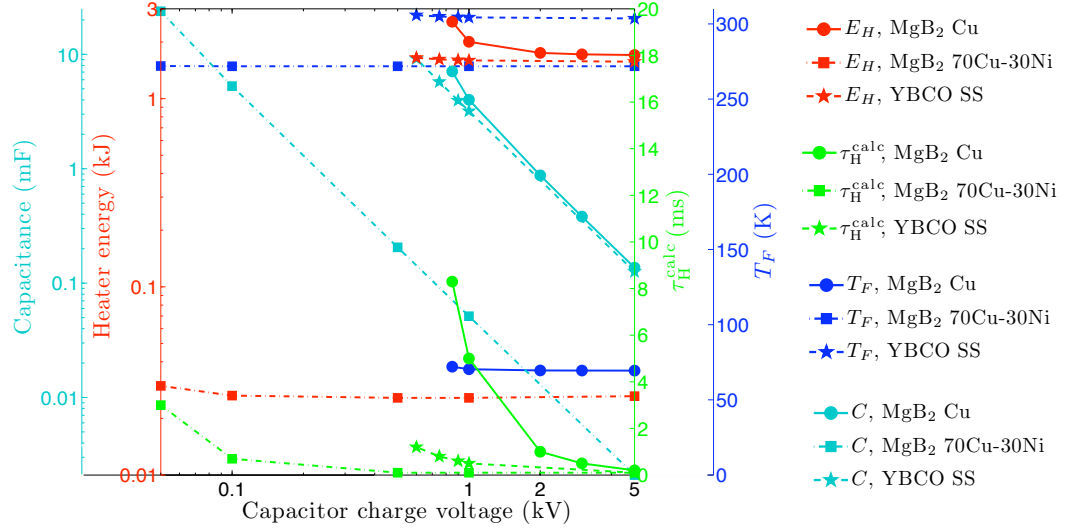


FIGURE 5.72: Effect of the heater capacitor charge voltage on the required heater energy and capacitance, and the resulting heater discharge time and final temperature for dump-switches that operate at 20 K and have 50  $\mu\text{m}$  thick heaters formed of copper (RRR 100).

needed and so the discharge time of the capacitor may increase. The lower thermal mass of a thinner heater switch may also result in higher final temperatures, which may lead to an increase in the heater resistance. The reduction in thermal mass may also result in higher final temperatures and lower thermal gradients. The required length of switch that meets the magnet discharge requirements and results in the minimum heater energy must be recalculated for switches that have different heater thicknesses. The required length and heater energy of  $\text{MgB}_2$  based switches that operate at 20 K are shown in Table 5.13. The  $\text{MgB}_2$  is in a 70Cu-30Ni matrix and one tape is required to carry the 600 A magnet current.

$\delta_H$ ( $\mu\text{m}$ )	$L_{tot}$ (m)	$E_H$ (J)
100	4.8	45.3
50	4.7	26.5
10	4.3	12.6
5	4.2	13.6

TABLE 5.13: Parameters of  $\text{MgB}_2$  in 70Cu-30Ni matrix based dump-switches that operate at 20 K and have different thickness heaters ( $\delta_H$ ) formed of stainless steel. One tape is needed to carry the magnet current and the lengths are set to meet the discharge requirements for the minimum heater energy.

The thermal profiles of dump-switches having stainless steel heaters of thicknesses 5  $\mu\text{m}$ , 10  $\mu\text{m}$ , 50  $\mu\text{m}$ , and 100  $\mu\text{m}$  are shown in Figure 5.73. The switches with thicker heaters have lower final temperatures as they have higher heat capacities due to the increase in heater area and the increase in length. The reduction in the final temperature is non-linear as the heater energy must also be increased with increasing heater thickness. The average thermal gradients are lower in switches that have thinner heaters as the lower thermal

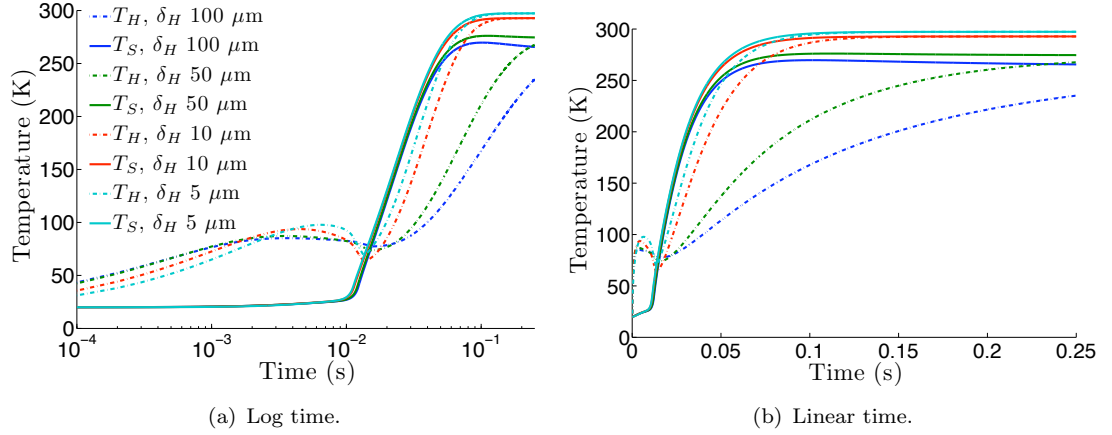


FIGURE 5.73: Thermal profiles of  $\text{MgB}_2$  based dump-switches that have different stainless steel heater thicknesses ( $\delta_H$ ) that have a capacitor charge voltage of 1 kV. A log time scale (a) is used to show the differences at early times and a linear time scale (b) to show differences at later times. The legend is the same for both figures.

mass of the heater means that its temperature follows that of the superconductor more closely.

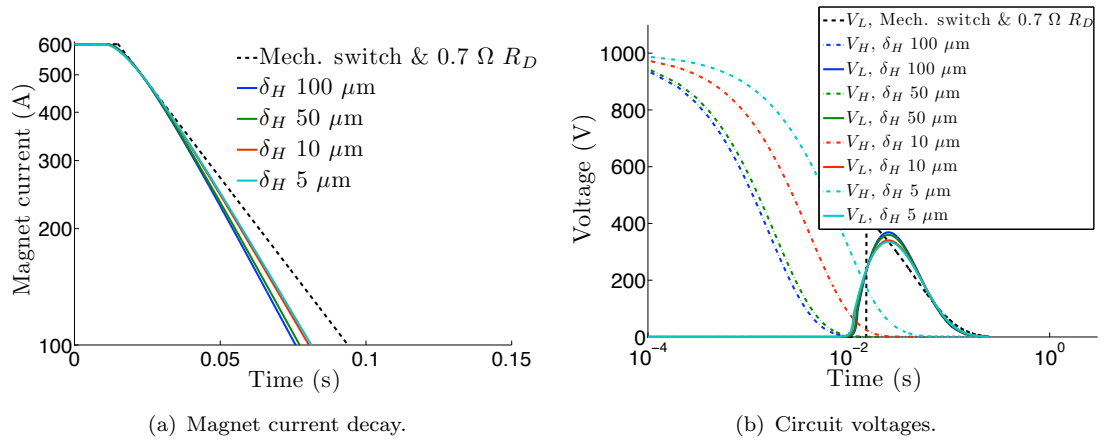


FIGURE 5.74: Effect of using different thicknesses stainless steel heaters in  $\text{MgB}_2$  based dump-switches on the current decay (a) and on the circuit voltages (b).

The magnet current decay curves (Figure 5.74(a)) and therefore the energy dissipation are similar as the length of the switch is set to meet the magnet discharge requirements. The switch with the thinnest heater has the lowest peak voltage (Figure 5.74(b)) as it has the lowest dump resistance. This lower dump resistance also means that it has a slightly slower magnet current decay than the switches with thicker heaters.

Reducing the heater thickness reduces the average thermal gradients within the switch but also results in a higher final temperature (Figure 5.75). This is due to the reduction in thermal mass of the heater which means that less energy is required to heat it to the temperature required to trigger the switch. As the heater also acts as a heat sink the reduction in thermal mass means that it can not limit the overall temperature rise of the

switch and so there is a higher final temperature. Reducing the heater thickness causes an increase in the resistance of the heater and so the discharge time of the heater increases with decreasing heater thickness. For the copper heater switches, which have a discharge time  $\leq 0.1$  ms, decreasing the heater thickness results in a corresponding reduction in the heater energy as the thermal mass of the heater is less. However, for switches with stainless steel heaters there is a minimum in the heater energy because as the time constant of the capacitor discharge is increased the heater energy must also increase to compensate for the reduced initial heat conduction through the insulation. For a switch formed of  $\text{MgB}_2$  in a 70Cu-30Ni matrix, the heater thickness that results in the minimum heater energy is  $8 \mu\text{m}$ , when it is formed of stainless steel and the capacitor charge voltage is 1 kV. The final temperature of this switch is  $\approx 300$  K.

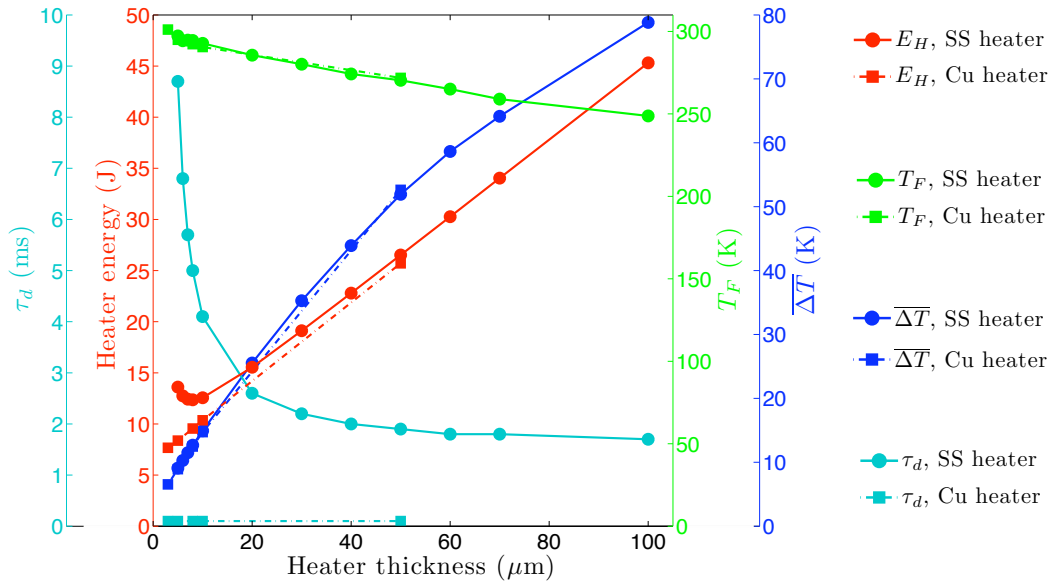


FIGURE 5.75: Required heater energy and resulting capacitor discharge time ( $\tau_H^{\text{calc}}$ ), average thermal gradients and final temperatures for  $\text{MgB}_2$  in 70Cu-30Ni based dump-switches that have different thickness heaters formed of either copper (RRR 100) or stainless steel. The capacitor charge voltage is 1 kV.

Figure 5.75 showed the results for copper heaters where the capacitor charge voltage was 1 kV. In the previous section (Figure 5.72) it was shown that with copper heaters,  $\text{MgB}_2$  in 70Cu-30Ni switches are short enough and have low enough energy requirements for them to have fast capacitor discharges when the charge voltage is only 100 V. Figure 5.76 shows the effect of heater thickness when either a 100 V or a 1 kV capacitor charge voltage is used. The final temperatures and average thermal gradients do not change with the change in charge voltage as the energy input into the switch is dominated by the 5.5 kJ of energy from the magnet circuit. When a 1 kV charge voltage is used the capacitance is low and so the discharge time of the capacitor is less than 0.1 ms even when the thin and thus higher resistance heaters are used. This allows a reduction in heater energy with reducing heater thickness due to the reduction in thermal mass. When a 100 V charge voltage is used the heater has fast discharge times when the heater thickness is greater than  $10 \mu\text{m}$ . Below

this the heater resistance and higher capacitance required to provide the energy with a  $V_{HI}$  of 100 V results in slow capacitor discharge times. These slower discharging heater systems require more energy to compensate for the reduced initial thermal gradients.

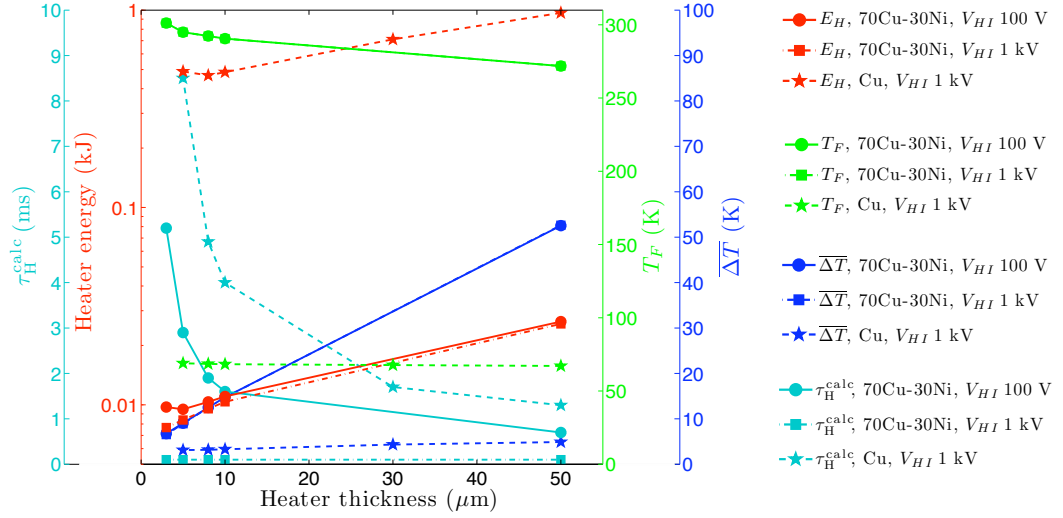


FIGURE 5.76: Required heater energy and resulting capacitor discharge time ( $\tau_H^{\text{calc}}$ ), average thermal gradients and final temperatures for MgB<sub>2</sub> based dump-switches that have different thickness copper heaters (RRR 100).

For the switch powered that has a capacitor charge voltage of 100 V there is a minimum in the required heater energy when a 5  $\mu\text{m}$  copper heater is used. With this thickness of heater the final temperature of the switch is  $\approx 300$  K and the average thermal gradient is less than 10 K making this a suitable design of switch to use for the 5.5 kJ MCD magnet circuits. However, this switch only has limited scope for use with higher energy circuits as even with a 50  $\mu\text{m}$  heater the final temperature is  $\approx 275$  K and so not much more magnet energy can be dissipated in the switch. Longer switches have a greater thermal mass and may have a lower final temperature. Copper stabilised MgB<sub>2</sub> has a lower resistivity and so a longer length is needed to meet the magnet discharge requirements. Even though more energy is required to trigger this switch the final temperature is reduced by  $\approx 200$  K (Figure 5.76). The heater discharge time increases due to the longer length of switch. A 1 kV capacitor charge is needed so that the higher energy requirements can be met without further increasing the discharge time with a high capacitance. The heater energy can be reduced to a minimum without significantly increasing the final temperature by reducing the heater thickness to 8  $\mu\text{m}$ . This copper stabilised switch is suitable for use in the MCD magnet circuits and has a lower final temperature but a higher energy requirement than the MgB<sub>2</sub> switch with a 70Cu-30Ni matrix. The copper stabilised switch also greater potential to be scaled to higher energy circuits; scaling to higher magnet energy circuits is discussed in Section 5.4.

## 5.4 Application of Superconducting Switches to Higher Energy Circuits

The optimisation of a switch dump was described in Section 5.3 using the LHC MCD circuits as an example magnet circuit. This circuit had a transport current of 600 A and a stored energy of 5.5 kJ that was dissipated in a  $0.7 \Omega$  dump resistor. Due to the resistance and energy requirements of this circuit dump-switches were shown to be more suited than bypass-switches that were not practical in this situation (Section 5.2.4). The 5.5 kJ circuit allowed the investigation and optimisation of different parameters that affected the switching characteristics and performance. However, there are many magnet circuits that have higher stored energies and require energy extraction with mechanical switches and dump resistors. Superconducting switches may find applications in these circuits. This section describes the scaling of superconducting switches to higher energy circuits that have the same current and dump resistance as the MCD circuit, for example other LHC corrector magnet circuits such as the 22.2 kJ MCS circuit or the 77.8 kJ MS, and also the application of superconducting switches to higher current but lower dump resistance circuits such as the 1.3 GJ LHC main dipole circuits.

### 5.4.1 Higher Energy Circuits with the Same Current and Dump Resistance

Dump-switches can be formed of a variety of different materials to meet the discharge requirements of a magnet circuit having a specified current and dump resistance. The magnet energy that can be dissipated by the switch is a function of the change in enthalpy of the switch between the operating temperature and the upper limit of 300 K. The  $\text{MgB}_2$  based switches can accept more magnet energy per volume than the YBCO switches as they have a lower operating temperature, 20 K compared to 50 K (Section 5.3.5). The  $\text{MgB}_2$  based switches can all accept  $\approx 0.67 \text{ J/mm}^3$  as the matrix metals have the around the same volumetric heat capacity. The copper stabilised  $\text{MgB}_2$  switch is 3.6 mm wide, the superconductor is 0.6 mm thick, and the heater is  $8 \mu\text{m}$  thick. The cupronickel matrix  $\text{MgB}_2$  switches are 1.4 mm wide, the superconductor is 1.4 mm thick, and the heater is  $5 \mu\text{m}$  thick. Due to differences in geometry, the different switches can accept different amounts of energy per length ( $\phi$ ). Due to its larger area the copper stabilised  $\text{MgB}_2$  switch can accept 1.68 kJ/m whereas the cupronickel matrix switches can accept 1.3 kJ/m. Due to their higher operating temperature of 50 K, the YBCO based switches can accept less energy per length;  $\phi$  is 0.45 kJ/m for the stainless steel clad switch and  $\phi$  is 0.6 kJ/m for the copper clad switch. The copper stabilised YBCO switch is 4 mm wide, the superconductor is  $78 \mu\text{m}$  thick, and the heater is  $21 \mu\text{m}$  thick. The stainless steel clad YBCO switch is 4.3 mm wide, the superconductor is  $150 \mu\text{m}$  thick, and the heater is  $5 \mu\text{m}$  thick. The

copper stabilised MgB<sub>2</sub> based switch can accept the highest amount of energy per length and has a long length making it suited for use in higher energy circuits.

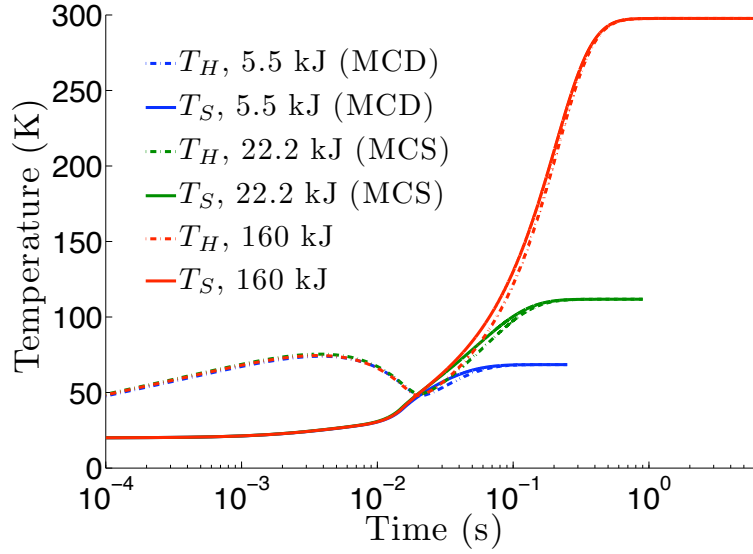


FIGURE 5.77: Thermal profiles of MgB<sub>2</sub> with copper stabilization based dump switches when they are used in magnet circuits that have different stored energies but the same current and dump resistance requirements. For a constant  $R_D$  of 0.7  $\Omega$ , the magnet discharge times are 44 ms (5.5 kJ), 0.18 s (22.2 kJ), and 1.3 s (160 kJ)

A reference design formed of copper stabilized MgB<sub>2</sub> was optimized using the procedure described in Section 5.3 for the 5.5 kJ MCD magnet circuits as an example circuit. In this situation the switch had a final temperature of 68 K and so the switch has the potential to be scaled to higher energy circuits. The reference design can be directly used if the required dump resistance and transport current remains unchanged. This is because the same total length of conductor is required to develop the required dump resistance. Switches for higher energy circuits may require a slight reduction in length due to the increase in matrix resistivity with the higher final temperatures. As the same length is used then the same heater energy will also be required. This will result in similar thermal gradients. The enthalpy change of the reference design from 20 K to 300 K ( $H_{20\text{ K}}^{300\text{ K}}$ ) is such that the switch can accept an energy input of 1.68 kJ/m. As the heater energy remains unchanged the magnet circuit energy that will result in the switch having a final temperature of 300 K is  $E_M^{300\text{ K}}$ .

$$\begin{aligned}
 E_M^{300\text{ K}} &= L_{tot} H_{20\text{ K}}^{300\text{ K}} - E_H \\
 &= 95 \times 1.68 - 0.45 \\
 &= 160 \text{ kJ}.
 \end{aligned} \tag{5.6}$$

To confirm this scaling the switching characteristics of a higher energy (22.2 kJ) LHC circuit and a 160 kJ magnet are described below.

The copper stabilised  $\text{MgB}_2$  dump-switches that were described in Section 5.3.11.3 had low final temperatures and thermal gradients but required more heater energy than the cupronickel matrix  $\text{MgB}_2$  switches described in Section 5.3.9. For scaling to higher magnet energy circuits the copper stabilised  $\text{MgB}_2$  has more potential as its lower resistivity means that a longer length is required and so the thermal mass is increased. The increase in heater energy is proportionally less than the increase in the magnet energy. These switches could be triggered with a capacitor charged to 1 kV if an 8  $\mu\text{m}$  copper (RRR 100) heater was used.

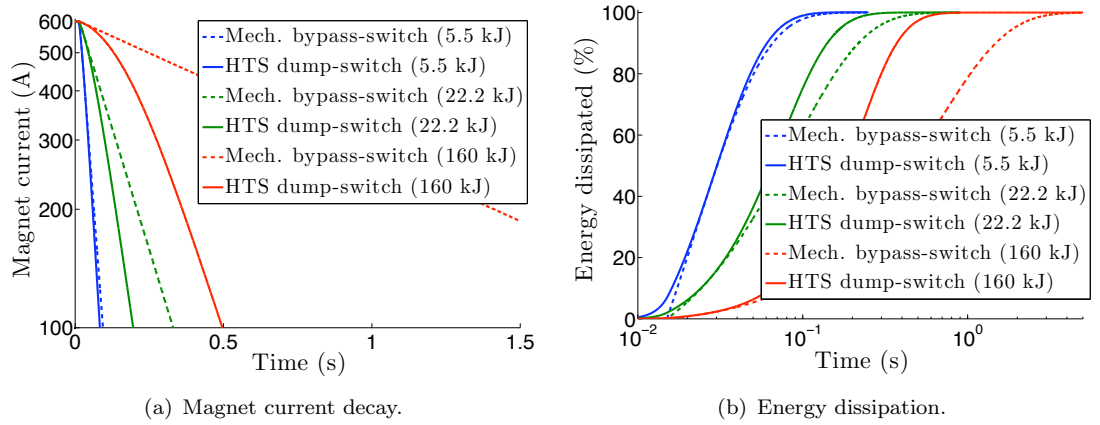


FIGURE 5.78: Current decay profiles (a) and energy dissipation profiles (b) of  $\text{MgB}_2$  with copper stabilization based dump switches when they are used in magnet circuits that have different stored energies but the same current and dump resistance requirement.

The thermal profiles of switches for use in magnet circuits that have stored energies of 5.5 kJ (similar to the MCD magnet circuits), 22.2 kJ (similar to the MCS magnet circuits), and 160 kJ (greater energy than the largest LHC 600 A circuit) are shown in Figure 5.77. The initial thermal profiles of these switches are almost identical as they all have similar lengths and input heater energies. Once the magnet current (Figure 5.78(a)) starts to decay the temperature of the higher energy circuits rises faster to a higher final temperature. The higher final temperature of the switch means that it has a higher dump resistance (Figure 5.79(b)) that causes the magnet decay to be much faster than that of the mechanical switch and dump resistor. The resulting energy dissipation (Figure 5.78(b)) is also faster.

The maximum discharge voltage (Figure 5.79(a)) obtained with the mechanical switch is the same irrespective of magnet energy as there is a constant  $0.7 \Omega$  dump resistor. For this constant resistance case the discharge time of the magnet ( $\frac{L_m}{R_D}$ ) is 44 ms for the 5.5 kJ circuit, 0.18 s for the 22.2 kJ, and 1.3 s for the 160 kJ circuit. The non-linear dump resistance caused by the temperature rise of the dump-switches means that the magnet discharge times do not scale in this way and the maximum discharge voltage depends upon the magnet energy. For low energy circuits the maximum voltage is less than that achieved with the mechanical switch due to the earlier initiation of current decay and the similar



final dump resistances. For higher magnet energy circuits the final temperature and hence dump resistance is higher and so the  $\frac{dI}{dt}$  is higher than for the mechanical switch case, resulting in a higher maximum voltage.

The heater voltage decays for all of the switches are similar as the heater energy and resistance is about the same in each case. The discharge time is sufficiently fast due to the use of low resistivity heaters and a 1 kV capacitor charge voltage. As the length's and temperatures (during discharge) are the same the heater resistances are also the same.

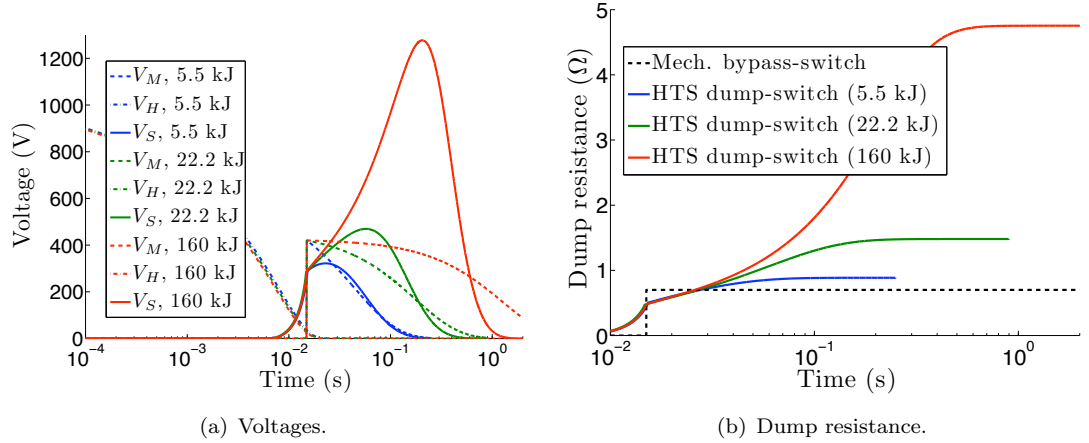


FIGURE 5.79: Voltage traces (a) and dump resistance evolutions (b) of MgB<sub>2</sub> with copper stabilization based dump switches when they are used in magnet circuits that have different stored energies but the same current and dump resistance requirement.  $V_M$  is the voltage obtained with the mechanical switch and dump resistor,  $V_S$  is the voltage obtained with the HTS switch, and  $V_H$  is the heater voltage.

As the magnet energy is increased the final temperature of the switch increases (Figure 5.80) due to more magnet energy being deposited in the switch. The increase in temperature necessitates a slight reduction in the switch length due to the increase in resistivity with temperature. This shorter length results in a correspondingly small decrease in the heater energy required to trigger the switch. The maximum magnet discharge voltage increases as the inductance of the magnet increases with energy.

#### 5.4.2 Higher Energy Circuits with a Higher Current and Lower Dump Resistance

Switches that require different dump resistances or have higher magnet currents necessitating the use of a greater area of superconductor will require a different length to achieve the correct dump-resistance. In these cases the switch would need to be re-optimised. The LHC main dipole circuits have a magnet current of 13 kA and an inductance of 15.4 H that results in a large stored energy (1.3 GJ). These circuits have a lower dump resistance (150 m $\Omega$ ) that gives a lower  $\frac{dI}{dt}$  in order to reduce the large discharge voltages that would otherwise occur due to the high inductance. The switch for the 600 A circuits can not



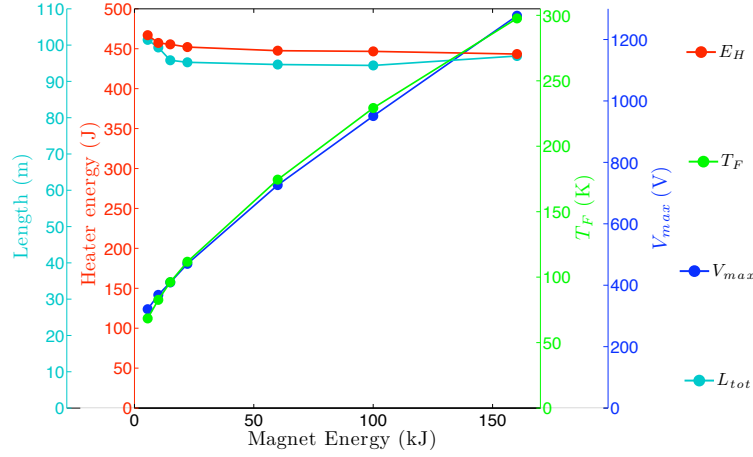


FIGURE 5.80: Required length and heater energy and the resulting final temperature and magnet discharge voltage when using MgB<sub>2</sub> with copper stabilization based dump-switches in higher energy magnet circuits.

be directly scaled to this circuit as the required length is significantly different due to the lower dump resistance and greater number of tapes in parallel.

The energy that causes the switch to rise to 300 K ( $E_{EST}^{300\text{ K}}$ ) can be estimated from the material properties of the switch if the required dump resistance and magnet current are known.

$$E_{EST}^{300\text{ K}} = \frac{\phi R_D I I_{SF}}{\rho J_{ce}}. \quad (5.7)$$

The amount of energy that the switch can accept per unit length ( $\phi$ ) was described at the start of the previous section and depends upon the operating temperature. The engineering critical current density ( $J_{ce}$ ) is divided by some safety factor ( $I_{SF}$ ) to provide current and temperature margin. Materials with a high RRR will have an error in the estimation as resistivity required by the estimation depends strongly on the temperature at which the dump resistance is developed. Table 5.14 shows the estimated energies that cause MgB<sub>2</sub> based switches to warm to 300 K. Due to its low resistivity the copper stabilised MgB<sub>2</sub> switch has the most potential for scaling to higher energy circuits. For copper stabilised MgB<sub>2</sub> dump-switches for the above 600 A and 0.7  $\Omega$  circuits,  $E_{EST}^{300\text{ K}}$  is  $\approx 200$  kJ if the resistivity is evaluated just above  $T_c$ . This is an overestimate compared to the calculated 170 kJ of the reference switch; for this energy the estimation requires the dump resistance to be evaluated at just under 50 K.

An increase in the magnet current requires a corresponding increase in the number of tapes. This increase in conductor area lowers the resistance and so the switch length must be increased from the reference to keep the same dump resistance. If there is a corresponding decrease in the required dump resistance the length will remain largely unchanged. When

Stabiliser	$\phi$ (kJ/m)	$\rho(40\text{ K})$ ( $\mu\Omega\text{ cm}$ )	$E_{\text{EST}}^{300\text{ K}}$ (kJ)
70Cu-30Ni	1.3	6.5	28
90Cu-10Ni	1.3	5.1	35
Cu	1.7	1.2	200

TABLE 5.14: Estimated energies that cause MgB<sub>2</sub> based switches that operate at 20 K to warm to 300 K. The switches have an  $I_c$  of 700 A ( $J_{ce}$  (20 K) of  $\approx 0.35\text{ kA/mm}^2$ ) The magnet current is 600 A and the dump resistance is  $0.7\ \Omega$ .

$$IR_D = \text{constant}; \quad (5.8)$$

- the switch length remains the same as the reference and hence the heater energy also remains the same;
- there will be a higher  $T_F$  if the magnet energy is increased;
- there may be a higher  $V_{max}$  if the inductance or rate of magnet decay are increased ( $V = -L \left( \frac{dI}{dt} \right)$ ).
  - Higher voltages would require the use of thicker insulation. This would increase the thermal mass of the switch and lower  $T_F$ . Thicker insulation that has a slow diffusion time may require the solution with the PDE model (Section 3.6).

If the magnet energy is increased due to an increased inductance then the discharge time of the magnet will also increase as in this case  $R_D$  remains constant (Equation 5.8). The  $V_{max}$  of the mechanical switch system will remain the same as the current and constant dump resistance remain unchanged. The dump-switch has a non-linear resistance and so the  $V_{max}$  will increase as the increased heating will lead to a more resistive switch and a higher rate of magnet decay. If the magnet energy is increased due to an increase in current, the dump resistance will decrease and the time constant will increase. The  $V_{max}$  obtained with both the mechanical switch with a constant dump resistance and with the dump-switch will increase.




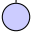
If  $IR_D \neq \text{constant}$ , then the required switch length will change from the reference design. For a new circuit that has a current of

$$I_{\text{NEW}} = pI_{\text{REF}}, \quad (5.9)$$

and a required dump resistance of

$$R_{\text{NEW}} = qR_{\text{REF}}, \quad (5.10)$$

then the thermal mass of the new design will be  $\Delta H_{\text{NEW}}$  (Equation 5.11).

- Increase in thermal mass due to increase in length caused by more tapes being required to carry an increase magnet current. 
  - New thermal mass. 
- $$\Delta H_{\text{NEW}} = \Delta H_{\text{REF}} (p) (pq). \quad (5.11)$$
- Thermal mass  of the reference design.
  - Increase in thermal mass due  to an increase in length to achieve a higher dump resistance.

For the same final temperature the energy that can be dumped in the new switch is

$$E_{\text{NEW}} = E_{\text{REF}} (p^2 q). \quad (5.12)$$

The reference design was shown for a circuit that had an energy of 5.5 kJ ( $E_{\text{REF}}^{5.5 \text{ kJ}}$ ); this resulted in a final temperature of 68 K. For a final temperature of 300 K the energy ( $E_{\text{REF}}^{300 \text{ K}}$ ) that can be dissipated in the reference design is 160 kJ, about 1.7 kJ/m. If the new switch is also to have a final temperature of 300 K then the allowable magnet energy is

$$E_{\text{NEW}}^{300 \text{ K}} = E_{\text{REF}}^{300 \text{ K}} (p^2 q). \quad (5.13)$$

If the earlier copper stabilized  $\text{MgB}_2$  dump switch for a 600 A circuit that has an  $R_D$  of  $0.7 \Omega$  and  $E_M$  of 5.5 kJ is scaled to a 13 kA circuit that has an  $R_D$  of  $150 \text{ m}\Omega$ , then the maximum magnet energy that can be dissipated is

$$\begin{aligned} E_{\text{NEW}}^{300 \text{ K}} &= 160 \text{ kJ} \times \left( \frac{13000}{600} \right)^2 \times \left( \frac{150}{700} \right) \\ &= 16 \text{ MJ}, \end{aligned} \quad (5.14)$$

so about 80 switches would be required to dissipate the 1.3 GJ of stored energy in the main dipole circuits. The length of these switches would be required to be increased from the reference, with each switch requiring a length of  $L_{\text{REF}} p^2 q$ . About 35 km of conductor would be required in total.

For magnets such as the LHC main quadrupoles that require slow discharges with a dump resistances of  $7.7 \text{ m}\Omega$ , the energy that can be dumped in the switch is

$$\begin{aligned} E_{\text{NEW}}^{300 \text{ K}} &= 160 \text{ kJ} \times \left( \frac{13000}{600} \right)^2 \times \left( \frac{7.7}{700} \right) \\ &= 0.83 \text{ MJ}. \end{aligned} \quad (5.15)$$

The main quadrupole circuits have a stored energy of 24 MJ and so about 30 switches would be required to dissipate the energy.

**Bypass-switches** may find application in high energy circuits that require low dump resistances as shorter lengths of conductor may be required to develop the required resistance than the length of conductor required in a dump-switch to avoid overheating. For 13 kA bypass-switches,  $\text{MgB}_2$  in a 70Cu-30Ni matrix operating at 20 K is a potential combination as it has a higher critical current than YBCO tape so less area is required to carry the magnet current and it has a higher resistivity than copper stabilised  $\text{MgB}_2$  so less length is needed to develop the required resistance. To completely bypass the switch would require the switch resistance to be much greater than the parallel dump resistor; this would require long lengths of tape. However, some energy can be dissipated in the switch itself with the limiting factor being the maximum temperature in the switch. The amount of energy dissipation is limited by the maximum allowable temperature is 300 K, the same as for the dump switches. For a required dump resistance of  $R_D$  and a fraction ( $f$ ) of current flowing in the switch, the required switch resistance is given by

$$R_S = \frac{R_D}{f}. \quad (5.16)$$

For operation at 20 K, 20 tapes of  $\text{MgB}_2$  are required to be used in parallel giving a switch  $I_c$  of 1.39 kA. The length of switch that results in a final temperature  $T_F$  can be estimated by

$$L_{\text{est}} = \sqrt[3]{\frac{L_m I^2 R_D^2 \delta_S^2 W_S^2 N^2}{\rho(T) 2(\Delta H(T_{op}, T_F) - E_H)}}. \quad (5.17)$$

$\Delta H$  is the enthalpy change of the switch from the operating temperature to the final temperature and is

$$\begin{aligned} \Delta H = & \gamma_S \delta_S W_S \int_{T_{op}}^{T_F} C_S dT \\ & + \gamma_H \delta_H W_H \int_{T_{op}}^{T_F} C_H dT \\ & + \gamma_I \delta_I W_I \int_{T_{op}}^{T_F} C_I dT. \end{aligned} \quad (5.18)$$

Due to the non-linear resistivity of the superconductor the dump resistance is not constant and so the required length is estimated at a specified temperature. The heater energy  $E_H$  only makes a noticeable contribution to the final temperature for long lengths where most of the current bypasses the switch. For short switches the self heating of the switch is much greater than the heating due to the heater. The final temperature as a function of length with this estimation is shown in Figure 5.81. Modelled results that take into account the non-linear resistivity are also shown.

The switching characteristics of such a bypass-switch are shown in Figure 5.82. If the

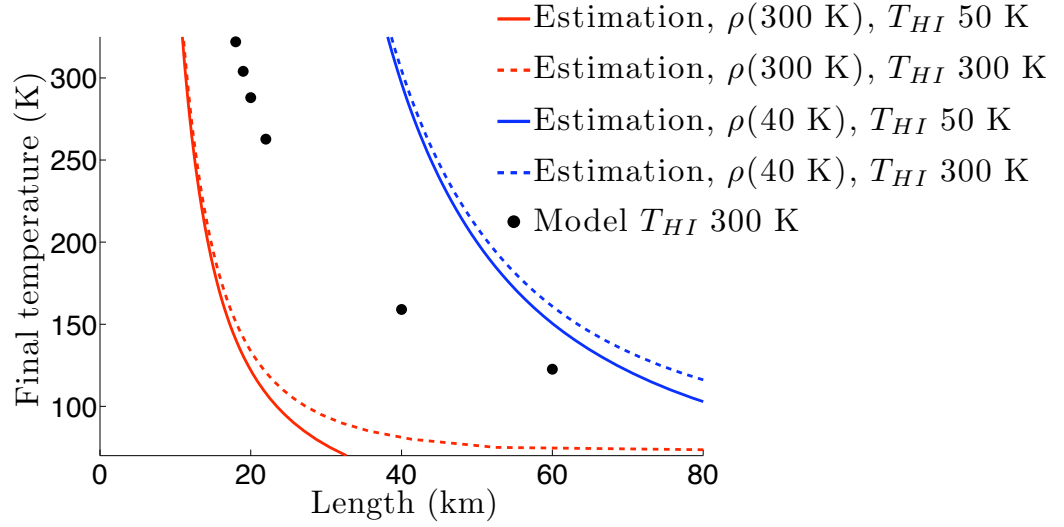


FIGURE 5.81: Final temperature of the bypass-switch as a function of length. The estimations have a constant dump resistance of  $0.15 \Omega$ .

resistance is developed just above  $T_c$  then  $\approx 19$  km of superconductor is required. Increasing the current margin would require an increase in the number of tapes and therefore the length. Reducing the self heating of the switch due to the portion of current that is not shunted into the dump also requires a longer length switch. For these long switches the heater would have to be segmented in order to reduce the discharge time constant to the required levels. Each segment of the heater would have a shorter length and thus a lower heater resistance. Superconducting bypass-switches, that also dissipate some of the magnet energy, may find applications in high energy circuits that require a low dump resistance.

## 5.5 Summary of Design Parameters and Reference Designs of HTS Switches

### 5.5.1 Summary of Design Parameters for Superconducting Switches

The optimization of HTS switches was described in Section 5.3 using the MCD magnet circuits as an example. The scaling of these switches to higher energy circuits that had the same current and dump resistance requirements was described in Section 5.4.1. The applicability of these switches to circuits that have different currents and dump resistances was described in Section 5.4.2. A summary of the design parameters is shown below and a description of the reference designs is in the following section (Section 5.5.2).

**The switch length** is not a free parameter as it is set so that the resistance of the switch allows it to meet magnet discharge requirements. The switch must develop a high enough

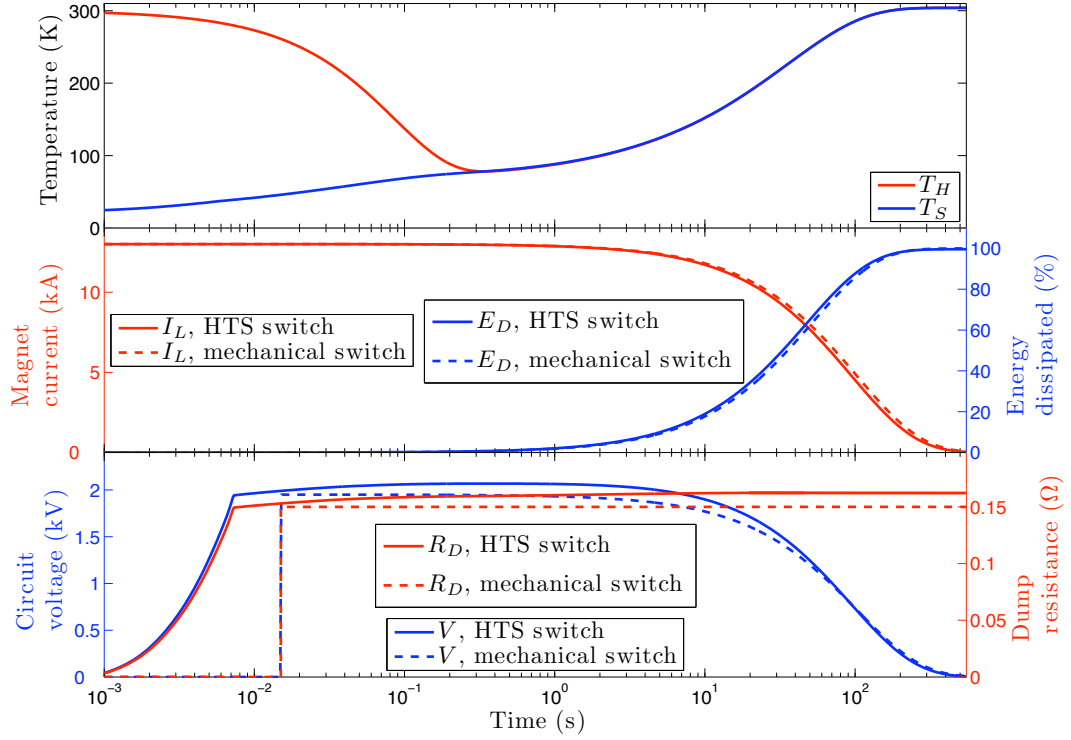


FIGURE 5.82: Switching characteristics of a 19 km long  $\text{MgB}_2$  in a 70Cu-30Ni matrix based bypass-switch for the 13 kA dipole circuits. The top pane shows the thermal histories of the heater ( $T_H$ ) and superconductor ( $T_S$ ). The middle pane shows the magnet current ( $I_L$ ) decay and energy dissipated ( $E_D$ ) for the HTS bypass-switch and for a mechanical switch with a 150 m $\Omega$  dump resistor. The bottom pane shows the circuit voltage ( $V$ ) and the dump resistance ( $R_D$ ) for the two systems. In the LHC there are two energy extraction facilities, one of which is grounded at its midpoint, thereby reducing the discharge voltage to < 500 V.

resistance soon enough after triggering in order that the magnet current is never more than that achieved with a mechanical switch and external dump resistor.

**The operating temperature and choice of superconductor** of the switch is dependent upon the cryogenic system of the magnet circuit. Operation above 40 K requires the use of YBCO based switches, below this  $\text{MgB}_2$  based switches may also be used. BSCCO based superconductors can operate above 40 K but due to the use of predominately silver matrices their resistivity means that they are not suitable for use in switches. Operation at 4.2 K is less suited for switches due to the cryogenic cost and complexity of depositing the magnet energy at this temperature and also the high heater energy that is required by bypass-switches. Operating YBCO switches at 20 K means that there is a large current sharing regime and so high heater energies are needed to drive the switch fully normal. Operating  $\text{MgB}_2$  based dump-switches at 20 K means that the integrated specific heat capacity is high, so if long low resistivity superconductors are used high energy circuits can be protected. Higher heater energies are required to trigger the YBCO based switches that operate at 50 K due to the higher thermal mass at these temperatures. The higher operating temperature reduces  $\overline{E}_H$  so there may be overall cost savings.

**The number of tapes** must be enough to carry the magnet current with appropriate current and temperature margins. Increasing the number of tapes will mean that longer switches are required as the resistance per length of switch decreases. This increase in total length allows higher energy circuits to be protected as  $E_M^{300\text{ K}}$  is also increased. Higher heater triggering energies are required due to the increase in thermal mass and is compounded by the increase in temperature margin.

**The critical current density** of the superconductor determines the minimum number of tapes that can be used. Increases in the critical current density of the tape are useful for dump-switches for low energy magnet circuits as it reduces the required number of tapes and thus the required length of superconductor. Increases are less suitable for dump-switches that are used with high energy magnet circuits as the thermal mass of the switch must be high enough to absorb the magnet energy without over heating. Increases in critical current are useful for high energy circuits that use bypass-switches as the switch is not required to dump all of the magnet energy and so the reduction in the number of tapes leads to a reduction in the required total length of superconductor. The dependence of critical current density on temperature also determines the temperature margin; operating with a low temperature margin allows low heater triggering energies to be used.

**The normal state resistivity** of the tape is a key factor in setting the switch length and therefore the size of magnet circuit that the switch can protect. Dump-switches that utilise superconductor that have high resistivity matrices are suitable for use in low energy circuits as short lengths are required to develop the required dump resistance. The short length means that  $E_M^{300\text{ K}}$  is low. The short length and low heater triggering energy means that the short capacitor discharge times can be achieved with low capacitor charge voltages. Dump-switches that utilise superconductor that have low resistivity matrices are suitable for use in high energy circuits as long lengths are required to develop the required dump resistance. The long length means that there is a large enthalpy change in the switch from  $T_{op}$  to 300 K and so the switch can absorb dissipate higher magnet energies. The higher heater energies that are required to trigger the switch are less significant when high magnet energy circuits are to be protected. However, the long heater length means that high capacitor charge voltages are required in order to achieve fast capacitor discharge times.

**The heater dynamics** are optimised to give fast capacitor discharges for low capacitor charge voltages. For long switches copper heaters are necessary in order to reduce the resistance of the heater to achieve short capacitor discharge times. For short switches the use of copper heaters allows a reduction in the capacitor charge voltage whilst still achieving fast capacitor discharge times. The low resistivity of copper (RRR 100) at 20 K means that thin heaters, or low  $V_{HI}$ , and sometimes both, can be used with  $\text{MgB}_2$  switches at 20 K. Reducing the heater thickness reduces the required heater energy if very high (10 kV) capacitor charge voltages are used. For realistic capacitor charge voltages ( $\leq 1\text{ kV}$ ) the increase in capacitance means more heater energy is required to compensate for

the slower discharge time; this results in a minimum heater energy that varies with the switch length.

**The insulation thickness** must be enough to provide good electrical protection between the heater layer and the superconductor layer. Thin insulation allows fast thermal diffusion times and so low heater energies can be used to trigger the switch. Thick insulation is necessary where there is a high magnet discharge voltage or a high heater charge voltage. The heat capacity of polyimide insulation is high at low temperatures so thicker heaters may contribute to an increase in  $E_M^{300\text{ K}}$  even if the required heater energy is also increased.

### 5.5.2 Reference Designs of HTS Dump-Switches

Super-conductor	Stabiliser	$T_{op}$ (K)	$L_{tot}$ (m)	$\delta_H$ ( $\mu\text{m}$ )	$E_H$ (J)	$V_{HI}$ (kV)	$E_M^{300\text{ K}}$ (kJ)
YBCO	SS clad	50	38	5	1.3e3	0.75	17
YBCO	Cu (25 $\mu\text{m}$ )	50	122	21	9.2e3	1	72
MgB <sub>2</sub>	70Cu-30Ni	20	4.3	5	9.5	0.1	5.7
MgB <sub>2</sub>	90Cu-10Ni	20	11	5	22	0.25	14.5
MgB <sub>2</sub>	Cu	20	100	8	467	1	167

TABLE 5.15: Reference designs of switches that transport 600 A and develop a dump resistance of 0.7  $\Omega$ .

Reference designs of dump-switches formed of different superconductors are shown in Table 5.15. The reference designs are for magnet circuits that have a transport current of 600 A and a dump resistance of 0.7  $\Omega$ . All of the switches meet the magnet discharge requirements and dissipate the magnet energy faster than the mechanical switch setup. The maximum discharge voltage ( $V_{max}$ ) of all the switches is about the same as they are required to develop the same dump resistance. For the MCD magnet circuits this voltage less than that obtained with the mechanical switch by about 100 V. These reference designs can be scaled up to higher energy circuits; the magnet energy that causes the switches to reach a final temperature of 300 K is  $E_M^{300\text{ K}}$ . The application of these switches to circuits that have different transport currents and dump resistances is described in Section 5.4.2. All of the switches have copper (RRR 100) heaters in order to reduce the discharge time of the capacitor to allow fast acting heaters. The heater thickness ( $\delta_H$ ) is optimised in conjunction with the capacitor charge voltage ( $V_{HI}$ ) for each switch design. Generally longer switches require thicker heaters and higher discharge voltages in order to deposit the required energy fast enough. There is 76.2  $\mu\text{m}$  of insulation between the heater and the superconductor and the switches are designed to switch adiabatically. The thermal profiles of the reference switches when used with the 5.5 kJ MCD magnet circuits is shown in Figure 5.83. Description of the individual designs are given below.

**YBCO with stainless steel cladding** is a potential superconductor for switches that operate at 50 K in conjunction with magnet circuits that have an energy levels less than



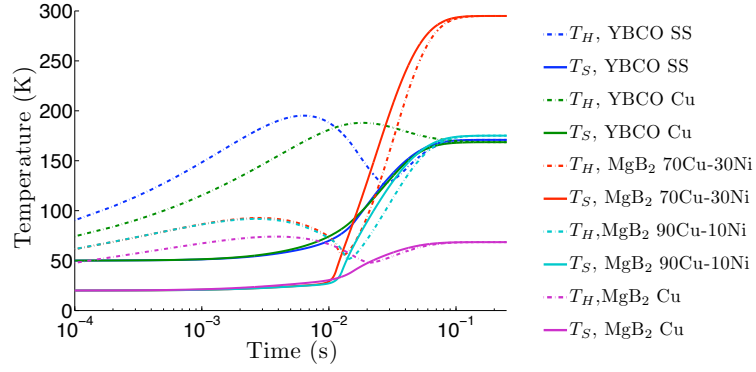


FIGURE 5.83: Temperature evolutions of the reference design dump-switches when used with the 5.5 kJ MCD magnet circuits.

20 kJ. YBCO based switches are necessary for HTS magnet circuits or where cryogenic savings due to the higher temperature energy dissipation are required. At 50 K, three tapes are required to carry the magnet current and so the thermal mass of the switch can be used to absorb more magnet energy. The superconductor is produced by American Superconductor and has an  $I_c$  of 60 A at 77 K giving a switch  $I_c$  of 700 A at 50 K. The switch requires 1.3 kJ of heater energy to be triggered, but due to the low heater resistance due to the short length and large area the discharge time of the heater is low and so a capacitor charge voltage of 750 V can be used. The  $V_{HI}$  could be lowered to 500 V; this would require an increase in heater thickness to 10  $\mu\text{m}$ , the heater energy to 2 kJ, and would require a 16.3 mF capacitor. Operating at 20 K would mean that less tapes are required to carry the magnet current. This may mean that less energy can be absorbed by the switch. Higher heater energies may be needed to trigger to the normal state due to the extended current sharing regime where little magnet energy is dumped.

**YBCO with 25  $\mu\text{m}$  of copper stabilisation** is a potential choice of superconductor for switches that operate at 50 K in conjunction with magnet circuits that have an energy levels up to 70 kJ. The superconductor is produced by SuperPower and has an  $I_c$  of 60 A at 77 K giving a switch  $I_c$  of 700 A at 50 K. The SuperPower tape has a higher critical current density than the American Superconductor tape but it has a smaller area resulting in the same  $I_c$ . Due to the low resistivity matrix long lengths of conductor are required to develop the required discharge resistance. This longer length means that the copper stabilised YBCO switch can be used with higher energy magnet circuits than the more resistive stainless steel clad YBCO switch. The larger thermal mass means that more heater energy is required to trigger the copper stabilised switch. Due to the long length of conductor and high heater energies, the heater has a thickness about four times greater than the YBCO SS switch in order to reduce the heater resistance. A  $V_{HI}$  of 1 kV is needed to provide sufficiently fast capacitor discharge times. The copper clad YBCO switch is more suited to higher energy magnet circuits as it has high  $E_M^{300\text{ K}}$  and the high heater energy is less significant for larger circuits.

**MgB<sub>2</sub> in a 70Cu-30Ni matrix** is well suited for use in switches to protect low energy circuits. The superconductor is produced by Columbus and only one tape is required to give the switch an  $I_c$  of 693 A at 20 K. Its high resistivity means that only a short length is required in order to develop the required dump resistance. The short length and low specific heat at 20 K means that the required triggering energy is also low. The low resistivity of the copper heater at 20 K means that thin heaters and a low capacitor charge voltage (100 V) will give a fast enough heater. The short length means that  $E_M^{300\text{ K}}$  is low and so the switch is only suitable for protecting low energy circuits (<6 kJ). low energy

**MgB<sub>2</sub> in a 90Cu-10Ni matrix** is based on the 70Cu-30Ni matrix MgB<sub>2</sub> produced by Columbus. The less resistive matrix means that a longer switch is required allowing circuits with energies up to 15 kJ to be protected. The critical current remains unchanged at 693 A at 20 K. The length is approximately twice that of the more resistive MgB<sub>2</sub> switch and so the required heater energy is also doubled. The increase in length means that the  $V_{HI}$  must be increased to 250 V to have a sufficiently fast heater capacitor discharge time.

**MgB<sub>2</sub> with copper stabilisation** requires 100 m of conductor in order to develop the required dump resistance. The large enthalpy change of the switch from operation at 20 K to 300 K means that it can be used to protect circuits up to  $\approx 170$  kJ. The increase in  $\int_{T_{op}}^{300\text{ K}} c_p dT$  is the reason why the switch can dissipate  $\approx 2.3$  times the magnet energy of the longer copper stabilized YBCO switch. The longer length and means that more heater energy is required than the resistive MgB<sub>2</sub> switches, but the lower specific heat at 20 K means that less heater energy is required than the YBCO switches that operate at 50 K. The longer length requires an increase in the heater thickness to 8  $\mu\text{m}$  and the higher heater energy an increase in  $V_{HI}$  to 1 kV. The heater is thinner than the long YBCO Cu switch due to the low resistivity of the copper (RRR 100) heater at 20 K.

**The performance metrics** of the reference designs are shown in a star plot Figure 5.84 with the 5.5 kJ MCD magnet circuits as an example circuit. The chosen design will depend upon the cost and availability of the superconductor and upon the available cooling scheme. The switches which utilise superconductors that have low resistivity matrices and thus require long lengths to develop the required dump resistance are more suited to higher energy circuits as they have a higher  $E_M^{300\text{ K}}$ . Due to their higher thermal masses these switches require higher heater energies in order to be triggered. For low energy circuits, switches that utilise superconductors that have high resistivity matrices are more suited as they require short lengths to develop the required dump resistance. The correspondingly lower thermal mass means that less heater energy is needed to trigger the switch. Due to the shorter lengths, which give lower heater resistances, and the lower heater energy requirements the charge voltage of the capacitor can be reduced. For switches based on MgB<sub>2</sub> in a 70Cu-30Ni matrix it can be as low as 100 V.

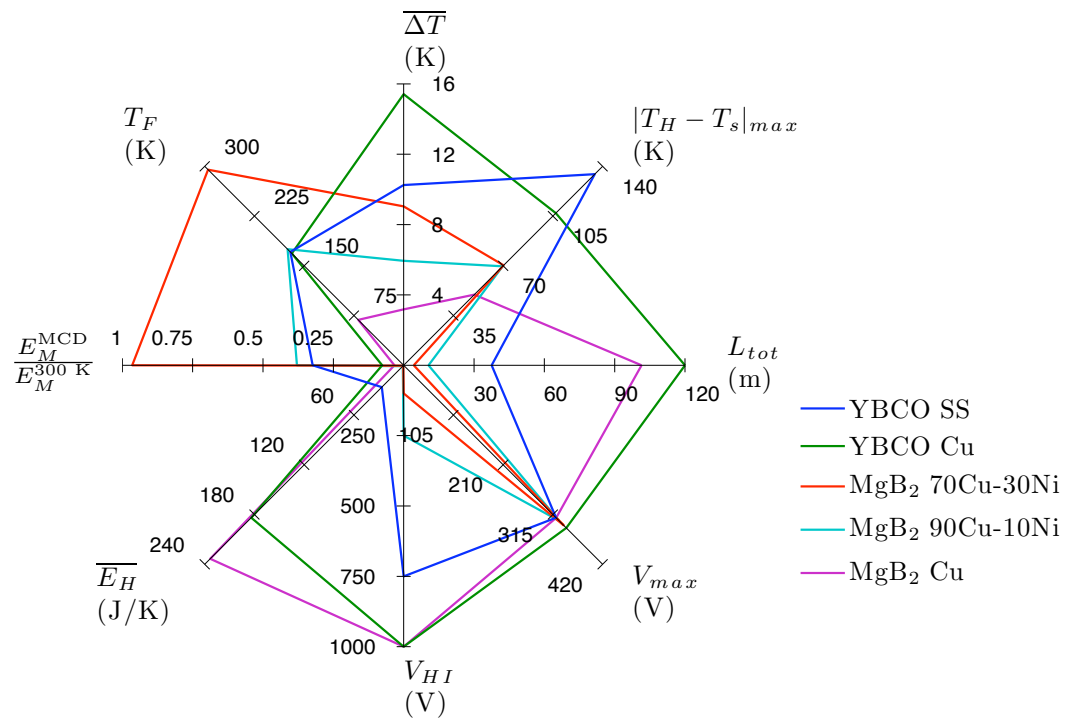


FIGURE 5.84: Star plot of the performance metrics of the reference design dump-switches when used with the 5.5 kJ MCD magnet circuits.

## Chapter 6

## Conclusions

**Superconducting switches**, of either the bypass type or the dump type, may find application in superconducting magnet systems that require energy extraction, for example in certain LHC magnet circuits. Superconducting switches may provide advantages in such circuits as they do not suffer from arcing and erosion that is a problem for mechanical switches. Furthermore, they may allow cryogenic savings or the removal of the dump resistor depending upon the type of energy extraction circuit.

**Superconducting bypass-switches** that are operated in conjunction with a parallel dump resistor can be used as a replacement for conventional mechanical switches. The switch must develop a resistance high enough to shunt the magnet current into the external resistor. Bypass-switches are suited to higher energy circuits as the majority of the energy is dissipated in the external dump resistor. Together these parallel connected switch and resistor make up the total dump resistance that must allow the required magnet discharge characteristics to be met. Superconducting bypass-switches may provide cryogenic savings in long magnet chains where there are multiple energy extraction facilities as they allow the replacement of certain full rated current leads that always carry the magnet current with lower heat leak leads that only carry the current during energy extraction.

**Superconducting dump-switches** allow all of the magnet energy to be dissipated in the switch itself removing the need for the parallel resistor. Dump-switches require less material and triggering energy than bypass-switches as a lower switch resistance is needed to achieve the required total dump resistance. Dump-switches can have cryogenic savings over bypass-switches as the extra current leads that allow the switch to be bypassed are not required. The energy that can be dissipated in a dump-switch is limited by the enthalpy change from the operating temperature to the the maximum allowable temperature.

**Thermally triggering** superconducting switches can result in switching times that are comparable to conventional mechanical switches ( $\approx 15$  ms). Thermal triggering allows simpler powering schemes than over-current triggered switches, a simpler triggering mechanism than field triggered switches, and does not have the erosion problems of mechanical switches. The heater, which is co-wound with the superconductor and the insulation, can be powered by a capacitor discharge. Such a system is similar to quench heaters that are widely used to protect superconducting magnets. For long switches, fast capacitor discharges can be achieved by using a heater with a low resistivity. After triggering and during the magnet discharge the heater can act as a heat sink limiting the overall temperature rise of the switch.

**Operating at HTS temperatures** allows cryogenic savings over switches that utilise LTS materials that operate at 4.2 K. Utilising HTS materials allows a greater range of operating temperatures to be considered, for example using helium gas at 20 K that is recovered from the magnet boil off. Extracting the magnet energy and depositing the heater energy at higher temperatures will also reduce the load on the overall cryogenic system during switching and energy extraction. For magnet circuits that are based on

high temperature superconductors the switch must also be formed of HTS material. Due to the approximately  $T^3$  dependence of specific heat capacity, switches that operate at higher temperatures have slower heat diffusion times and require higher triggering energies than those operating at low temperature. YBCO based dump-switches and YBCO based bypass-switches were tested in liquid nitrogen to show that the required switching time could be achieved at these high temperatures.

**A variety of superconducting materials** are suitable for use in superconducting switches. Switches based on stainless steel clad YBCO, which operate at HTS temperatures, can be formed into dump-switches for low to medium energy circuits or as bypass-switches for low current circuits. Their suitability to higher current bypass-switches increases with improvements to the critical current of the superconductor. Copper stabilised YBCO switches that operate at HTS temperatures can be formed into dump-switches for medium energy circuits. Magnesium diboride in a cupronickel matrix based switches are suitable for use as low energy dump-switches or as bypass-switches. Increasing the matrix resistivity increases the suitability for use as a bypass-switch. Reducing the matrix resistivity increases the magnet energy that can be dissipated when it is used in a dump-switch. Magnesium diboride with copper stabilisation can be formed into dump-switches that are suitable for use with high energy circuits.

**Reference designs of HTS dump-switches** were optimised for magnet circuits that have a transport current of 600 A and a dump resistance of  $0.7\ \Omega$  that is switched into the circuit with a conventional mechanical switch with an opening time of 15 ms; these circuits are similar to certain LHC magnet circuits. Stainless steel clad YBCO, produced by American Superconductor, can be formed into dump-switches that operates at 50 K. These switches would require 38 m of superconductor and could absorb 17 kJ of magnet energy for a final temperature of 300 K ( $E_M^{300\text{ K}}$ ). YBCO with  $25\ \mu\text{m}$  of copper stabilisation that is produced by SuperPower can be formed into a dump-switch that operates at 50 K with an  $E_M^{300\text{ K}}$  of 72 kJ when 122 m of conductor is used.  $\text{MgB}_2$  produced by Columbus can be formed into dump-switches that operate at 20 K. With a 70Cu-30Ni matrix, the required length is 4.3 m and  $E_M^{300\text{ K}}$  is 5.7 kJ. With a 90Cu-10Ni matrix, the required length is 11 m and  $E_M^{300\text{ K}}$  is 14.5 kJ. For copper stabilised  $\text{MgB}_2$ , the required length is 100 m and  $E_M^{300\text{ K}}$  is 167 kJ. These reference designs can be applied to circuits that have different dump resistances or operating currents.  $E_M^{300\text{ K}}$  increases with the square of the relative increase in transport current and increases linearly with the relative increase in required dump resistance.

**In conclusion,** high temperature superconducting materials can be used in power switches. These switches may find application in energy extraction schemes where the majority of the energy is dissipated in a parallel resistor or in schemes where all of the energy is dissipated in the switch itself. Thermal triggering of these switches can provide switching times comparable to conventional mechanical switches.

# Bibliography

- [1] T. J. Berners-Lee, “Information management: A proposal,” Tech. Rep. CERN -DD-89-001-OC, CERN, March 1989.
- [2] F. Close, *Particle Physics: A Very Short Introduction*. Oxford University Press, 2004.
- [3] O. S. Brüning, P. Collier, P. Lebrun, S. Myers, R. Ostojic, J. Poole, and P. Proudlock, *LHC Design Report*. CERN, 2004.
- [4] K. Dahlerup-Petersen, F. Rodriguez-Mateos, R. Schmidt, and F. Sonneman, “Energy extraction for the LHC superconducting circuits,” LHC Project Report 484, CERN, 2001.
- [5] M. R. Palmer and A. E. Dabiri, “Electromagnetic space launch: A re-evaluation in light of current technology and launch needs and feasibility of near term demonstration,” *Magnetics, IEEE Transactions on*, vol. 25, no. 1, pp. 393–399, 1989.
- [6] K. Dahlerup-Petersen, J. Coelingh, N. Kusnetsov, B. Kazmin, A. Vassilevski, E. Kuper, A. Medvedko, and V. Ovchar, “The CERN/LHC energy extraction switches and their arc detector systems,” in *Power Modulator Symposium, 2004 and 2004 High-Voltage Workshop. Conference Record of the Twenty-Sixth International*, pp. 580–583, May 2004.
- [7] V. Anushat, K. Dahlerup-Petersen, A. Erokhin, A. Kussul, and A. S. Medvedko, “Modeling and computer simulation of the pulsed powering of mechanical d.c. circuit breakers for the CERN/LHC superconducting magnet energy extraction systems,” Tech. Rep. LHC-Project-Report-442. CERN -LHC-Project-Report-442, CERN, Geneva, Nov 2000.
- [8] K. Dahlerup-Petersen, F. Rodriguez-Mateos, R. Schmidt, and F. Sonneman, “Engineering specification: General parameters for energy extraction of the LHC superconducting circuits,” LHC project Document No LHC-DQ-ES-00001, CERN, 2002.
- [9] K. Dahlerup-Petersen, “Safety aspects related to commissioning of the LHC energy extraction facilities.” CERN Internal Presentation, October 2007.

- [10] D. L. Ameen and P. R. Wiederhold, "Fast-acting superconducting power switches," *Review of Scientific Instruments*, vol. 35, no. 6, pp. 733–737, 1964.
- [11] M. Biltcliffe and P. Hanley, "A method for safely discharging a superconducting magnet in persistent mode when the helium supply becomes exhausted," *Journal of Physics E: Scientific Instruments*, vol. 4, no. 8, pp. 622–624, 1971.
- [12] D. Hagedorn and P. Dullenkopf, "A fast-acting superconducting switch for protection of superconducting coils in the persistent current mode," *Cryogenics*, vol. 14, pp. 429–430, August 1974.
- [13] H. D. Glass, G. W. Foster, P. J. Limon, E. J. Malamud, P. H. Garbinicus, S. G. Peggs, J. B. Strait, M. Syphers, J. C. Tompkins, and A. Zlobin, "Design study for a staged very large hadron collider," Tech. Rep. Fermilab-TM-2149, Fermilab, 2001.
- [14] H. Piekarz and Foster, "Quench detection and protection." Fermilab Unpublished VLHC Note.
- [15] S. Hays, H. Piekarz, H. Pfeffer, and B. Claypool, "Design considerations of a power supply system for fast cycling superconducting accelerator magnets of 2 tesla B-field generated by a conductor of 100 kA currents," *Applied Superconductivity, IEEE Transactions on*, 2007.
- [16] E. Thuries, V. Pham, Y. Laumond, T. Verhaege, A. Fevrier, M. Collet, and M. Bekhaled, "Towards the superconducting fault current limiter," *Power Delivery, IEEE Transactions on*, vol. 6, pp. 801–808, Apr 1991.
- [17] P. Tixador, O. Belmont, E. Floch, J. Barbut, J. Noudem, L. Porcar, D. Bourgault, and R. Tournier, "Current limitation using high  $T_c$  materials," *Applied Superconductivity, IEEE Transactions on*, vol. 7, pp. 1017–1020, Jun 1997.
- [18] P. Tixador, L. Porcar, E. Floch, D. Buzon, D. Isfort, D. Bourgault, X. Chaud, and R. Tournier, "Current limitation with bulk Y-Ba-Cu-O," *Applied Superconductivity, IEEE Transactions on*, vol. 11, pp. 2034–2037, Mar 2001.
- [19] R. F. Tournier, D. Isfort, D. Bourgault, X. Chaud, D. Buzon, E. Floch, L. Porcar, and P. Tixador, "c-axis YBCO domains for current limiting applications," *Physica C: Superconductivity*, vol. 386, pp. 467–463, 2003.
- [20] A. Heinrich, J. Muller, A. Hiebl, K. Numssen, H. Kinder, W. Wechk, A. Muller, and H. Scholderle, "Y-Ba-Cu-O thick films as active high power switches," *Applied Superconductivity, IEEE Transactions on*, vol. 11, pp. 1952–1955, 2001.
- [21] V. Braccini, D. Nardelli, R. Penco, and G. Grasso, "Development of ex-situ processed  $\text{MgB}_2$  wires and their application to magnets," *Physica C: Superconductivity*, vol. 456, pp. 209–217, 2007.



- [22] L. Ye, M. Majoros, A. M. Campbell, T. Coombs, D. Astill, S. Harrison, M. Husband, M. Rindfleisch, and M. Tomsic, "Experimental studies of the quench behaviour of MgB<sub>2</sub> superconducting wires for fault current limiter applications," *Superconductor Science and Technology*, vol. 20, no. 7, pp. 621–628, 2007.
- [23] J. Bock, F. Breuer, H. Walter, S. Elschner, M. Kleimaier, R. Kreutz, and M. Noe, "CURL 10: Development and field-test of a 10 kV/10 MVA resistive current limiter based on bulk MCP-BSCCO 2212," *Applied Superconductivity, IEEE Transactions on*, vol. 15, pp. 1955–1960, 2005.
- [24] X. Yuan, K. Tekletsadik, L. Kovalsky, J. Bock, F. Breuer, and S. Elschner, "Proof-of-concept prototype test results of a superconducting fault current limiter for transmission-level applications," *Applied Superconductivity, IEEE Transactions on*, vol. 15, pp. 1982–1985, June 2005.
- [25] A. P. Malozemoff, S. Fleshler, M. Rupich, C. Thieme, X. Li, W. Zhang, A. Otto, J. Maguire, D. Folts, J. Yuan, H.-P. Kraemer, W. Schmidt, M. Wohlfart, and H.-W. Neumueller, "Progress in high temperature superconductor coated conductors and their applications," *Superconductor Science and Technology*, vol. 21, no. 3, p. 034005 (7pp), 2008.
- [26] H.-P. Kraemer, W. Schmidt, M. Wohlfart, H.-W. Neumueller, A. Otto, D. Verebelyi, U. Schoop, and A. P. Malozemoff, "Test of a 2 MVA medium voltage HTS fault current limiter module made of YBCO coated conductors," *Journal of Physics: Conference Series*, vol. 97, p. 012091 (6pp), 2008.
- [27] K. Nemoto, S. Saito, Y. Sanada, K. Sasaki, S. Miyake, and H. Hashiguchi, "Niobium-tin persistent-current switch for the superconducting magnet of Maglev," *Applied Superconductivity, IEEE Transactions on*, vol. 9, no. 2, pp. 181–184, 1999.
- [28] M. Tomita, M. Murakami, S. Nariki, and K. Sawa, "Mechanical persistent current switch made of resin-impregnated bulk superconductors," *Superconductor Science and Technology*, vol. 15, p. 846, 2000.
- [29] Y. Tsuda, A. Ohara, S. Nakamura, N. Oomyou, T. Numato, and M. Yamamoto, "Development of superconducting mechanical persistent current switch," *Applied Superconductivity, IEEE Transactions on*, vol. 10, pp. 804–807, 2000.
- [30] F. Rodriguez-Mateos and F. Sonnemann, "Quench heater studies for the LHC magnets," *Particle Accelerator Conference, 2001. PAC 2001. Proceedings of the 2001*, vol. 5, pp. 3451–3453 vol.5, 2001.
- [31] H. K. Onnes, "The superconductivity of mercury," *Comm. Phys. Lab. Univ. Leiden*, pp. 122–124, 1911.

- [32] M. M. Masaru Tomita, Ken Nagashima and T. Herai, “Resin-impregnated bulk YBCO current leads for maglev,” *Physica C: Superconductivity*, vol. 357-360, pp. 832–836, 2001.
- [33] M. Wilson, *Superconducting Magnets*. Oxford Science, 1983.
- [34] W. Meissner and R. Ochsenfeld *Naturwissenschaften*, vol. 21, November 1933.
- [35] W. Buckel and R. Kleiner, *Superconductivity*. Wiley-VCH, second ed., 2004.
- [36] J. Demko, I. Sauers, D. James, M. Gouge, D. Lindsay, M. Roden, J. Tolbert, D. Willen, C. Trholt, and C. Nielsen, “Triaxial HTS cable for the AEP Bixby project,” *Applied Superconductivity, IEEE Transactions on*, vol. 17, pp. 2047–2050, June 2007.
- [37] L. Rossi, “The LHC superconducting magnets,” *Particle Accelerator Conference, 2003. PAC 2003. Proceedings of the*, vol. 1, pp. 141–145 Vol.1, 12-16 May 2003.
- [38] Y. Iwasa, “HTS and NMR/MRI magnets: Unique features, opportunities, and challenges,” *Physica C*, vol. 445-448, pp. 1088–1094, 2006.
- [39] M. Al-Mosawi, C. Beduz, and Y. Yang, “Construction of a 100 kVA high temperature superconducting synchronous generator,” *Applied Superconductivity, IEEE Transactions on*, vol. 15, pp. 2182–2185, June 2005.
- [40] M. Ono, S. Koga, and H. Ohtsuki, “Japan’s superconducting Maglev train,” *Instrumentation & Measurement Magazine, IEEE*, vol. 5, no. 1, pp. 9–15, Mar 2002.
- [41] J. Bardeen, L. N. Cooper, and J. R. Schrieffer, “Theory of superconductivity,” *Phys. Rev.*, vol. 108, pp. 1175–1204, Dec 1957.
- [42] J. G. Bednorz and K. A. Müller, “Possible high  $T_c$  superconductivity in the Ba-La-Cu-O systems,” *Zeitschrift für Physik B Condensed Matter*, vol. 64, pp. 189–193, June 1986.
- [43] P. Dai, B. C. Chakoumakos, G. F. Sun, K. W. Wong, Y. Xin, and D. F. Lu, “Synthesis and neutron powder diffraction study of the superconductor  $\text{HgBa}_2\text{Ca}_2\text{Cu}_3\text{O}_8 + \delta$  by Tl substitution,” *Physica C: Superconductivity*, vol. 243, no. 3-4, pp. 201 – 206, 1995.
- [44] American Superconductor. AMSC Corporate Headquarters, 64 Jackson Road, Devens, MA 01434-4020, USA. <http://www.amscom.com>.
- [45] American Superconductor, “2G HTS wire fact sheet,” Tech. Rep. WFS\_344CP\_0807\_A4, American Superconductor, 2007.
- [46] American Superconductor, “344S wire fact sheet,” Tech. Rep. WFS\_344S\_0808\_A4, American Superconductor, 2008.

- [47] W. Zhang, M. Rupich, U. Schoop, D. Verebelyi, C. Thieme, X. Li, T. Kodenkandath, Y. Huang, E. Siegal, D. Buczek, W. Carter, N. Nguyen, J. Schreiber, M. Prasova, J. Lynch, D. Tucker, and S. Fleshler, “Progress in AMSC scale-up of second generation HTS wires,” *Physica C: Superconductivity*, vol. 463-465, pp. 505 – 509, 2007. Proceedings of the 19th International Symposium on Superconductivity (ISS 2006).
- [48] American Superconductor, “Service note SN002,” Service Note SN002-0409, American Superconductor, April 2009.
- [49] L. J. Masur, D. Buczek, E. Harley, T. Kodenkandath, X. Li, J. Lynch, N. Nguyen, M. Rupich, U. Schoop, J. Scudiere, E. Siegal, C. Thieme, D. Verebelyi, W. Zhang, and J. Kellers, “The status of commercial and developmental HTS wires,” *Physica C: Superconductivity*, vol. 392-396, no. Part 2, pp. 989 – 997, 2003. Proceedings of the 15th International Symposium on Superconductivity (ISS 2002): Advances in Superconductivity XV. Part II.
- [50] M. Gouge, J. Demko, R. Duckworth, D. Lindsay, C. Rey, M. Roden, and J. Tolbert, “Testing of an HTS power cable made from YBCO tapes,” *Applied Superconductivity, IEEE Transactions on*, vol. 17, pp. 1708–1711, June 2007.
- [51] J. Lu, E. S. Choi, and H. D. Zhou, “Physical properties of Hastelloy C-276 at cryogenic temperatures,” *Journal of Applied Physics*, vol. 103, no. 6, p. 064908, 2008.
- [52] R. A. Matula, “Electrical resistivity of copper, gold, palladium, and silver,” *Journal of Physical and Chemical Reference Data*, vol. 8, no. 4, pp. 1147–1298, 1979.
- [53] Cryogenics Technologies Group, “Material properties: Online database,” tech. rep., National Institute of Standards and Technology, 2009.
- [54] L. Rossi and M. Sorbi, “MATPRO: a computer library of material property at cryogenic temperatures,” Tech. Rep. CARE-NOTE-2005-018-HHH, CARE, 2005.
- [55] S. A. March, A. Ballarino, C. Beduz, K. H. Meß, and Y. Yang, “Towards the design of power switches utilizing HTS material,” *Journal of Physics: Conference Series*, vol. 97, p. 012002 (6pp), 2008.
- [56] SuperPower. SuperPower Inc., 450 Duane Avenue, Schenectady, NY 12304, USA. <http://www.superpower-inc.com>.
- [57] SuperPower, “Superpower 2G HTS wire specifications,” tech. rep., SuperPower, 2009.
- [58] SuperPower, “Superpower fault current limiter application,” tech. rep., SuperPower, 2009.
- [59] R. Bhattacharya, “Electrodeposited Cu-stabilizer layer and biaxially textured buffer layers for YBCO superconductors,” in *Superconductivity Program for Electric System*, 2007.

- [60] V. Selvamanickam, Y. Chen, X. Xiong, Y. Xie, M. MarTchevskii, A. Rar, Y. Qiao, R. Schmidt, A. Knoll, K. Lenseth, and C. Weber, "High performance 2G wires: From R&D to pilot-scale manufacturing," *Applied Superconductivity, IEEE Transactions on*, vol. 19, pp. 3225–3230, June 2009.
- [61] Y.-Y. Xie, Y. Chen, X. Xiong, X. Zhang, A. Rar, M. MarTchevskii, Y. Qiao, A. Knoll, K. Lenseth, R. Schmidt, J. Herrin, D. Hazelton, and V. Selvamanickam, "Recent results in 2G HTS wire technology development at SuperPower," in *Korea Superconductivity Society Annual Meeting*, July 2008.
- [62] SuperPower, "Superpower 2G HTS wire spec sheet-fault current limiter application," Tech. Rep. Rev. 0808, SuperPower, 2008.
- [63] SuperPower, "Soldering instructions," tech. rep., SuperPower, 2009.
- [64] Y. Chen, X. Xiong, Y. Xie, X. Zhang, J. Reeves, Y. Qiao, A. Rar, K. Lenseth, and R. Schmidt, "Status of 2G manufacturing & development at SuperPower," in *DOE Wire & Applications Workshop*, January 2007.
- [65] D. W. Hazelton, "2G HTS high field magnet demonstration," in *Magnet Technology Conference, MT-20*, 2007.
- [66] Z. Chen, F. Kametani, Y. Chen, Y. Xie, V. Selvamanickam, and D. C. Larbalestier, "A high critical current density MOCVD coated conductor with strong vortex pinning centers suitable for very high field use," *Superconductor Science and Technology*, vol. 22, no. 5, p. 055013 (5pp), 2009.
- [67] V. Selvamanickam, Y. Chen, X. Xiong, Y. Xie, X. Zhang, A. Rar, M. MarTchevskii, R. Schmidt, K. Lenseth, and J. Herrin, "Progress in second-generation HTS wire development and manufacturing," *Physica C: Superconductivity*, vol. 468, no. 15–20, pp. 1504 – 1509, 2008. Proceedings of the 20th International Symposium on Superconductivity (ISS 2007).
- [68] D. R. Smith and F. R. Fickett, "Low-temperature properties of silver," *Journal of Research of the National Institute of Standards and Technology*, vol. 100, no. 2, pp. 119–171, 1995.
- [69] Columbus Superconductors. Columbus Superconductors SpA, Corso Perrone 73r, 16152 Genova, Italy. <http://www.columbussuperconductors.com>.
- [70] Hyper Tech Research. Hyper Tech Research Inc., 1275 Kinnear Road, Columbus, OH 43212, USA. <http://www.hypertechresearch.com>.
- [71] M. D. Sumption, M. Bhatia, X. Wu, M. Rindfleisch, M. Tomsic, and E. W. Collings, "Multifilamentary, in situ route, Cu-stabilized MgB<sub>2</sub> strands," *Superconductor Science and Technology*, vol. 18, no. 5, pp. 730–734, 2005.

- [72] E. A. Young, W. Bailey, and Y. Yang, "Thermal-electrical properties of  $\text{MgB}_2$  wire and bulk conductors," *EUCAS*, vol. 1, pp. P-111, 2009.
- [73] Columbus Superconductors, "Magnesium diboride from Columbus." Private Communication, August 2008.
- [74] P. D. Desai, "Thermodynamic properties of nickel," *International Journal of Thermophysics*, vol. 8, pp. 763–780, Nov. 1987.
- [75] C. Y. Ho, M. W. Ackerman, K. Y. Wu, S. G. Oh, and T. N. Havill, "Thermal conductivity of ten selected binary alloy systems," *Journal of Physical and Chemical Reference Data*, vol. 7, no. 3, pp. 959–1178, 1978.
- [76] C. Y. Ho, M. W. Ackerman, K. Y. Wu, T. N. Havill, R. H. Bogaard, R. A. Matula, S. G. Oh, and H. M. James, "Electrical resistivity of ten selected binary alloy systems," *Journal of Physical and Chemical Reference Data*, vol. 12, no. 2, pp. 183–322, 1983.
- [77] L. F. Goodrich, T. C. Stauffer, J. D. Splett, and D. F. Vecchia, "Measuring residual resistivity ratio of high-purity Nb," vol. 711, pp. 41–50, AIP, 2004.
- [78] C. Y. Ho, R. W. Powell, and P. E. Liley, "Thermal conductivity of the elements: A comprehensive review," *Journal of Physical and Chemical Reference Data*, vol. 3(Supplement 1), no. 4, pp. 1–796, 1974.
- [79] P. D. Desai, "Thermodynamic properties of iron and silicon," *J phys chem ref data*, vol. 15, no. 3, pp. 967–983, 1986.
- [80] W. R. G. Kemp, P. G. Klemens, and G. K. White, "Thermal and electrical conductivities of iron, nickel, titanium and zirconium at low temperatures," *Australian Journal of Physics*, vol. 9, p. 180, June 1956.
- [81] A. Ballarino, "Current leads for the LHC magnet systems," *Applied Superconductivity, IEEE Transactions on*, vol. 12, pp. 1275–1280. 6 p, Mar 2002.
- [82] K. H. Meß, "Quench Protection at HERA," in *Proceedings of the 12th IEEE Particle Accelerator Conference. 16-19 Mar 1987, Washington, DC, p.1474*, p. 1474, 1987.
- [83] P. S. Martin, "Design and operation of the quench protection system for the Fermilab Tevatron," vol. 184, pp. 2073–2097, AIP, 1989.
- [84] A. Ballarino, K. H. Meß, and T. Taylor, "Extending the application of HTS in particle accelerators," in *EUCAS (Brussels)*, 2007.
- [85] X. Wang, U. P. Trociewitz, and J. Schwartz, "Near-adiabatic quench experiments on short  $\text{YBa}_2\text{Cu}_3\text{O}_{7-\delta}$  coated conductors," *Journal of Applied Physics*, vol. 101, no. 5, p. 053904, 2007.

- [86] S. March, A. Ballarino, and Y. Yang, “Power switches utilizing superconducting material for accelerator magnets,” *Applied Superconductivity, IEEE Transactions on*, vol. 19, pp. 1182–1185, June 2009.
- [87] Y. A. Cengel, *Heat Transfer A Practical Approach*. McGraw-Hill, 1997.
- [88] F. Rodriguez-Mateos, P. Pugnati, S. Sanfilippo, R. Schmidt, A. Siemko, and F. Sonnemann, “Quench heater experiments on the LHC main superconducting magnets,” *EPAC*, vol. Vienna, Austria, p. 4 p, Sep 2000.
- [89] D. Larbalestier, A. Gurevich, D. M. Feldmann, and A. Polyanskii, “High- $T_c$  superconducting materials for electric power applications,” *Nature*, vol. 414, pp. 368–377, 2001.
- [90] A. Godeke, A. den Ouden, A. Nijhuis, and H. ten Kate, “State of the art powder-in-tube niobium-tin superconductors,” *Cryogenics*, vol. 48, no. 7-8, pp. 308 – 316, 2008. Special Issue: Low- $T_c$  Superconducting Materials.
- [91] “European High Temperature Superconductors.” URL: [www.bruker-eHTS .com](http://www.bruker-eHTS.com), 2008.
- [92] C. R. Walters, “Brookhaven national laboratory informal report BNL 18928 (AADD 74-2) 30-1,” tech. rep., Brookhaven National Laboratory, 1974.
- [93] E. Barzi, L. D. Frate, D. Turrioni, R. Johnson, and M. Kuchnir, “High temperature superconductors for high field superconducting magnets,” *AIP Conference Proceedings*, vol. 824, no. 1, pp. 416–424, 2006.
- [94] “Superconductivity - part 3: Critical current measurement - dc critical current of Ag- and/or Ag alloy-sheathed Bi-2212 and Bi-2223 oxide superconductors,” April 2006.
- [95] W. Bailey, E. A. Young, Y. Yang, and C. Beduz, “Boiling heat transfer to a liquid nitrogen pool from Ag sheathed BiPb2223 tapes carrying over-current,” *Superconductor Science and Technology*, vol. 19, no. 4, pp. 276–279, 2006.
- [96] E. H. Brandt, “The flux-line lattice in superconductors,” *Reports on Progress in Physics*, vol. 58, no. 11, pp. 1465–1594, 1995.
- [97] D. M. J. Taylor, S. A. Keys, and D. P. Hampshire, “ $E-J$  characteristics and  $n$ -values of a niobium-tin superconducting wire as a function of magnetic field, temperature and strain,” *Physica C: Superconductivity*, vol. 372-376, pp. 1291–1294, 2002.
- [98] A. K. Ghosh, “ $V-I$  transition and  $n$ -value of multifilamentary LTS and HTS wires and cables,” *Physica C: Superconductivity*, vol. 401, pp. 15–21, Jan. 2004.

- [99] B. Dutoit, M. Sjoström, and S. Stavrev, “Bi(2223) Ag sheathed tape  $I_c$  and exponent  $n$  characterization and modelling under DC applied magnetic fields,” *Applied Superconductivity, IEEE Transactions on*, vol. 9, pp. 809–812, Jun 1999.
- [100] T. Kiss, M. Inoue, S. Nishimura, T. Kuga, T. Matsushita, Y. Iijima, K. Kakimoto, T. Saitoh, S. Awaji, K. Watanabe, and Y. Shiohara, “Angular dependence of critical current properties in YBCO coated tape under high magnetic field up to 18 T,” *Physica C: Superconductivity*, vol. 378–381, pp. 1113–1117, Oct. 2002.
- [101] Y. Inoue, H. Kurahashi, Y. Fukumoto, and M. Shimada, “Critical current density and  $n$ -value of NbTi wires at low field,” *Applied Superconductivity, IEEE Transactions on*, vol. 5, pp. 1201–1204, Jun 1995.
- [102] B. Seeber, A. Ferreira, V. Abacherli, and R. Flukiger, “Critical current of a Nb<sub>3</sub>Sn bronze route conductor under uniaxial tensile and transverse compressive stress,” *Superconductor Science and Technology*, vol. 20, no. 9, pp. S184–S188, 2007.
- [103] T. J. Arndt, A. Aubele, B. Fischer, H. Krauth, B. Sailer, and A. Szulczyk, “Bi-2223 tapes for applications at high temperatures and/or high fields—designs, long length processing and properties,” *Physica C: Superconductivity*, vol. 372–376, pp. 887–890, 2002.
- [104] T. M. Qu, C. Gu, M. Li, and Z. Han, “ $V - I$  properties and  $n$ -value of degraded Bi-2223/Ag superconducting tapes,” *Physica C: Superconductivity*, vol. 426–431, pp. 1159–1163, 2005.
- [105] K. Inoue, N. Sakai, and Murakami, “ $E - J$  characteristics and  $n$  value of melt-textured REBa<sub>2</sub>Cu<sub>3</sub>O<sub>x</sub> (RE: Nd, Y),” *Applied Superconductivity, IEEE Transactions on*, vol. 13, pp. 3109–3112, 2003.
- [106] E. Martinez, M. Martinez-Lopez, A. Millan, P. Mikheenko, A. Bevan, and J. S. Abell, “Temperature and magnetic field dependence of the  $n$ -values of MgB<sub>2</sub> superconductors,” *Applied Superconductivity, IEEE Transactions on*, vol. 17, pp. 2738–2741, June 2007.
- [107] A. Kuijper, A. P. Verweij, and H. H. J. ten Kate, “Correlation between voltage-current relation and current distribution in superconducting cables,” *Physica C: Superconductivity*, vol. 401, pp. 129–134, 2004.
- [108] M. H. Sohn, S. Kim, K.-D. Sim, C.-H. Min, E.-Y. Lee, K.-C. Seong, Y.-K. Kwon, and H.-J. K. and, “A study on  $I - V$  characteristics of conduction-cooled HTS coils,” *Physica C: Superconductivity*, vol. 463–465, pp. 1276–1280, 2007.
- [109] P. W. Anderson and Y. B. Kim, “Hard superconductivity: Theory of the motion of Abrikosov flux lines,” *Rev. Mod. Phys.*, vol. 36, pp. 39–43, Jan 1964.

- [110] G. L. Dorofeev, A. B. Imenitov, and E. Y. Klimenko, "Voltage current characteristics of type II superconductors," *Cryogenics*, vol. 20, pp. 307–312, 1980.
- [111] A. Clark and J. Ekin, "Defining critical current," *Magnetics, IEEE Transactions on*, vol. 13, no. 1, pp. 38–40, 1977.
- [112] DuPont, "DuPont Kapton HN, polyimide film," Data sheet K-15345, DuPont, March 2006.
- [113] J. D. Hoffman, *Numerical methods for engineers and scientists*. New York, NY: McGraw-Hill, 1992.
- [114] S. Caspi, L. Chiesa, P. Ferracin, S. Gourlay, R. Hafalia, R. Hinkins, A. Lietzke, and S. Prestemon, "Calculating quench propagation with ANSYS," *Applied Superconductivity, IEEE Transactions on*, vol. 13, pp. 1714–1717, June 2003.
- [115] T. Huang, A. Johnstone, Y. Yang, C. Beduz, and C. Friend, "Finite element modeling of thermal stability and quench propagation in a pancake coil of PbBi2223 tapes," *Applied Superconductivity, IEEE Transactions on*, vol. 15, pp. 1647–1650, June 2005.
- [116] J. Grundmann, M. Lindmayer, R. Röckelein, and W. Schmidt, "Simulation of HTS switching with the finite element analysis program ANSYS," *Superconductor Science and Technology*, vol. 16, p. 562, 2003.
- [117] R. D. Skeel and M. Berzins, "A method for the spatial discretization of parabolic equations in one space variable," *SIAM Journal on Scientific and Statistical Computing*, vol. 11, pp. 1–32, 1990.
- [118] W. Schmidt, H. P. Kraemer, H. W. Neumueller, U. Schoop, D. Verebelyi, and A. Malozemoff, "Investigation of YBCO coated conductors for fault current limiter applications," *Applied Superconductivity, IEEE Transactions on*, vol. 17, pp. 3471–3474, June 2007.
- [119] C. R. Acosta, M. Acosta, V. Sosa, O. Ares, and E. H. Brandt, "Comparative analysis of the complex susceptibility of YBCO films at different temperatures and magnetic fields," *Physica C: Superconductivity*, vol. 398, no. 3-4, pp. 152 – 156, 2003.
- [120] M. M. Abu-Samreh, "Viscous flow in Al-doped YBCO high- $T_c$  superconductor thick tapes," *Physica B: Condensed Matter*, vol. 321, no. 1-4, pp. 368 – 374, 2002.
- [121] A. Ballarino, K. H. Mess, and T. Taylor, "Extending the use of HTS to feeders in superconducting magnet systems," *Applied Superconductivity, IEEE Transactions on*, vol. 18, pp. 1455–1458. 6 p, Jul 2008.
- [122] A. Ballarino, "Large-capacity current leads," *Physica C*, vol. 468, pp. 2143–2148. 19 p, Jan 2008.